AD-A034 324 ADVISORY GROUP FOR AEROSPACE RESEARCH AND DEVELOPMENT--ETC F/G 14/2
NUMERICAL METHODS AND WINDTUNNEL TESTING.(U)
OCT 76

UNCLASSIFIED AGARD-CP-210 NL

1 OF 3
AD-A
034 324

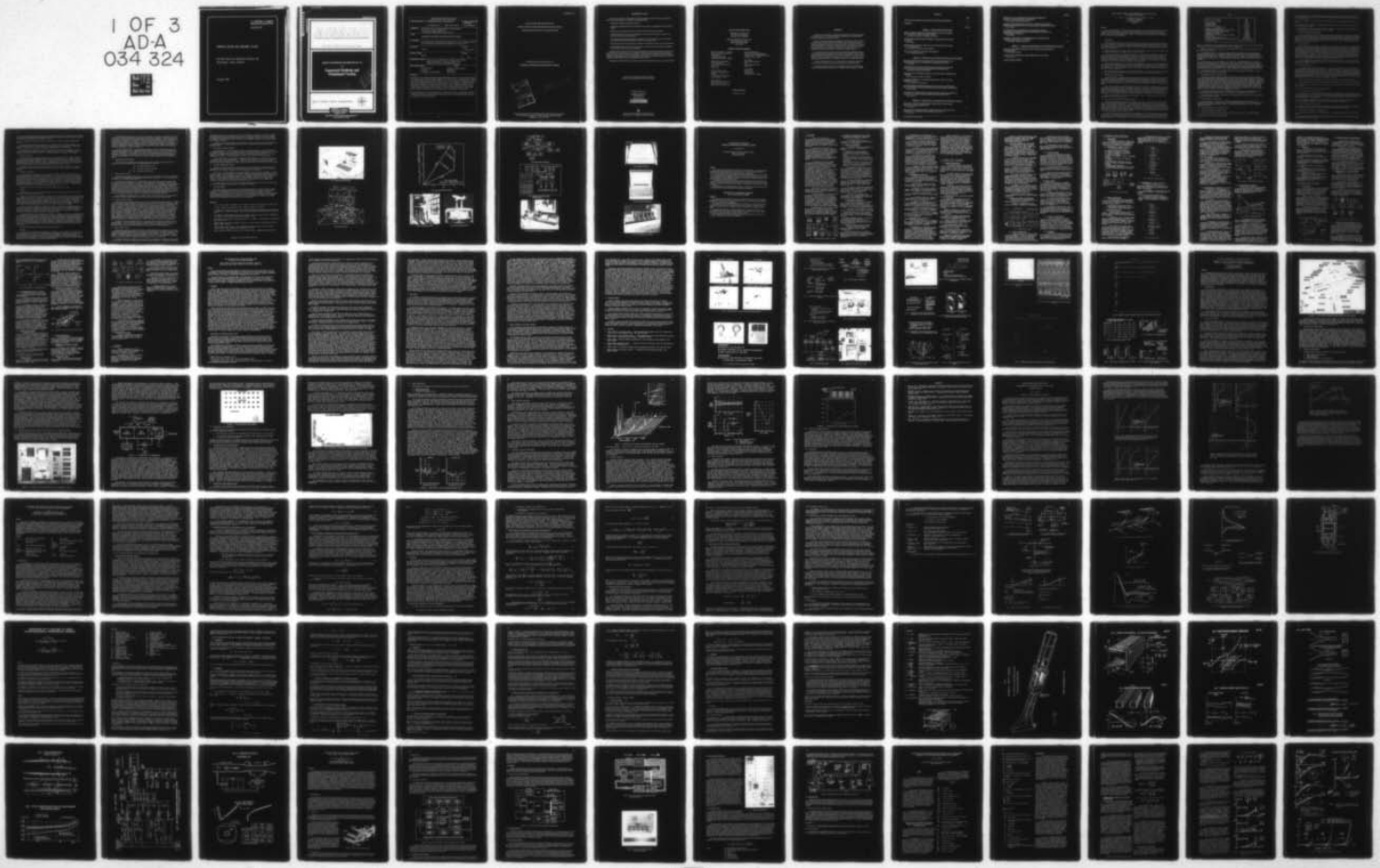

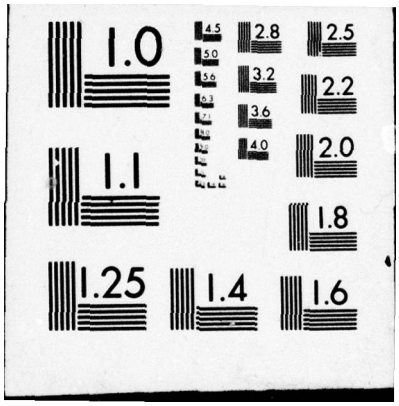
1.0
1.1
1.25
1.4
1.6
1.8
2.0
2.2
2.5
2.8
3.2
3.6
4.0
4.5
5.0
5.6

NUMERICAL METHODS AND WINDTUNNEL TESTING

ADVISORY GROUP FOR AEROSPACE RESEARCH AND
DEVELOPMENT, PARIS (FRANCE)

OCTOBER 1976

AGARD-CP-210

AGARD-CP-210

AGARD

ADVISORY GROUP FOR AEROSPACE RESEARCH & DEVELOPMENT

7 RUE ANCELLE 92200 NEUILLY SUR SEINE FRANCE

AGARD CONFERENCE PROCEEDINGS No. 210

on

Numerical Methods and Windtunnel Testing

NORTH ATLANTIC TREATY ORGANIZATION

DISTRIBUTION AND AVAILABILITY
ON BACK COVER

REPORT DOCUMENTATION PAGE			
1. Recipient's Reference	2. Originator's Reference AGARD-CP-210	3. Further Reference ISBN 92-835-0178-0	4. Security Classification of Document UNCLASSIFIED

5. Originator Advisory Group for Aerospace Research and Development
North Atlantic Treaty Organization
7 rue Ancelle, 92200 Neuilly sur Seine, France

6. Title

NUMERICAL METHODS AND WINDTUNNEL TESTING

7. Presented at

the Fluid Dynamics Panel Specialists' Meeting held at the Von Kármán Institute for Fluid Dynamics, Rhode-St-Genèse, Belgium, 23–24 June 1976.

8. Author(s)	9. Date
Various	October 1976
10. Author's Address	**11. Pages**
Various	214

12. Distribution Statement This document is distributed in accordance with AGARD policies and regulations, which are outlined on the Outside Back Covers of all AGARD publications.

13. Keywords/Descriptors

Windtunnel tests	Computer systems programs
Computers	Windtunnels
Computer systems hardware	Effectiveness

14. UDC

14. Abstract

Proceedings of the Fluid Dynamics Panel Specialists Meeting held at the Von Kármán Institute for Fluid Dynamics, Rhode-St-Gènese, Belgium, 23–24 June 1976, containing seventeen papers and a Round Table Discussion which focused on the role of computers in windtunnel testing. Discussions highlighted the manner in which computers can be utilized complementary with windtunnels to enhance the utility and effectiveness of both. Computer systems for windtunnel automatic real-time control, operation, and data collection-analyzation, which significantly increase operating efficiency and reduce power consumption, were discussed.

Recommendations were made for planned key experiments to obtain selected data to further validate and develop the computational methods, thus enhancing and significantly improving our prediction and design capability.

NORTH ATLANTIC TREATY ORGANIZATION

ADVISORY GROUP FOR AEROSPACE RESEARCH AND DEVELOPMENT

(ORGANISATION DU TRAITE DE L'ATLANTIQUE NORD)

AGARD Conference Proceedings No.210

NUMERICAL METHODS AND WINDTUNNEL TESTING

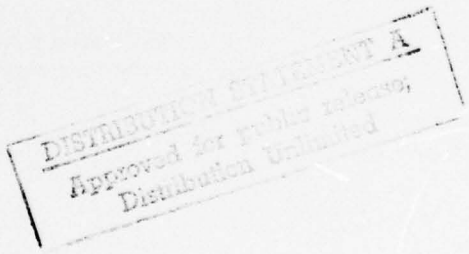

Papers presented at the Fluid Dynamics Panel Specialists' Meeting held at the Von Kármán Institute for Fluid Dynamics, Rhode-St-Genèse, Belgium, 23–24 June 1976.

THE MISSION OF AGARD

The mission of AGARD is to bring together the leading personalities of the NATO nations in the fields of science and technology relating to aerospace for the following purposes:

- Exchanging of scientific and technical information;
- Continuously stimulating advances in the aerospace sciences relevant to strengthening the common defence posture;
- Improving the co-operation among member nations in aerospace research and development;
- Providing scientific and technical advice and assistance to the North Atlantic Military Committee in the field of aerospace research and development;
- Rendering scientific and technical assistance, as requested, to other NATO bodies and to member nations in connection with research and development problems in the aerospace field;
- Providing assistance to member nations for the purpose of increasing their scientific and technical potential;
- Recommending effective ways for the member nations to use their research and development capabilities for the common benefit of the NATO community.

The highest authority within AGARD is the National Delegates Board consisting of officially appointed senior representatives from each member nation. The mission of AGARD is carried out through the Panels which are composed of experts appointed by the National Delegates, the Consultant and Exchange Program and the Aerospace Applications Studies Program. The results of AGARD work are reported to the member nations and the NATO Authorities through the AGARD series of publications of which this is one.

Participation in AGARD activities is by invitation only and is normally limited to citizens of the NATO nations.

Published October 1976

ISBN 92-835-0178-0

Printed by Technical Editing and Reproduction Ltd
Harford House, 7–9 Charlotte St, London W1P 1HD

AGARD FLUID DYNAMICS PANEL

CHAIRMAN: Mr J.P.Hartzuiker
NLR, Anthony Fokkerweg 2,
Amsterdam 1017, Netherlands

DEPUTY CHAIRMAN: Mr J.Lloyd Jones
NASA Ames Research Center
Moffett Field, California 94035
United States

PROGRAM COMMITTEE MEMBERS

Professor J.J.Smolderen – Chairman
Director, Von Kármán Institute for
Fluid Dynamics
72, Chaussée de Waterloo
1640 Rhode-Saint-Genèse – Belgium

Professor Dr Ing. C.Buongiorno
Universita degli Studi
Scuolo d'Ingegneria Aerospaziale
Via Salaria
Roma – Italy

M.l'Ing. Général P.Carrière
Directeur Scientifique Central
ONERA
29 Avenue de la Division Leclerc
92 320 Châtillon – France

Mr J.Lloyd Jones
Chief, Planning & Analysis Office
NASA Ames Research Center
Moffett Field, Ca. 94035 – USA

Dr K.J.Orlik-Rückemann
National Aeronautical Establishment
Montreal Road – National Research Council
Ottawa K1A 0R6 – Canada

Dr G.G.Pope
Head Aerodynamics Dept.
RAE
Farnborough GU 14 6 TD
Hants – UK

Dr F.W.Riegels
DFVLR-AVA
3400 Göttingen
Bunsenstrasse 10 – Germany

PANEL EXECUTIVE

Mr Michael C.Fischer

FOREWORD

The purpose of the Meeting was to illustrate through specific examples how computers and computer systems can be utilized integrally and complementary with windtunnels to enhance the efficiency and effectiveness of both.

Papers were presented indicating the advantages of computers for automatic real-time control, operation, and data collection for windtunnel facilities, which permit greatly increased operating efficiency and reduced power consumption. Additionally, it was discussed how the large computer, recognized as a powerful tool in numerical simulation and computational aerodynamics, can be utilized in combination with carefully chosen selected experiments to further validate and develop our prediction and design capability.

The computer can be used to simulate flow conditions either prohibitively expensive or physically impossible to accomplish in windtunnels, screen preliminary design concepts, perform aerodynamic optimization studies, etc. while the windtunnel can be used to obtain selected key data on refined geometric configurations at full scale (or near) design and off-design flight conditions which are not amenable to calculation by computational methods.

A Round Table Discussion, led by experts and joined by participants, discussed the Session Topics and recommended actions and planning for future research activities.

The Specialists' Meeting was held at the Von Kármán Institute for Fluid Dynamics, Rhode-St-Genèse, Belgium at the invitation of the Belgium National Delegates to AGARD.

CONTENTS

* Not available at time of publication.

DIGITAL COMPUTER ASPECTS OF THE INSTRUMENTATION AND CONTROL OF THE NEW RAE 5 METRE LOW SPEED TUNNEL

R. J. North, R. W. Jeffery, Mrs. J. A. Dolman, A. N. Tuck
Aerodynamics Department
Royal Aircraft Establishment
Farnborough, Hants
England

SUMMARY

After a brief description of the new 5m pressurised low speed tunnel at RAE Farnborough, an account is given of the applications of online and offline minicomputers in its instrumentation and control systems. Some of the hardware and software design considerations, and the choices made, are discussed: various options for future development are outlined. The connections with the RAE central computers and other ancillary systems are mentioned.

1 INTRODUCTION

Any new large wind tunnel will utilise digital computers in some way: the questions of interest are how and to what extent? This paper is essentially concerned with the part digital computers will play in the context of the new 5m pressurised low speed tunnel at RAE Farnborough. However, in order to set the scene a brief general description of the facility as a whole including the instrumentation and data handling system is given first.

Although minicomputers are commonly used in connection with wind tunnels, at RAE and elsewhere, they are more widely exploited on this tunnel than ever before in the UK.

The object has been to use the speed and versatility of these devices to simplify the tasks of the tunnel user, to make available the information necessary to control effectively the course of the tests whilst in progress, and to make available at least some of the results as soon as possible thereafter. The tunnel control system is itself computer-based and there are several other directions in which the properties of minicomputers facilitate or simplify control of apparatus. In all these cases the machines are unobtrusive in that the users do not need any computer expertise.

As well as the operational use of the tunnel, the development and testing of the various hardware and software sub-systems both before and after initial commissioning have to be taken into consideration. All these factors favour a system architecture which could be dealt with in modular parts during construction and subsequent use. Such an arrangement offers the advantage of being able to continue in operation in the face of partial malfunction.

Thus the overall intention has been to bring digital computers to the aid of the users in all facets of tunnel operation without imposing on them any additional burdens or introducing unreliability.

2 GENERAL DESCRIPTION OF TUNNEL

The RAE 5m tunnel is a high-Reynolds-number facility which will improve substantially the reliability and accuracy achievable in assessing the low speed aerodynamic characteristics of modern aircraft from wind-tunnel tests; the representation of the complex high lift systems which are used during take-off and landing is an important aspect. Its utilisation should lead to the design of aircraft with better low speed performance and should reduce the risk of expensive modifications being necessary at the flight test stage.

By virtue of the size of its working section (5m wide by 4.2m high), its pressure range and its main drive power, the tunnel can be used to test models of aircraft of the size of the HSA Hawk or GD YF 16 at full-scale values of Reynolds number. For models of transport aircraft of the size of the European airbus (A300B), Reynolds numbers nearly a quarter of full-scale values can be achieved; the capability to test over a 3 to 1 range of Reynolds number at constant Mach number then enables the effects of scale and compressibility to be separated, and gives a firm base from which to extrapolate to full-scale conditions.

The main characteristics of the tunnel are summarised in Table 1. Model tests in the tunnel are scheduled to start in the Spring of 1977.

2.1 Tunnel circuit, working section and model supports

The general arrangement of the facility is shown in Figs.1 and 2. The tunnel circuit is of welded steel construction and is aerodynamically a conventional return circuit except for the rapid expansion between the fourth corner and the cooler. The pressure shell is everywhere circular in cross-section, but liners are incorporated at the settling chamber, the contraction and the working section to make the air-swept surfaces rectangular (with corner fillets). The shape of the cross-section is similar through the latter parts in order to preclude secondary cross-flows. The main drive consists of an ac motor of 11000kW and a dc motor of 1640kW, used separately or together, turning a ten-bladed single-stage fixed-pitch fan. The tunnel performance envelope is shown in Fig.3.

One of the main features of the design is the arrangement made to ensure easy access to the working section, Fig.4. Two concentric spheres surround this, and parts of it at the upstream and downstream ends can be retracted, so that pressure doors on the outside of the inner sphere can be swung across the air passage and closed on to the inner sphere. This can then be depressurised to give access to the working

Table 1

Working section: width	5.0m
height	4.2m
Circuit length	186m
Contraction ratio	7.64
Pressure range	1 to 3 bar
Maximum speed at 3 bar	M = 0.27
at 2½ bar or less	M = 0.31
Maximum total temperature	40°C
Maximum Reynolds number (based on 0.5m chord)	8×10^6
Main drive, maximum continuous power	12.6MW
Compressors, maximum power	6.6MW
Pump-up time to 3 bar	45 minutes
Access time to model from operating condition	6 minutes
Restart time	5 minutes
Time to interchange model carts	30 minutes
Kinetic pressure variation across working section	±0.1 per cent
Turbulence level	0.10 to 0.15 per cent

section. Alternatively, the whole working section may be rotated to line up with an access tube through which a model on its cart can be removed into one of four rigging bays.

These carts effectively form the floor of the working section when in place in the tunnel. Three will be available initially:

(1) The mechanical-balance cart, from the turntable of which is suspended a particularly compact, virtual-centre balance, Fig.5. It measures and separates six components of force and moment through suitably-arranged mechanical lever systems and automatic weighbeams. Model incidence is changed by a telescopic strut at nose or tail. Sideslip, or the incidence of a half-model, is changed by rotating the turntable. The load ranges are lift ±90kN (±20000 lb), drag ±22kN (±4950 lb) and side force ±127kN (±28500 lb).

(2) The sting-support cart on which models are attached via a strain gauge balance and a sting to a quadrant which can be moved in pitch through ±19°. A lift force of 82kN (18500 lb) can be supported at any angle of roll together with a rolling moment of 20kN m (15000 lb ft). A straight sting and one with a 10° crank will be provided initially. With the cranked sting a second roll unit will normally be incorporated between the strain gauge balance and the sting which will enable small sideslip angles to be obtained without the model being rolled. The cranked sting allows an incidence range from -9° to +29°.

(3) A simple general-purpose cart for miscellaneous tests, including tunnel calibration. It also provides for models supported on a single-pole.

2.2 Instrumentation and data handling system

This system[3] provides the means of measuring, monitoring, recording and processing any physical quantities of interest which can be presented in the form of electrical signals. These will be principally forces, measured by either the mechanical balance or strain gauge balances mentioned above, or pressures. For pressure measurements a modular Scanivalve system is used with low-hysteresis transducers typically in three ranges. Up to 45 ports on each of eight Scanivalves are available in each module at scanning rates of 2½ ports/second. The present limit of capacity is 1200 ports, which can be increased if necessary. Interleaved scanning is used so that all the ports can be recorded in 2 minutes. The transducers are calibrated during the scans using a set of calibration pressures which span the pressure range of the tunnel. The modular system is sufficiently compact to mount inside the fuselages of conventional models but when this is not possible it will be accommodated on the cart.

Other physical quantities from up to 128 transducers can be dealt with by an adaptation of the pressure measuring system regarding them as an extra module of 128 single-port Scanivalves.

The instrumentation system as a whole exploits the capabilities of minicomputers and these aspects are dealt with in section 3 below.

2.3 Tunnel and plant control system

It is necessary to control the total pressure, the Mach number or kinetic pressure and the temperature in the tunnel. Changes in any of the three parameters interact with the other two and all of them are affected by changes in drag or thrust of a model in the working section. Thus an automatic computer-based system

(a) controls conditions in the working section;

(b) controls and monitors the tunnel plant;

(c) provides the interlock and sequence control for rapid and safe access to the working section.

In regard to tunnel air conditions, the system:

(a) sets and maintains a required value of the total pressure in the working section by assuring a sufficient inlet of air into the tunnel from the auxiliary compressors and controlling the rate of blow-off to the atmosphere;

(b) sets and maintains a required value of either Mach number or kinetic pressure by control of fan speed;

(c) minimises rate of change of air temperature by controlling the water temperature to the cooler, through a recirculation system.

Required values of tunnel parameters can be set manually or through the data system computers. The tunnel plant computer system is described in section 6 below.

3 DATA SYSTEM COMPUTER CONSIDERATIONS

The use of computers with wind tunnels has followed their development for scientific and commercial purposes. At first they were used for batch processing of wind tunnel data and later they were linked to one or more tunnels via relatively slow terminals. When they became cheaper and more powerful it became possible to use them online providing at least some results in real time and performing some control functions. This is the state of the art at the present time[4]: evidence of contemporary ideas in France and USA is given in Refs.5, 6 and 7.

3.1 Design objectives

The situation that faced us at the beginning of the 1970s when the 5m tunnel data system was being planned was that the use of minicomputers was generally accepted and the appearance of a new generation of machines with more powerful hardware and software was encouraging users to think of improvements to existing systems. The overall objective was a system which would acquire and record the desired raw data and at the same time process and display enough of it in real time for the tunnel users to assess and control the progress of the test. This of course implied that it should be possible for the user to interact with the test in progress. The ability to process locally large parts of the data to a more or less final form between tunnel runs would be advantageous. All this should be accomplished without the necessity for computer expertise on the user's part. Since the time in the tunnel is only part of the total activity the extraneous work should be computer-aided also if possible.

As well as meeting these requirements it was obviously desirable to have a flexible basic design which would be adaptable in the light of experience, the increased expectations of future users, and the demands of new types of testing.

3.2 System architecture

An early question was whether a multiplicity of minicomputers should be used in a distributed (or federal) system[8] or whether there should be one, or two, central machines. One machine may be the most economical solution once everything is working but it does not provide any redundancy in case of failure nor free access for development whilst the tunnel is running. For these reasons two-computer systems had been used previously both at NPL and RAE one of the machines being dedicated to real-time functions such as data acquisition and storage and the other to subsequent processing and analysis. This simplified the programming problems especially with the limited choice of real-time executives at the time. The second machine could also be used as a standby for development if need be.

When the 5m tunnel was considered it was clear that more than one computer would be needed

(i) during development of various parts of the system, which might not all take place on the same site;

(ii) during simultaneous tunnel operation and preparation for subsequent tests or calibration of strain gauge balances;

(iii) for software development or offline processing; and

(iv) for replacement in case of malfunction.

Since it would not be practicable to equip ourselves for all eventualities it was decided to use a number of machines in a two-tier hierarchy[3]. The first tier of machines, the so-called front end machines, are each dedicated to one of the main types of measurement (mechanical balance, strain gauge balance, pressure measurement). Each sub-system

(a) controls the instrumentation, the model attitude and the tunnel conditions according to the operator's commands via push-buttons or decade switches from a special control panel;

(b) records the raw data on disc files;

(c) converts the data to coefficient form and displays the last eight points together with information on the current tunnel conditions. Pressure distributions are shown in bar chart form;

(d) logs progress and alarms on a teletypewriter.

The second-tier machine is of the same basic type. The complete system can be operated in three modes:

(i) with the front end machines operating as stand-alone devices each with its own control panel and links with the tunnel plant computer;

(ii) as an integrated system in which the front-end machines operate under the supervision of the second-tier machine with a comprehensive control panel. The supervisory computer carries out additional processing, recording and display tasks under operator control;

(iii) in an automatic mode in which the test is controlled by the supervisory machine under program control.

When the front-end machines are operating in a stand-alone mode the supervisory machine can be used for development or for offline processing. The normal means of data transfer to the RAE central computers or the customer's own will be by computer-compatible tape from this machine.

The ensembles of instrumentation, computer and software are referred to as packages. Further packages can be added for special functions, for example, the balance calibration package (section 6.2). The tunnel plant computer system (section 6.1) can also be regarded as a package in this respect.

3.3 Operator interaction

The problems of users in communicating with one or more computers have been tackled by providing each machine with a specially-designed operating console consisting essentially of a number of push buttons and decade switches through which all data and demands for model position, tunnel conditions, operating modes, and display formats are entered. Though different for each machine these control panels share many common features: that for the supervisory machine embraces the functions of all the others. The control panel for the balance calibration machine is shown as an example in Fig.7.

The principal means of rapid communication between the system and the operators are the visual displays which are a feature of both the data system and the control system and which are discussed in section 4.

3.4 Hardware configurations

At an early stage we envisaged the front end machines as rather simple and austere devices but detailed consideration of the data storage requirements of the pressure measurement system particularly and the wish to have Fortran facilities soon made it clear that disk storage was essential. The present front end configuration consists of a PDP 11/40 processor with 24k words of core storage and hardware floating point, an RK05 1.2M word exchangeable disk, a VT05 alphanumeric crt display, an ASR33 teletype-writer and, in the case of the pressure measurement system, a Tektronix 4010 storage-type crt display. The supervisory machine, also a PDP 11/40, has a second RK05 disk, two TU 10 nine-track magnetic tape transports (800 bits/inch, 45 inch/second), an LS 11 line printer (60 lines/minute), a high-speed paper tape reader and punch and a VR17 large-screen refresh-type crt display.

A general view of the control panels, displays and computers is shown in Fig.8.

4 DISPLAYS

The displays are of course the principal means by which the computers communicate with the users and they are the data window on the tunnel.

Numerical data and information on model and tunnel conditions are presented on the VT05 crt displays, Fig.9. Twenty lines of up to 72 characters are available. The precise allocation varies according to the package function but in general a number of lines is devoted to the last 8 or 9 sets of values and is updated every time a new set is recorded. This gives the effect of a scrolled display. The rest of the screen is devoted to such information as demanded and achieved model attitude and tunnel conditions, current instrumentation readings, the type of test, the package status and error messages. Because of the large number of pressure measurements only a selection of the readings can be presented.

The Tektronix 4010 storage-type crt displays are peculiar to the pressure measurement system. A selection of the pressures is shown in the form of a bar graph, reminiscent of a liquid manometer but with the length of each bar in non-dimensional form, Fig.10. The computer stores the readings in the order taken and sorts them into the order required for display. The values of a previous set of readings can also be displayed as indicated by the shorter interdigital lines.

The supervisory machine has a larger and more versatile crt display than the front end machines and will be enhanced further as the need becomes clear. As has been suggested, a separate display package with its own computer may be appropriate. Initially we are providing the commonly-used graphical displays featuring lift, drag and pitching moment coefficients, incidence, Mach number and Reynolds number together with pressure distributions. We do not intend to develop the capabilities of the supervisory machine very rapidly during the early use of the tunnel, expecting to be guided by user experience. Since that part of the system already defined will be a great advance on anything previously available to low-speed tunnel users, in the United Kingdom at least, we feel that we should obtain the user reactions before proceeding too far.

The tunnel and plant control displays are mentioned in section 6.1.

5 SOFTWARE

Although we have discussed mainly the hardware the importance of the software was very much in our minds from the outset. It was clearly necessary for it to be designed so that it could be easily understood and modified as necessary later on, which implied documentation to professional standards. The software system has been planned in conjunction with Computer Analysts and Programmers (Reading) Ltd. and they have written the majority of the front end programs, working on site in close collaboration with RAE staff and using the actual machines for testing and development.

The operating system to be used for the front end machines was a matter of considerable discussion at the time (1973) and the possibility of writing one specially was considered. However, we were most anxious to use standard DEC software wherever possible to gain the advantages of their developments and the experience of other users. We therefore chose a fairly simple single-user executive, DOS Level 9 and accepted its shortcomings for our purposes. The question arose again in relation to the supervisory machine which has rather different functions from the front end machines and more scope for parallel activities (communications with the front end machines, processing operator commands, data logging, data reduction, supporting an interactive display). By this time (1975) a wider choice of DEC operating systems was available RT 11, RSX 11M and RSX 11D.

Our choice has been RSX 11M. We have considered whether it would be worthwhile converting the already-written programs so that a common operating system could be used. We have concluded that since we expect the programs for front end machines to reach a stable state fairly early in the life of the tunnel the extra effort is not justified. If, however, after some experience it seems necessary to standardise on one system it will be RSX 11M or a successor. None of this should bother a prospective user who would presumably only be concerned with Fortran processing programs run on the supervisory machine.

6 COMPUTER CONTROL APPLICATIONS

Apart from the data acquisition and recording system there are several other areas in which computers are used for combined control and computing purposes. These are:

(i) the tunnel and plant control;

(ii) the balance calibration machine;

and (iii) the model attitude control.

6.1 Tunnel and plant control

The plant control computer system, Fig.11, carries out the tasks mentioned in section 2.3 above and in addition performs comprehensive alarm signalling and logging of plant data. It is the responsibility of Ferranti Ltd., Automatic Systems Division.

The computer is interfaced to the two fused-quartz bourdon-tube precision pressure gauges which measure the tunnel speed and pressure, to the two digital valves one for charging the tunnel the other for blowing-off, the cooling water control valve, to two keyboards, four crt displays, two teletypewriters and a paper tape reader and a punch. In addition, there are links to the instrumentation computers and provision for 192 unipolar and 64 bipolar analogue inputs and 256 digital inputs. Three of the crt's are small monitors (4 lines of 16 characters) for tunnel users: one displays the set points and the others display the measured values and the percentage errors. The set points are entered from one of the keyboards which also allows set point control to be transferred to the instrumentation computers. The fourth crt is a large-screen display which responds to entries from the main keyboard mounted in front of it. Control loop parameters, alarms, and the various information being logged are displayed.

This comprehensively-equipped machine is a Ferranti Argus 500 with 32k words of core storage and a 2 microsecond cycle time operating under a real-time executive, small machine organiser (SMO).

6.2 Balance calibration machine

Associated with the mechanical balance and for use in calibrating strain-gauge balances is a computer-controlled balance calibration machine[4]. This machine has been designed in the light of experience with earlier calibration machines at RAE and exploits the state of the art in two areas of technology in novel fashion. As will have been noted the force balance loads are inconveniently large if they are to be applied by weights. In any case this is a slow process not amenable to mechanisation and the weights are bulky. Further, the calibration machine needs to be transportable initially between the factory and the tunnel site, and then between locations on site. So pairs of pneumatic double-acting force generators with rolling rubber diaphragms controlled by commercially-available precision pressure generators have been used instead of deadweights. The calibration machine designed around these devices relies on a digital computer to control and monitor the loading actions demanded. It performs initial testing for leaks, calculation of the forces necessary, interpolation between the pressure generator calibration points, application of the necessary pressures with temperature corrections, monitoring of the various displacement sensors and the balance outputs, and displays and records the calibration data. Without a digital computer the sum of these tasks would be at best tedious and slow and at worst unmanageable.

The balance calibration package operates in a stand-alone mode and borrows the mechanical balance package computer. This is acceptable because it is expected that the calibration machine will be used only occasionally. It has its own control panel of which the layout is shown in Fig.7. Both the mechanical balance and the calibration machine have been constructed by TEM Engineering Ltd.

6.3 Model attitude control

The attitude of the model on the sting support or the mechanical balance turntable is controlled by servomechanisms commanded either manually or via the data system computers. The control equipment, common to both the sting and mechanical balance carts, employs a PDP 11/03 computer to translate the control commands into appropriate signals for the servomechanisms. This computer is a microprocessor version of the PDP 11, being effectively the rack-mounted version of the LSI 11. It is at present the only example of the latest wave of computer technology in this system but it will not be the last.

The angular position of the model in pitch and roll will be measured by force-balance accelerometers mounted on board. The yaw will be measured by an optical system consisting of a rotating fan beam from a

laser mounted in the roof of the tunnel and a set of photodetectors on the model. The actual incidence and sideslip angles will be calculated from the outputs of these instruments by the front end computer and compared with the demanded incidence and sideslip. Any necessary corrections will be calculated by the computer and relayed to the control system so that the demanded attitudes will be obtained independent of support deflections.

For models, such as those designed for other tunnels, not fitted with the necessary accelerometers and photodetectors the calibrated support deflections will be taken into account by the front end computer software.

7 LINKS WITH RAE CENTRAL COMPUTERS

As stated earlier, it will be possible to operate the supervisory machine in an offline mode for processing and analysis. It is also being provided with a PDP 11/7020 Emulator, a combination of hardware and software components which equips the PDP 11 with ICL 7020 Remote Job Entry capability. It is connected to the RAE ICL 1906S central computer via a Datel 2400 (2400 bits/second) line and ICL 7900 communications equipment. A MOP teletypewriter terminal is also connected via a Datel 100 line.

Work has been started in conjunction with RAE Mathematics Department on a database system for use in conjunction with the ICL 1906S filestore. A subset of this data base will be operable on the supervisory machine with its graphical facilities. Another PDP 11/40 machine with interactive graphical facilities in Mathematics Department is linked to the ICL 1906S and can be used for access to the database.

8 ANCILLARY COMPUTER-BASED SYSTEMS

The period 1972-1975 has seen the rapid proliferation of computer-based systems in Aerodynamics Department RAE, and several others are in use for wind-tunnel data processing. Two should be mentioned particularly since they may be regarded as facilities available to the 5m tunnel.

A PDP 11/45 is available nearby which has been extensively used for software development for the 5m and other tunnels. It is equipped with a 44-channel simultaneous sample-and-hold, multiplexer and 12-bit analogue-to-digital converter primarily intended for digitising and processing 42-channel analogue magnetic tape. It employs a software package developed at ISVR, Southampton, which provides a wide range of functions for processing and analysing unsteady data and supports a Tektronix 4010 graphical display terminal. Users' own Fortran programs can be incorporated. Multichannel (up to 42) analogue tape recorders are available for use in conjunction with this facility.

For online processing of unsteady data a transportable Hewlett-Packard 5451A Fourier analyser based on the HP 2100A computer is available with two analogue input channels.

9 CONCLUDING REMARKS

This paper has given a broad picture of the philosophy underlying the computer systems installed in the RAE 5m low speed tunnel and has indicated the nature and extent of the facilities that will be available. The basis adopted for them has been justified by subsequent developments in computer technology (e.g. microcomputers) which can readily be incorporated in this framework. Interaction between systems designers and tunnel users is of course vital in the development of such systems and, although much previous RAE experience has been incorporated, the future enhancements are likely to be strongly influenced by user experience when the facility comes into operation.

REFERENCES

1 J.Y.G. Evans, A. Spence: Development of wind tunnels at the RAE. RAE Technical Report 71040 (1971)

2 M. Wilson: The RAE 5m low speed wind tunnel. Flight, 22 March 1973, 478a-482

3 R.J. North, D.W. Partridge, E.C. Brown: A multicomputer instrumentation system for a new pressurised low speed tunnel. Fifth International Congress on Instrumentation in Aerospace Simulation Facilities (1973)

4 A.A. Wingrove: Computer-based data and control systems in three wind tunnels at RAE. Proceedings of IEE Conference on Use of Digital Computers in Measurement (1973)

5 Marcel Pierre: La soufflerie subsonique pressurisée F-1 de l'ONERA. L'Astronautique et l'Aeronautique No.48-1974-5, 48-59

6 Michel Delattre: Evolution des systemes de mesure et de controle dans les installations d'essai de l'ONERA. ONERA TP 1975-19

7 Joseph M. Cambra, Geno P. Tolari: Real-time computer data system for the 40- by 80-foot wind-tunnel facility at Ames Research Center. NASA TN D-7970 (1975)

8 James H. Crewshaw: Federated versus integrated computer systems. AGARDograph 158, February 1972

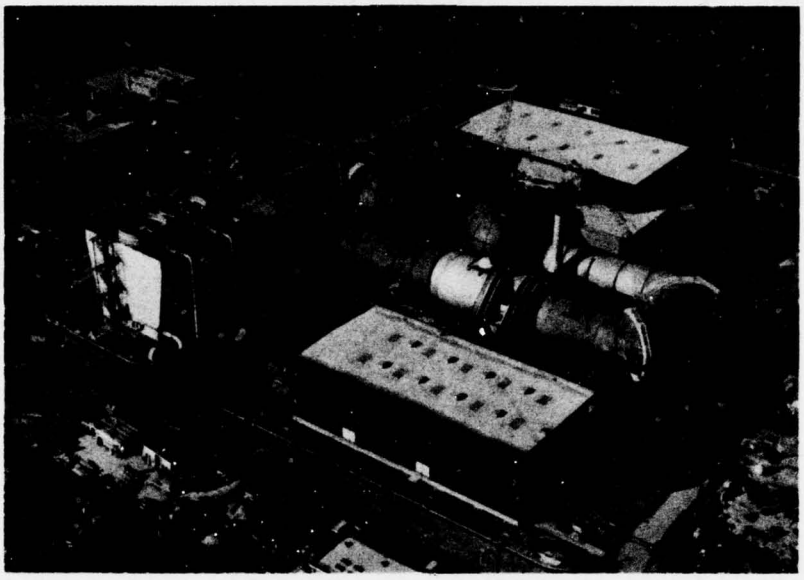

Fig.1 Aerial view of 5m tunnel (1975)

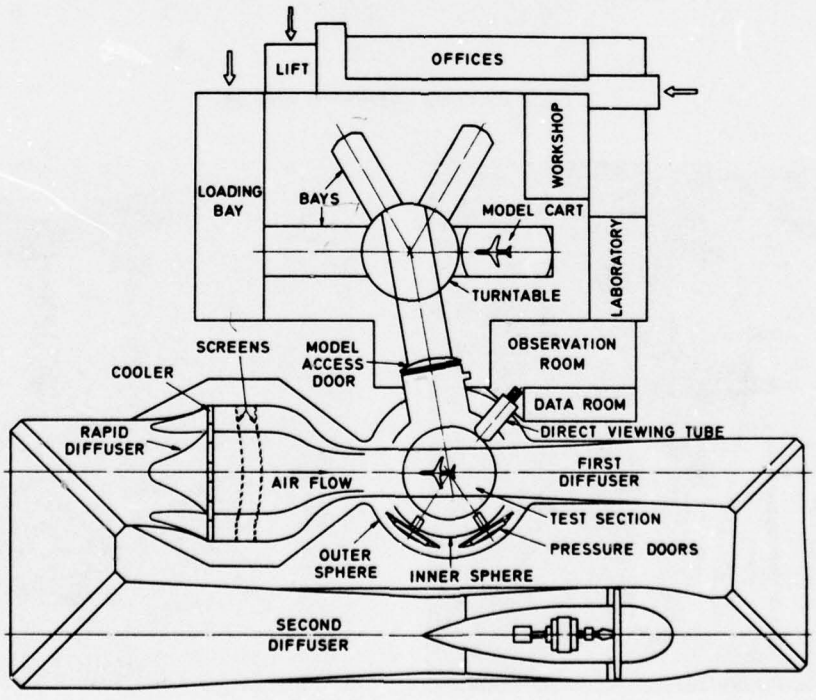

Fig.2 Plan of 5m tunnel

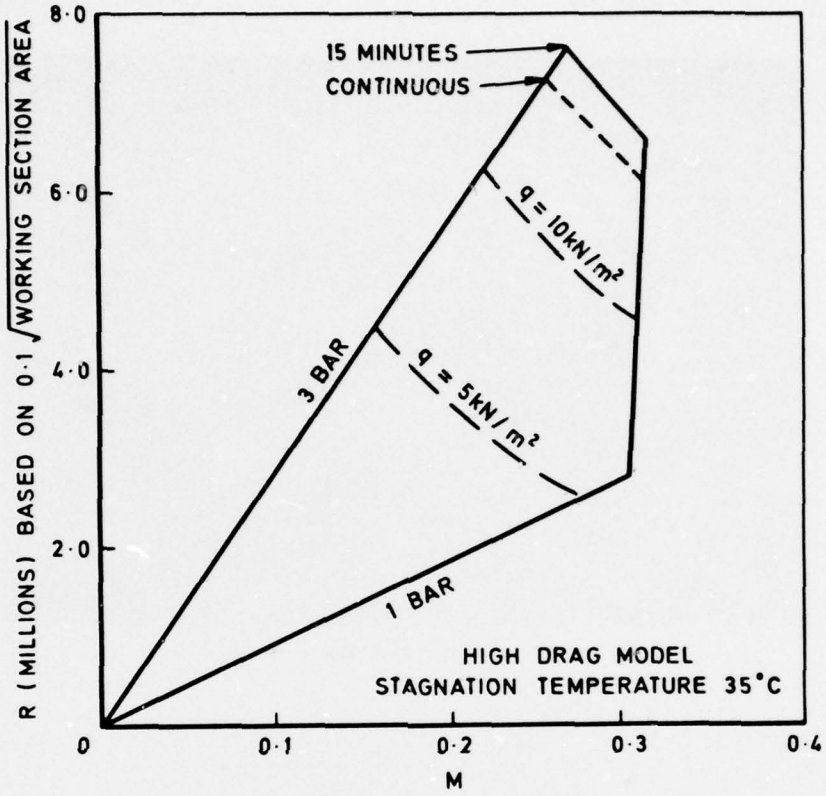

Fig.3 5m tunnel performance envelope

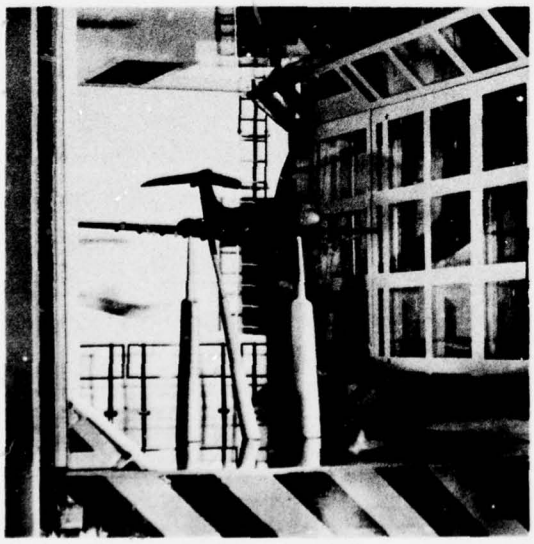

Fig.4 Model of working section

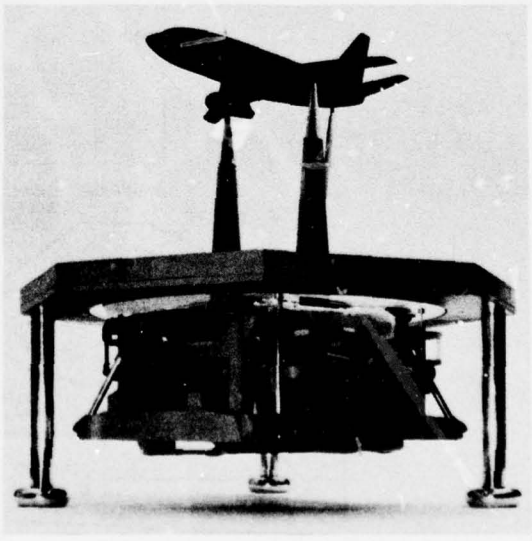

Fig.5 Model of mechanical balance

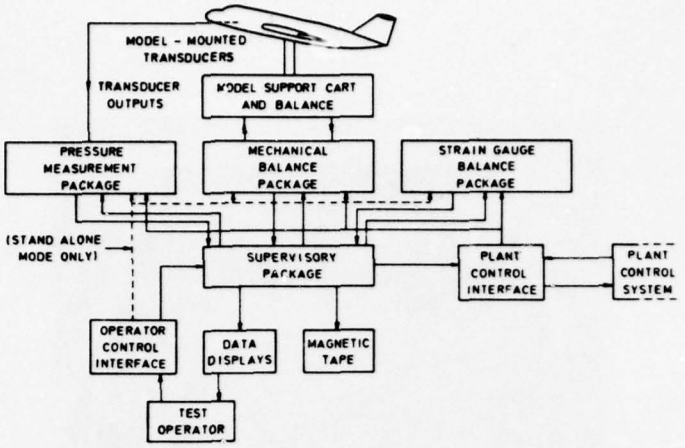

Fig.6 Block diagram of data system

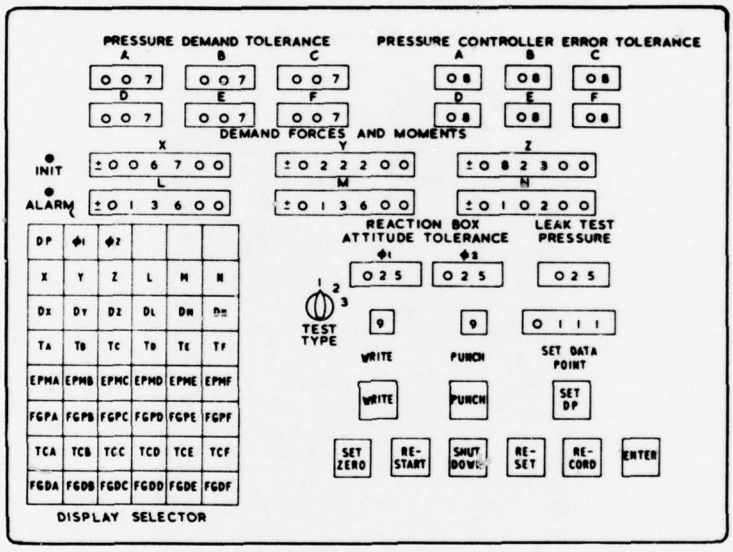

Fig.7 Operators control panel for balance calibration machine

Fig.8 General view of observation room and data room

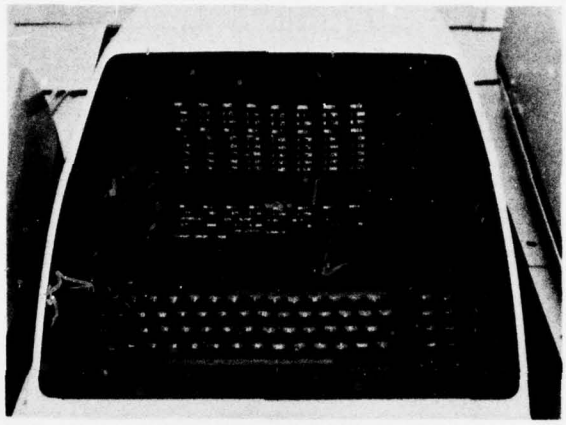

Fig.9 Alphanumeric display

Fig.10 Pressure distribution display

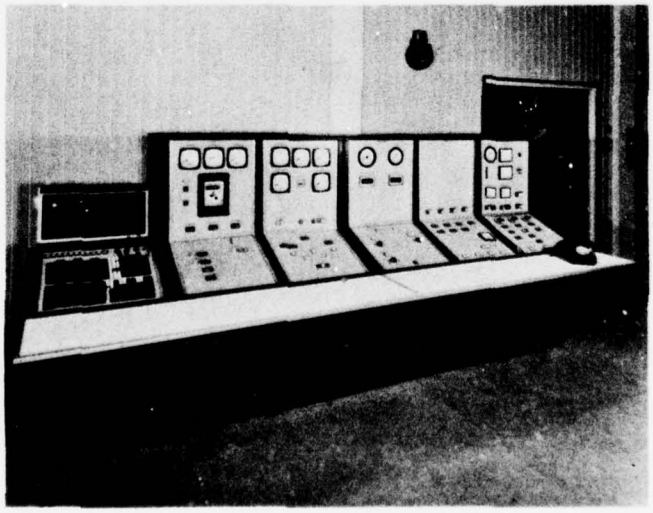

Fig.11 Tunnel and plant control desk

UTILISATION DES ORDINATEURS ASSOCIÉS AUX SOUFFLERIES DU CENTRE DE MODANE

par Gérard GRENAT

Office National d'Etudes et de Recherches Aérospatiales (ONERA)
92320 CHATILLON (France)
Centre de Modane-Avrieux

RÉSUMÉ

Les chaînes de mesure des souffleries de l'ONERA, Centre de Modane-Avrieux, ont été dotées progressivement de mini-ordinateurs destinés à en assurer la gestion. Ceux-ci assurent les fonctions suivantes : gestion d'acquisition des mesures, contrôle et surveillance de l'essai, asservissements.

Pour ce type particulier d'utilisation, l'ONERA a développé son propre logiciel. Celui-ci est multi-tâches, il offre une grande souplesse de dialogue avec l'opérateur et permet l'échange d'informations avec l'extérieur, à des cadences proches de celles réalisables avec l'ordinateur fonctionnant sans système ("stand alone"). L'ensemble du système est en service depuis avril 1975.

Trois applications sont décrites : essais de profils en courant plan, essais de rotor de convertible avec simulation en temps réel du basculement du rotor, dispositif de pesée d'engins sous avion, qui doit permettre de restituer la trajectoire de l'engin par rapport au porteur, en la calculant pas à pas (méthode de la "trajectoire captive").

Ces exemples donnent un aperçu des fonctions confiées aux ordinateurs associés aux chaînes de mesure, des charges qui peuvent leur être demandées, et des limites de leurs possibilités.

OPERATIONAL USE OF COMPUTERS ASSOCIATED WITH THE MODANE WIND TUNNELS

SUMMARY

The measuring units of the ONERA wind tunnels of the Modane-Avrieux Centre have been gradually equipped with mini-computers for ensuring the following functions : measurement acquisition management, test control and monitoring, automatic operations.

For this particular kind of use, ONERA developed its own software. This is of multi-task type, offers a great flexibility for dialogue with the experimenter and allows an exchange of informations with the outside, at a rate close to that of a "stand alone" computer. The whole system is operational since April 1975.

Three applications are described : two-dimensional profile tests, convertible rotor tests with real time simulation of rotor tilting, device for weighing missiles close to the aircraft with a view to calculate step by step the missile relative trajectory ("captive trajectory" method).

These examples outline the functions entrusted to the computers associated to measuring units, the loads they can withstand and the limits of their possibilities.

1 - HISTORIQUE

L'évolution progressive de la technologie des essais en soufflerie a amené l'Office National d'Etudes et de Recherches Aérospatiales à doter peu à peu les chaînes de mesures de son Centre de Modane-Avrieux en matériel numérique et analogique de plus en plus performant.

Les premières utilisations d'un ordinateur ont vu le jour lors de la définition et de la réalisation d'une chaîne d'acquisition numérique, nommée Unité d'Acquisition Numérique (UAN), destinée à automatiser la gestion de l'ensemble multiplexeur-convertisseur, le stockage des informations sur une bande magnétique numérique ainsi que l'enchaînement de certaines actions sur les périphériques de la chaîne.

L'utilisation de ces UAN a permis d'augmenter considérablement les cadences d'acquisition et de stockage des mesures ainsi que leur volume, mais la conception du logiciel de l'ordinateur associé à l'UAN interdit son utilisation en tant qu'outil de calcul arithmétique et logique à des fins autres que la pure gestion d'acquisition. La tendance à l'élargissement des fonctions de la chaîne de mesure en vue d'assurer la surveillance des points fragiles du montage, les calculs locaux destinés à assurer la sécurité de l'essai, le transfert des informations vers l'ordinateur central pour permettre le suivi de l'essai par un traitement en temps réel, ainsi que le besoin d'accélération et d'automatisation de certaines fonctions mécaniques ont nécessité l'utilisation d'un deuxième ordinateur, couplé à l'UAN ou autonome, dont le rôle ne soit pas limité à celui d'un automate de gestion d'appareils.

Cette évolution explique la coexistence, dans une même chaîne de mesure, de plusieurs ordinateurs de nature différente auxquels ont été confiées diverses missions.

La tendance actuelle de l'évolution est de supprimer cette disparité en confiant la gestion de la chaîne de mesure à un ordinateur qui dispose de toutes les actions souhaitables sur les appareils numériques ou analogiques qui la constituent ; les fonctions d'asservissement spécifiques d'un essai particulier pourront toutefois être confiées à un second ordinateur en cas de saturation de l'ordinateur principal ou pour des raisons de sécurité de fonctionnement.

La configuration de la chaîne de mesure de la soufflerie à rafales S3MA, qui sera détaillée lors de l'étude des essais dits "en courant plan", préfigure les chaînes futures qui équiperont les souffleries du Centre de Modane dans un avenir proche (schéma de la planche 1).

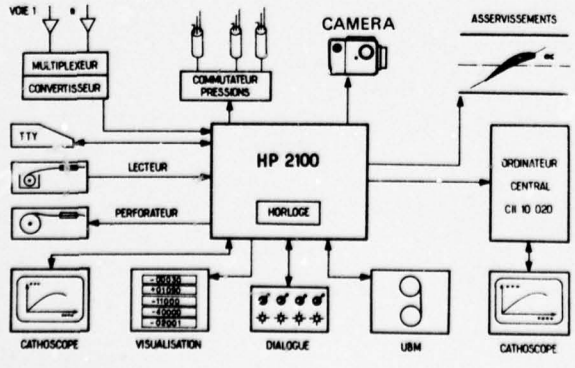

Pl. 1 – Fonctions assurées par les ordinateurs de chaîne.

2 - PRESENTATION SCHEMATIQUE DES DIFFERENTES FONCTIONS DES ORDINATEURS (planche 1) :

Les fonctions assurées par les ordinateurs de chaîne peuvent être grossièrement classifiées en quatre groupes.

2.1. Gestion d'acquisition :

L'ordinateur dispose, pour réaliser la gestion d'acquisition, des périphériques suivants :

- un commutateur de voies analogiques
- un convertisseur analogique-numérique réalisant une pesée sur 14 bits plus un signe
- un disque constitué d'une partie fixe et d'une partie mobile, chacune pouvant stocker 2,5 millions d'octets, ou une unité de bande magnétique
- une liaison directe avec l'ordinateur central (CII 10020) qui permet la transmission de mots de 16 bits en parallèle à une cadence maximale de l'ordre de 20 000 Hz.

Le processus d'acquisition consiste à sélectionner les voies à explorer dans un ordre pré-établi défini par le contenu d'une table d'adresses, puis à déclencher la pesée par le convertisseur. L'ensemble des mesures découlant d'une table d'adresses ou d'un sous-ensemble logique d'une table d'adresses constitue un lot d'informations. Ce lot sera généralement stocké localement sous sa forme brute.

Les lots sont ensuite (ou simultanément) transmis à l'ordinateur central après avoir éventuellement subi une transformation simple (moyenne, changement d'unités, correction de zéros, etc.).

Les cadences instantanées de multiplexage et conversion peuvent atteindre 16 000 Hz en mode aléatoire (fourniture de l'adresse à chaque pesée) et 60 000 Hz en mode séquentiel (fonctionnement en commutateur).

Les cadences de transfert vers l'ordinateur sont en moyenne assez faibles (200 mots/seconde), elles atteignent 4000 à 5000 Hz pour les essais instationnaires.

2.2. Automatismes et régulations :

Les fonctions confiées à l'ordinateur dans le domaine des asservissements et des régulations sont assez diversifiées car elles dépendent du but recherché, de l'appareillage mis en oeuvre, du type de fonctionnement recherché.

Deux modes de fonctionnement distincts, qui seront détaillés ultérieurement, sont utilisés:

- les asservissements par valeur de consigne : l'ordinateur est à l'origine, mais ne réalise pas l'asservissement qui est confié à un dispositif extérieur.

- les asservissements complets : l'ordinateur dispose des commandes élémentaires de positionnement (marche, arrêt, sens, etc.) et réalise lui-même l'asservissement à partir d'un algorithme pré-défini.

2.3. Contrôles et surveillance de l'essai :

Cette activité des ordinateurs de soufflerie présente plusieurs aspects complémentaires :

- Surveillance globale de la chaîne de mesure et de la qualité des mesures (détection des saturations, des fuites, contrôle de validité, détection des décalages des appareils à commutation...)

- Surveillance des points fragiles du montage (dépassement de la capacité des balances, surpressions, ...) ou des configurations dangereuses préjudiciables à la tenue du matériel.

- Fourniture de paramètres semi-élaborés destinés à assurer la conduite macroscopique de l'essai et surveillance des paramètres clés de l'expérimentation en cours afin d'en contrôler le suivi et la qualité.

Le premier aspect est assez systématique quel que soit le type d'expérimentation en cours, le deuxième et le troisième aspect sont à la discrétion de l'expérimentateur qui définira les contrôles à effectuer en cours d'essai.

Les informations en provenance des différents contrôles sont en général envoyées sur des visualisations numériques quand elles demandent un contrôle immédiat et permanent. Elles sont envoyées sur un cathoscope ou une télétype quand elles présentent un intérêt dans le suivi de l'essai sans mettre en aucun cas en cause la sécurité du matériel ou des personnes.

La cadence des rafraîchissements de ces informations dépend de l'importance des traitements à réaliser mais reste toujours proche des possibilités de préhensions et de réactions d'un opérateur humain (de l'ordre de 0,2 secondes à 2 ou 3 secondes).

2.4. Enchaînement des opérations.

La coordination et l'enchaînement des fonctions définies précédemment sont assurés par le déroulement d'un ou plusieurs programmes d'application contrôlés par le moniteur du système de gestion du calculateur.

L'acquisition des mesures ainsi que les traitements à réaliser dépendent en général de trois rythmes distincts :

- le rythme le plus élevé H1 définit la cadence instantanée de multiplexage-conversion pendant le déroulement de l'acquisition d'un lot.

- le rythme H2, encore appelé récurrence, définit la fréquence du renouvellement d'un lot.

- le rythme H3 détermine la cadence de renouvellement de l'acquisition d'un ensemble logique de plusieurs lots (polaire).

Le rythme H1 est déterminé par le mode de fonctionnement de l'ensemble multiplexeur-convertisseur (aléatoire ou séquentiel) ou par le réglage de l'horloge associée à cette commutation.

Le rythme H3 est déterminé par un évènement extérieur à la disposition de l'opérateur et du responsable de l'essai (bouton poussoir).

Le rythme H2 ou récurrence est fonction du mode d'acquisition associé à la partie numérique de la chaîne de mesure. On distingue deux orientations différentes :

- Le programme est à l'origine du déclenchement de l'acquisition :
La récurrence est dans ce cas déterminée par la durée des opérations à réaliser (stockage, pré-traitement, transferts) ou synchronisée sur un évènement attendu par le programme.

- Le programme subit l'arrivée des mesures :
La récurrence est déterminée par le rythme de l'arrivée des informations dans l'ordinateur. Les programmes entrant dans cette catégorie se classent en deux sous-ensembles ; ceux pour lesquels il est impératif que la durée du traitement soit inférieure, en moyenne, à la période de l'acquisition et ceux qui sont autorisés à ne traiter qu'un lot de temps en temps en fonction de leur récurrence propre.

Dans tous les cas où il est nécessaire que le rythme du traitement d'un lot soit au moins égal à celui de son renouvellement, la cadence d'acquisition doit pouvoir s'adapter à la durée du traitement qui est, en général, incompressible. L'utilisation d'un stockage de masse (disque) permet dans certains cas de reculer les limites imposées par la durée des traitements ; ce type de fonctionnement entraîne cependant un retard croissant entre acquisition et traitement, retard qui peut être préjudiciable au suivi et à la sécurité de l'essai. Cette procédure ne peut donc être mise en oeuvre que pour les traitements secondaires ne nécessitant pas une surveillance très serrée.

3 - LOGICIEL DE BASE - SYSTEME CMA.

3.1. Définition des besoins.

Les premières réalisations de gestion de tout ou partie d'une chaîne de mesure par un ordinateur ont vu le jour lors de l'écriture du premier processus courant plan et lors de la mise en service de la liaison directe avec l'ordinateur central.

Le premier processus courant plan avait été écrit (en 1972) en prenant l'ordinateur brut sans logiciel associé (fonctionnement dit en "stand-alone"), la liaison directe avait été écrite en utilisant comme support un logiciel séquentiel fourni par le constructeur (Basic Control System) dont les deux avantages étaient de gérer les entrées-sorties et de permettre l'emploi du Fortran.

L'extension progressive des fonctions confiées à ces ordinateurs, en particulier la surveillance des points fragiles d'un montage et de tout point relatif à la sécurité d'un essai a amené l'ONERA à désirer un logiciel de base plus sophistiqué présentant entre autre les caractéristiques suivantes :

- possibilité de mener en parallèle plusieurs travaux indépendants

- indépendance des travaux vis à vis des périphériques qu'ils n'utilisent pas et en particulier lors d'une panne de l'un d'eux, ceci pour éviter par exemple l'arrêt d'un programme de surveillance par suite d'un fonctionnement déficient de la liaison directe avec l'ordinateur central qui est rarement, de fait, indispensable à l'essai.

- temps de commutation de tâches et temps de réponse aux sollicitations extérieures (arrivée d'un lot d'informations) de l'ordre de la milli-seconde.

- cadence de transfert (Entrées-Sorties) instantanée en mode programmé de l'ordre de 15 000 Hz sans programmation spéciale.

- cadence de transfert instantanée en mode canal au minimum égale à 80 000 Hz (ensemble multiplexeur-convertisseur, disque ...)

- encombrement mémoire réduit ; les ordinateurs du Centre de Modane-Avrieux ne disposent que de 32 K.octets.

- verrouillage du système d'interruption limité à 20 micro-secondes afin d'être sûr de ne jamais perdre d'information à destination ou en provenance d'un périphérique rapide.

- possibilité de création ou d'extension d'un catalogue de commande personnalisé pour résoudre les problèmes de dialogue entre l'opérateur et la chaîne de mesure.

- interface utilisateur-système aussi simple que possible permettant l'emploi des langages évolués comme le FORTRAN compte tenu d'une bibliothèque existante (compilateurs, bibliothèque mathématique).

3.2. Présentation générale du logiciel CMA.

Le logiciel multi-tâches standard, fourni par le constructeur, dont l'ONERA s'est porté acquéreur afin d'en connaître les possibilités, répond à un certain nombre des points ci-dessus mais présente, vis à vis de cette demande, de grosses lacunes, notamment dans le domaine des Entrées-Sorties. L'ONERA a donc entrepris de réaliser un logiciel correspondant à ses besoins propres.

Le logiciel réalisé est un multi-tâches. Le temps de commutation d'une tâche à l'autre est de l'ordre de 500 micro-secondes. Les cadences d'Entrées-Sorties en mode programmé mono-directionnel sont de 30 000 Hz, elles sont de 17 000 Hz en mode programmé adressable (transfert d'une adresse et d'une information).

Le système de base comportant le moniteur et la gestion des périphériques standards (Télétype, lecteur/perforateur de ruban, disque ou unité de bandes magnétiques) occupe environ 12 K.octets de mémoire.

L'interface utilisateur-système a été volontairement rendue identique à celle du système équivalent du constructeur dans le but évident d'en utiliser les processeurs standards ; de ce fait les programmes d'applications écrits pour tourner sous le système du constructeur sont compatibles avec le système CMA mais n'en utilisent pas toutes les ressources.

Le langage le plus couramment utilisé pour la programmation des applications (gestion, surveillance, traitements locaux) est le Fortran, le langage d'assemblage n'étant utilisé que pour traiter les cas de manipulation de bits difficilement accessibles au Fortran.

L'écriture des modules de gestion d'entrées-sorties est faite par contre en langage d'assemblage.

3.3. Architecture générale du système CMA.

L'architecture du système figure sur le schéma synoptique de la planche n° 2.

L'ensemble du système est articulé autour d'un réseau de communications de messages.

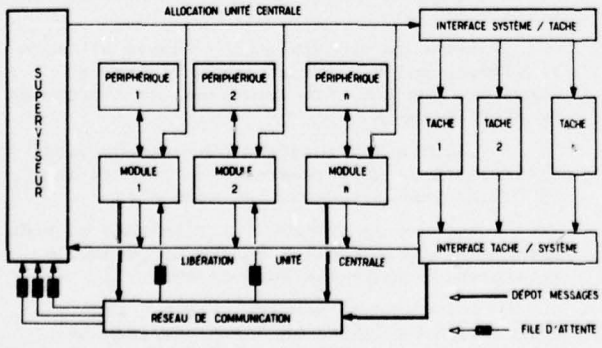

Pl. 2 – Architecture du système CMA.

3.3.1. Rôle du Superviseur.

Le Superviseur est un allocateur passif de l'unité centrale. Il dispose d'une liste de travaux privilégiés, associés aux évènements de fin d'entrées-sorties, qu'il fait passer en priorité par rapport aux travaux d'une autre nature qui sont déposés dans les files d'attentes.

L'exploration des files d'attentes n'est faite que si aucun travail privilégié n'est validé ; à chaque file est associée une priorité logicielle déterminée par un ordre d'exploration, chaque file n'étant traitée que si la précédente était vide.

Le Superviseur n'a aucun rôle de décision quant aux modules à faire travailler, chaque message contenant dans ses informations le module destinataire.

3.3.2. Notion de Module.

Un module est constitué d'une série d'instructions destinées à assurer une fonction définie et autonome. Les modules sont connus du superviseur par l'adresse d'une zone de variables associées, l'adresse de la première instruction exécutable et l'identificateur du module (numéro). Ils peuvent être découpés en traitements qui sont définis comme une série d'instructions exécutées entre deux retours au Superviseur.

Le Superviseur ignore la notion de traitement qui est géré par le module et qui fait partie intégrante des messages déposés dans les files.

Les modules sont en général associés à un périphérique, une partie des instructions étant exécutée sous le niveau d'interruption du périphérique, ils sont par ailleurs raccordés au réseau général de communications.

3.3.3. Notion de tâche.

Une tâche est en pratique un programme d'applications. Ces programmes d'applications, dont les prérogatives sont moindres que celles des modules (qui peuvent à peu près tout se permettre) sont accrochés au Superviseur et au réseau de communication par l'intermédiaire de deux interfaces.

L'interface système/tâche contrôle la logique de déroulement des programmes et le bien-fondé de leur reprise lors des mises en attente par suite des opérations d'entrées-sorties.

L'interface tâche/système contrôle la syntaxe et la formulation des demandes et les traduit, sous forme d'un message destiné au réseau de communication ; elle tient à jour l'état des évènements associés à ces demandes (actif, fini, attendu).

Les tâches se présentent sous forme d'un ruban contenant les instructions, l'identité, les implantations mémoire et les assignations (correspondance entre étiquette opérationnelle et périphérique) nécessaires à la bonne exécution de celle-ci.

3.3.4. Réseau de communication.

Le réseau de communication est en pratique un sous-programme qui est appelé à chaque fois qu'un module désire communiquer un message à un autre module. Comme dans tout système de communication, l'émetteur fournit le message à transmettre, message dont la syntaxe est une constante du système, ainsi que le destinataire du message sous forme de la file d'attente dans laquelle doit être déposé le message en question.

3.3.5. Extension.

Une extension du système est en cours de réalisation dans le but de permettre l'accès et la gestion de fichiers créés et catalogués sous le système DOS (Disc Operating System) du constructeur des ordinateurs HP 2100.

4 - DISPOSITIF D'ESSAI EN COURANT PLAN.

4.1. Présentation.

Le dispositif d'essai en courant plan a été réalisé dans la soufflerie à rafales S3MA dans le but d'automatiser le déroulement des opérations pour en améliorer les prestations.

4.2. Description de la chaîne (planche 3).

La chaîne de mesure comprend :

- l'ensemble multiplexeur-convertisseur
- la logique de commutation de pression
- la logique de commande de prise de vue
- le clavier de dialogue
- la logique de commande de position (incidence, peigne)
- la commande de protection des capteurs autonomes
- les périphériques classiques, Télétype, lecteur de rubans, perforateur de rubans
- l'horloge
- l'unité de bandes magnétiques
- la télécommande d'une chaîne analogique pour les mesures instationnaires s'il y a lieu.

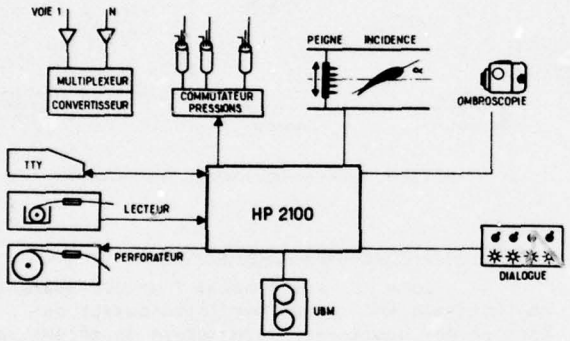

Pl. 3 – Chaîne pour essais en courant plan.

4.3. Gestion d'acquisition.

L'ordinateur déroule automatiquement, en fonction d'un programme d'essai pré-établi fourni au début de chaque rafale, les opérations suivantes, dans cet ordre :

1 - Acquisition des zéros avant rafale.
2 - Déclenchement et exécution de la rafale.
3 - Acquisition des zéros après rafale.

4.4. Acquisition des zéros.

L'acquisition des valeurs de zéros des capteurs, réalisée systématiquement avant et après la rafale, procède des principes schématisés sur la planche 4.

L'ordinateur, auquel a été préalablement fourni le programme général sous la forme reproduite sur la planche 8, prévient l'opérateur soufflerie du début de la procédure à l'aide de voyants lumineux disposés sur le boîtier de dialogue.

Par l'intermédiaire du même boîtier, l'opérateur fera savoir à l'ordinateur s'il peut ou non continuer sa procédure. Dans le cas favorable, l'ordinateur positionnera l'incidence à la valeur fournie dans le programme d'essai, prendra une photo s'il y a lieu et déclenchera l'acquisition du lot d'informations défini par la table d'adresses fournie avant la rafale.

Les valeurs sont imprimées sur la télétype locale à des fins de contrôle.

Le programme général permet l'acquisition de deux zéros simultanés. Le premier est en général réalisé avec la pression atmosphérique comme contre-pression sur les capteurs, le deuxième est réalisé avec la contre-pression de l'essai.

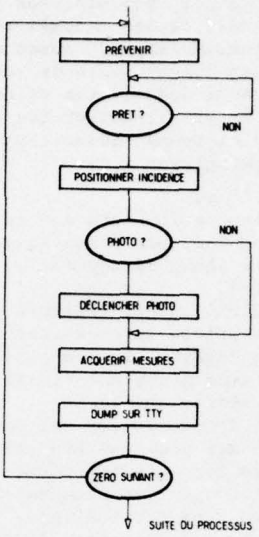

Pl. 4 – Courant plan – Acquisition des zéros.

4.5. Déroulement de la rafale (planche 5).

Le principe du déroulement est sensiblement le même que pour l'acquisition des zéros ; les acquisitions des mesures sont par contre plus complexes.

Le programme de l'essai définit le type d'acquisition à réaliser. Ces types sont les suivants :

- Acquisition des pressions pariétales :
  L'acquisition consiste à explorer, à l'aide de prises de pressions réparties sur le profil, le champ aérodynamique au niveau du profil.

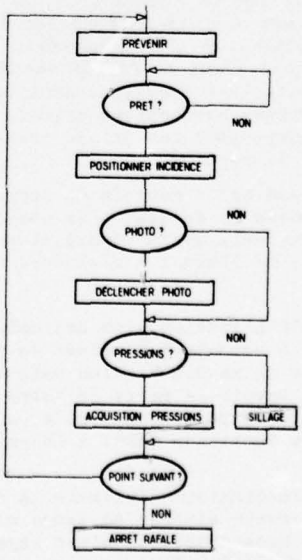

Pl. 5 – Courant plan – Rafale.

Les prises de pressions sont réparties sur six commutateurs de pressions de type scanivalve comportant chacun quarante huit prises.

Le lot d'information est constitué des six signaux en provenance des capteurs associés aux commutateurs, de quelques pressions caractéristiques (pi, po) mesurées par des capteurs autonomes et des paramètres de position.

L'ordinateur explore successivement les 48 positions des commutateurs de pression en donnant l'ordre de commutation et en vérifiant à chaque fois la stabilisation des signaux en provenance des capteurs (asservissement de commutation, paragraphe 4.6).

- Peignage de sillage :

Le principe de cette acquisition consiste à explorer, par un balayage vertical de la veine, le champ aérodynamique en aval du profil (sillage).

L'exploration est réalisée par un peigne comportant des prises de pressions statiques et totales qui se déplace sur une glissière verticale à l'aide d'une motorisation appropriée assurant une vitesse constante.

Le lot d'acquisition est constitué des capteurs autonomes généraux (po, pi, contre-pressions), des capteurs autonomes du peigne et des capteurs associés aux commutateurs de pressions (pressions pariétales).

Pendant le déplacement du peigne, qu'il a déclenché, l'ordinateur procède, avec une récurrence constante (10 lots/seconde), à l'acquisition des lots en déclenchant la commutation (non asservie) des pressions pariétales avec une récurrence qui est un sous-multiple de la précédente.

4.6. Asservissement de commutation (planche 6).

Le principe de l'asservissement de commutation repose sur l'allure générale de la courbe de réponse qui est présentée sur la figure n° 1. Le temps de stabilisation du signal est fonction de l'écart entre la pression de départ et la pression d'arrivée ainsi que du niveau de pression général Po. Ce temps est donc variable d'une prise à l'autre.

En dehors de tout asservissement le schéma d'une série de commutations se présente comme indiqué sur la figure n° 2. La cadence de commutation est choisie en fonction du temps de réponse le plus long afin d'acquérir pour chaque prise un signal ayant de fortes chances d'être stabilisé. Certaines pressions sont réparties sur plusieurs prises successives afin de ne pas trop perdre de temps pour les prises présentant un court temps de réponse.

Dans cette méthode de commutation, le compromis entre la fréquence de commutation minimale, maximale et la répartition des prises est fonction de l'essai à réaliser, donc non répétitif.

L'utilisation d'un ordinateur pour déclencher la commutation permet de remédier aux deux défauts de la commutation automatique cadencée, à savoir la perte de temps ou l'utilisation de prises en double ou triple, et le manque de certitude quant à la validité de la mesure.

L'ordinateur déclenche la commutation puis, après avoir attendu un temps minimum constant en deçà duquel il n'est physiquement pas possible que la stabilisation soit atteinte, lit à intervalle régulier la réponse du capteur et compare à chaque fois le signal obtenu avec le précédent. Si la différence entre deux signaux successifs est inférieure à la plage de stabilisation imposée, le calculateur stocke les mesures et déclenche la commutation afin d'explorer le plot suivant ; dans le cas contraire l'ordinateur continue à suivre la stabilisation du signal.

Au delà d'un certain temps, traduit par un nombre de lectures maximum des signaux, le calculateur déclare le signal instable, le stocke en le marquant et passe au plot suivant.

Cette méthode, qui est appliquée en parallèle sur plusieurs commutateurs (six actuellement), permet d'une part d'explorer les pressions aussi vite que leur stabilisation l'autorise et d'autre part d'être sûr que la mesure est stable ou instable.

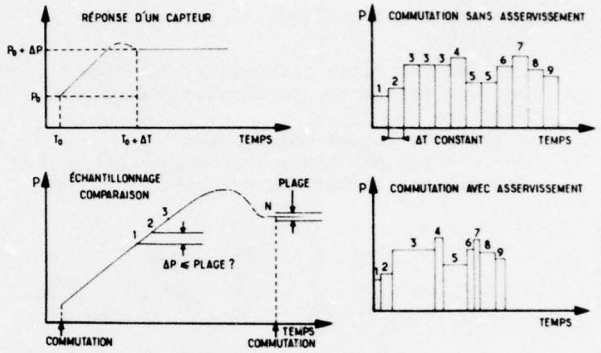

Pl. 6 – Courant plan – Asservissement de commutation.

4.7. Asservissement d'incidence.

Dans ce type d'essai l'asservissement en incidence est assuré par l'ordinateur qui dispose des commandes élémentaires de sélection du sens du déplacement et de marche-arrêt (schéma synoptique planche 7).

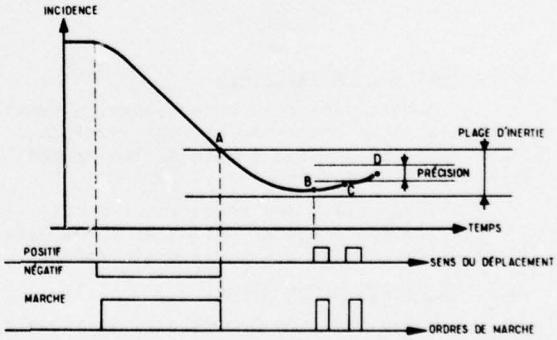

Pl. 7 – Courant plan – Asservissement d'incidence.

L'algorithme adopté est basé, comme dans tout asservissement, sur l'écart entre la valeur de consigne et la valeur actuelle.

Au delà d'un certain écart, lié à l'inertie du système, le déplacement est continu à grande vitesse. L'ordre d'arrêt est donné au point A du graphique, l'arrêt est effectif au point B. Si le point B est situé dans la fourchette déterminée par la précision souhaitée, l'ordinateur s'arrête, sinon il continue en donnant une série d'ordre de marche-arrêt de durée calibrée jusqu'à ce que l'arrêt se fasse dans la fourchette imposée.

Le choix de la plage d'inertie est fait après identification du modèle de façon à ce que l'arrêt déclenché en A aboutisse à un arrêt effectif dans la fourchette, ce qui est vrai dans

plus de 90 % des cas étudiés. Dans le cas contraire tout phénomène de pompage est supprimé par la limitation du nombre de changement de sens de déplacement ; si ce nombre est atteint, le point de mesure est fait à la dernière incidence obtenue et l'anomalie est signalée à l'opérateur par un message.

4.8. Conclusion.

L'utilisation d'un ordinateur pour gérer la chaîne de mesure de la soufflerie à rafales S3MA a permis des améliorations dans les domaines suivants :

- gain de temps et de qualité dans l'exploration des 48 plots d'un commutateur de pression.

- gain de temps et suppression de fonctions manuelles du fait de l'enchaînement automatique, suivant programme, des différents types d'acquisition.

- gain de temps dû à la commande des motorisations.

- recoupements avec des essais antérieurs rendus possibles grâce à la reproductivité du positionnement en incidence.

- augmentation du nombre d'informations utiles acquises dans une même rafale.

- augmentation de la sécurité du matériel grâce aux détections des anomalies de fonctionnement et à la rapidité des actions entreprises s'il y a lieu.

5 - ESSAI D'UN ROTOR DE CONVERTIBLE.

5.1. But de l'essai.

L'essai de rotor de convertible réalisé dans la soufflerie transsonique S1MA de Modane-Avrieux pour le compte de la Société Nationale des Industries Aérospatiales se propose de simuler le décollage, le vol de croisière et l'atterrissage d'un avion convertible.

Dans la phase de décollage, le rotor dont l'axe est au départ vertical dans la position hélicoptère bascule au fur et à mesure que l'avion monte et prend de la vitesse jusqu'à devenir horizontal dans la position hélice qui est celle de croisière. Dans la phase d'atterrissage le basculement a lieu dans le sens inverse. Ces deux phases durent, en vol réel, environ 12 secondes.

L'équilibre aérodynamique de l'avion en vol veut qu'il y ait une relation bi-univoque entre la vitesse linéaire de l'avion et les paramètres de positions et de motorisations, et c'est cette relation que l'essai se propose de simuler (planche 8).

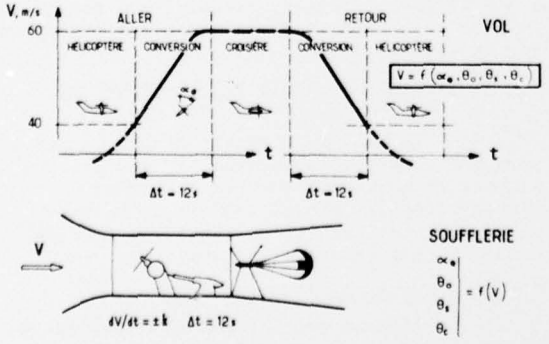

Pl. 8 – Rotor de convertible – Simulation de conversion.

5.2. Caractéristiques de l'asservissement

La simulation du décollage et de l'atterrissage de l'avion convertible nécessite le passage d'une vitesse de l'ordre de 30 m/s à une vitesse de l'ordre de 70 m/s et réciproquement dans un intervalle de 12 secondes.

L'accélération et la décélération correspondantes sont du même ordre de grandeur que l'accélération maximale de démarrage ou la décélération maximale de la soufflerie S1MA de l'ONERA. De ce fait, l'impossibilité de piloter la vitesse de la soufflerie dans ces deux zones limites de fonctionnement, a amené l'ONERA et la SNIAS à concevoir un asservissement inverse de celui du vol, c'est-à-dire à asservir les paramètres du rotor à la vitesse de la soufflerie.

Les paramètres asservis sont l'inclinaison du rotor par rapport à la verticale α_e et les composantes du pas cyclique à savoir le pas général, le pas latéral et le pas longitudinal. La vitesse de rotation du rotor ne fait pas pour le moment l'objet d'un asservissement, la conversion se fait à vitesse constante.

5.3. Description de la chaîne de mesure (planche 9).

La chaîne de mesure comporte deux postes indépendants. Le premier poste correspond à la chaîne normale de surveillance et d'acquisition de la soufflerie S1MA, le deuxième poste correspond à la chaîne d'asservissement.

La séparation des deux fonctions, acquisition générale et asservissement, qui par nature peuvent être réalisées dans le même ordinateur, est liée à un souci de sécurité ainsi qu'à des problèmes d'encombrement mémoire des programmes de gestion.

Le poste d'asservissement comprend un ordinateur HP 2100 nanti des périphériques d'accès classique, un ensemble de multiplexage et de conversion des mesures et quatre sorties de consignes d'asservissement.

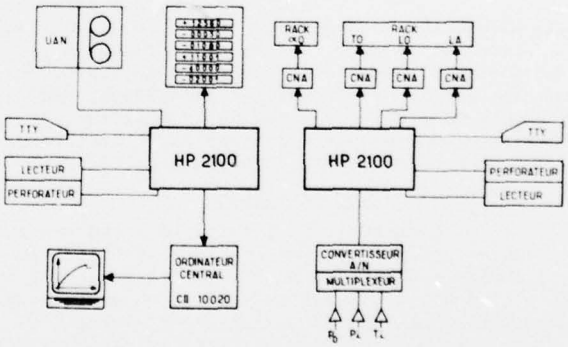

Pl. 9 – Essai de convertible - Chaîne de mesure.

5.4. Principe de l'asservissement (planche 10).

Les courbes de correspondance entre la vitesse du vent et chacun des paramètres asservis sont fournies à l'ordinateur sous forme d'une loi linéaire pour une vitesse inférieure à 30 m/s, d'une courbe définie point par point pour une vitesse comprise entre 30 m/s et 70 m/s et à nouveau d'une loi linéaire pour une vitesse supérieure à 70 m/s.

L'ensemble multiplexeur-convertisseur permet l'acquisition des valeurs Po, Pi et Ti à partir desquelles est calculée la vitesse du vent qui donnera, compte tenu des lois définies, les valeurs de consignes à envoyer, par l'intermédiaire

d'un convertisseur numérique/analogique sur les racks d'asservissement qui sont commandés en tension.

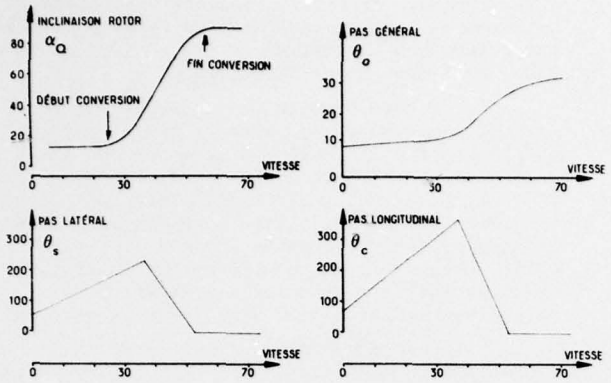

Pl. 10 – Essai de convertible – Consignes d'asservissement.

5.5. Fonctionnement général de la chaîne.

L'ordinateur de gestion de la chaîne d'acquisition et l'ordinateur d'asservissement sont indépendants.

Le programme d'asservissement fonctionne en suiveur. Il est lancé au début de l'essai et envoie des consignes à l'extérieur environ quinze fois par seconde pendant toute la durée de la rotation.

Le programme de gestion d'acquisition est lancé par l'opérateur au début de chaque conversion. Les mesures sont acquises à un rythme régulier en asynchronisme complet avec les consignes de position et sont envoyées sur une unité de bande magnétique et vers l'ordinateur central où elles subiront les traitements demandés par l'essai. Les informations élaborées, par exemple les trajectoires réelles de chacun des paramètres rotor, seront restituées sur le cathoscope relié à l'ordinateur central.

Le programme de surveillance fonctionne en permanence avec une récurrence de l'ordre de 2 secondes et calcule la vitesse du vent, le paramètre d'avancement, les informations de pas et les efforts encaissés par le montage. Ces valeurs sont affichées sur des visualisations numériques afin d'être disponibles à tout moment pour contrôler le bon déroulement de l'essai.

5.6. Essai de qualification.

L'ensemble du dispositif a été mis au point en juillet 75. Une première vérification de la chaîne a été faite en simulant les signaux Po, Pi, Ti donc la vitesse du vent et en envoyant les consignes analogiques sur un enregistreur graphique pour vérifier la validité des commandes. Une deuxième simulation plus complète a été réalisée avec un rotor sans pales, la soufflerie étant en marche et les paramètres de position étant asservis dans les conditions réelles de l'essai. Ces deux simulations ont prouvé le bon fonctionnement de l'ensemble.

L'essai réel du convertible étudié par la SNIAS aura lieu prochainement dans la soufflerie S1MA de l'ONERA.

6 - DISPOSITIF DE PESEE D'ENGIN SOUS AVION.

6.1. Pose de problème.

Ce dispositif, étudié par l'ONERA, est destiné à la simulation des trajectoires d'engins largués par un avion porteur.

La méthode utilisée jusqu'à présent pour étudier les interactions aérodynamiques entre un engin et son porteur, dite "méthode de la grille", consiste à explorer systématiquement par déplacements successifs suivant deux axes le champ aérodynamique entourant l'avion ; la trajectoire de l'engin est ensuite déduite des mesures obtenues par cette exploration du champ aérodynamique et des lois régissant le mouvement de cet engin.

Cette exploration systématique est longue et coûteuse, le nombre de points de mesures acquis étant très grand par rapport au nombre de points utiles, ce qui a amené l'ONERA, vu l'intérêt montré par les constructeurs pour ce type d'essai, à étudier un dispositif automatique de restitution de trajectoire par asservissement en position d'un engin par rapport à un avion porteur, la trajectoire étant calculée au fur et à mesure compte tenu des efforts mesurés et de l'équilibre de l'engin.

6.2. Description du dispositif (planche 11).

Le dispositif mécanique consiste en une glissière permettant de simuler le déplacement longitudinal de l'engin à laquelle est accroché un bras mobile, articulé suivant deux axes perpendiculaires, lui-même accroché à un équipage mobile par deux articulations perpendiculaires. Le dernier équipage mobile, auquel est fixé l'engin, possède un mouvement de rotation en roulis. L'ensemble possède donc six degrés de liberté, soit une translation, deux mouvements de tangage, deux mouvements de lacet et un mouvement de roulis.

Les six mouvements sont motorisés et chaque position est géométriquement connue par un codeur numérique associé.

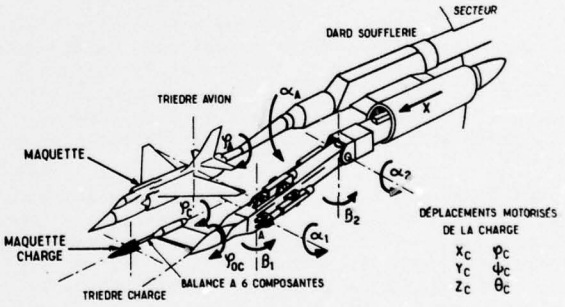

Pl. 11 – Dispositif pour l'étude de la trajectoire en présence de l'avion.

6.3. Type d'asservissement.

L'asservissement est fait par valeur de consigne. Les consignes sont fournies numériquement à une logique de pilotage associée à six modules de puissance, chaque mouvement étant distingué par un système d'adressage.

6.4. Description de la chaîne de mesure (planche 12).

La chaîne de mesure comprend, outre les périphériques standards, une logique de commande adressable pour réaliser les consignes d'asservissement et une logique de lecture, adressable également, des états des diverses motorisations (codeurs de position).

6.6. Principe de l'essai.

L'essai peut se dérouler suivant deux modes distincts, le mode "grille" et le mode "trajectoire".

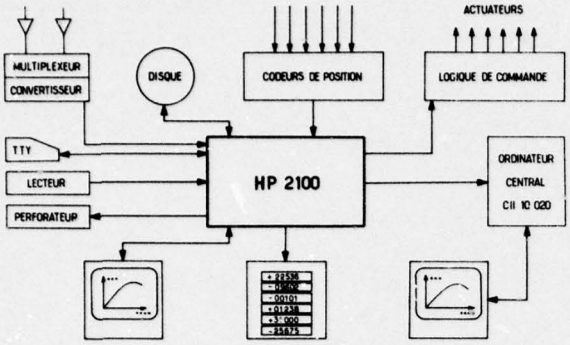

Pl. 12 – Dispositif à six degrés de liberté – Chaîne de mesure.

En mode grille la position de départ est définie par le responsable d'essai et l'ordinateur actionne le dispositif de translation pour avancer d'un pas constant à chaque fois. Dans ce cas, outre la responsabilité de l'enchaînement des actions translation/acquisition, l'ordinateur doit tenir compte des efforts encaissés par le montage et corriger les autres paramètres de position compte tenu des déformations.

En mode trajectoire le fonctionnement de l'ordinateur est entièrement autonome à partir du moment où il lui est demandé de réaliser la trajectoire. La position d'emport ainsi que les impulsions de départ (poussées axiales, poussées longitudinales) ou les conditions initiales (vitesse et accélération) sont connues ; la suite de la trajectoire est déterminée pas à pas par l'ordinateur qui tient compte de la position actuelle, des efforts encaissés par l'engin, des équations de la mécanique du vol et des déformations du montage pour déterminer la position complète de l'engin au point suivant, deux points étant conventionnellement séparés par un intervalle de temps constant.

La trajectoire est explorée complètement par l'ordinateur qui enchaîne automatiquement les calculs de positions, les ordres d'asservissement, l'acquisition des mesures, l'affichage des paramètres de position, le stockage et le transfert des mesures vers l'ordinateur central et qui en fin de trajectoire se prépare à exécuter la trajectoire suivante compte tenu des nouvelles consignes de départ.

6.6. Essai de qualification.

L'essai de qualification du dispositif et des opérations associées aura lieu dans la soufflerie S2MA de l'ONERA dans le courant du dernier trimestre 1976.

7 - CONCLUSION.

Depuis la réalisation en 1973 du premier dispositif automatique de conduite d'une rafale par un ordinateur, le rôle dévolu à l'ordinateur n'a cessé d'augmenter.

La réalisation d'un essai, la mise en service d'un nouveau poste d'essai ou la rénovation d'un autre poste ne se conçoit plus sans l'aide d'un ordinateur dont la souplesse d'adaptation et d'emploi est un facteur déterminant.

Actuellement, au seul Centre de Modane de l'ONERA, et en sus des dispositifs qui ont fait l'objet de cette description, plusieurs processus basés sur l'emploi d'un ordinateur sont en cours de réalisation parmi lesquels :

- Une chaîne d'acquisition pour un banc de dynalpie pour lequel le taux d'automatisation sera au moins égal à celui du processus Courant Plan.

- Une chaîne destinée à gérer un dispositif de simulation de décollage et atterrissage court qui équipera prochainement la soufflerie S1MA.

- Une chaîne destinée à la réalisation d'un essai d'entrée d'air en instationnaire pour lequel les cadences d'acquisition et le volume d'informations à stocker nécessitent l'emploi d'un ordinateur et d'un disque associé.

D'autres réalisations de ce genre verront certainement encore le jour dans les années qui viennent à moins, évidemment, d'une révolution dans la technologie des essais ou des matériels.

APPLICATIONS OF THE REAL-TIME DATA ANALYSIS SYSTEM IN THE AMES 40- BY 80-FOOT WIND TUNNEL

Mark W. Kelly,* Stanley O. Dickinson,** and Everett E. Maynard†
Ames Research Center, NASA, Moffett Field, California 94035, U.S.A.

SUMMARY

The first major overhaul and refurbishment of the Ames 40- by 80-Foot Wind Tunnel since it was put into operation in 1944 has recently been completed. A substantial part of this refurbishment was devoted to providing this wind tunnel with a modern real-time data acquisition and analysis system to increase the safety, efficiency, and accuracy of experimental investigations in this facility.

This paper summarizes the background leading to the requirements for the new system, describes the major elements of the system, and discusses some of the applications of the system. The concluding section of the paper discusses the potential of computerized data acquisition systems for wind tunnels in terms of long-term trends in hardware and software costs, and the constraints which must be dealt with to achieve the full potential of computerized data acquisition systems.

1. BACKGROUND

Figure 1 shows some typical test installations in the 40- by 80-foot wind tunnel and is presented to illustrate some of the general test requirements that influenced the design of the new data acquisition system. For tests of conventional aircraft or wind-tunnel models, conventional wind-tunnel data processing ordinarily is sufficient, although the efficiency and quality of the test is, of course, directly related to the timely availability of test results to guide the investigation. However, the need to test experimental VTOL aircraft (such as the XV-5B) with their propulsion systems operating in the wind tunnel, places a severe constraint on the wind-tunnel test time, since the aircraft and propulsion system hardware generally have a limited life, or at least limited time between major overhauls. This means that, to obtain the essential data with a minimum of operating time on the test hardware, the wind-tunnel test must be closely controlled; on-line data analysis is essential to achieve this. In the case of wind-tunnel tests of full-scale experimental rotor systems, the time constraints are generally even more severe because of limited life of the test hardware. In addition, the possibility of encountering catastrophic dynamic instabilities in the rotor system provides unique requirements for on-line data analysis, and is discussed more completely in a later section of this paper.

Figure 2 illustrates the primary data acquisition systems utilized in the 40- by 80-foot wind tunnel prior to the installation of the new system. The mechanical scale system shown on the left is still the heart of the force and moment measuring subsystem in the new system, because more modern devices with a superior combination of accuracy and capacity were unavailable. The multitube manometer board shown at the right of this figure was the primary means of measuring pressures. As summarized on this figure, both the mechanical scales and the manometer boards provided measuring systems that were simple and highly reliable. Also, they were almost fool-proof in use, with malfunctions announced by a mechanical fouling alarm for the scales, and by air bubbles in the manometer tubes or puddles on the floor for the manometer boards. Thus, they were almost ideal systems for the rapid and reliable acquisition of vast quantities of raw data. The sole disadvantage was the exorbitant time required to calculate meaningful engineering parameters from the raw data. For example, to obtain one set of six-component aerodynamic coefficients from the raw force data for one test condition requires 166 arithmetic operations. For pressure distribution investigations, which often require about 500 channels of pressure data, the computational work load was even worse than for the force and moment computations. Thus, the time lag in getting meaningful test data back to the test engineer meant that he was forced to run the test blind. This ordinarily resulted in a matrix approach to the selection of the test conditions, which meant that considerably more data were taken than actually needed to assure that the critical conditions were adequately covered. The number-crunching power of the digital computer was obviously the answer to these problems.

2. DESCRIPTION OF THE NEW DATA ANALYSIS SYSTEM

The overall objectives used in formulating the design requirements for the new data system are summarized on Fig. 3, as follows: (a) to increase test efficiency by providing rapid access to test results in meaningful engineering parameters; (b) to improve test safety by providing highly visible monitoring and/or alarms to identify the proximity of critical test conditions or test limits, and to provide on-line assessment of helicopter rotor dynamic stability; and (c) to reduce the test time for limited-life experimental hardware.

The interpretation of the preceding objectives in terms of the design requirements for the new data acquisition system is summarized on Fig. 4. To aid the test engineer in establishing the desired test conditions, the force and moment measuring subsystem was required to continuously compute and display critical test parameters (such as drag and moment trim). The steady-state pressure and temperature subsystem was required to provide on-line calculation and to display selected channels as needed to conduct the test. The dynamic loads subsystem was required to provide on-line monitoring of numerous channels, including test-limit alarm provisions. The rotor dynamic stability and flutter subsystem was required to provide an

*Chief, Large Scale Aerodynamics Branch.

**Computational Analysis Group Leader, Large Scale Aerodynamics Branch.

†Instrumentation Group Leader, Large Scale Aerodynamics Branch, Ames Directorate, U. S. Army Air Mobility Research and Development Laboratory.

on-line assessment of the damping of critical modes. All subsystems were required to record the appropriate data in convenient form for off-line processing.

The design constraints used to configure the new data acquisition system are summarized on Fig. 5. A major consideration was that the system should be easy to operate so that the test engineer could concentrate on the test results rather than on the operation of the system. This meant that the system must forgive minor setup errors, and that it must communicate meaningful diagnostic information to the user when problems occurred. It must forgive minor mistakes on the part of the operator, and only terminate operation when the integrity of the data is threatened. The other major constraint was that the system should be configured so that failure of any subsystem would not inactivate the entire system, but, rather, would only temporarily degrade the on-line analysis and data turnaround capability of the system.

Figure 6 is a block diagram of the data acquisition system designed around the requirements and constraints just described. As may be observed from this block diagram, the data acquisition system is comprised of several special-purpose subsystems, all of which are interconnected to a master computer. The output of the master computer feeds monitoring information to the operator's console, or to various peripheral equipment which provide plots and tabulation of the data, or storage on digital magnetic tape for off-line processing. Provision is also made for the master computer to communicate with the Ames Research Center's central computer facility. The following paragraphs summarize the overall features of the main elements of the data acquisition system from an operational viewpoint. Additional information regarding the detailed characteristics of this system, as well as those of each of the subsystems, may be found in Ref. 1.

The operator's console is the central control point for conducting a test. When the system is in the monitoring mode, critical test parameters are computed and displayed continuously to assist in directing the test. Also, raw scale data and other information is provided to determine the health and/or state of the various subsystems. When the desired test conditions are met, the console operator presses a "record" button, at which time the master computer switches from the monitoring mode to the record mode and issues appropriate instructions to the various subsystems. When all subsystems have finished their recording cycle, the master computer directs the subsystems to resume the monitoring mode, and notifies the operator's console that the recording cycle has been completed.

The static force subsystem consists of the wind tunnel's original mechanical scale system, which is equipped with optical analog-to-digital converters to transmit data to both the operator's console and the master computer for real-time processing. This subsystem also records raw data on punched cards and paper tape for backup.

The special instruments subsystem provides digitized data to the master computer regarding wind-tunnel operating conditions, (i.e., angle of attack and angle of yaw), propulsion system conditions (i.e., engine or rotor rotational speed and nozzle total pressure) as required to provide on-line calculation of parameters for test monitoring.

The static-pressure subsystem can accept low-level signals on each of 10 channels which are commutated by a 48-position stepping switch. Thus, this subsystem can record a total of 480 channels of steady-state data. This subsystem transmits digital data to the master computer once per record session and records the raw data on punched cards as a backup.

The signal conditioning subsystem is used to condition dynamic signals for acquisition by the analog tape recorder, the time series analyzer, the raw data displays, and/or the master computer. The analog tape recorder is operated continuously as a backup unit on all hazardous tests.

The time series analyzer provides for quick analysis and display of the dynamic characteristics of the test article. It provides the capability to do complex dynamic stability calculations in near real time, so that potentially unstable operating conditions can be identified and avoided. The results of these calculations may be displayed immediately on a cathode ray tube, an X-Y plotter, or a printer.

At this point, it might be noted that many of the subsystems can operate either under the control of the master computer or in a stand-alone mode. This flexibility of operation provides much of the fail gracefully requirement demanded of the system. The manner in which the master computer controls the various subsystems is determined by the system software, which can be arranged to meet the requirements of each test. The system software has three primary modes: setup, record, and monitor. During the setup mode, the software specifies the characteristics of the system, verifies the operation of the system, and verifies that the data received from the various subsystems are within tolerance. Following completion of the system setup, the test is begun, and the system software operates in either the monitor or the record mode, as shown on Fig. 7. In the monitor mode, the software updates the data from the scale system and the special instrumentation system every 1.25 seconds and provides the test engineer with computed engineering parameters on the lamp-bank display. (At the same time, the computer is permitted to process, tabulate, and plot the data obtained in the previous record mode.) When the test engineer is ready to record the next data point, he initiates the record mode of operation. This command brings in the record software and locks out the monitor mode. The record software provides a number of functions, including verification that the required subsystems are on line, checking the calibration of various data channels, writing the data into the computer core (or onto disk or magnetic tape storage), and informing the test engineer when the recording is completed. The record mode software also prints error messages if any of the subsystems fail to perform as anticipated.

Figures 8, 9, and 10 show various components of the data acquisition system as installed in the 40- by 80-foot wind tunnel control room. Figure 8 shows the operator's control console. The lamp-bank displays in the center of the panel are utilized to display final computed data transmitted from the computer. The lamp banks on the right side of the panel are used to display raw scale data to assure the health of the scale subsystem. The two TV monitors directly above the console are used to provide visual monitoring

of the test article. Figure 9 shows the dynamic loads monitoring console. The large cathode ray tube at the upper left of the panel displays eight simultaneous time histories of critical loads and dynamic information. The direct-writing oscillograph at the lower right of the panel records up to 36 channels of dynamic information for both on-line monitoring and as a data backup. The cathode ray tube directly above the oscillograph provides for a bar-chart display of peak-to-peak dynamic loads for easy monitoring of critical stress. This bar-chart display is also equipped with an alarm system to insure that test limits are not inadvertently exceeded. Figure 10 shows the time series analyzer used for performing on-line dynamic stability calculations. On-line displays of system transfer functions, Fourier transforms, etc., are provided on the small cathode ray tube at the center right of the panel. The time series analyzer also provides for hard copy output via the X-Y plotter, shown just above the cathode ray tube, and the typewriter terminal at the lower left of this picture.

As previously stated, a design constraint for the new system was that no single failure would cause a test to be terminated. This requirement has been met in various ways for the various subsystems. An example of the performance of the force data acquisition subsystem with various failures is provided on Fig. 11. When all components of the force data subsystem are operational, the time to obtain final computed data is essentially zero. If the real-time subsystem becomes inoperative, force data can still be computed through the master computer by manually feeding the backup punched cards into the computer with about a 1 minute turnaround. For most purposes, this is essentially on-line. If the Master Computer becomes inoperative, force data can still be computed within 15 minutes to 8 hours after completion of a run, depending upon the priority placed on the information relative to other demands on the Ames Research Center's central computer facilities. If the scale system analog-to-digital converters become inoperative, the data are still not lost, because they are printed on the paper tapes at the scale heads. However, it will now require approximately 8 hours for calculation of six-component force data.. Of course, when the balance itself becomes inoperative, no valid data are obtained, and the run must be terminated.

3. APPLICATIONS

The advantages of real-time data analysis for wind-tunnel tests of conventional aircraft are summarized on Fig. 12. First, real-time data analysis provides maximum information to the test engineer in a timely fashion so that (a) an unexpected result can be checked immediately, and (b) test parameter increments can be adjusted to fit the need. This means that the number of data points required to meet the test objectives is minimized. Another advantage of real-time data analysis is that it provides the ability to assess the adequacy of the data in terms of meaningful statistical parameters. An example of this is discussed later in connection with rotor dynamics testing.

As mentioned previously, in the absence of real-time data, it is often necessary to resort to a matrix approach to insure adequate covering of all the test parameters. This often results in more data being obtained than are actually required to meet the minimum test objectives. An example of this is illustrated on Fig. 13 (from Ref. 2) which shows a plot of rotor lift coefficient as a function of rotor longitudinal force coefficient obtained for a typical helicopter rotor test. The information of primary interest is associated with trimmed 1-G level flight and is indicated by the target at zero $C_{X_{R/\sigma}}$ and a value of $C_{L_{R/\sigma}}$ of about 0.07. In the absence of on-line data, it would be necessary to run collective pitch sweeps for at least three values of angle of attack (in this example, collective pitch sweeps were run at five angles of attack). With real-time data available to the test engineer, it is possible to set directly the left coefficient and longitudinal force coefficient values for 1-G level flight and to then make collective pitch sweeps, angle-of-attack sweeps, and control sweeps, as required to establish the appropriate stability and control derivatives. It is obvious that this will result in considerably less test time. Furthermore, the interpretation of the wind-tunnel test results in terms of the flight vehicle are more direct and are achieved with a minimum of time-consuming cross-plotting of wind-tunnel data.

As mentioned previously, one of the prime requirements for on-line data processing is in connection with the assessment of rotor dynamic stability. The method used prior to the acquisition of the new dynamic analysis system is indicated on Fig. 14. The rotor system under test was excited by means of a shaker vane or rotor cyclic pitch to induce a steady-state excitation at the desired frequency. At the appropriate time, the excitation was turned off, and the decay of the resulting motion was recorded. The instrumentation normally used was a direct-writing oscillograph, and the data reduction was done manually. This method had two general shortcomings. First, the accuracy of the damping assessment was poor, which had serious implications with regard to test safety. Second, the method was extremely time consuming for complex dynamics systems, since it required excitation at the natural frequency of each important mode of the system. An example of the difficulty in obtaining accurate rotor dynamic stability assessments from the transient decay method is illustrated in Fig. 15 (from Ref. 3) which presents the results of experiments made to establish the dynamic stability of an experimental tilt rotor system. As shown here, the accuracy of the stability assessment left much to be desired, particularly when it is recognized that the consequences of negative damping could be catastrophic failure of full-scale test hardware or the loss of a multimillion dollar aircraft. One fundamental factor involved in the poor accuracy illustrated here is that the transient decay method does not provide any mechanism to average out extraneous noise inputs from either wind-tunnel turbulence, extraneous mechanical excitation, or instrumentation noise.

With the new data analysis system, the rotor dynamics tests may be conducted in a steady-state fashion, as illustrated on Fig. 16. The left-hand side of this figure illustrates the procedure for an ideal situation, that is, with no instrumentation errors and no turbulence. The dynamic system, H, is excited by a measured input, w, and the response, x, is measured. The transfer function, H, is determined as the ratio of the Fourier transform of the output divided by the Fourier transform of the input. This calculation and a graphical plot of the transfer function can be displayed in real-time by the time series analyzer. Furthermore, the damping ratio of the critical mode can be determined from the shape of the transfer function, as indicated by the equation at the lower left of this figure; this can also be determined on-line. The time required to obtain the transfer function is minimized if the input signal, w, is broad-band pseudo random (that is, if it has a flat frequency response over the range of frequencies of interest). This avoids the necessity of making time-consuming tests at a number of discrete frequencies of input signal.

The real advantage of the forced-response transfer function analysis for determining rotor damping is more apparent when consideration is given to the presence of noise and turbulence in the input and output signals. This situation is illustrated on the right-hand side of Fig. 16. As shown here, the measured input, z, includes the desired input, w, an unknown input, u (due, for example, to aerodynamic turbulence), and instrumentation noise, v_I. Similarly, the measured output, y, is the sum of the output due to the measured input, w, the output due to the unknown input, u, and the unknown noise, v_O, in the output measurement. In this situation, the transfer function of the system, H_W, is estimated by the ratio of the input-output cross-spectrum, S_{zy}, and the input auto spectrum, S_z, which are, in turn, estimated by taking the ensemble average of the spectra over any desired number of samples. As shown here, the error in the determination of the cross-spectra and the auto-spectra is inversely proportional to the number of averages taken, which is, of course, under the control of the experimenter. Also, the error in the estimate of the transfer function can be assessed by computing the coherence function, $\hat{\gamma}_{zy}$, which establishes the degree to which the measured output, y, was really determined by the measured input, w. All of these calculations can be done essentially on-line with the time series analyzer. A typical on-line display of a transfer function relating in-plane acceleration at the rotor hub to in-plane force is illustrated on Fig. 17. The picture shown is a direct photograph of the display on the cathode ray tube. The responses shown at slightly over 2 and 4 Hz are associated with the coupled response of the rotor test module, the wind-tunnel struts, and the balance platform to horizontal force, and could be of possible concern relative to rotor ground-resonance type instabilities. The response at high frequencies is not of concern in rotor stability assessments but, of course, could be important relative to various rotor vibratory modes.

Additional information relative to the on-line assessment of rotor dynamic stability from analysis of the system transfer function, and the use of broad-band pseudo-random excitation of the system to obtain the transfer function, may be found in Ref. 4. A discussion of the effects of noise on the accuracy of the system transfer function and damping ratio obtained by the use of various experimental techniques and analysis methods may be found in Ref. 5.

The power of the computerized data analysis system in interpreting dynamic loads information is illustrated on Figs. 18 through 21. For comparison purposes, Fig. 18 shows the raw data from a helicopter rotor test as recorded by a direct-writing oscillograph. The difficulty in reading these traces, let alone making meaningful interpretations of their meaning, is obvious. As shown on Fig. 19, the computer makes it possible to single out any one of these traces, and to display it in time history form. More importantly, as shown on Fig. 20, it is possible to perform a Fast Fourier Transform on this time history and to display the predominant harmonics in the signal so that some assessment of the source of loads can be made.

An example of the usefulness of this kind of information was provided during full-scale wind-tunnel tests of the Controllable Twist Rotor. During these tests, it was noted that the rotor behaved in a progressively more erratic fashion as the wind-tunnel test speed was increased, showing some similarity to a rotor out-of-track condition. However, the rotor was checked for track and tracked well at hover and low speeds. Figure 21 shows the ratios of the flap-wise bending moments on one blade divided by the corresponding flap-wise bending moments on another blade, and R_1, R_2, R_3, and R_4 correspond to the first, second, third, and fourth harmonics of these bending moments, respectively. As indicated by the R_1 values, the rotor was in reasonably good track relative to once-per-rev flap-wise bending loads. However, as indicated by the R_2, R_3, and R_4 values, there were significant differences in the higher harmonic dynamic response of the two blades. Moreover, the accuracy of these measurements, as indicated by the root-mean-square variation around the average value of the various harmonics, shows that the dynamic mismatch indicated is really there, and is not due to inaccuracies in the measurement. From these measurements, it was concluded that the basic problem was a dynamic mismatch of the blades, which resulted in dissimilar bending response in the higher harmonic modes.

4. TRENDS, CONSTRAINTS, AND FUTURE POTENTIAL

As illustrated by the preceding examples of applications of computer to wind-tunnel testing, the availability of moderately-priced small computers and special-purpose digital processing equipment provides a high potential for improving the efficiency, quality, and safety of wind-tunnel testing. However, as with all new developments, a number of constraints and problems must be recognized and dealt with in order to realize the full potential of computerized data acquisition systems. The following paragraphs discuss some recent trends in the performance and costs of data analysis systems, and the overall impact of these trends on wind-tunnel testing.

The performance and cost trends of data analysis system hardware are summarized on Fig. 22 (from Ref. 6). As shown on the left-hand plot of this figure, the ratio of the cost of computer hardware to computing power (as indicated by the number of channels per second which can be processed) has decreased dramatically over the last 15 years. As a result, Ames Research Center has invested, and is continuing to invest a considerable amount in this hardware, as illustrated in the central plot on this figure. In addition, as shown on the right-hand plot of this figure, maintenance costs of this equipment represent an additional significant investment. While not shown here, the project costs occasioned by malfunctioning data systems during major experimental investigations can be considerable, and represent a hidden "maintenance cost" over and above that shown here. The conclusion to be drawn from this is that considerably more attention must be paid to reliability and maintainability of data system hardware if the full potential of this equipment is to be realized.

Another factor which constrains the realization of the full potential of computerized data analysis systems is the cost of software. Figure 23 (from Ref. 6) summarizes two points relative to software and programming costs. First, as illustrated on the left side of this figure, the cost of software and programming relative to system hardware costs has been steadily increasing over the last 20 years. Second, as illustrated on the right-hand side of this figure, the cost of programming is related to the degree to which the central processing unit and memory are utilized. As the utilization of memory increases over about 70 percent capacity, the cost of programming begins to show an exponential increase. A major difficulty here is that many of the software and programming costs are difficult to assess until the system is put into operation, while the hardware costs are accurately identified with system capacity at the outset

of the procurement cycle. Thus, there are strong pressures to make an initial hardware selection which places undue emphasis on hardware costs, with the result that inadequate memory and CPU capability are provided, and excessive software and programming costs are ultimately encountered. Distributed computer systems such as described herein, and provisions for memory addition, are both means for dealing with this problem. Additional aspects of distributed computer data acquisition and analysis systems are discussed in Ref. 6.

One aspect of data system programming which provides a favorable spinoff is the discipline that the programming effort places on the planning of a wind-tunnel test; this is illustrated on Fig. 24. The left-hand side of this figure illustrates the data reduction and analyses tasks as a function of time-to-complete the overall investigation for the situation which prevailed prior to the availability of computerized data analysis equipment. The pretest tasks consisted primarily of preparation of the basic data reduction programs and the necessary calibrations and measurements. Since much of the data could not be reduced while the tests were underway, a matrix test plan was prepared, and many judgmental tasks were postponed until after the test. However, with a computerized data system, where a substantial amount of computed results are to be presented on-line, a number of pretest judgments have to be made, as illustrated on the right of Fig. 24. For example, a judgment has to be made relative to which results must be presented on-line, and which are to be recorded for later analyses. Further, for the data which are to be presented on-line, detailed instructions as to desired output format, range and scale, etc., must be made. In the process of selecting these priorities and making these judgments, the researcher is forced to answer some very basic questions concerning the purpose of the test, such as the relative importance of multiple test objectives, anticipated level of the results, etc. The reward for proper pretest planning is that abundant on-line information is provided during the test, which can be used by the experimenter to guide and enhance the value of the test. The penalties for inadequate test planning are severe, in that the data analysis system will either be programmed to answer the wrong question, or, in extreme cases, will not provide intelligible output in a timely manner, and, thus, may become essentially useless. These rewards and punishments provide considerable incentive for thorough test planning, and this will do much to increase the efficiency and safety of experimental investigations conducted in wind tunnels.

5. CONCLUDING REMARKS

Technical progress in the field of small computers and digital processors have provided the capability of configuring powerful and flexible data analysis systems for wind tunnels. Experience with such a system installed in the Ames 40- by 80-Foot Wind Tunnel shows that these systems can substantially improve the quality and safety of the experiment by providing the researcher with timely information presented in meaningful scientific terms.

The major constraints preventing full realization of the potential of digital data analysis systems are inadequate hardware reliability and the high cost of programming and software. While there has been progress in the alleviation of these problems, more attention to these factors is required.

The programming effort required to prepare for a complex experimental investigation utilizing on-line digital data analysis systems provides high incentives for thorough test planning and severe penalties for inadequate planning. The discipline thus enforced on the experimenter is responsible for a significant share of the increased efficiency and safety of test operations realized through the use of modern data analysis systems.

In general, it may be concluded that the wind-tunnel capability of producing large quantities of data, and the digital computer capability of processing vast amounts of information, coupled with the increasing complexity of modern aircraft, will provide a long-term need for further progress in the harnessing of digital data analysis systems to the needs of experimental investigations in wind tunnels.

6. REFERENCES

1. Cambra, Joseph M., and Tolari, Geno P.: "Real Time Computer Data System for the 40- by 80-Foot Wind-Tunnel Facility at Ames Research Center," 1975, NASA TN D-7970.

2. McCloud, John L. III, and Biggers, James C.: "An Investigation of Full-Scale Helicopter Rotors at High Advance Ratios and Advancing Tip Mach Numbers," 1968, NASA TN D-4632.

3. Johnson, Wayne: "Analytical Modeling Requirements for Tilting Proprotor Aircraft Dynamics," 1975, NASA TN D-8013.

4. Johnson, Wayne, and Biggers, James C.: "Shake Test of Rotor Test Apparatus in the 40- by 80-Foot Wind Tunnel," 1975, NASA TM X-62,418.

5. Johnson, Wayne: "A Discussion of Dynamic Stability Measurement Techniques," 1975, NASA TM X-73,081.

6. Cambra, Joseph M., and Trover, William F.: "The Revolution in Data Gathering Systems," 1975, NASA TM X-62,452.

SPACE SHUTTLE MODEL

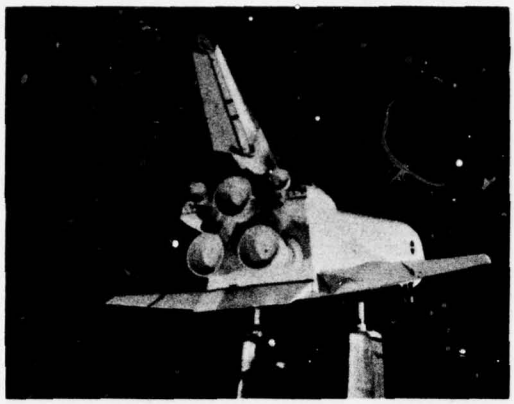

F-14 MODEL

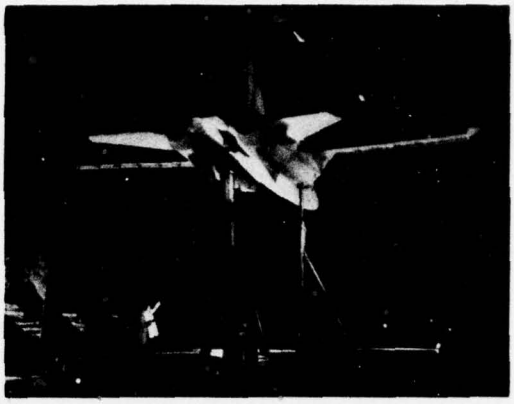

XV-5B VTOL AIRPLANE

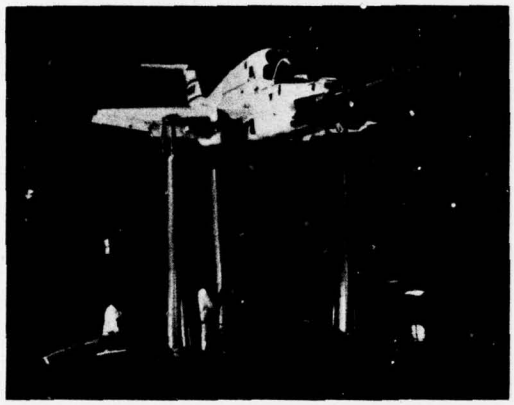

CONTROLLABLE TWIST ROTOR

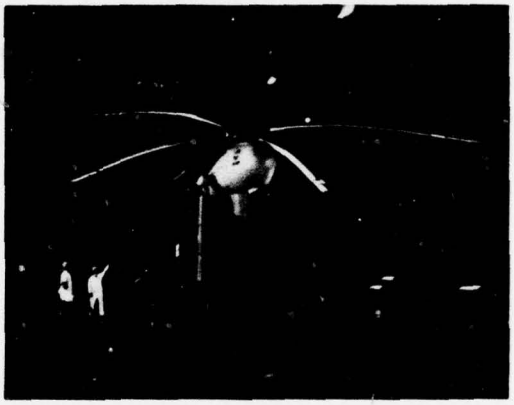

Fig. 1 Typical tests in the Ames 40- by 80-Foot Wind Tunnel.

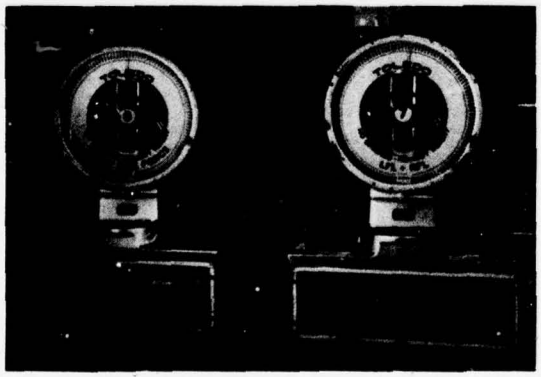

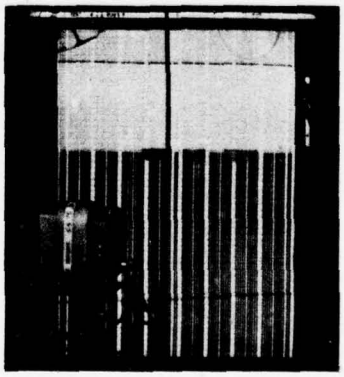

ADVANTAGES:

- SIMPLICITY, HIGH RELIABILITY
- PRIMARY STANDARD, NO CALIBRATION REQUIREMENTS
- RAPID ACQUISITION OF RAW DATA

DISADVANTAGE

- EXCESSIVE TIME REQUIRED TO CONVERT RAW DATA TO MEANINGFUL ENGINEERING FORM

Fig. 2 Original primary data acquisition systems.

- INCREASE TEST EFFICIENCY
- IMPROVE TEST SAFETY
  - MONITORING AND ALARMS
  - ON-LINE ROTOR DYNAMIC STABILITY ANALYSIS
- REDUCE TEST TIME FOR LIMITED-LIFE HARDWARE

Fig. 3 Objectives of conversion to the real-time data acquisition system.

SUBSYSTEM	MONITORING	RECORDING
FORCE AND MOMENT	DISPLAY IN ENGINEERING TERMS	RECORD IN DIGITAL FORM
PRESSURE, TEMPERATURE	DISPLAY OF SELECTED CHANNELS IN ENGINEERING TERMS	" "
DYNAMIC LOADS	DISPLAY CRITICAL CHANNELS, ALARMS FOR TEST LIMITS	" "
ROTOR DYNAMIC STABILITY	DISPLAY DAMPING AND FREQUENCY	" "

Fig. 4 Design requirements for the real-time data system.

OPERATING CHARACTERISTICS

- MUST OPERATE IN SPITE OF MINOR SETUP ERRORS
- MUST COMMUNICATE MEANINGFUL DIAGNOSTICS
- MUST FORGIVE OPERATOR'S MISTAKES

FAILURE MODES

- DEGRADE ON-LINE PERFORMANCE
- DEGRADE DATA TURN AROUND

Fig. 5 Design constraints for the real-time data acquisition system.

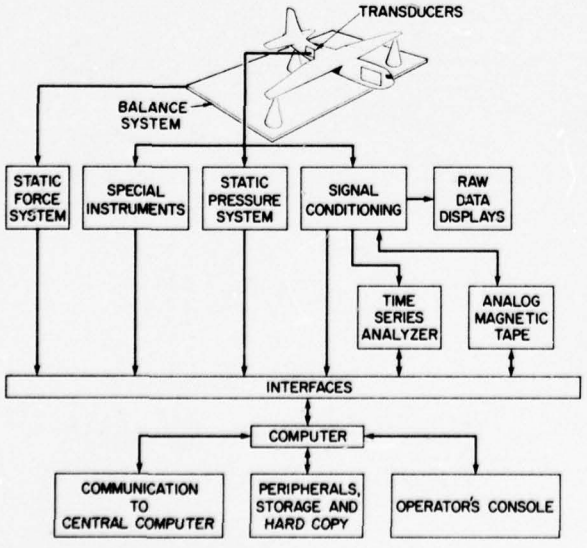

Fig. 6 System block diagram.

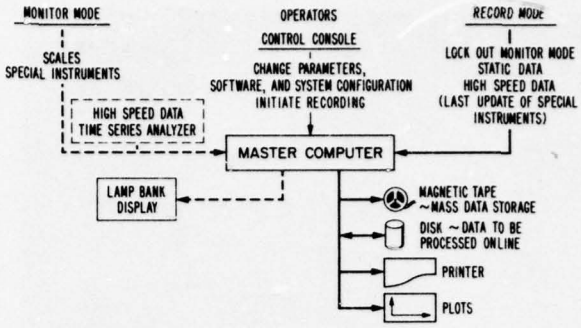

Fig. 7 On-line modes of operation.

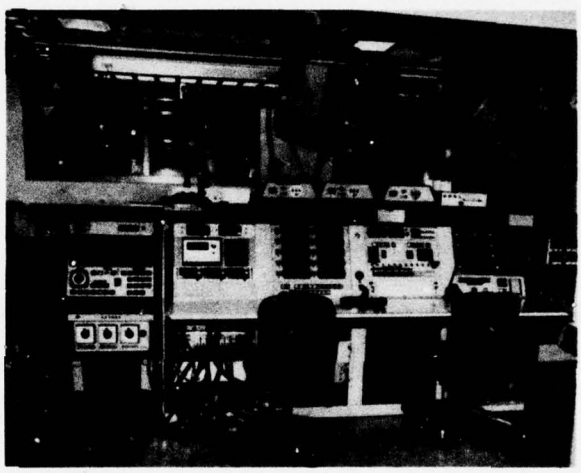

Fig. 8 Operator's control console.

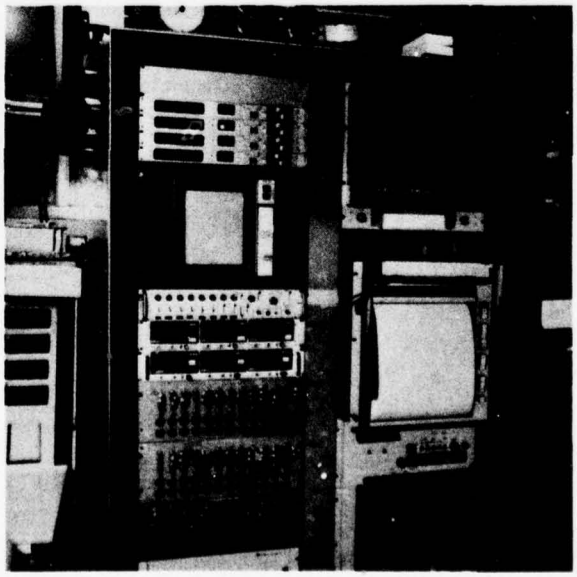

Fig. 9 Dynamic loads monitoring console.

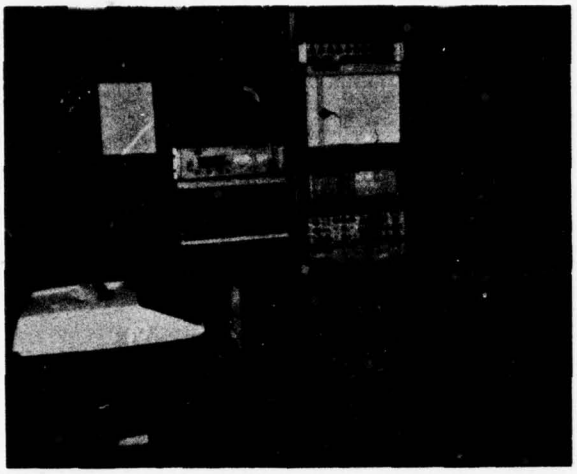

Fig. 10 Time series analyzer for dynamics analysis.

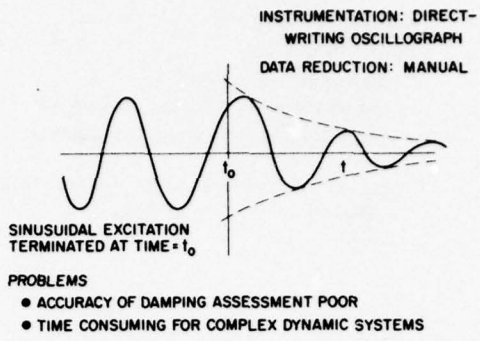

Fig. 14 Old method used for rotor dynamic stability measurement.

SYSTEM CONDITION	TIME TO OBTAIN FINAL DATA
ALL SYSTEMS OPERATIONAL	ON-LINE
REAL-TIME SUBSYSTEM INOPERATIVE	I minute BY MANUALLY FEEDING COMPUTER
MASTER COMPUTER INOPERATIVE	15 minutes TO 8 hours AFTER COMPLETION OF RUN, ON CENTER'S COMPUTER
SCALE SYSTEM ADC INOPERATIVE	8 hours FOR 6 COMPONENT DATA
BALANCE INOPERATIVE	NO VALID DATA

Fig. 11 Performance of force data acquisition system with various subsystem failures.

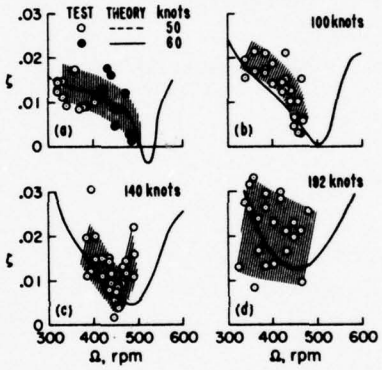

Fig. 15 Example of rotor dynamic stability assessment obtained from transient decay.

MAXIMUM INFORMATION PROVIDED TO TEST ENGINEER
- UNEXPECTED RESULTS CAN BE CHECKED IMMEDIATELY
- TEST PARAMETER INCREMENTS CAN BE ADJUSTED TO FIT THE NEED
- NUMBER OF DATA POINTS REQUIRED IS MINIMIZED

PROVIDES DATA ASSESSMENT IN STATISTICAL TERMS

Fig. 12 Advantages of real-time data analysis for wind-tunnel tests of conventional aircraft.

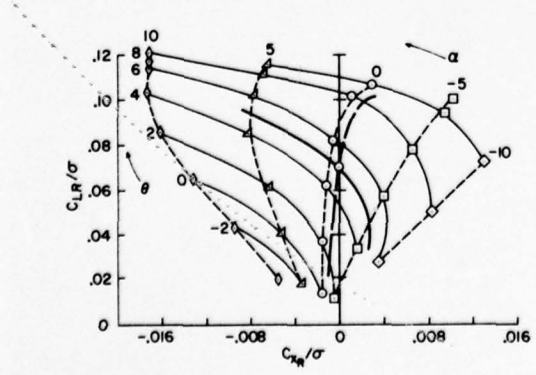

Fig. 13 Comparison of 1-g flight to matrix approach to wind-tunnel testing.

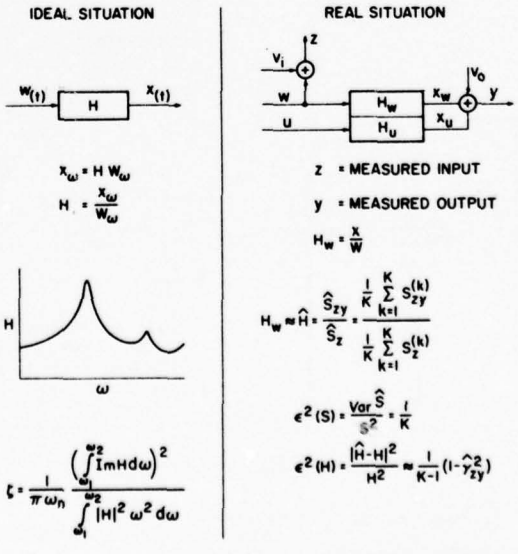

Fig. 16 Transfer function analysis for rotor damping.

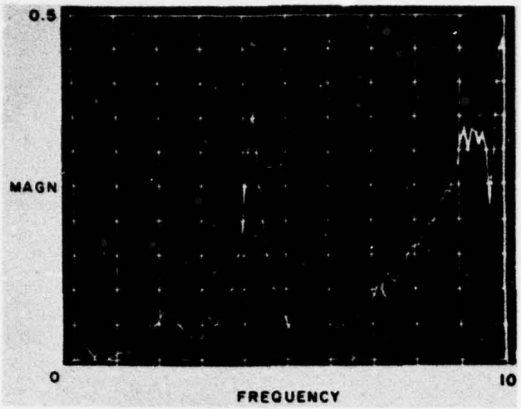

Fig. 17 Typical on-line display of transfer function.

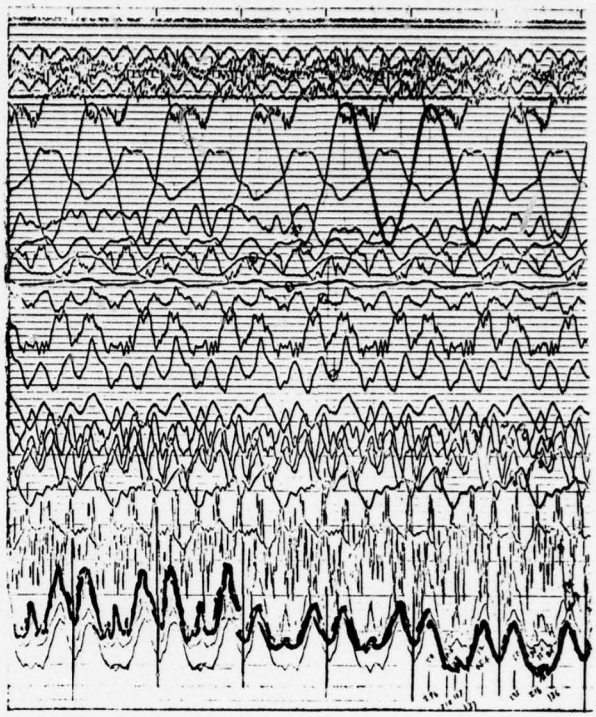

Fig. 18 Typical oscillograph record from helicopter test.

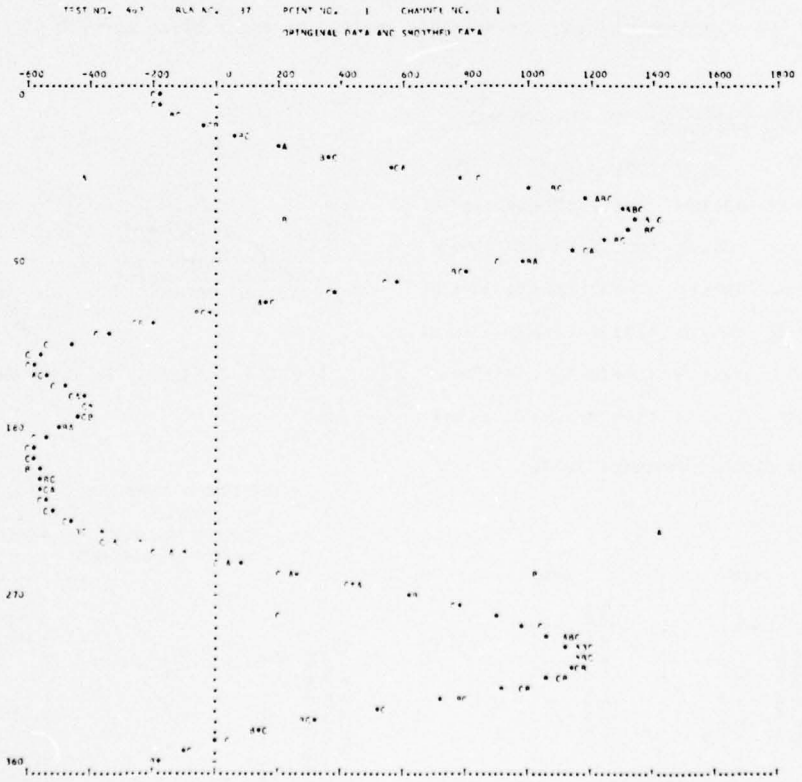

Fig. 19 Computer printout of rotor blade torsion time history.

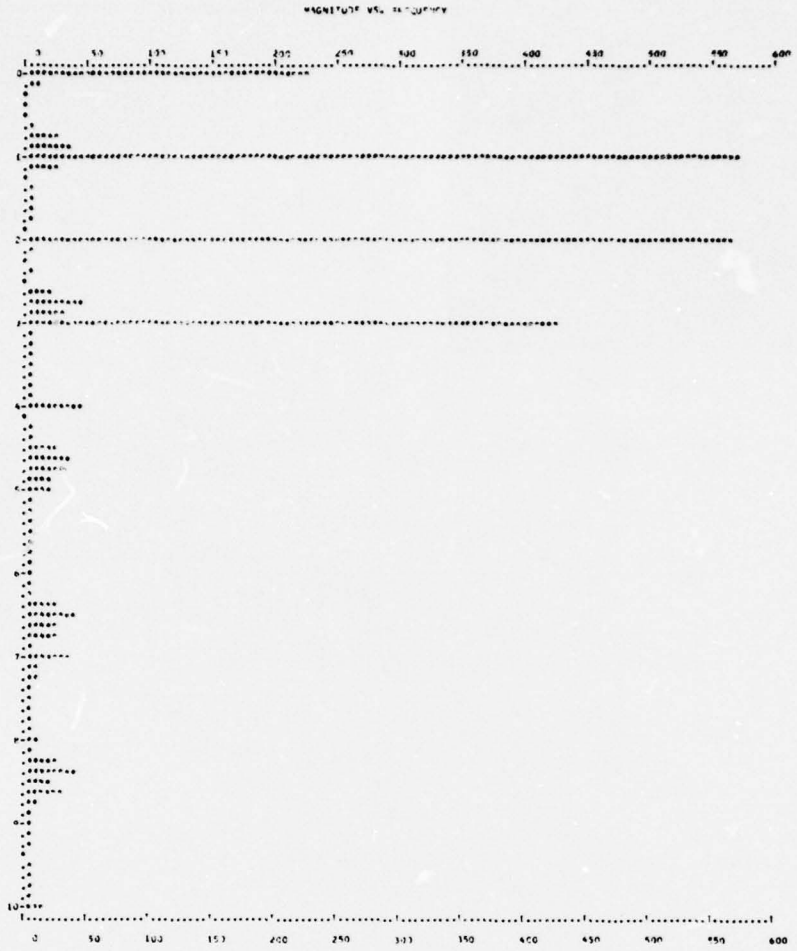

Fig. 20 Computer printout of harmonic content of rotor blade torsion signal.

$R = \frac{\text{FLAPWISE BENDING, YELLOW BLADE}}{\text{FLAPWISE BENDING, RED BLADE}}$ FOR EACH HARMONIC

CONFIG	V, knots	α_s	θ_0	R1	R2	R3	R4
BLADE	120	-5°	8°-15°	0.98±.04	1.26±.18	1.20±.06	1.14±.27
BLADE	120	-8°	10°-16°	1.03±.01	1.12 ±.16	1.10 ±.15	0.96±.13
BLADE	135	-5°	8°-14°	0.99±.04	1.17 ±.15	1.33 ±.20	1.32±.30
BLADE	135	-8°	10°-15°	1.01 ±.10	1.25±.15	1.27±.10	1.08±.09
CTR	135	-8°	10°	0.98±.04	1.29±.08	1.11 ±.08	1.38±.13
CTR	135	-8°	12°	1.02±.04	1.30±.08	1.12 ±.06	1.43±.16

Fig. 21 Blade dynamic response ratios.

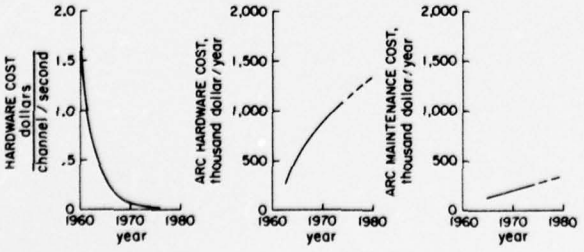

Fig. 22 Data system performance and cost trends.

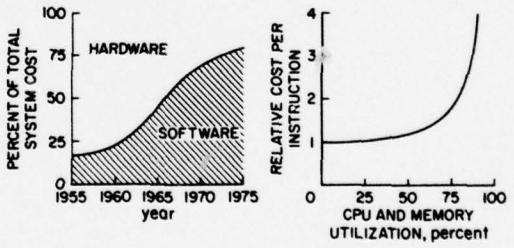

Fig. 23 Software and programming costs.

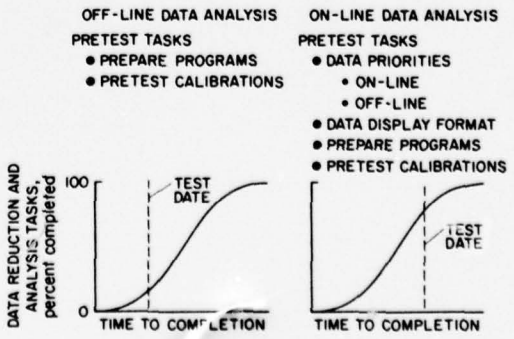

Fig. 24 Impact of real-time data analysis system on test planning.

THE USE OF COMPUTERS IN ROTARY WING TESTING

William G. S. Hardy, Supervisor of Model Testing Group
Edward J. Pyne, Supervisor of Model Instrumentation

Boeing Vertol Company
P.O. Box 16858
Philadelphia, Pa. 19142

SUMMARY

Advancements in wind tunnel testing of rotary wing aircraft have been paced by the ability to build dynamically similar, Mach scaled models. Within the past few years, materials and design technology have advanced to the point where such models are now technically possible to design and are economically feasible to fabricate. With this development, there was an accompanying growth in test techniques and data acquisition and processing methods. The computer requirements for testing rotary wing aircraft models are discussed and a general purpose processing system is described. Some considerations for data acquisition and presentation are presented. The types of analyses required for rotary wing models are covered in some detail. Both real time and off-line analysis methods are reviewed.

1.0 INTRODUCTION

Until recently, advancements in testing rotary wing aircraft models were not as rapid as those made in fixed wing aircraft testing. Model design, the economics of fabrication, the reliability of the instrumentation, and not having the type of instrumentation required to investigate phenomena, all contributed to the slow growth of this field. This has all changed. With the availability of advanced composite materials, "mini" bearings, improved strain gage technology, and high speed, noise free slip-rings, it is now possible to manufacture dynamically similar, Mach scaled models at a reasonable price. Rotary wing testing has come of age. This was demonstrated dramatically by the Boeing UTTAS Program which had over 5000 hours of wind tunnel testing associated with its design and development. We are now in an era where no major rotor craft will be built without extensive wind tunnel testing. Recognizing this has forced re-evaluation of data acquisition and processing methods. We no longer can rely on punch card, paper and magnetic tape, and oscillographs as our data record. Hand reduction of data is too time consuming to keep up with volume of data produced by our models nor the demand for rapid turnaround of data. In addition, as testing methods have grown in sophistication, the data analysis has become more complex requiring computerization.

In the sections which follow, we will describe one computer system developed for rotary wing testing. We will discuss its design criteria, how it functions, and some of the analysis methods used. But before we get into the details of the computer system, we need to take a brief look at rotary wing models and how they are tested. In doing so, we can gain an understanding of some of the unique problems which arise.

2.0 ROTARY WING MODELS

There are two approaches to designing rotary wing models as described in Reference 2, Mach scaling and Froude scaling. In Mach scaling, the model is operated at full scale tip speed, advance ratio, and disc loading. The blades are designed so that they are dynamically scaled in the first five elastic modes. The blades, hub, and fuselage are geometrically faithful to full scale. Mach scaled models are designed to measure aircraft and rotor performance, rotor blade loads, rotor downwash, blade and fuselage interactions, rotor downwash loads, and to understand rotary wing aerodynamics. Such models are highly-powered and usually operate in a high load environment.

In Froude scaling, the model is designed to investigate aeroelastic stability and flying qualities. The model is designed in much the same way as airplane flutter models are. Deflections due to gravity are geometrically scaled thus achieving scaled inertia and weight. This approach allows the model to be operated at reduced tip speeds and therefore at reduced stress and power requirements.

In both approaches, the model is usually designed to incorporate as many remotely operated control surfaces as possible eliminating the need for frequent model changes and allowing the model operator to "fly" the model through high load operating conditions. Figure 1 shows a Froude scale model recently tested in Boeing's V/STOL Wind Tunnel. Many of the remote features are pointed out: collective pitch, lateral and longitudinal cyclic, and pedestal pitch. Mach scaled models usually include at least one six-component, internal, strain gage balance and have been built to include up to five.

Model instrumentation usually consists of the model control surface positions, the strain gage balance signals, a 60 per rev pulse for the rotor RPM, and a 1 per rev pulse as a rotor blade position reference. All rotating system signals are transferred to the fixed system by means of slip rings. The blades are minimally strain gaged for safety of flight. Usually, however, they are instrumented with strain gage bridges to measure the blade loads and mode shapes. We have recently tested blades having hot film anemometers at five radial stations. Reference 4 describes testing of blades with pressure transducers buried in them to measure chordwise pressure distributions in forward flight, and with skin friction gages to measure skin friction distributions.

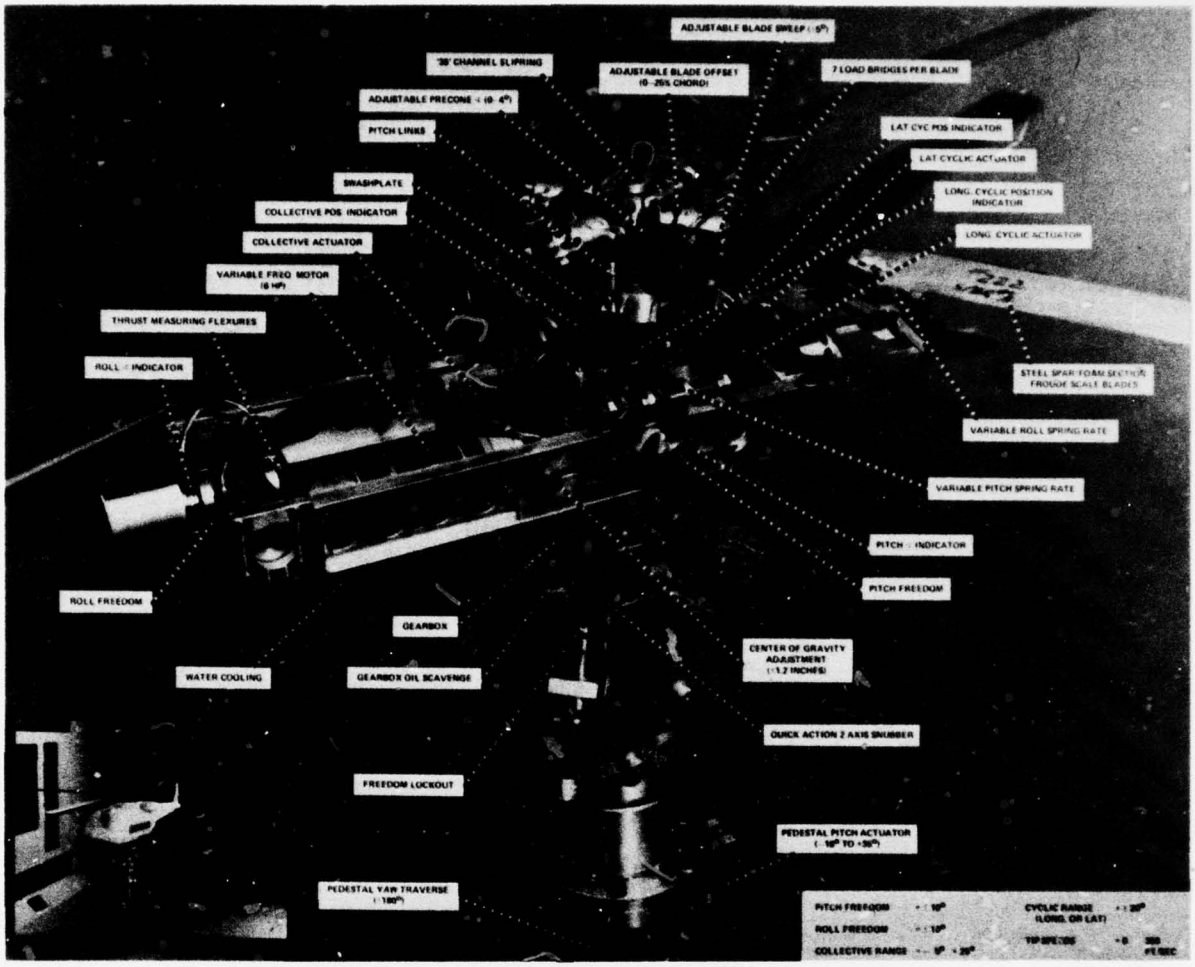

FIGURE 1. A PITCH/ROLL FREEDOM FROUDE SCALED HELICOPTER MODEL

Both types of models are required to operate in a high strain environment under high fatigue conditions. Therefore, strain gages, wire packs, and solder joints are subjected to constant flexing and require periodic repair and maintenance. Although we have made great progress in improving the mean time between failure, we are still too often shut down to repair the blade instrumentation.

3.0 TESTING ROTARY WING MODELS

The general approach to rotary wing testing is quite similar to other types of wind tunnel testing. Objectives are established, the data required is defined, and the experiment is carried out. The data is then analyzed and interpreted. The traditional practice in wind tunnel testing, however, is to acquire a matrix of test data from which we can derive data about specific design conditions. A set of parameters to be investigated is defined. These parameters are systematically varied until data from all of the conditions has been acquired. In testing rotor models, the high operating loads on the models and the survivability of the instrumentation become a factor in planning the test. There is no guarantee against a failure of one component or another. In this environment, it becomes imperative to obtain the important design related data first and then return to fill out the off design conditions. This approach has the added advantage of providing key data at a very early stage in the test. This does not suggest that matrix type testing is not useful. In some cases it is a necessary practice to develop enough data to approach the experiment selectively. In most cases, however, we have found acquiring the prime data first is more productive.

4.0 COMPUTER REQUIREMENTS

Computers serve several functions in rotary wing testing:

1. Monitoring test conditions.
2. Data acquisition.
3. Data analysis.
4. General processing for predictions.

Any computer system should provide these services, but it is not necessary for them to be provided by a single processor. The functions can be and often are shared by several

machines. Information to monitor test conditions is usually provided by a combination of special purpose, hardwired analog and digital devices and a general purpose, programmable computer. Data acquisition can be done in analog form and converted to machine readable form later, or it can be converted to machine readable form directly. Data analysis can be done on any general purpose processor. Prediction programs are usually located on large, central, batch processing machines.

In planning a computer system for rotary wing testing, a manager inevitably must choose between using a shared, multi-purpose, central computing system for data acquisition and analysis or making an investment in acquiring a processor which is dedicated to the tunnel facility. A shared system offers the advantage of distributing the computer's cost between several facilities, of maximizing the use of the computer's time, and of having a computer which is large in size and has great computing power. The disadvantage of a shared system is that it usually operates on either a priority system or a schedule system. The availability of the computer is not guaranteed. Priorities are a management decision based on apparent costs, or the program's importance, or political reasons. Scheduling assumes that the test's progress can be predicted ahead of time. This is not always the case. A dedicated system offers the advantage of instant access to the computer for data acquisition and analysis. The dedicated system can also be modified to do special functions. A dedicated system has immediate access to the data and can therefore operate in real time. For this reason, it is best suited for rotary wing testing.

A second decision that must be made in the planning stage is whether to attempt to do all of the processing in real time or whether to have a balance between real time and off-line processing. At the Boeing V/STOL Wind Tunnel (BVWT), the initial course was toward total real time processing. We have found, in our experience, that this is not the best approach. Errors in input require reprocessing the data, additional analysis is always requested, and, as the number of analysis methods grow, the presentation of all of the data simultaneously becomes unmanageable. Our approach now is to provide a standard set of analysis programs which operate both in real time and in batch processing mode and make the use of these programs selectible in real time by inputs to the computer. In this way, the analysis required for on-line evaluation of the results can be done without saturating the computer's ability to keep pace with the acquisition of data. At the same time batch work can be processed providing additional or more detailed data analysis.

5.0 GENERAL FEATURES OF THE BOEING V/STOL WIND TUNNEL'S COMPUTING SYSTEM

We have looked briefly at rotary wing models and discussed their limitations. We have seen how these limitations affect the testing process and have set the requirements for the computing system supporting the test. Now we will look at the computer system at the Boeing V/STOL Wind Tunnel (BVWT). This system was developed to support rotor testing. Although it is not the ideal system, it meets all of the major requirements described above that are needed to support rotor testing.

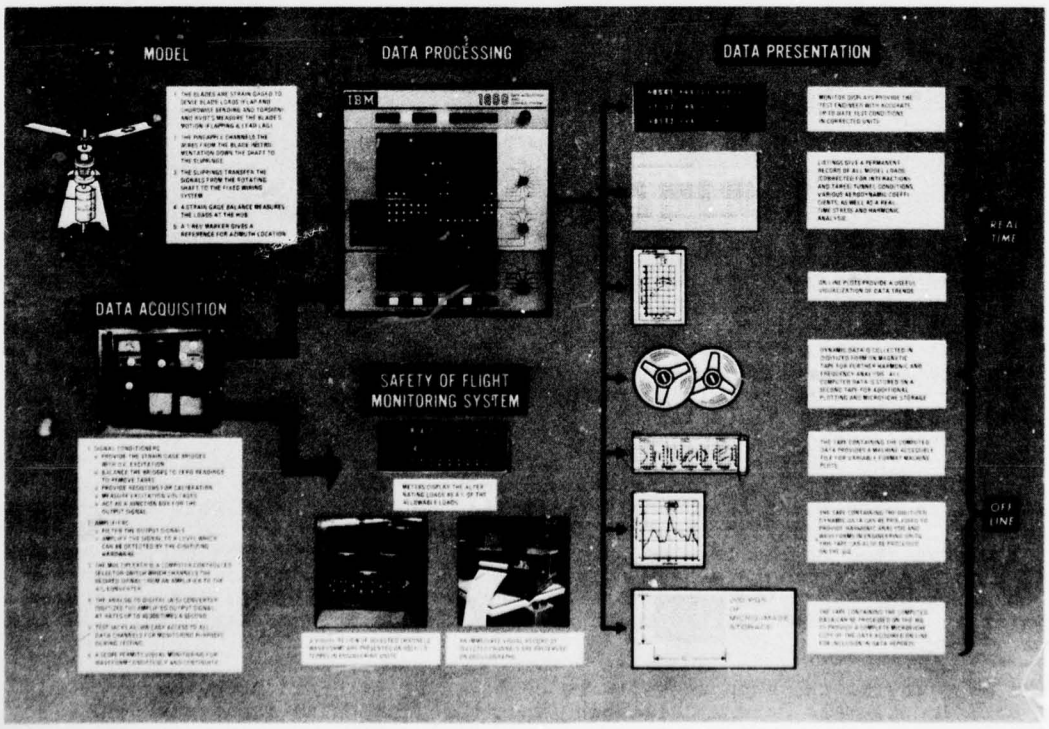

FIGURE 2. THE BOEING V/STOL WIND TUNNEL'S DATA MANAGEMENT SYSTEM

A general arrangement of the system and its functions is shown in Figure 2. The system was designed around an IBM 1800 Computer. The signals from the model are accessed by the computer after passing through signal conditioners, filters, and amplifiers. Up to 128 individual signals or channels of information are fed into two analog-to-digital converters (ADC). The computer's central processing unit (CPU) is structured to serve the four functions discussed earlier: test monitoring, data acquisition, data analysis, and test predictions. This is shown schematically in Figure 3. These functions could be done equally well by three machines operating separately but interfaced with each other. Our decision to partition one larger machine rather than have separate processors was based primarily on cost. It was cheaper to expand our core-size than it was to purchase a new system and interface it with the one we had. The one disadvantage of this machine is that the core cycle time is 2.25 μsec which is slow compared to those available in newer machines. Our real time analysis capability thus becomes saturated rather rapidly.

The data and the results of the analysis programs can be presented in a number of formats. All data can be listed in tabular form. The test's conditions are displayed on a series of nine light displays which are updated continuously by the computer. Six X-Y, flat bed plotters give a real time display of computed parameters. All data is temporarily stored on discs and permanently stored on magnetic tape. The discs provide a rapid random access to the data, letting it be recalled on demand for comparison with later runs. Off-line analysis usually accesses the data stored on the digital magnetic tapes and the results are plotted on a separate plotter which is interfaced with the computer by magnetic tape. The majority of our data output is in plotted form.

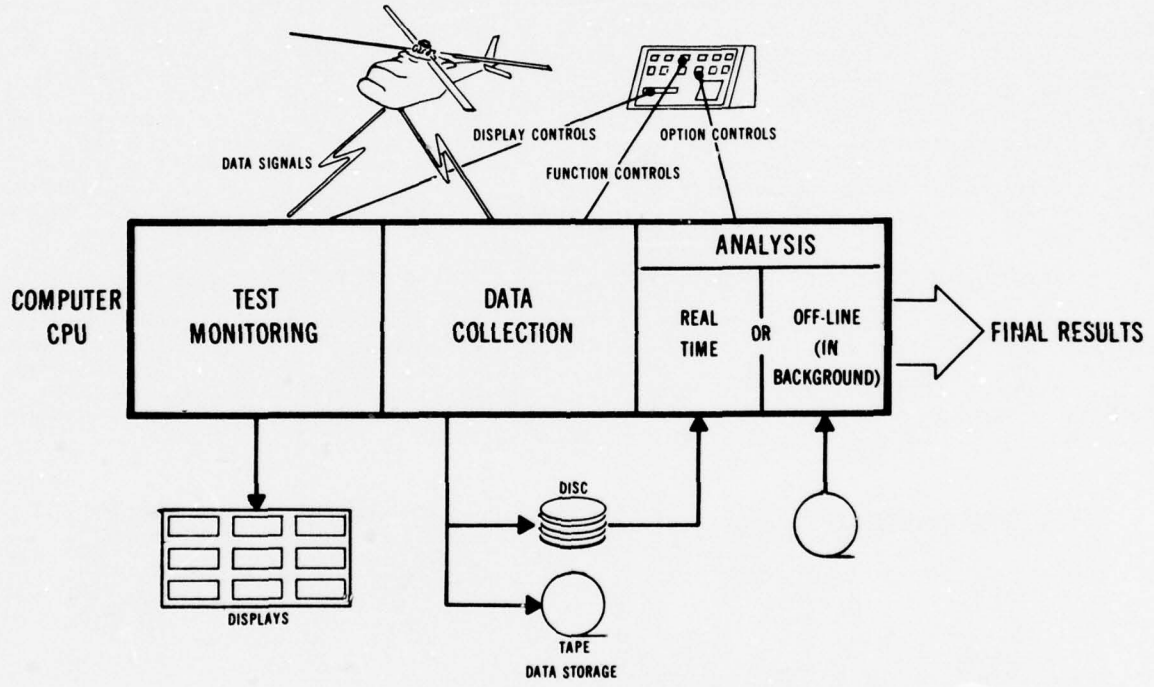

FIGURE 3. THE COMPUTER'S CPU ARRANGEMENT

The computer's functions are a prioritized set of programs. The highest priority to the computer is the acquisition of test data. The second is the monitoring of conditions. Third is real time analysis and last is off-line or batch analysis. The machine is structured so that there is usually very little conflict between functions. The three areas of core, although not totally separate, operate independently. The only exception to this is that information is not provided to the monitor light displays during periods of data acquisition. The reason for this is that the data acquisition programs have priority on accessing the ADC's. Since data acquisition lasts only a few seconds, the test conduct is not compromised. The data analysis area is almost totally partitioned from the other areas. Analysis is being done at all times while the test is being run. The real time analysis programs operate on the data in the order that it is acquired. It is possible for the analysis to lag the testing when data is being acquired at a high rate or the analysis required is exceptionally lengthy. In these cases, the results are presented to the test engineer several minutes after the data is taken. If the real time analysis programs have no data to process, the computer will automatically switch to batch mode analysis programs. As more data is available, the batch work will be temporarily interrupted so that the analysis area can be used again for real time programs.

The majority of the support software consists of standard programs controlled by punched card input. All data acquisition functions (including input changes) are initiated by a button on the data acquisition console, Figure 4. The functions are performed in the order the buttons are pushed. A set of option switches is located below

the function buttons. These switches control the processing and data presentation as well as provide a means for trouble shooting. Intermediate printouts can be turned on and off at will. Plotting can be suspended to service the plotters. The parameters displayed to monitor the test conditions can be changed. These features give us a lot of versatility.

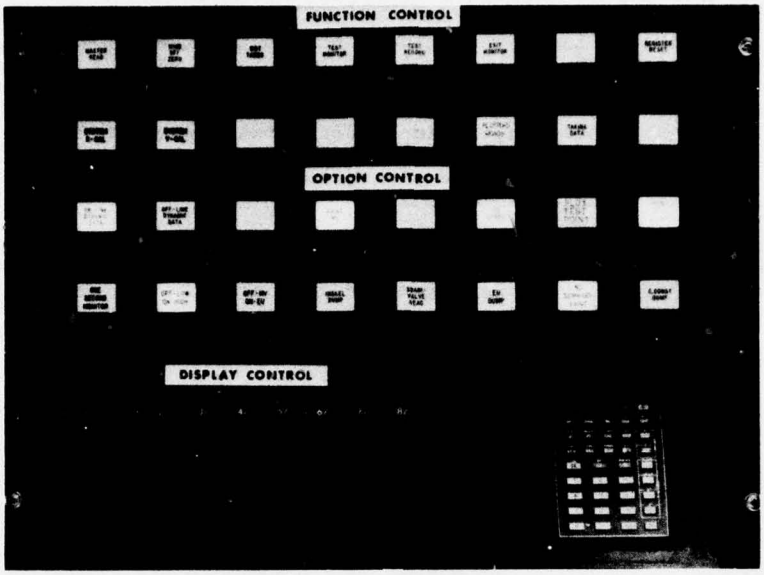

FIGURE 4. THE DATA ACQUISITION CONSOLE

6.0 MONITORING TEST CONDITIONS

While conducting a typical rotor experiment, two questions are constantly in the mind of the responsible engineer.

1. Are the tunnel and model at the conditions that are required to take data?

2. Is it safe to proceed to the next condition without endangering the model or any of the support equipment?

If these two questions cannot be answered affirmatively, the test should stop. To provide information to the engineer, we use both the digital 1800 Computer and some special purpose, hardwired devices which take the analog signals from the model as inputs.

6.1 Monitoring Using Digital Signals

It was pointed out in earlier discussions that rotary wing testing has departed from a matrix type approach to testing. Data acquisition is done selectively to obtain the data that is required in the least amount of time. To do this the test manager must know the conditions at which the model is operating and how the model responds to control inputs. This data is provided by the computer. The computer is set up so that it is in a continuous cycle of sampling data from the model through the ADC, processing the data, and displaying the results in the light displays. All data has been fully corrected and is consistent with the printed and plotted data. The processing programs are a series of standard acquisition, calibration, and correction programs which apply the normal tare corrections, remove zero references, and convert the raw data to useable and correct engineering values. A small analysis program then computes the values of interest to the engineer and displays them nine at a time in the light displays. The nine light displays are controlled by nine separate option switches on the data acquisition console. There is one switch for each display. Three computed parameters are assigned to each display. The computer determines which parameter to display from the switch position. Thus up to 27 final data parameters can be displayed. Once the items have been displayed, the computer begins the cycle of sampling, processing, and displaying again. Each cycle takes about two seconds.

This computer controlled monitor has two other modes of operation. In one, it is possible to display the steady component of the voltages being sensed by the computer for all 128 channels of input. In the other, these inputs can be converted to engineering units and displayed. These functions serve well in calibrating instrumentation and checking it daily. They provide a full and instantaneous end to end check on each data channel. The desired mode of operation is selected by option switches on the data console. Totally, this computer operated monitor provides a display of 155 engineering values. Using it, the engineer can easily move from one test condition to another.

6.2 Monitoring Using Analog Signals

To ensure a safe operation, an assortment of hardwired, special purpose devices which provide visibility on the safety of the model are available. The main concern in

operating rotor models mounted on force measuring systems is whether the combination of steady and vibratory loadings on critical components will ultimately yield that component or create a fatigue failure. Critical components are identified during the design of the model and are instrumented for safety monitoring. The allowable steadies and alternating loads are computed prior to the test. This is a vital part of the test preparation. In addition, pretest predictions of loads and performance serve to give advanced notice of test conditions which might create high loads.

In the simplest cases it is only necessary to monitor the vibratory load in one plane to ensure a safe operation. A pitch link load is an example. Single channel vibratory loads are usually displayed on oscilloscopes as a continuous waveform display. These waveforms are stationary because the horizontal sweep is controlled by a circuit which resets the sweep every rotor revolution. Red lines appear on the face of each scope denoting the operating limits. In addition to these scopes, vertical meters can be used to display the vibratory part of a signal as a percent of an allowable load. These too are red lined at the allowable limit.

In some instances, the testing envelope can be expanded by monitoring loads in more than one plane of a component and by properly accounting for their interaction. An oscilloscope is again used, but now one component is placed on the vertical axis and the other on the horizontal. The load envelope is then drawn on the face of the scope as shown in Figure 5. This display results in a Lissajou pattern of the loads. As long as the pattern lies within the envelope on the scope, testing can proceed.

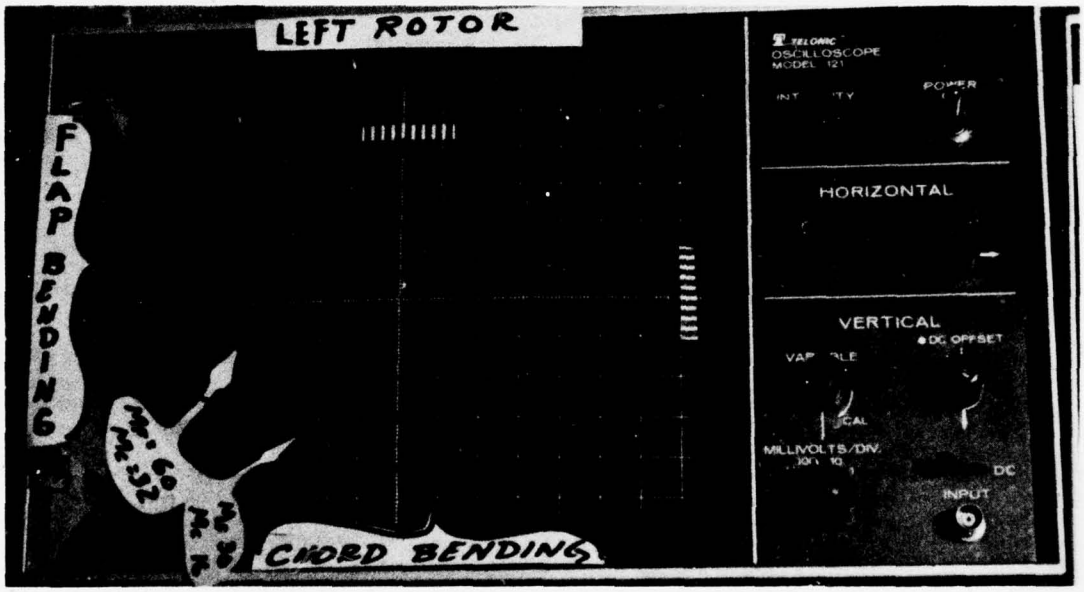

FIGURE 5. A MULTI-COMPONENT STRUCTURAL LOADS MONITORING OSCILLOSCOPE

This multicomponent loads analysis has been applied to our six component strain gage balances. We have built a hardwired, analog computer which has been programmed to analyze the signals from all of the balance components and output a single voltage which is proportioned to the load limit. The method derives a single equation which represents each component's contribution to the total stress on the most critical flexure. The computer separates the steady and vibratory loads, applies weighting factors to each and then sums them in the correct manner. In effect, it is giving a continuous output of the stresses in the critical flexure. This can be monitored on a vertical meter as a percentage of the allowable stress.

Besides these hardwired analog systems we have available a programmable analog computer. It has proved to be an invaluable tool in computing functions for real time display and for manipulating signals prior to being recorded by the digital computer. We use it quite often to transfer from the balance's moment reference center to the model's. Displaying the pitch and roll moments on an X-Y oscilloscope lets the operator keep the rotor in proper trim at all times.

The last special purpose device we want to mention is the frequency analyzer. This has become a standard piece of test hardware on rotor tests. With this device, an experienced test engineer can permit the model to approach unstable modes without catastrophe. He can visually monitor all of the modes at once and evaluate them. We also use these analyzers to determine non-rotating frequencies from "bang" tests.

The combination of digital, analog, and special purpose devices gives the test engineer the visibility he needs to operate safely and obtain data at very specific test conditions.

7.0 DATA ACQUISITION

Three types of permanent data records are acquired at each test condition:

1. Steady state data,
2. Time varying data,
3. Periodic or harmonic data.

Each is acquired in a different way for a different purpose. Sixty-four channels of steady state information and sixty-four channels of time varying information are available. All data is recorded in digital form and is permanently stored on disc and magnetic tape.

One of the two analog to digital converters is used exclusively for the steady state data. The signals from the model have been filtered by a 2 Hz low pass filter prior to being interfaced to the ADC. The signals from all 64 channels are averaged over a one second period at a sampling rate of 8 kHz. This essentially eliminates the 60 Hz noise from the data. One averaged value is obtained for each channel at each test condition and stored on disc.

Time varying signals are digitized at rates up to 40 kHz. Only those channels of interest are sampled. The computer is supplied by card input with the list of channels to sample and the sample period in seconds. The sampling rate is set externally by a quartz crystal clock. The channels are sampled in a rotational manner. Sampling starts with the first channel in the list. The second sample the computer samples the second channel in the list. It follows this sequence until the last channel in the list has been sampled. It then returns to the top of the list and continues sampling in the same channel sequence. This sampling technique provides histories for all of the channels over the same time period. The sampling period is around one second which is sufficient to cover 10 to 20 rotor revolutions. This time history data is acquired to analyze transients and non-harmonic responses. The raw counts of data are identified so that cyclic phenomenon can be studied. This is accomplished by changing the lowest order bit on the data input register every revolution. This change is accomplished using the 1/rev marker from the model to trigger a circuit which changes the bit. Thus, if cyclic analysis is required, the computer can distinguish between cycles in the time history because all of the data in one cycle will be odd and in the next cycle even and so forth.

Nearly all of our periodic or harmonic data is acquired by a special sampling technique which synchronizes the initiation of sampling to the start of a rotor revolution and the sampling period to the period of a rotor revolution. In developing this technique, the objectives were to improve the consistency of the periodic data acquired by compiling a time average of the data over the period of one rotor cycle and to reduce the volume of data by reducing the length of analysis to one cycle. Prior to sampling the computer determines the sampling period from the rotor's RPM. It then signals the sampling circuitry that it is ready for data. The circuitry inhibits the computer from sampling until the 1/rev marker is received. Sampling then commences and continues for one rotor revolution. The computer stores this array of data temporarily. It then signals that it is ready to sample again. The circuitry again inhibits sampling until the 1/rev marker is received. Then sampling starts again. The point to be made here is that the first sample is always taken with the rotor in the same azimuth position as are the second, third, fourth, etc. Thus the n-th sample of data from one cycle can be added to the n-th sample from another without any phase errors. The sampling method guarantees that samples will be taken when the rotor is in the same azimuth position. By accumulating data over a number of rotor cycles and averaging the samples at the fixed azimuth locations, data for an "average" rotor cycle is obtained, non-harmonic responses have been averaged out of the data, and harmonic responses reinforced. Figure 6 shows a comparison of an unaveraged signal and the same signal averaged over 32 rotor cycles.

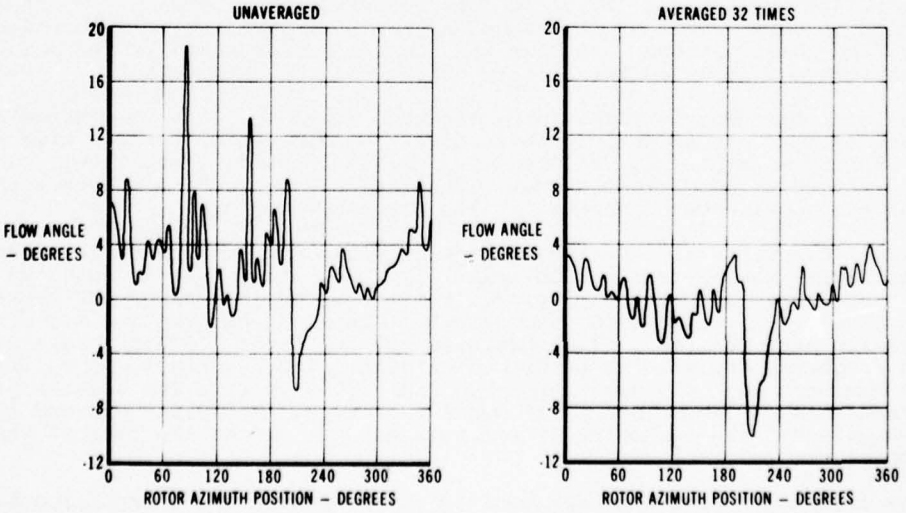

FIGURE 6. THE EFFECT OF TIME AVERAGING PERIODIC DATA

The sampling rates for the time varying and periodic signals are selected after considering the frequency content of the signal and the number of channels being sampled. The general rule of thumb is to acquire five samples for each harmonic. For example, if we want to obtain data to the tenth harmonic on 15 channels of information, and the rotor was turning at 20 cps we would have to sample at a minimum rate of 15,000 Hz (= 5/harmonic x 10 harmonics x 20 cps x 15 channels). Since this rate is not available we would select the next higher rate which is 20 kHz.

For each test condition, we acquire twenty to twenty-five thousand data values. The time varying signal is stored permanently on magnetic tape and is not generally analyzed in real time. The steady state and periodic data are retained on disc and analyzed in real time. Subsequent to the test, the data is transferred to tape for storage.

8.0 REAL TIME DATA ANALYSIS

The computer arrangement, you will recall from Figure 3, is such that a portion of its CPU is dedicated to the analysis of test data. The data is analyzed as it is recorded. A backlog of data to be analyzed can accumulate, but the computer will continue to analyze until all of the data has been processed. No other computing can be done until the computer has caught up. In general, the delay between data acquisition and final presentation is no longer than 90 seconds.

The analysis of the steady state data is similar to other facilities. The data, in counts, is converted to engineering units with zero references removed if required. Interactions are removed from the strain gage balance data as are weight tare conditions. The analysis program can process data from ten, six component force balances. The balance data is finally rotated to the desired model axis system and transferred to the correct moment reference center. Following this, special application programs compute the desired rotor and aircraft coefficients applying all known corrections including wall effects. The final results are kept on disc and may be listed or plotted as desired.

Currently two types of analysis are performed on the periodic data. The first analysis does a quick look evaluation of the averaged waveform for each channel of data sampled. This analysis is directed towards providing an evaluation of the stresses and loads on the rotor and model. The waveform is analyzed to determine the steady load, the maximum and minimum loads and the vibratory or peak-to-peak divided by two amplitude. When it is important to understand the dynamic content of the waveform, a Fourier series curve is fitted to the data. Up to ten harmonics can be analyzed and presented for each channel. These analyses provide the experimenter with a tabulated listing of both the loads and dynamics being experienced by the rotor. The computer has done in seconds what previously took weeks of hand reduction of oscillograph tapes. The results are listed along with the rotor's performance and can be plotted as a function of the performance parameters.

The value of real time analysis is that it makes rotor testing cost effective. The test can approach a question directly, evaluate the results, and probe where necessary. Real time analysis loses its value when it affects the progress of the test or when the results of the analysis cannot be presented effectively in real time. For these reasons, we have chosen to perform other analyses off-line. We will now turn our discussion towards these.

9.0 FREQUENCY ANALYSIS TECHNIQUES

As rotor technology has advanced from articulated to hingeless blades, new problems have been encountered which have required improved analysis techniques. Hingeless rotors characteristically have highly coupled modal characteristics which change as the loading on them changes. As these modes change so does the structural damping. A rotor blade chord mode which is very stable at low thrust may move as the thrust is increased and couple with a flap mode. At the same time its damping may decrease to the point where the model experiences a flap-lag instability which could be detrimental.

By means of a Fast Fourier Transform, the time histories from the chordwise and flapwise moment bridges can be analyzed effectively. This method takes a time history and converts it into an amplitude vs. frequency plot. In this format modes are easily identified and traced as conditions change. Coupling can be seen as a growth in amplitude of one mode or the appearance of another in the frequency spectra.

Reference 1 describes an experimental approach used to map the rotating natural mode shapes to verify the pretest predictions. Typically the model is operated at a constant ratio of tunnel speed to tip speed. The tip speed is varied, but the angle of attack, collective pitch, and cyclic pitch are held constant keeping the non-dimensional aerodynamic environment constant. Time histories of the rotor loads are taken at each tip speed and frequency analysis is performed on each. The resultant map of frequency spectra shows how each mode changes with RPM. The ridges on this map are then transferred to a "fan" diagram which shows the modal variation. A typical map and fan diagram are shown in Figure 7. The harmonics or per revs are plotted as the ribs of the fan. The natural modes cut across these.

From the frequency spectra we can compute power spectra and correlation functions. We have used them to analyze the energy dissipation in wakes behind the rotor to evaluate the effectiveness of aerodynamic fairings. Vibratory data can be analyzed as well as

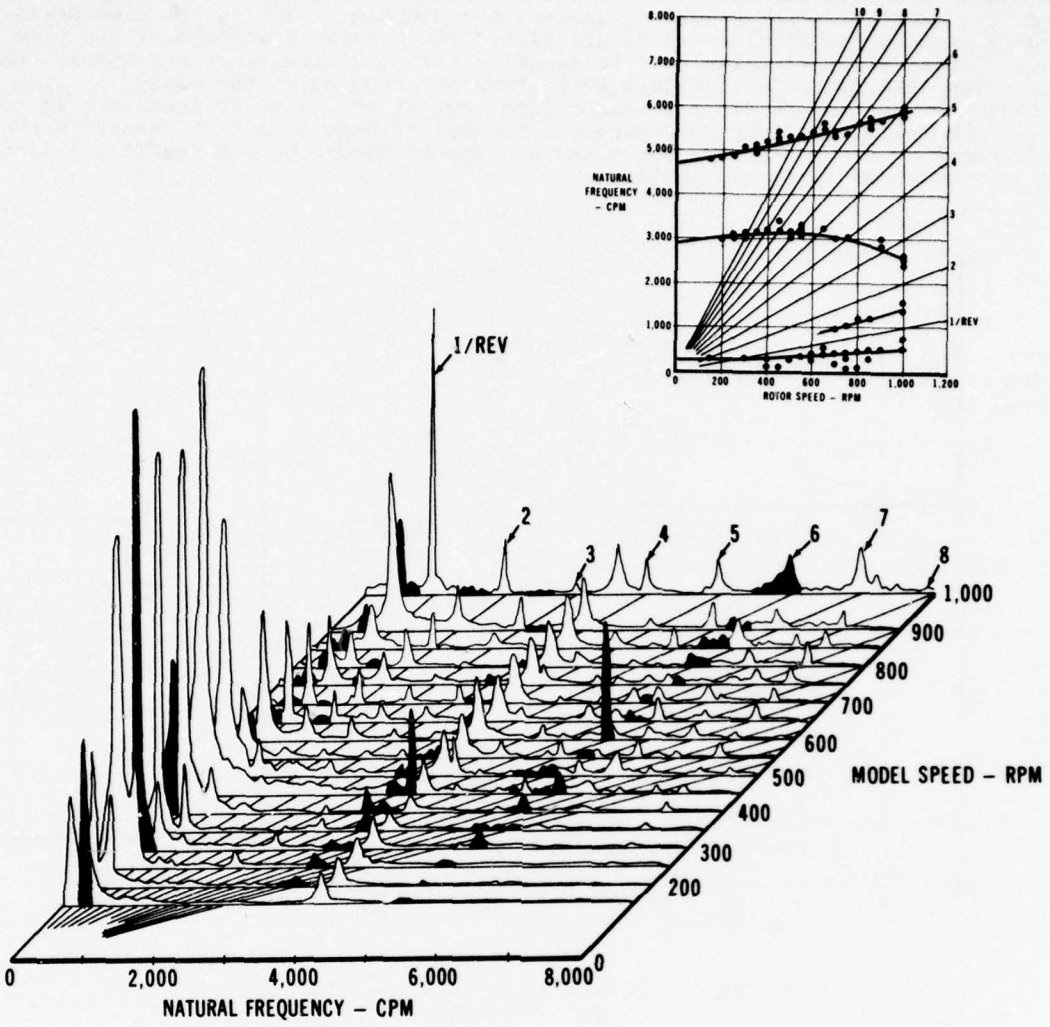

FIGURE 7. MAPPING ELASTIC MODES USING FREQUENCY ANALYSIS METHODS

noise measurements. Octave and 1/3 octave band analyses can be done.

The advantage of using the computer for this work instead of a hardwired real time analyzer is that the computer is always working a permanent data base which can be analyzed and reanalyzed. It never gets lost. Also, the data for one channel is acquired at the same time as all of the other channels so the transfer from one mode to another can be studied.

10.0 DAMPING ANALYSIS

The Fast Fourier Transform (FFT) has proven to be a powerful analysis technique when applied to modal identification and analysis. It is of even greater value when applied to analyzing the damping characteristics of these modes. The analysis is applied to the time history of a transient response. The frequency of the mode is identified from the frequency spectrum. Having identified the frequency, a block of the transient is selected to be analyzed. The block size is selected based on the frequency accuracy required, the length of the time history and the frequency of interest. Starting at the beginning of the transient, an FFT is performed on the block of data and the amplitude of the mode of interest is determined and saved. The block is then moved an increment in time. This increment can be one sample or a number of samples. We have selected to make the increment one half the period of the modal frequency. Again an FFT is done and the amplitude at the mode's frequency is determined and saved. The block is moved again the same increment and the process is repeated. The scheme of moving the block and FFT analysis is continued over a prescribed time period which is usually six periods of the modal frequency. After completing this process the computer has a history of the transient nature of the mode's response to a forcing function. The computer then takes the logarithm of the amplitudes it has recorded. Plotting these against the time in the history each block was started gives a curve from which the damping can be calculated.

Figure 8 shows the results of such an analysis. During the test, the model shown in Figure 1 was excited by oscillating the lateral cyclic pitch control. The object

of this was to excite the rotor at the first chord mode's natural frequency. At the instant the excitation force was terminated, the computer recorded the time history of the chord bending moment shown in Figure 8(a). The Fourier Transform of the time history, Figure 8(b), was then used to identify the modal frequency and the moving block analysis was then performed. Figure 8(c) shows the results of the analysis. You will note that the results are not a straight line, but it can be shown that this is to be expected. We will not cover this aspect. A complete description of theory is available in Reference 3. Because of the sometimes non-linear nature of the results, a linear least squares curve is fitted to them.

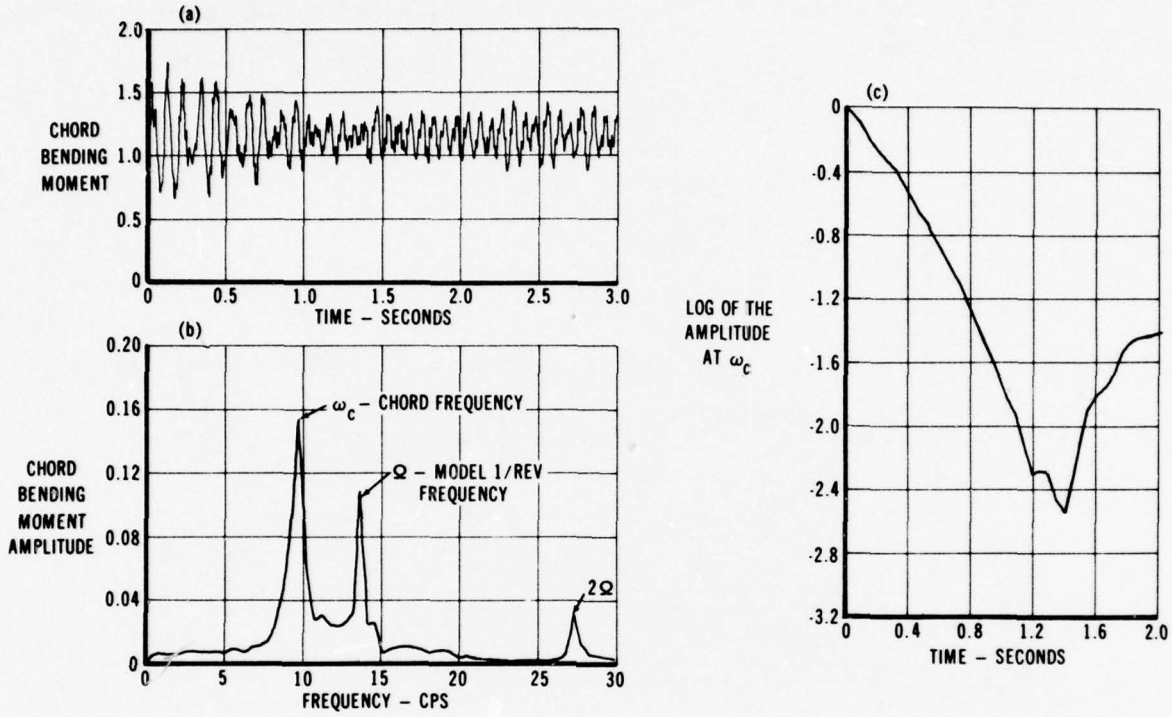

FIGURE 8. MOVING BLOCK DAMPING ANALYSIS
(a) TIME HISTORY
(b) FREQUENCY SPECTRUM
(c) ANALYSIS RESULTS

This method has been called the moving block damping analysis. It is used to its best advantage with an interactive CRT scope. This is not a necessity, however. A real advantage of this technique is that the excitation does not need to be mechanically induced. It can be induced by random aerodynamic forces arising from air turbulence. For this reason, it can be used in conventional flutter testing to predict flutter boundaries without having to go to those boundaries. This special application of FFT techniques has made damping analysis rigorous.

11.0 DATA VISIBILITY

One problem that computer acquisition and processing has created is that the data is not visible to the analyst. There are people today who would still prefer oscillograph records because they can hold the data in their hands and look at it. They can understand where their results come from. The fixed wing experimenter does not have this problem. All of his data appear on six X-Y plotters. The rotary wing experimenter is faced with twenty to twenty-five thousand points per test condition. Still, we must provide access to the data.

Our solution to this problem has been to provide the analyst with a presentation of his data which includes the data plotted against azimuth position along with the results of loads and harmonic analysis performed in real time. This presentation is done using printer plots shown in Figure 9. These plots usually serve to show waveforms sufficiently well to answer questions arising from the analyses. The advantages of printer plots are that they only require the use of the computer's printer, and they can be done in bulk very inexpensively. One of the plots can be produced every 15 seconds on our computer. A more formal presentation can be produced using the off-line plotting unit mentioned earlier.

Those facilities that have CRT terminals which can act inter-actively with the computer have a very useful tool. Using these the analyst can address the data, have it displayed in any format, and direct the analysis after viewing the data. This is a time consuming process but in many cases it is the only way that effective analysis is possible. The speed with which such terminals operate give them a tremendous advantage over any mechanical plotters.

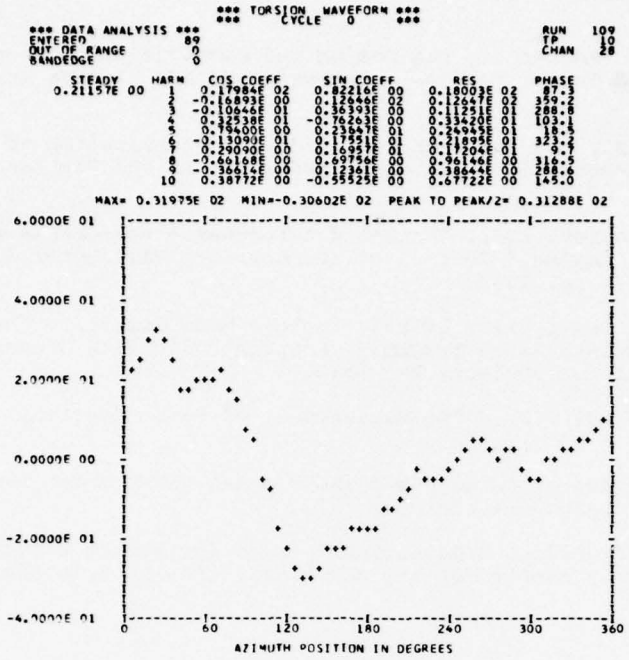

FIGURE 9. A PRINTER PLOT OF ONE ROTOR CYCLE OF DATA

12.0 SPECIAL COMPUTER ANALYSES

Generally, we strive to make our computer analysis programs capable of supporting any test situation, but occasionally standard programs will not provide the required information. We, as an industry, must vigorously approach these non-standard requirements and develop them to their full potential. Usually, these requirements develop into the standard programs as time goes on. The frequency analysis programs described above were originally developed to investigate a blade stall phenomenon, not to trace modal frequencies and measure damping. The methods used in handling data from hot wires was applied to the frequency and damping analyses. The requirement to do transient load analysis during start up and shut down tests forced us to depart from the traditional harmonic analysis used by the rotary wing aircraft community. The examples are plentiful and they all demonstrate the need to experiment with analysis techniques. In this way, computer methods can move ahead with model making and testing technology to develop the V/STOL aircraft of the future.

13.0 CONCLUSION

We have seen that the advancing state of the art in model building has placed renewed emphasis on wind tunnel testing of rotary wing aircraft and rotor systems. To accomplish efficient testing of the models and productive and effective analysis of the data, we must rely on a computer system which has features tailored to rotor testing. A continuous monitor of test conditions is important not only to set up the proper conditions but to operate safely. Real time data analysis has been stressed because of the importance of acquiring specific data rather than a matrix of data. It is also important to maintain the proper balance between real time and non-real time analysis. The real time analysis should be limited to a digestible amount of data and ought to proceed at the pace of the experiment. Off-line analysis should proceed as quickly as possible. Many times these analyses provide answers which are vital to the success of the test. The suggestion here is that the computer facility should be dedicated to the test facility.

We have found that the best analysis tool in rotor testing today is a Fast Fourier Transform analysis. The FFT provides a visibility of the data which was previously unavailable. Its application to the moving block damping analysis is one example of its utility. It is also applicable in computing power spectra, correlation coefficients and energy characteristics.

The computer has many uses in rotary wing testing. As long as there are imaginative engineers in the rotary wing community, there will be a need for wind tunnels and a computer system supporting it. This combination will continue to be an irreplaceable tool in the design of future V/STOL aircraft.

REFERENCES

1. Harris, F.D., "Aerodynamic and Dynamic Rotary Wing Model Testing in Wind Tunnels and Other Facilities," paper presented at the AGARD/von Karman Institute Lecture Series No. 63, April 1973.

2. Albrecht, Carl O., "Factors in the Design and Fabrication of Powered Dynamically Similar V/STOL Wind Tunnel Models." Proceedings, AHS Mideast Region Symposium, October 1972.

3. Hammond, Charles, E., Doggett, Robert V., Jr., "Determination of Subcritical Damping by Moving Block/Randomec Applications," presented at the Flutter Testing Techniques Symposium, October 1975.

4. Fisher, R.K., McCroskey, W.J., "Detailed Aerodynamic Measurements on a Model Rotor in the Blade Stall Regime," Journal of the American Helicopter Society, Vol. 17, No. 1, January 1972, pp. 20-30.

5. Anderson, W.D., "Investigation of Reactionless Mode Stability Characteristics of a Stiff Inplane Hingeless Rotor System." Preprint 734, 29th Annual National Forum of The American Helicopter Society, May 1973.

6. Blackman, R.B., Tukey, J.W., "The Measurement of Power Spectra," Dover Publications, 1959.

7. Loewy, R.G., "A Review of Aerodynamic and Dynamic VSTOL Model Testing." Proceedings, AHS Mideast Region Symposium, October 1972.

8. Wood, Edward R., "Significant Development Areas for Future V/STOL Wind Tunnel Testing." Comments presented at the AHS Mideast Region Symposium, October 1972.

SOME EXPERIENCES WITH THE EXPLOITATION OF MEASUREMENTS OF THE PERTURBATION FIELD IN A WIND TUNNEL TO IMPROVE SIMULATION

by W. R. Sears

University of Arizona and Calspan Corporation

I shall assume that my audience is already aware of the adaptive-wall scheme independently proposed a few years ago by the late Professor Antonio Ferri and the speaker. Briefly, the scheme consists of joining the flow field within a wind tunnel to a computed exterior flow field that satisfies the required boundary condition at large distances. The matching of these two flow fields is carried out to an arbitrary, convenient, matching surface S within the tunnel.

The essential feature of this proposal is that both the flow within the tunnel and the computed exterior field are iteratively adjusted to achieve the matching. The tunnel flow is adjusted by mechanical changes of tunnel-wall geometry -- for example, by varying the pressures in subdivided plenum chambers surrounding the working section and communicating with the tunnel through porous walls or slots. The exterior flow field is adjusted by altering the boundary values prescribed at S, on the basis of measurements of flow-perturbation distributions at or near S.

In practice, the most suitable perturbation quantities to be used for this purpose appear to be static pressure and flow inclination -- or, what is equivalent, streamwise and normal (to S) velocity components, u and v.

A way to carry out the procedure is to introduce one or the other of the two measured distributions, say v_m, as interior boundary values for the exterior field, and to extract from the computer the distribution u consistent with the (unconfined) exterior flow. We call this result $u[v_m]$, denoting that it is a functional of the distribution v_m. The discrepancy function δu, defined as $u[v_m]-u_m$, is a measure of wind-tunnel wall interference, and is the basis for the next wall modification.

Let the superscript n denote the number of the iteration arrived at; thus $u_m^{(n)}$ and $v_m^{(n)}$ are the measured distributions at the n-th iteration, and $\delta^{(n)}u \equiv u[v_m^{(n)}]-u_m^{(n)}$ is the corresponding discrepancy.

The procedure is to adjust the tunnel-wall geometry so as to change the measured u-distribution from $u_m^{(n)}$ to $u_m^{(n)} + k\delta^{(n)}u$, say, where k is a constant. If k is taken to be 1, the phenomenon of "overshoot" seems always to occur -- the function $\delta^{(n+1)}u$ will be generally of opposite sign to that of $\delta^{(n)}u$ -- convergence may occur, but it will be slow. One of the interesting problems associated with this scheme is to find optimal values for k.

It is possible to simulate analytically the iterative process for certain categories of models in two-dimensional or circular tunnels, for flow that is either incompressible or is subsonic in the Prandtl-Glauert approximation. For example, Lo and Kraft of ARO, Inc. have shown very elegantly that the process converges, for any value of k within $0 < k \leq 1$, for any two-dimensional nonlifting model in a two-dimensional wind tunnel. Both Dr. Lo and I have carried out the extension to axisymmetric models in circular tunnels, and I have applied R. T. Jones' low-aspect-ratio using theory to study the case of a lifting wing in a circular tunnel. In each case, the process converges to the correct, unconfined flow, for a range of k's, regardless of the initial wall configuration. That is, it does not matter whether the iteration begins with a closed, open or ventilated tunnel, so far as the conclusion regarding convergence is concerned. (The tunnel-wall configuration must, at every step, have the assigned symmetry: two-dimensional or axisymmetric.)

The Calspan one-foot transonic tunnel is an embodiment of the Ferri-Sears scheme; namely, a two-dimensional tunnel having perforated top and bottom walls communicating with subdivided plenum chambers whose pressures are controllable. Flow quantities u and v are measured by means of a longitudinal static-pressure pipe and flow-inclination tubes, respectively. Experiments have been carried out using a 0012 wing with force, moment, and pressure instrumentation. The wing chord is 0.5 ft.

Under conditions where the flow at surface S (in this case, plane surfaces above and below the model) is wholly subsonic, the outer-flow calculation has been based on the Prandtl-Glauert approximation. Thus, for given $v_m(x)$ at surface S, the calculation of $u[v_m(x)]$ is relatively straightforward, involving only inversion of a Hilbert transform on the infinite interval. The only complication is that the measured data must be extrapolated to large values of x and -x. This has been done by fluid-mechanical principles.

For higher Mach numbers, the exterior flow becomes supercritical (mixed), and must be calculated from the nonlinear small-disturbance transonic theory. To date, the finite-difference technique of Murman and Cole has been used. The inner boundary (plane) is unusually simple, but again there are some complications because the boundary is infinite in extent, and extrapolation of measured data is necessary.

Figures 1-3 are examples of the experimental data obtained at Calspan in the one-foot tunnel described above. They show 3-component data for the 0012 airfoil at Mach numbers 0.55, 0.65 and 0.725. The points identified with the symbol Δ are the results obtained when the one-foot tunnel was run in a configuration roughly simulating a conventional ventilated tunnel; namely, the plenum chambers were set so as to give uniform static pressure in the absence of the airfoil (empty tunnel) and their valves were fixed in those positions. When the airfoil was tested in this configuration, of course, there was communication between the plenum chambers through the piping; no further wall adjustments were made.

The data identified with the symbol ○ were obtained in the Calspan 8-foot, ventilated, transonic wind tunnel using the same model of 0.5-foot chord and, therefore, can be interpreted, to good approximation, as data obtained in unconfined flow. It will be seen that the discrepancies between the one-foot-conventional data and the 8-foot data are substantial, especially at Mach numbers 0.65 and 0.725 and especially as regards moment coefficient.

In figure 3 are also shown the results of iterative wall adjustments using the measurement techniques and computations described above, at an angle of attack of 2 degrees. These data are designated with the symbol □. The numbers 1, 2 and 3 indicate successive approximations, the first being a configuration suggested by simple calculations representing the theoretical perturbation distributions for the 0012 airfoil in unconfined flow. For points 2 and 3 the iterative procedure described above was carried out. This Mach number (0.725) is above the theoretical critical value for all α's. The measured pressure distribution at $\alpha = 2°$ confirmed this, and a strong upper-surface shock wave was present.

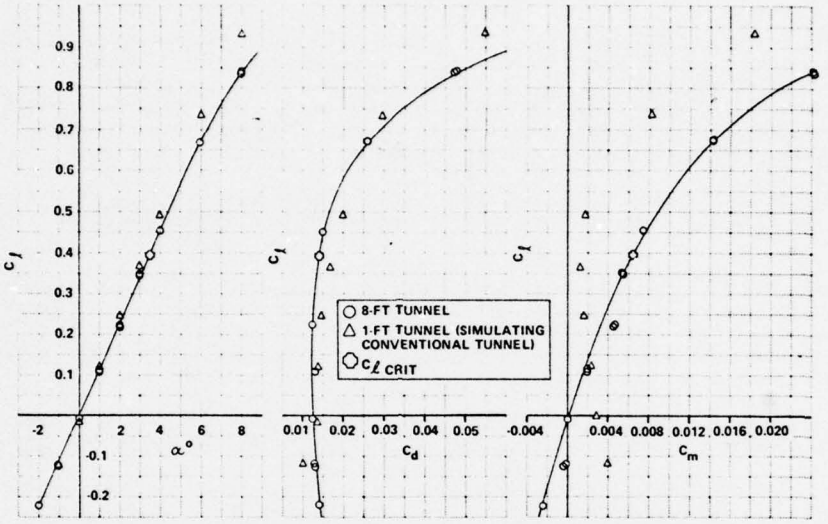

Figure 1: Three-component data for 0012 airfoil in 8-foot and 1-foot Calspan tunnels at Mach number 0.55. The 1-foot tunnel was run in the configuration simulating conventional ventilated tunnels. The theoretical critical α for this Mach number is 3.6°.

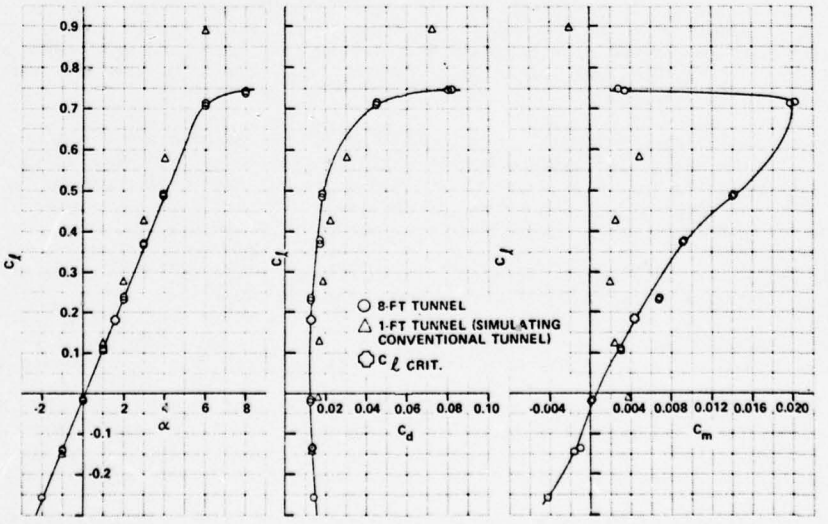

Figure 2: Same as Figure 1 but at Mach number 0.65. The theoretical critical α for this Mach number is 1.6°.

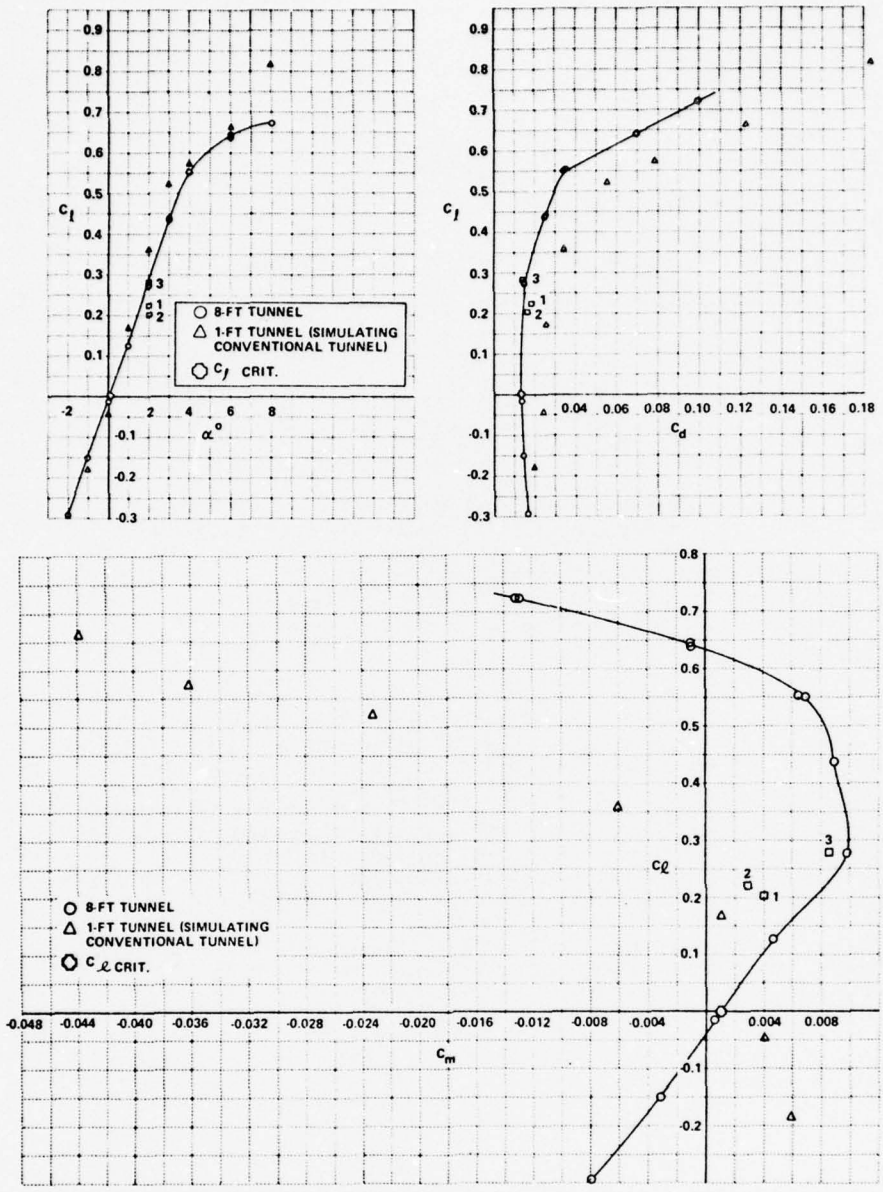

Figure 3: Same as Figure 1 but at Mach number 0.725; also results of three iterative adjustments of plenum pressures according to Ferri-Sears scheme at $\alpha = 2°$. The airfoil is above critical at all angles of attack at this Mach number.

We conclude that the conventional ventilated wind tunnel may have large wall interference at these Mach numbers when such a large model is tested. We also conclude that the iterative adjustments of plenum pressures rapidly remove boundary interference.

Experimental data are not yet available for higher Mach numbers. Numerical simulations have been carried out, however, for an airfoil in a tunnel at Mach number 0.9. For these studies the Murman-Cole technique was used for both interior and exterior flow fields -- separately, of course. Convergence is found to be rapid especially if small values of k are used -- e.g. 1/4 to 1/10.

Figure 4 shows some results of this numerical simulation. The model was assumed to be a double-circular-arc profile at zero incidence in a stream of Mach number 0.9. Starting with a very poor approximation ("Iteration No. (1) "), the process of iterative matching at the interface at h = 0.75c was carried out successively. After 11 iterations the pressure distribution on the airfoil was not distinguishable from that of unconfined flow. The third iteration already brought the distribution close to the final one.

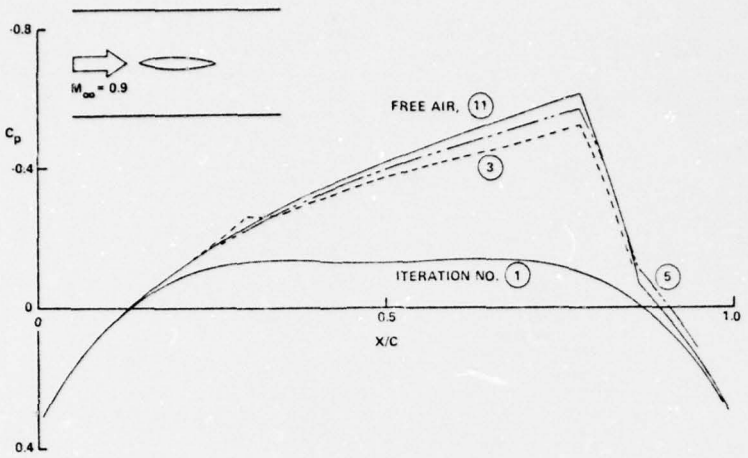

Figure 4: Results of numerical simulation of successive iterations at Mach number 0.9. Double-circular-arc airfoil at $\alpha = 0$. Inner and outer flow regions calculated by transonic small-distrubance approximation.

By present-day standards the Murman-Cole finite-difference approximation is rather old-fashioned. More modern methods include formulations in which the differencing scheme is fully conservative. That is, before the derivatives are approximated by finite differences the differential equation is written in divergence form. The finite-difference equation is then a statement that mass is conserved. Experience has shown that substantial improvements in flow-field prediction are often achieved by this refinement -- especially that the positions of shock waves are more accurate. We have therefore repeated some of the calculations of the external flow field just mentioned, using a fully conservative differencing scheme prepared by Dr. N. J. Yu of the University of Arizona. The result shows that in this case there is very little difference between the conservative and non-conservative results. Of course, the fully conservative scheme is preferred for future applications.

Finally, an observation concerning the process of wall adjustment in response to an error distribution $\delta u^{(n)}$: how does one adjust one's plenum pressures to change $u_m^{(n)}$ to $u_m^{(n)} + k\delta u^{(n)}$? For the two-dimensional tunnel, this has turned out to be rather straightforward. The tunnel operator simply begins at the plenum chambers farthest upstream -- top and bottom; he adjusts their valves to give the desired $\delta u^{(n)}$ at the measuring station immediately downstream, and proceeds to set each valve in this way, working from up-to downstream. Each change affects stations downstream but has only small effects upstream; therefore, when this process is repeated two or three times, the desired u-distribution is obtained. It is predicted that it will not be a serious problem in three-dimensional embodiments as well.

APPLICATION OF THE COMPUTER FOR ON-SITE DEFINITION AND CONTROL OF WIND TUNNEL SHAPE FOR MINIMUM BOUNDARY INTERFERENCE

by
M. Judd, M.J. Goodyer and S.W.D. Wolf,
Department of Aeronautics and Astronautics,
The University, Southampton SO9 5NH, Hants, U.K.

SUMMARY

The use is described, of flexible top and bottom walls, as a means of eliminating or minimising wall interference effects on two-dimensional wind tunnel models. Strategies for producing streamline contours and their extension to three dimensions are discussed. Errors due to theoretical assumptions and practical implementation are explored so that computational resolution can be made consistent. The need for efficient and rapidly convergent algorithms for wall adjustment is stressed and discussed. These must be developed in order to reduce the current data acquisition times and make feasible the present aim to incorporate an on-line minicomputer for automatic wall control. Results are presented showing the correctness of the strategies used to date with manual wall adjustment.

SYMBOLS

$a, a(\eta)$	Cross section coordinates	M	Mach number
a_1	Lift curve slope	R_c	Reynolds number based on chord
c	Wing chord	$u,v,w,$ $U,v_n,\underline{dv}$	Velocity components
C_L, C_D	Lift and drag coefficients	x,x_1,y,y_1 $\xi,\underline{ds},\underline{r}$	Coordinates
C_p, C_{pi}	Pressure coefficients	β	$\sqrt{1 - M^2}$
E_1,E_2,K_1,K_2 R,R_1	Functions used in the three-dimensional strategy	δ	Velocity error function
h	Tunnel height	$\gamma_v, \underline{d\Gamma}$	Vorticity
L	Tunnel semi-length	η,ψ,θ,γ	Angular coordinates

1. INTRODUCTION

The practice of correcting wind tunnel data arises because the test flowfield is restricted in extent in all directions by the dimensions of the test section, while the aircraft represented by the model operates normally in a flowfield which extends effectively to infinity in all directions. The constraints of the bounds of the test section interfere with the flow over the model and it is unfortunate that the magnitudes of the required corrections for the interference are somewhat uncertain. However, since the corrections reduce with increasing size of test section and by the employment of test section wall ventilation, it has been normal practice to reduce the uncertainty by the exploitation of one or both of these devices. These considerations coupled with the fact that test values of Reynolds number are usually rather low in comparison with flight values have resulted in present and planned wind tunnels which are large and expensive in terms of capital outlay and operating costs.

A further source of flow interference which is again of uncertain magnitude is the model support sting and strut. In wind tunnel testing the interference can be eliminated by the use of magnetic suspension for the model, where the magnetised model is restrained by an electro-magnet system outside the test section. However the bulkiness of the conventional types of test section, particularly the ventilated type having a plenum chamber around the test section, has so far prevented the large scale exploitation of magnetic suspension because costs rise rapidly with increase of the distance between model and electro-magnets.

As a possible means for reducing this separation a proposal was made in 1972[1] that the test section walls should be curved around the model in such a way that they followed a stream tube that would have existed around the same model in free flight. In this way the wall interference would be eliminated, removing the need for a plenum chamber and also allowing the walls and therefore the electro-magnets to be positioned close to the model. Since the shapes of such stream tubes change strongly with model attitude and also with Mach number in the transonic range the walls would need to be flexible, capable of accepting double curvature. In view of the apparent mechanical complexity of such a test section, it was decided to exploit the notion first in two-dimensional testing, since important economic advantages would reward its successful development. In such a test section the stream tube can be regarded simply as a pair of streamlines, only two of the four walls are required to be curved and these only in single curvature.

It was crucial to devise reliable means for checking that the curved walls follow streamlines. A streamlining criterion was proposed[1], which has been used for the past

three years in two-dimensional testing, and is illustrated in Fig.1.1. A set of streamlines is shown as would have existed around the two-dimensioanl aerofoil in an infinite flowfield. Two arbitrary streamlines are selected to be followed by the curved walls. Since the pressure field is continuous in the absence of shock waves it was proposed to use the local equality at the wall of static pressure produced by the real part of the flow inside the test section with a static pressure on the outside computed for an imaginary flowfield passing over the same streamline contour. In general there is a mismatch between the pressures, and the walls are moved in an iterative manner with a jacking system until a satisfactory match is obtained, independently for the two walls. At this stage, data can be taken on the model. Note that the viscous effects at the model are contained within the test section. The walls reside in portions of the flowfield which behave essentially as though inviscid, and therefore the computations of the imaginary flowfields can be utilised with confidence.

Although a two-dimensional example has been used to illustrate the streamlining criterion, and the majority of this paper is devoted to two-dimensional work, the same criterion is equally valid for the more general case of three-dimensional model testing. Section 2.3 outlines a method which allows the computation of the three-dimensional imaginary flowfield, and promises the means for convergence of walls in very few iterations.

It should be noted that the wind tunnel itself provides, from measurements at the walls, all the information needed for the streamlining process. The local sign and magnitude of the mismatch between real and imaginary wall pressures indicates the direction and magnitude of the wall movement required locally. There is a continuous exchange of information between tunnel wall and computer, hence the use of the term "self streamlining". The process also is ideal for closed-loop control by on-line computer, because rapid acquisition of wall pressures coupled with the rapid computation and setting of the next contour is of vital importance since this time is unproductive in terms of model data acquisition.

The self streamlining wind tunnel is still in development, and is moving progressively from an initial stage involving the use of a low speed wind tunnel operated in an open-loop mode with a modest involvement of computers, towards the development of a transonic test section with automated adjustment of wall contours by online computer. The ultimate development might be the three-dimensional flexible walled test section. This report is a statement of the recent stage of development.

2. WALL ADJUSTMENT STRATEGY AND COMPUTATIONAL IMPLEMENTATION

2.1 Initial two-dimensional method

This method has been developed in conjunction with a low speed wind tunnel and minicomputer. A schematic cross section through the test section of the low speed tunnel is given on Fig.2.1. Indicated are the manual jacking points on the top and bottom walls from which data is taken for use in the streamlining process. The essential data are the wall contours and wall centreline static pressure distributions and the free stream reference conditions. Since the section has finite length, the streamlines near the two ends are not parallel to the free stream, an effect which is particularly apparent in the important case of lifting models. Therefore adapter portions are included to blend the non-horizontal ends of the streamlined portion into the other horizontal and fixed portions of wind tunnel circuit. The nominal depth of the test section is 1.1 wing chords, and the length of streamlined wall is about 5.1 chords equally disposed about the wing quarter-chord point. The wing chord is 13.72cm, 5.4 inches. It is shown in section 3.3 that the truncation of the test section length in this manner introduces only a small end-interference.

The first step in computing an imaginary flowfield (one of these passes over the top wall, the other under the lower wall) is to correct the geometrical wall contour for boundary layer displacement thickness, since it is the contour of this thickness which is effective. A program solving the momentum integral equation provides the correction and the effective contour. In a second program the wall is represented by the envelope of the flow of a set of sources and sinks distributed along a straight line lying parallel to the freestream and positioned fairly close to the wall. In the case of lifting models it was found necessary to represent the slope of a wall streamline well upstream and downstream of the ends of the test section in order to achieve sufficiently accurate predictions of wall pressures. The necessary information allowing the computation of the wall slopes beyond the extremities of the test section is again available from wall measurements in the test section.

An example of part of a wall contour for which an exact solution for surface pressure coefficient is available is shown on the upper half of Fig.2.2. The contour represents the lower test section wall streamlined around a non-lifting two-dimensional cylinder. The exact pressure coefficient distribution is given, together with that computed (C_{pi}) for the lower imaginary flowfield from the source/sink model. There is satisfactory agreement.

The strategy for wall adjustment has been to move the wall, where significant differences between the measured pressure and C_{pi} exist, towards the higher of the two by an amount proportional to the difference. The convergence on to the streamline shape is usually monotonic, taking around eight iterations.

The procedure so far developed allowed principles to be proved, but is unsatisfactory for regular use because of its slowness arising from several sources. Much of the work was manual, for example the setting of the jacks, the measurement of pressures, and the feeding of data into the computer. The computation of the imaginary flowfields itself was lengthy on the mini-computer, taking typically one hour of computer time per pair of computations. It can be seen that many hours of work are required in order to establish just one pair of streamlines. Following this lengthy process, just one set of data can be taken on the model. Tunnel users will see that a reduction of the time for streamlining by perhaps three orders of magnitude is required if this type of test section is to be practical.

In the following sections are introduced the means by which it is proposed to implement the necessary speed-up. It is proposed to reduce the required number of iterations per streamlining, and to couple a larger computer to the tunnel for the closed-loop control of wall contours.

2.2 A predictive method for two-dimensional wall adjustment

In order to increase the rate of convergence of wall adjustment, an alternative strategy to the one used successfully to date (as outlined in the previous section) was sought. Rapid convergence and as simple a program as possible are needed in order to realise the aims of an on-line computer application.

The basis of this second method is illustrated here by application to a single wall in a form suitable for iteration. Iteration is still necessary because the pressure and velocity fields of the model will change after the wall adjustment and resultant interference reduction. In the case of the Southampton tunnel, streamline flow is obtained by solid wall contouring using surface pressure measurements, rather than by velocity component adjustment at a control surface, as in the Calspan approach[2]. This allows the mismatch between internal measured and external calculated tangential velocity components at the wall to be regarded as determining a local strength of vorticity in a sheet replacing the wall. Moreover, the normal velocity induced at the wall by this vorticity just balances the components from the undisturbed free stream and the model. The free stream component is known because the wall-shape is given; the model component normal to the wall is therefore obtained as the difference between the free stream and vortex sheet components. The predictive method for wall adjustment now requires:-

(1) the calculation of a change in local wall slope so that an increment in free stream normal velocity component just cancels that due to the model, and

(2) the integration of wall slope to give the new wall position.

This may be formulated mathematically using the arrangement shown in Fig.2.3 for a single (upper) wall. A wall shape $y_{n-1}(x)$ has been set and the internal velocity distribution $u_{n-1}(x)$ measured using the wall static pressures. The external velocity distribution $v_{n-1}(x)$ can be calculated for shape $y_{n-1}(x)$ in a free stream flow U. The new wall position is given by:-

$$y_n(x) = y_{n-1}(x) + \Delta y_{n-1}(x)$$

where the increment $\Delta y_{n-1}(x)$ is obtained from:-

$$U \frac{d\Delta y_{n-1}(x)}{dx} \simeq \frac{1}{2\pi} \int_{-\infty}^{+\infty} \frac{\left[u_{n-1}(\xi) - v_{n-1}(\xi)\right]}{(\xi - x)} \, d\xi \qquad 2.1$$

It should be noted that no assumption need be made here about how the model produces its velocity field. Indeed, the interference from the lower wall would also be included in $u_{n-1}(x)$. The form of equation 2.1 is similar to that used for the unconstrained incompressible flow condition[2,3] but is an approximation here because the wall and hence the vortex sheet, is not flat in general. Since all self-correcting or self-streamlining tunnel principles involve the use of an imaginary and calculated external field, it is imperative that the theoretical bases should be justified at all stages and that the errors resulting from any simplification be consistent with the errors associated with numerical analysis and mechanical setting tolerances. The simplifications in deriving equation 2.1 are considered further in Section 3.1.

Computational care is required in obtaining the principal value of the integral in equation 2.1. The method adopted has been to use a piecewise cubic spline fit and local analytic integration followed by numerical summation. The numerical integration to obtain $\Delta y_{n-1}(x)$ is straightforward.

When the strategy of equation 2.1 is applied to a single wall, a slight but desirable overshoot in wall adjustment, as verified by application to simple flows with known exact solutions. No attempt is therefore made to factor the adjustment because of a major advantage in the calculation of the external flow field obtained by retaining an unmodified equation 2.1. The external velocity $v_n(x)$ for the shape $y_n(x)$ is shown in Fig.2.4 and can be determined by representing the boundary again as a vortex sheet. The

normal velocity boundary condition results in an approximate equation identical with equation 2.1 but inverse in nature. Comparison of the two equations shows that

$$v_n(x) \simeq \tfrac{1}{2}\left[u_{n-1}(x) + v_{n-1}(x)\right] \qquad 2.2$$

It is therefore not necessary to calculate the external velocity for the new shape $y_n(x)$ since it can be obtained from velocity components already available, provided the strategy in equation 2.1 is used to determine $y_n(x)$. However, it is necessary to have a known initial external velocity distribution and this can be achieved simply by starting with a straight wall so that

$$v_o(x) = U, \text{ constant.}$$

When the strategy is applied to both tunnel walls, a divergent process can result. This arises from the strong interaction between the walls which, for long wavelength components of wall movement, may be regarded as a one-dimensional continuity effect. Convergence can be obtained by feeding a proportion of the demanded movement for one wall to the other.

2.3 Wall adjustment strategy for three-dimensional subsonic flow

The extension of the method of section 2.2 to three-dimensional flow is conceptually straightforward. A close parallel can be drawn with the extension of thin aerofoil section theory to finite wings of arbitrary plan form. A lifting surface representation of the tunnel surface is therefore sought which, because of its non-planar nature, will lead to kernel functions in the surface integrals which are much more complicated than for the flat wing. Various developments of lifting surface theory are possible. Here an elemental vortex system is used and, by summing over the tunnel surface, the velocity normal to the boundary is found at any position. The normal velocity is used as before to determine the required streamwise slope of the streamline boundary and hence the new coordinates.

A general formulation has been developed with the tunnel shape represented as a cylinder of general cross-section. The difference between inner and outer velocities at the wall gives the local strength of the vorticity component normal to the tunnel flow. In order to satisfy the Helmholtz condition on circulation, this vorticity must be associated with a trailing vortex pair. This is shown in Fig.2.5 as the line ABCD. A section through the tunnel at the vortex head is shown in Fig.2.6 where the cross-section is defined in terms of polar coordinates $a(\eta)$ and η. The vortex element BC is given in vector form as

$$\underline{d\Gamma} = \gamma_v(x_1,\eta)dx_1\ \underline{ds} \qquad 2.3$$

where $\gamma_v(x_1,\eta)$ is the local vorticity strength and $\underline{ds}$ is the vector corresponding to the element of circumference with magnitude ds. The velocity $\underline{dv}$ induced at a general point Q is given formally by the Biot-Savart law in the form:-

$$\underline{dv} = \frac{1}{4\pi}\frac{\underline{d\Gamma} \times \underline{r}}{|\underline{r}|^3} \qquad 2.4$$

where $\underline{r}$ is the vector position of Q with respect to the vortex element.

Equation 2.4 is also used for the vortex leg AB in Fig.2.5 where the element at P has a strength

$$\underline{d\Gamma} = \gamma_v(x_1,\eta)dx_1\ \underline{d\xi} \qquad 2.5$$

This can be integrated with respect to ξ over the length AB and the corresponding contribution from vortex DC found in a similar way. The difference between the contributions is proportional to $d\eta$, the angular difference between the polar coordinates of B and C in Fig.2.6. At the general point Q in Fig.2.5, the total normal velocity $v_n(x,\theta)$ is found from equation 2.4 by integrating $\gamma_v(x_1,\eta)$ over the whole surface.

The result may be presented in various ways and, in practice, the best form will be determined by the arrangement of jacks for controlling wall position. For example, it may be convenient to move a wall portion according to its Cartesian rather than polar coordinates. For the present paper, a simplified result is given for a tunnel of circular cross-section (radius a). The normal velocity component is then the radial component and wall control could be obtained by simple jack movements along radial directions. The induced velocity is

$$v_n(x,\theta) = \frac{1}{4\pi}\int_{-\infty}^{+\infty} dx_1 \int_0^{2\pi} d\eta\ \gamma_v(x_1,\eta)\{E_1(\theta,\eta)K_1(x,x_1,\theta,\eta)$$

$$+E_2(\theta,\eta)\left[2K_1(x,x_1,\theta,\eta) + K_2(x,x_1,\theta,\eta)\right]\} \qquad 2.6$$

where

$$E_1(\theta,\eta) = -a\, R_1(\theta,\eta)\cos(\eta - \theta)$$

$$E_2(\theta,\eta) = a^3[\sin(\eta + \theta) - \sin 2\theta]\sin(\eta - \theta)$$

$$R_1(\theta,\eta) = 2a^2[1 - \cos(\eta - \theta)]$$

$$K_1(x,x_1,\theta,\eta) = [1 + (x - \xi)/R(x,x_1,\theta,\eta)]/R_1^{\,2}(\theta,\eta)$$

$$K_2(x,x_1,\theta,\eta) = \beta(x - \xi)/R_1(\theta,\eta)R^3(x,x_1,\theta,\eta)$$

$$\text{and } R^2(x,x_1,\theta,\eta) = (x - \xi)^2 + \beta^2 R_1(\theta,\eta)$$

The result has been developed for subsonic flow through the use of the Prandtl-Glauert correction factor

$$\beta = \sqrt{1 - M^2}$$

M being the flow Mach number. As usual in lifting surface integrals, the numerical integration requires care in dealing with the singularities associated with $x_1 = x$ and $\eta = \theta$, but a method of local analytic integration similar to that used in Section 2.2 is expected to be adequate. A double cubic spline surface fit would now be required.

In the general application of the three-dimensional method, there is an infinite number of stream tubes which can be chosen, although only one will have a cross-section at the upstream end which matches the fixed tunnel geometry. If this particular stream tube is chosen then there will not in general be a matching at the downstream end and some tailoring is required. It may be better to choose a stream tube whose cross-section shape at the model is convenient from an implementation point of view. Tailoring would be required upstream and downstream but stream tube discrepancies in these regions produce much smaller interference errors than similar discrepancies in the model region.

In this section, the foundation has been laid for a wall adjustment strategy in three-dimensional flow. The exact formulation and computer program have not been attempted because they will be determined by the physical way that wall movement is obtained. At the present time, it is not clear what would be the best engineering approach.

2.4 Test data

The low speed test section illustrated on Fig.2.1 has been utilised in demonstrating the effectiveness of the wall streamlining concept, with two types of two-dimensional model. The aim in these tests was to show from measurements of pressure distributions around their surfaces that they were experiencing within the narrow confines of the test section the same aerodynamic forces as in an infinite flowfield.

The first model was a circular cylinder, chosen for its simplicity and because its surface pressure distribution is well known, and also because the flow separation and therefore thick wake would provide a fairly severe test of the new test section and proposed methods of streamlining. Some of the data taken on this model with the walls straight and also streamlined is shown on Fig.2.7, together with other published data at the same Reynolds number for comparison. The data marked 29.2% blockage is entirely uncorrected and was taken in the self streamlining test section. Blockage is the ratio of cylinder diameter to depth of test section. The other data at lower levels of blockage were taken by Fage and Falkner[4] in a straight-walled test section and is shown uncorrected and also corrected for blockage effects by the methods of Allen and Vincenti[5]. The agreement between this corrected data and that taken in the self streamlining wind tunnel at high blockage but with the walls streamlined is very good, demonstrating the ability of the streamlining procedure to accommodate separated flows.

The second model is a wing of NACA 0012-64 section which has been tested in a deep test section to obtain its free-air behaviour. The tests were carried out in LTPT at NASA Langley Research Center, the test section being 213.4cm (84 inches) deep and the wing chord is 13.72cm (5.4 inches). The LTPT pressure distribution data with the wing at 6 degrees angle of attack is shown on Fig.2.8, together with data taken on the same wing and at the same Reynolds number in the 15.24cm (6 inch) deep flexible walled test section. The wing pressure distribution obtained with the flexible walls straight is included in order to illustrate the magnitude of the wall interference effects that would have been present had it not been possible to properly contour the walls to streamlines. It can be seen that in the presence of streamlined walls the surface pressure distribution reverts almost exactly to the LTPT data despite the fact of the flexible walled test section being shallower by about 93%. For clarity, the LTPT and straight wall results in Fig.2.8 are shown as lines although they are, in fact, discrete point measurements.

3. COMPUTATIONAL RESOLUTION AND ERROR ASSESSMENT

The major sources of error in obtaining interference free flow may be summarised as:-

(1) Theoretical bases of wall adjustment strategy.

(2) Numerical analysis and computation.

(3) Implementation problems such as finite length of adjustable test section.

(4) Mechanical tolerances in wall setting.

The computational error can readily be made less critical than the other three but at the expense of increased program sophistication and computer run time. For on-line control of wall position using limited capacity computers this trend is undesirable. It is then more efficient to develop as simple a program as possible with numerical process errors compatible with those from the other three sources. It is therefore important to have some knowledge of the magnitude of these to ensure total consistency. Economic penalties will also be incurred if too close a practical tolerance is demanded at any particular stage. Consideration is given in this section to some of the error sources in order to obtain test section design parameters. The errors have been expressed in terms of the aerodynamic interference at the model since this is the ultimate measure of acceptability.

3.1 Error due to wall adjustment strategy (two-dimensional)

The predictive strategy represented by equations 2.1 and 2.2 has an approximate theoretical basis because, in general, the walls and equivalent vortex sheets are not flat so that both the normal and tangential velocity components are in error. Since the first iteration away from the straight wall provides the bulk of the wall correction, this is used as the basis for the following error estimation.

For an internal velocity distribution $u_o(x)$ at the straight wall, equation 2.1 gives the new wall position as $y_1(x) = \Delta y_o(x)$ where

$$\frac{dy_1}{dx} = \frac{1}{2\pi U} \int_{-\infty}^{+\infty} \frac{[u_o(\xi) - U]}{(\xi - x)}\, dx \qquad 3.1$$

The flow external to this shape $y_1(x)$ could be obtained by replacing the surface with a distribution of vorticity $\gamma_v(x)$ and satisfying the exact normal velocity boundary condition:-

$$U \frac{dy_1}{dx} = \frac{1}{2\pi} \int_{-\infty}^{+\infty} \gamma_v(\xi) \frac{\left[(x - \xi) + (y_1(x) - y_1(\xi))\frac{dy_1}{dx}\right]}{\left[(x - \xi)^2 + (y_1(x) - y_1(\xi))^2\right]} \sqrt{1 + \left(\frac{dy_1}{d\xi}\right)^2}\, d\xi \qquad 3.2$$

For all anticipated wall shapes it may be assumed that $|\frac{dy_1}{dx}| << 1$ and $(y_1(x) - y_1(\xi))^2 << (x - \xi)^2$ so that equation 3.2 can be expanded to give

$$U \frac{dy_1}{dx} = \frac{1}{2\pi} \int_{-\infty}^{+\infty} \frac{\gamma_v(\xi)}{(x - \xi)} \sqrt{1 + \left(\frac{dy_1}{d\xi}\right)^2} \left\{1 + \frac{(y_1(x) - y_1(\xi))}{(x - \xi)} \frac{dy_1}{dx} - \frac{(y_1(x) - y_1(\xi))^2}{(x - \xi)^2}\right\} d\xi \qquad 3.3$$

where terms of order $(\frac{dy_1}{dx})^4$ have been neglected in the integrand. To the same order of accuracy it is found that the external tangential velocity $v_{1e}(x)$ is given by the exact equation as:-

$$v_{1e}(x) = \frac{U}{\sqrt{1 + \left(\frac{dy_1}{dx}\right)^2}} - \tfrac{1}{2} \gamma_v(x) \qquad 3.4$$

The external tangential velocity $v_1(x)$ is given by the approximate strategy of equation 2.2 as:-

$$v_1(x) = \tfrac{1}{2}[u_o(x) + U] \qquad 3.5$$

The difference $\Delta v(x) = v_{1e}(x) - v_1(x)$ represents the error in tangential velocity resulting from the approximate strategy, correct to order

$$\left(\frac{dy_1}{dx}\right)^2 .$$

Some manipulation of equations 3.1 to 3.5 is necessary to put $\Delta v(x)$ in a convenient form for assessment. First the vorticity $\gamma_v(x)$ is replaced using the following substitution:-

$$\gamma_v(x) \sqrt{1 + \left(\frac{dy_1}{dx}\right)^2} = -[u_o(x) - U] + \delta(x) \qquad 3.6$$

where $\delta(x)$ will always be small in practice compared with $u_o(x) - U$. Equations 3.4, 3.5 and 3.6 then give to order $(\frac{dy_1}{dx})^2$:-

$$\Delta v(x) = -\tfrac{1}{2}\,\delta(x) - \frac{U}{2}(\frac{dy_1}{dx})^2 \qquad 3.7$$

To a consistent order, equations 3.1, 3.3 and 3.6 yield:-

$$\int_{-\infty}^{+\infty} \frac{\delta(\xi)}{(x-\xi)}\,d\xi = \int_{-\infty}^{+\infty} \frac{[u_o(\xi) - U]}{(x-\xi)} \left\{\frac{(y_1(x) - y_1(\xi))}{(x-\xi)} \frac{dy_1}{dx} - \frac{(y_1(x) - y_1(\xi))^2}{(x-\xi)^2}\right\} d\xi \qquad 3.8$$

Equation 3.8 can be inverted to obtain $\delta(x)$ and this has been carried out for a series of simplified forms for $u_o(x) - U$ and $y_1(x)$, representative of a model consisting of vortex, source and doublet. In all cases the maximum value $|\delta(x)|$ was negligible compared with that of

$$U(\frac{dy_1}{dx})^2 .$$

It may therefore be concluded that the velocity error at the wall is

$$\frac{\Delta v(x)}{U} \simeq -\tfrac{1}{2}(\frac{dy_1}{dx})^2$$

Because of the distributed nature of $\Delta v(x)$, the corresponding velocity error Δu at the model will be somewhat less than the maximum value of $\Delta v(x)$. A conservative estimate will therefore be given by

$$\frac{\Delta u}{U} = -\tfrac{1}{2}(\text{maximum wall slope})^2$$

If the model is a lifting wing section, this can be interpreted as a force error in the form

$$\frac{\Delta C_L}{C_L} = -\frac{C_L^2}{128\pi^2}(\frac{c}{h})^2$$

where c is the wing chord and h is the test section depth. Even with a lift coefficient of 5 and c/h = 1, the error is less than 2%. The accuracy of the wall adjustment strategy represented by equations 2.1 and 2.2 therefore appears adequate, although it is desirable to monitor the maximum wall slope as a measure of the error.

3.2 Practical wall setting errors

Regardless of the accuracy of the wall setting strategy, it is recognised that the flexible walls can never be set exactly to the contours computed, but must lie within a tolerance band. In this section, the interference effects of the wall setting errors at the test model are analysed and estimated.

In any given test section of this type, there are likely to be many jacks along each wall, and position errors are likely to occur in a totally random manner, both in location and magnitude, within the tolerance band. The current low speed test section, has a wall setting accuracy of approximately $\pm$ 0.127mm ($\pm$ 0.005 inch or 0.00093c) and this is used in the analysis. Since the resulting wall errors are small, interference effects are expected to vary linearly with the wall tolerance allowing simple scaling.

In the analysis, the wall setting error is modelled as a bump or series of bumps in an otherwise straight walled two-dimensional test section and represented in a potential flow model as an equal source/sink pair lying on the wall line, combined with a system of images. The source/sink separation is taken equal to multiples of the jack spacing (approx. ½c). While this analytical representation of the wall errors is less

than ideal, it gives reasonable results for the interference effects.

The random nature of the wall setting errors, provides an infinite number of magnitudes of intereference effects. Hence interest centres on the maximum values likely to occur. Probability analysis of the wall setting errors has shown that there is a small, but significant, chance of a single bump occurring in the flexible walls. The interference effects found for this situation is taken as the probable worst case. The bump must then be close to the test model for maximum effect, thereby limiting the number of jacks involved.

Analysis estimates of the interference for a test section of one chord depth are

Angle of Attack error	0.025 degrees
Induced Camber	0.05 degrees
C_p error	0.0018 degrees

These three effects can be related to the lift coefficient of the test model producing a maximum interference as a C_L increment of about 0.002, a value which is insignificant in currently envisaged wind tunnel tests.

It must however be noted that the error is un-correctable, since its occurrence is random and set by the mechanical limitations of the test section. Nevertheless, the designer is to a large extent free to choose the tolerance, within cost constraints, but a limit to the wall setting precision must exist by virtue of the walls being positioned by a finite number of jacks. Hence, there is no control over the portions of the flexible walls between the jacks. Significant reductions in the interference effects, could however be achieved at minimum cost by reducing the tolerance only on jacks near the test model.

3.3 Errors due to finite test section length

Limitations on the length of test section which can have adjustable contours mean that the tunnel interference cannot be eliminated but must be kept instead to an acceptable minimum. Consideration of two-dimensional lift flow indicates significant streamline angularity with respect to the tunnel centreline at moderate C_L values even at distances of 5 to 10 chords up and downstream of the model. The presence of fixed geometry terminations therefore leads to (1) interference because the free streamline is not correctly represented and (2) possible ambiguities in the reference line for model incidence measurement.

A theoretical investigation of truncation errors was therefore made using the idealised geometry shown in Fig.3.1, where the solid walls are represented by four semi-infinite slits. For the two-dimensional case, a conformal transformation can be found to map the region cut by the slits onto the upper half of the transformed plane as shown in Fig.3.1. The incompressible velocity fields of the vortex, source and doublet in the real plane are readily determined by developing the complex potential in the transformed plane. Details of the method are available elsewhere[6]. In the present paper general observations are made and important results presented.

The effect of the streamline section in Fig.3.1 may be regarded as moving the wall disturbances which are producing the interference away from the region of the model and confining them to the slits. For small values of the ratio of model chord c to test section semi-length L, estimates of interference based on replacing the model by vortex, doublet and source will therefore be much more reliable than those used currently for tunnel corrections with totally solid walls and the same model representation. Moreover, if the wall effects can be regarded as providing some sort of mirror image with respect to the slit ends, it can be seen intuitively that the vortex and source interferences will vary inversely with 2L and the doublet interferences inversely with $(2L)^2$.

The theory[6] suggests that an ideal arrangement for minimising truncation errors is as shown in Fig.3.2. Here the model (defined by its lift centre) is located on the centreline and mid-way between the ends of the flexible section. The symmetry of this arrangement produces a zero angle of attack error for all values of h/L. If the separation between the downstream walls cannot be increased by the wake displacement thickness, a wake blockage will occur. The lift interference will arise, as in the case of the fully solid tunnel, as a streamline curvature at the model which is interpreted here as an equivalent camber. For design purposes the following results, applicable to the case of large L/h, are useful:-

Streamline curvature: $$\frac{\Delta C_L}{C_L} \simeq - \frac{a_1}{2\pi} \cdot \frac{1}{16} \left(\frac{c}{L}\right)^2$$

Wake blockage: $$\frac{\Delta C_D}{C_D} \simeq - \frac{C_D}{4\pi} \frac{c}{L}$$

where a_1 is the model lift curve slope. An interference less than 1% is obtained by an adjustable section length of 5 to 6 chords. Using the Prandtl-Glauert compressibility factor, it is found that even at a tunnel flow Mach number of 0.8 the length requirement

only increases by about 30%.

In summary, it has been shown in the various parts of this section that acceptable interference levels can be achieved with reasonable tunnel dimensions and tolerances. These tolerances determine the resolution and accuracy required of the numerical methods and computation.

4. INCORPORATION OF ON-SITE COMPUTER FOR A NEW TRANSONIC FACILITY

It is intended that the new transonic self streamlining test section currently being designed, will be completely automated both for flexible wall contouring and data acquisition from the test model, thereby providing a rapid system for obtaining two-dimensional aerofoil data, and also progressing towards a fully operational self-streamlining facility.

The incorporation of the computer with self-streamlining test sections is not new, but an on-line computer interface efficiently replaces the present manual link. Current design work envisages a system as illustrated by the block diagram in Fig.4.1, employing an existing PDP 11/40 computer. It can effectively be split into three sections from left to right:- (1) the computer on-line wall streamlining control, (2) the wind tunnel itself and (3) the computer dealing with data reduction. The process of data acquisition would be as follows. Using the wall setting strategy described in Section 2, the flexible walls would be set initially straight, probably driven by the computer to pre-selected co-ordinates. Then with the wind tunnel running, the wall pressure Scanivalve would be activated and all the wall static pressure tappings scanned. The computer then uses this data to compute a new set of wall co-ordinates by methods previously described.

The control then enters the outer system loop deciding whether the movements computed at the jacks are significant or not. The first iteration will be the largest so control passes into the inner loop, where the errors between present and demanded jack positions are driven to zero by a system involving motorised jacks and wall position sensors at each of the jacks.

The criterion of zero error satisfied, control drops out of the inner loop and the outer loop is repeated because the wall setting strategy is an iterative process. When the computed jack movements are within the tolerance, the flexible walls are taken to be streamlined. The final phase of the operating procedure is then activated, pressure data is acquired by the computer from the test model, immediately reduced and the results displayed at the wind tunnel.

The design of the actual two-dimensional test section has been very much influenced by the on-line control system envisaged for it. At each jacking point on the flexible walls, three connections into the control system are required. These are the static pressure tapping, the screw jack motor drive and the output from the jack position sensor, as shown in the cross-section view in Fig.4.2. Employing the existing rigid contraction, diffuser and sidewalls, the basic design must accommodate the planned 40 jack controls in close proximity to one another. The required movements of the flexible walls have been analysed and the jacks are designed for a maximum movement of $\pm$.5" from a mean position.

The test section height will be variable between approximately 8in and 3in. With an envisaged test model of 3in chord, the minimum test section height will be of order 1 chord, while the test section length will be greater than 10 chords. Ultimately the closeness of the flexible walls to the test model will probably be limited by the shock-wave growth on the upper surface, which will be monitored by schlieren methods. Shock wave reflections from the walls are not permissible for interference free conditions at the test model.

The basis of incorporating on-line computer control for a self-streamlining section has been laid. Detail design is complicated by the interaction of electronic, mechanical, aerodynamic and cost constraints. However, the benefits of the complete system are threefold:

1) Massive reduction in wall setting time, leading to more efficient use of wind tunnel run time.

2) More systematic operation from run to run.

3) A basic procedure more readily adapted to three-dimensional testing.

The disadvantage is the increase of complexity of the whole self-streamlining test section.

5. CONCLUSIONS

1) Strategies for determining streamline wall contours in two-dimensional flow have been successfully developed. Comparison of model results with interference free data shows excellent agreement.

2) The two-dimensional algorithms have been extended for use with three-dimensional compressible flows.

3) Tunnel design parameters such as test section length and wall setting tolerance have been considered for their interference contributions and hence in determining computational resolution.

4) The features of a fully automated self-streamlining transonic tunnel design have been outlined. On-line computational aspects include:-

(i) Calculation of wall setting demand.

(ii) Control of wall movement.

(iii) Model data acquisition.

REFERENCES

1. Goodyer, M.J. — The Self-streamlining Wind Tunnel NASA TMX-72699, August 1975.

2. Sears, W.R. — Self Correcting Wind Tunnels Royal Aeronautical Society Journal, Feb. 1974, pp.80-89.

3. Chevallier, J.P. — Soufflerie Transsonique a Parois Auto-Adaptables AGARD CP No.174, Oct. 1975.

4. Fage, A. and Falkner, V.M. — Further Experiments on the Flow Around a Circular Cylinder British ARC R and M 1369, 1931.

5. Allen, H.J. and Vincenti, W.G. — Wall Interference in a Two-Dimensional Flow Wind Tunnel NACA Report 782.

6. Judd, M., Goodyer, M.J. and Wolf, S.W.D. — Analytical Work in Support of the Design and Operation of Two Dimensional Self Streamlining Test Sections NASA CR (To be published).

ACKNOWLEDGMENT

The present work is sponsored by NASA Langley Research Center under grant NSG - 7172.

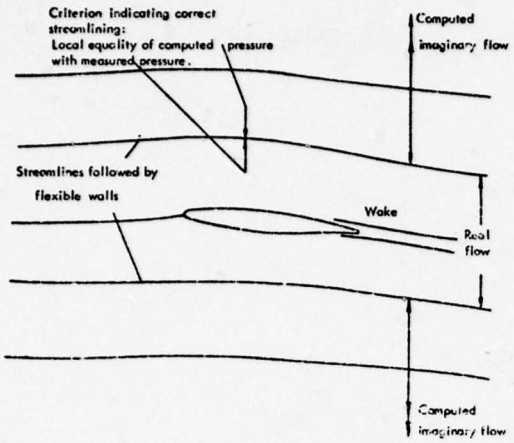

FIG.1.1 A TWO-DIMENSIONAL FLOWFIELD ILLUSTRATING THE PRINCIPLE OF TEST SECTION STREAMLINING.

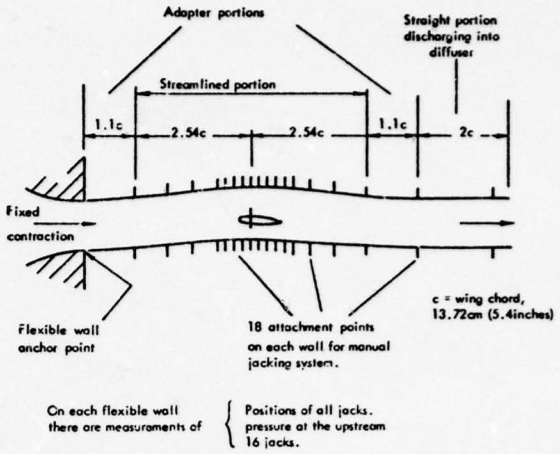

FIG.2.1 A SCHEMATIC DIAGRAM OF THE LOW SPEED TWO-DIMENSIONAL SELF STREAMLINING TEST SECTION.

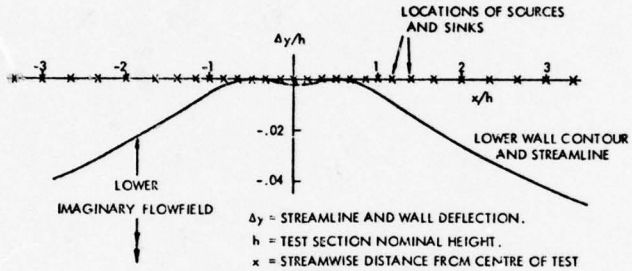

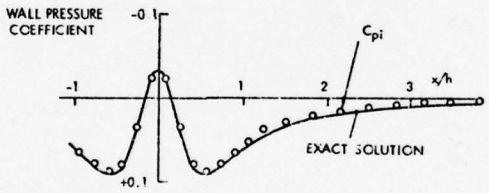

FIG.2.2A LOWER-WALL/STREAMLINE CONTOUR, AND COMPARISON BETWEEN THE EXACT WALL PRESSURE DISTRIBUTION AND THE WALL DISTRIBUTION C_{pi} COMPUTED WITH THE SOURCE/SINK GENERATION OF IMAGINARY FLOWFIELD.

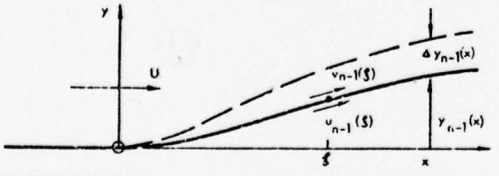

FREE STREAM VELOCITY, U

$y_{n-1}(x)$ PRESENT WALL POSITION.

$u_{n-1}(x)$ MEASURED INTERNAL VELOCITY FOR SHAPE $y_{n-1}(x)$

$v_{n-1}(x)$ CALCULATED EXTERNAL VELOCITY FOR SHAPE $y_{n-1}(x)$

ADJUSTMENT STRATEGY.

NEW WALL POSITION IS

$$y_n(x) = y_{n-1}(x) + \Delta y_{n-1}(x)$$

WHERE $$\frac{d\Delta y_{n-1}(x)}{dx} \simeq \frac{1}{2\pi U} \int_{-\infty}^{\infty} \frac{\left[u_{n-1}(\xi) - v_{n-1}(\xi)\right]}{(\xi - x)} d\xi$$

FIG.2.3 STRATEGY FOR RAPID WALL ADJUSTMENT.

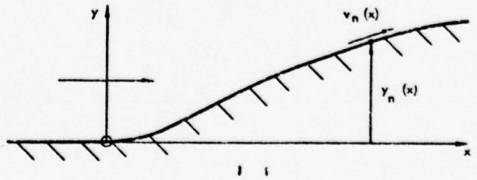

"CALCULATED" EXTERNAL VELOCITY FOR SHAPE $y_n(x)$ IS

$$v_n(x) \simeq \tfrac{1}{2}\left[u_{n-1}(x) + v_{n-1}(x)\right]$$

INITIAL EXTERNAL VELOCITY IS

$$v_o(x) = U$$

FOR THE STRAIGHT WALL.

FIG.2.4 EXTERNAL VELOCITY AT THE WALL.

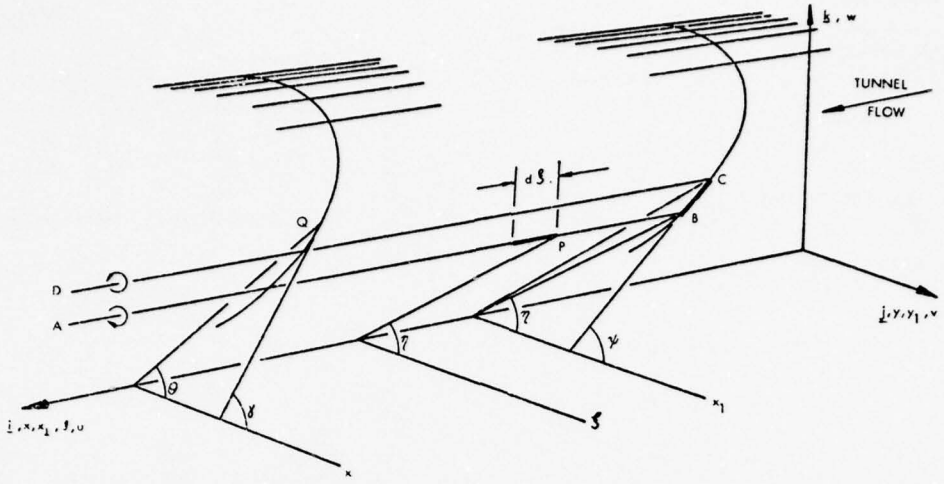

FIG.2.5 ELEMENTARY HORSESHOE VORTEX REPRESENTATION OF TUNNEL SURFACE.

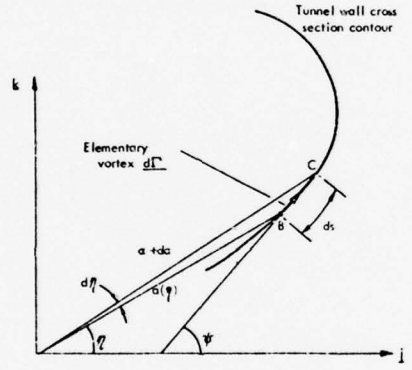

FIG.2.6 SECTION OF TUNNEL AT STATION x_1

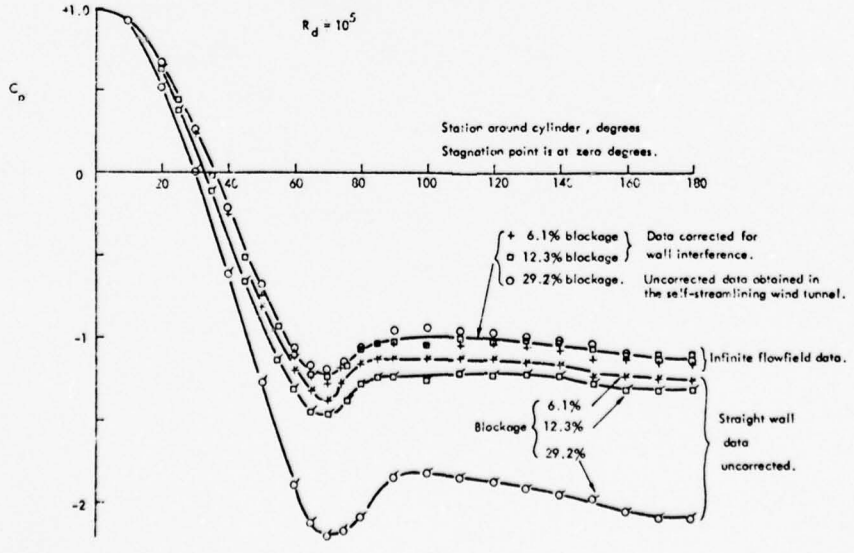

FIG.2.7 COMPARISONS OF PRESSURE DISTRIBUTIONS AROUND CYLINDERS MEASURED IN STRAIGHT WALLED AND STREAMLINED TEST SECTIONS.

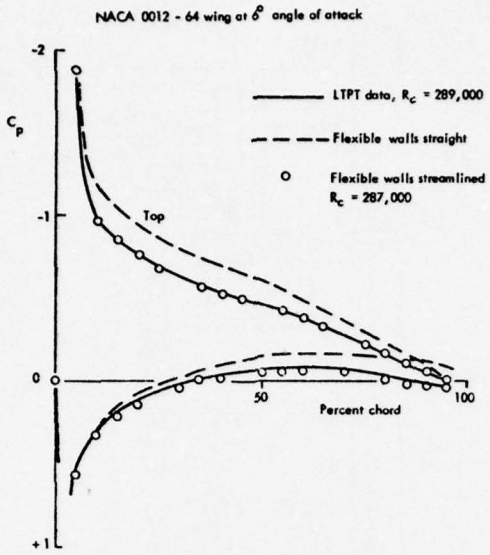

FIG.2.8 COMPARISON OF PRESSURE DISTRIBUTIONS AROUND A LIFTING WING.

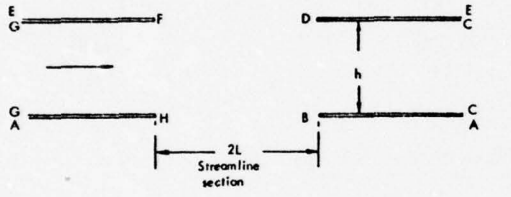

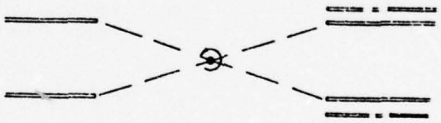

FIG.3.2 IDEAL MODEL POSITION FOR MINIMUM TWO-DIMENSIONAL INTERFERENCE DUE TO TRUNCATION.

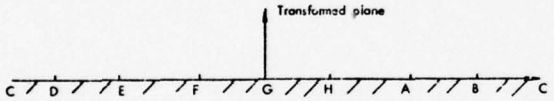

FIG.3.1 CONFORMAL TRANSFORMATION FOR DETERMINATION OF INTERFERENCE DUE TO WORKING SECTION TRUNCATION.

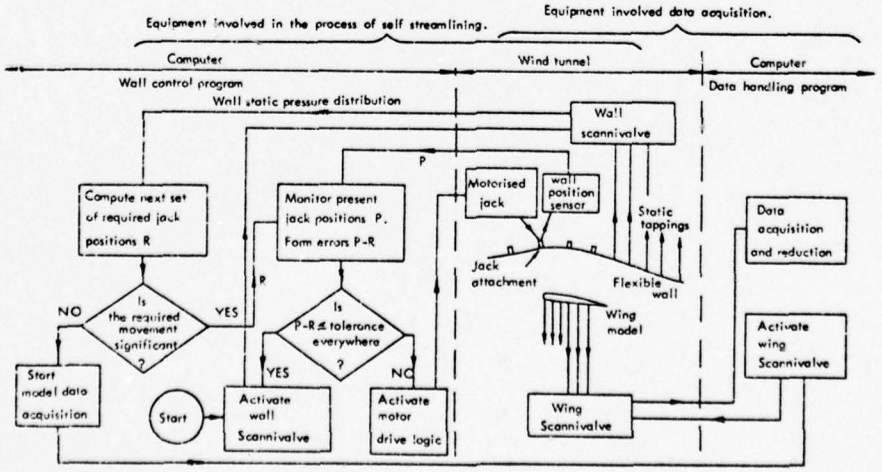

FIG.4.1 THE COMBINATION OF COMPUTER AND WIND TUNNEL FOR ON-LINE WALL STREAMLINING AND ACQUISITION OF TEST DATA.

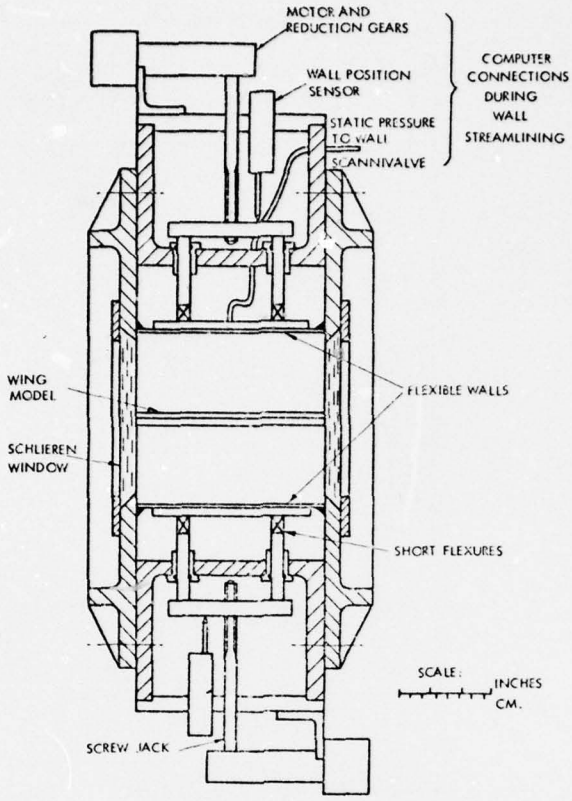

FIG.4.2 THE TRANSONIC SELF STREAMLINING TEST SECTION DESIGN – A VERTICAL CROSS SECTION LOOKING ALONG THE FLOW.

ADAPTATION DE LA METHODE DE JOPPA A UNE SOUFFLERIE A PERMEABILITE VARIABLE .

par

Jean-Ch. VAYSSAIRE

Avions Marcel Dassault - Breguet Aviation (AMD-BA)
92214 SAINT-CLOUD - France

M. LANGOT M. MENARD

Institut Aérotechnique St Cyr (IAT St Cyr)
78210 SAINT-CYR - France

RESUME

La méthode de calcul de JOPPA qui découpe les parois d'une veine de soufflerie en éléments rectangulaires d'intensité tourbillonnaire inconnue tient compte des dimensions de la veine et de la nature de ses parois. La position relative de la maquette dans la veine, ainsi que sa géométrie et sa répartition de circulation en envergure permettent de calculer les perméabilités théoriques nécessaires en tous points de parois ventilées pour minimiser ou annuler leur effet au droit du modèle.

A l'intérieur des caissons étanches qui entourent la veine d'essais de la soufflerie Sigma 4 (I.A.T. St Cyr) se trouvent des plaques flexibles, pleines et mobiles. Leur déplacement contribue à faire varier la perméabilité en tous points des parois perforées de la veine.

En présence de la maquette (dont les caractéristiques servent aux calculs), les perméabilités réelles sont connues par des relevés de pressions statiques.

En ajustant les perméabilités expérimentales réalisées par déplacement des plaques mobiles des caissons aux perméabilités théoriques calculées, il est possible de réaliser le but recherché correspondant à des besoins d'essais déterminés, notamment des effets de parois nuls.

En complément, la régulation de la vitesse dans la veine d'essais, au droit de la maquette, est asservie au calculateur qui fait varier la section du second col par pilotage de ses parois mobiles.

Acquisition des données au cours des essais, dépouillements et tracé des résultats expérimentaux sont effectués en temps réel par le calculateur de la Soufflerie.

SUMMARY

The Joppa calculation method divides the walls of a wind-tunnel working section into rectangular éléments with an unknown vortex ring strength and takes account of the test section dimensions and boundaries. The relative position of the model in the section,as well as its geometry and lift distribution spanwise allow the calculation of the theoretical permeability in any point of the ventilated walls to minimize or cancel its effect in the area of the model.

Inside the plenum chambers which are around the test section of the Sigma 4 wind tunnel (I.A.T. St-Cyr), flexible, solid and movable plates are found. The movement of the plates contribute to the variation of the permeability in any point of the working section perforated walls.

With the model present (whose characteristics are used in the calculations), the real permeabilities are known through static pressure holes.

By adjusting the permeabilites experienced by movement of movable plates in the plenum chamber with calculated theoretical permeabilities, it becomes possible to achieve the aim wanted which corresponds to the requirements of determined tests, namely zero wall effects.

In addition, the speed regulation in the working section, in the area of the model is connected with the computer which varies the cross section of the second throat by piloting its movable walls.

Data acquisition during the tests, processing and plotting of the test results are carried-out in real-time by the wind tunnel computer.

NOTATIONS

B	largeur de veine
C	section de veine = H^2
C_D	coefficient de traînée
C_L	coefficient de portance
C_M	coefficient de moment de tangage
H	hauteur de veine
K	coefficient de pression
L	longueur de veine
Mo	nombre de Mach
N	nombre de pavés = $N_s . N_x$
Q	porosité relative
R	facteur de porosité
V	vitesse du vent
XLEN	longueur d'un pavé
a	largeur d'un pavé
l_t	longueur de queue
$\bar{l}_a$	corde aérodynamique moyenne
p	pression
po	pression de référence
pc	pression dans le caisson
q	pression cinétique
2s	envergure de l'aile
v_n	vitesse normale à la paroi
w	vitesse induite
xyz	coordonnées cartésiennes
α	angle d'incidence
β	= $\sqrt{1 - Mo^2}$
Γm	circulation de l'aile
Γw	circulation de paroi
δ	facteur de correction d'incidence
δl	facteur de correction de courbure du champ
Δp	différence de pression
Λ°	flèche à 25 % de profondeur des cordes de l'aile
ρ	masse volumique
σ	= 2s/H
φ	potentiel
φ^*	potentiel unitaire = φ/Γ

1 INTRODUCTION

D'une manière générale, la possibilité d'appliquer des corrections de parois aux résultats d'essais en soufflerie procède du calcul des vitesses de perturbation induites par des potentiels représentatifs des parois supposées de longueur infinie en présence d'une ou plusieurs singularités qui schématisent la maquette.

Le développement du calcul numérique (méthode des singularités) proposé par Joppa (1) permet de calculer ces vitesses en tout point à l'intérieur de la veine d'essais en tenant compte des valeurs dimensionnelles relatives de l'ensemble maquette/veine considéré, c'est-à-dire de paramètres tels que :

- la forme géométrique réelle de la veine, quelles que soient sa section, ses dimensions (notamment sa longueur) et la nature de ses parois ;
- la forme géométrique de la maquette d'avion : envergure (avec sa répartition de circulation) et flèche de la voilure, corde aérodynamique moyenne, longueur de queue.

Ce principe de calcul numérique offre trois possibilités :

i) faire des études paramétriques de veines d'essais répondant à des besoins précis, en vue de leur réalisation future, tels que ceux nécessités, par exemple, par la mise au point d'avions du type A.D.A.C. (2) ;

ii) calculer et appliquer des corrections dans des soufflerie existantes en tenant rigoureusement compte de leur géométrie et de celle de la maquette quelle que soit la nature des parois : pleines (1) ou ventilées (3) ;

iii) réduire ou annuler l'effet des parois dans le cas précis où les parois ventilées possèdent une perméabilité adaptable.

Ces possibilités ont été exploitées par les Avions Marcel Dassault - Bréguet Aviation - AMD-BA - (4,5) - Les deux dernières, en particulier, sont utilisées dans la présente étude dont le but est de montrer comment dans une soufflerie existante, à Mach variable de 0,4 à 2.8 - Sigma 4 de l'Institut Aérotechnique de Saint-Cyr (Fig.1) - conçue avec des parois à perméabilité adaptable, il est possible d'ajuster la porosité expérimentale des parois perforées horizontales de la veine de section carrée (0,85 x 0,85 m) à une valeur théorique calculée pour une maquette en vue de rendre négligeables certaines corrections. On se propose plus spécialement d'annuler les corrections qui portent sur les moments de tangage(car les courbes C_L , Cm sont généralement les plus torturées et les moins linéaires) en régime sub/transsonique.

En outre, le second col de cette soufflerie, situé immédiatement en aval de la veine, est réalisé par des parois latérales mobiles dont la position permet de réguler le Mach tout en éliminant expérimentalement les effets de blocage dus à la présence de la maquette et à ses sillages dans la veine. La pression cinétique corrigée ou vraie est ainsi obtenue et elle demeure constante quelle que soit la position du modèle.

Enfin, cette soufflerie est commandée et contrôlée, en temps réel, par son propre ordinateur pendant toute la durée d'un essai au cours duquel la position angulaire de la maquette ou le nombre de Mach, par exemple, varient d'une façon continue, l'acquisition des mesures et la régulation en Mach étant assurées. De façon à réduire le temps de rafale, le dépouillement ne commence qu'à la fin de l'essai. L'ordinateur et ses périphériques permettent, quelques instants après, d'obtenir le tableau de chiffres et les courbes correspondantes.

Ainsi, grâce au calcul numérique, d'une part, qui impose des conditions théoriques d'essais et, d'autre part, à un ordinateur qui pilote une soufflerie munie d'éléments adaptables et mobiles, il est possible d'obtenir en moins de quatre minutes après l'essai le tracé des courbes [$C_L, C_D - C_L, C_M - C_L, \alpha$]

représentatives des résultats exempts pratiquement d'effets de parois. La durée de l'essai, au cours duquel l'incidence a varié de façon continue de 20 degrés, est toujours inférieure à 60 secondes, durée maximale qui correspond à M ~ 1.

2. CALCUL DES CORRECTIONS DE PAROIS PAR LA METHODE DES SINGULARITES - AVANTAGES - APPLICATIONS

2.1. Généralités

Grâce à la méthode de calcul numérique (Vortex Lattice Method) due à Joppa, il est possible de déterminer les vitesses induites par les parois guidées d'une veine de section arbitraire (1). Généralisée par Borovik aux parois ventilées (3), cette méthode fut alors adoptée et développée par A.M.D.B.A. (4,5).

Le calcul des corrections d'incidences et des moments de tangage est établi à partir de potentiels de tourbillons tridimensionnels :

$$\varphi_m = \varphi_{m_1}(y,z) + \varphi_{m_2}(x,y,z).$$

L'aile de forme en plan quelconque, d'envergure 2s, de flèche $\Lambda°$, découpée en 2M tourbillons d'envergure S/M, peut recevoir une répartition de circulation imposée a priori (Fig.2) - Introduisant le potentiel unitaire : $\varphi^*_m = \varphi_m / \Gamma_m$, la répartition de circulation est ainsi mise en évidence :

$$\varphi_m = \Gamma_m \left(\varphi^*_{m_1} + \varphi^*_{m_2} \right).$$

Une loi de circulation elliptique, jugée suffisante pour le but recherché, fut retenue par A.M.D.B.A.

2.2. Description

2.2.1. L'aile est placée au centre d'une veine de section carrée du type de celle de la soufflerie Sigma 4. Dans ces conditions, un quart de la veine peut être considéré (Fig. 2).

Les parois sont découpées en rectangles dont les côtés sont désignés par XLEN et a. Leur nombre $N=N_s.N_x$. La méthode de calcul numérique demande de prendre quelques précautions dans le choix de leur allongement XLEN/a.

AMDBA a développé cette méthode en portant la valeur de N à 160 , soit $N_s = 8$ et $N_x = 20$. Ainsi un bon compromis est réalisé entre la précision recherchée dans le calcul des facteurs de corrections et le temps d'utilisation de l'ordinateur. Des études paramétriques ont montré que pour N = 160, l'allongement XLEN/a pouvait prendre indifféremment n'importe quelle valeur comprise entre 0,7 et 1.9 - Grâce à ce résultat, l'effet de la longueur de la veine $L = N_x.XLEN$ sur les facteurs de correction peut être mis en évidence.

Dans le cas de calcul présenté Fig.3 , qui correspond à une demi-maquette à la paroi, N = 240 avec $N_s = 12$.

2.2.2. La méthode de calcul repose sur une double application de la loi de Biot - Savart.

Si $\varphi^*_{w_j} = \varphi_{w_j} / \Gamma_{w_j}$ représente le potentiel tourbillonnaire unitaire de chaque pavé de la paroi, alors :

$$\varphi_w = \sum_{j=1}^{N} \varphi^*_{w_j} \Gamma_{w_j}$$

$$(j = 1,2 \ldots N = N_s.N_x)$$

De même, si $\varphi^*_{m_n} = \varphi_{m_n} / \Gamma_{m_n}$ représente le potentiel unitaire de chaque tourbillon d'aile d'envergure S/M :

$$\varphi_m = \sum_{n=1}^{M = 10\sigma} \varphi^*_{m_n} \Gamma_{m_n}$$

$$(\sigma = 2s/H)$$

L'influence du potentiel unitaire de chaque pavé et celle du potentiel unitaire de chaque tourbillon d'aile sont introduites dans une suite d'équations linéaires :

$$\sum_{j=1}^{N} A_{ij} \Gamma_{w_j} = \sum_{n=1}^{M=10\sigma} B_{in} \Gamma_{m_n}$$

$$(i = 1,2 \ldots N = N_s.N_x)$$

ou $A \cdot \Gamma_w = B \cdot \Gamma_m$.

Connaissant la répartition de circulation Γ m, par une inversion de matrice, on en déduit Γw en s'imposant des conditions aux limites qui tiennent compte de la nature des parois qui, en l'occurence dans notre cas, sont des parois perforées de porosité R. Alors la matrice A :

$$A = \varphi^{*}_{w_x} + \frac{1}{R} \varphi^{*}_{w_n} \qquad (n = y, z)$$

fixe les dimensions et la forme de la veine ainsi que le nombre et la position des points de contrôle. La matrice B :

$$B = \varphi^{*}_{m_x} + \frac{1}{R} \varphi^{*}_{m_n} \qquad (n = y, z)$$

définit l'influence de l'aile sur les parois.

La connaissance de Γw permet le calcul des vitesses normales induites par les parois w(x, y), d'où les facteurs de correction d'incidences δ (x, y) et de courbure du champ aérodynamique δ_1(x, y) :

$$\delta = \frac{w\ H^2}{4s\ \Gamma_m} \qquad \delta_1 = \frac{H^3}{4s\ \Gamma_m} \frac{\partial w}{\partial x}$$

en considérant la veine de section carrée $C = H^2$.

Pour chaque valeur de x en aval de la ligne portante, il convient de prendre la valeur moyenne de δ et celle de δ_1 en envergure soit : $\bar{\delta}$ (x) et $\bar{\delta}_1$ (x).

Sur I.B.M. 370/168, le calcul de $\bar{\delta}$ (x) et de $\bar{\delta}_1$ (x), pour 20 valeurs de x/ β H, pour une aile ($\Lambda°$, σ), et une porosité R donnée, se fait en 1 minute 15 secondes si N = 160 et 2 minutes 55 secondes si N = 240.

Le contrôle du premier cas de calcul en double précision demande 1 minute 41 secondes mais s'est avéré inutile de façon usuelle.

2.3. Effets de la longueur et de la géométrie de la section de la veine

Le calcul des facteurs de corrections δ_0 (x = 0) et δ_1 (x) a été effectué pour une même aile ($\Lambda = 0°$) d'envergure relative σ = 0,6 placée dans trois veines d'essais différentes (V_1 , V_2 , V_3) de section carrée (Fig.4).

La Fig.5 donne, pour les trois veines, la variation de δ_0 en fonction de la porosité relative Q=1/1+ β/R. On constate que l'effet de la longueur de la veine est d'autant plus sensible que la porosité des parois horizontales croît et tend vers celle de parois libres. Les bandes latérales horizontales pleines augmentent la valeur de Q pour laquelle $\delta_0 = 0$ et en conséquence diminuent les valeurs de δ_0 lorsque Q tend vers 1.

La Fig.6 donne, pour les trois veines, la variation de δ_1 en fonction de l'abscisse relative x/β H. Le facteur δ_1 n'est pas sensible à l'effet de la longueur de la veine guidée. Mais cette sensibilité apparait et croît avec R.

Pour une valeur de x/ β H fixée, pour annuler δ_1, des parois perforées munies de bandes latérales pleines nécessitent une porosité supérieure à celle qui correspond à des parois perforées qui occupent toute la largeur de la veine.

2.4. Annulation des corrections de moments de tangage

Le principe consiste à trouver, pour toute valeur du Mach, une porosité R qui annule le facteur de correction δ_1(x) au droit de l'empennage horizontal (dans le cas, par exemple, d'un avion de transport) ou aux trois quarts de la corde aérodynamique moyenne (aile delta) (15).

Ainsi pour une maquette définie par la flèche $\Lambda°$ de l'aile et son envergure relative σ , les éléments d'un réseau de courbes $\delta_1 = f(x/\beta H)$ sont d'abord calculés pour plusieurs valeurs de R/β (Fig.7). La courbe $R/\beta = f(x/\beta H)$ qui correspond à $\delta_1 = 0$ en est déduite.

La maquette est définie aussi géométriquement par sa longueur de queue relative : lt/H.

Le calcul de R qui annule δ_1 pour toute valeur de M_o est résumé dans le schéma qui suit. La valeur du facteur δ_0 qui correspond à R/β s'obtient alors à partir de $\delta_0 = f(Q)$. Cette valeur est d'ailleurs faible.

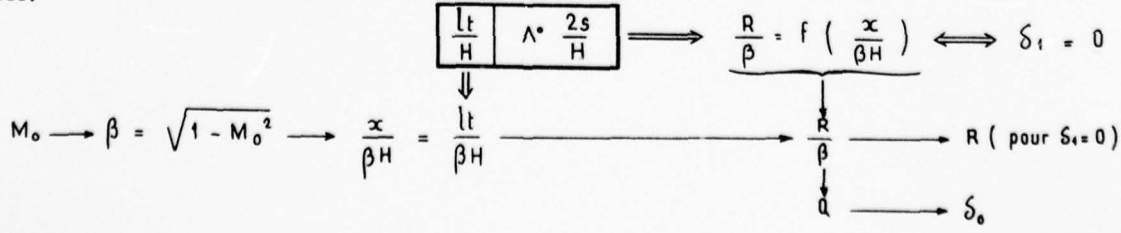

La Fig.8 donne les résultats de ces calculs pour deux maquettes, qui diffèrent par leurs échelles, d'un avion de transport ($\Lambda = 30°$). Cette figure donne aussi les résultats de calculs relatifs à une aile delta.

On constate que pour obtenir $\delta_1 = 0$, la porosité R varie peu en fonction du nombre de Mach. La valeur de R croît avec la taille de la maquette. Une grande maquette est donc à suggérer pour profiter des avantages d'essais dus à une porosité élevée (4,11). Néanmoins les effets du blocage limitent ces dimensions (4).

3. LABORATOIRE D'ESSAIS ($0.4 < M_0 < 2.8$) SOUFFLERIE SIGMA 4 - I.A.T. St-CYR

3.1. Généralités

SIGMA 4, soufflerie sub/trans/supersonique, à rafales, est entrée en exploitation en 1960. La genèse de sa conception, ses caractéristiques et ses possibilités d'essais ont été présentées en 1962 (6). Elle est à circuit ouvert. Sa pression génératrice est sensiblement celle de l'atmosphère.

Son tunnel aérodynamique, seul, nous intéresse (Fig.1). Il comporte un collecteur, la veine d'essais de section carrée et un diffuseur. Chacune de ces parties est mobile ou possède des éléments mobiles. Il se présente ainsi sous la forme d'une tuyère à deux cols réglables (7,8). Ces cols sont disposés en amont et en aval de la veine dont les parois horizontales, perforées, sont à porosité adaptable.

La réalisation d'essais à tous les nombres de Mach compris entre 0,4 et 2,8 est donc possible. La variation continue du Mach est obtenue grâce au déplacement de deux bulbes profilés qui régit la grandeur de la section droite de la tuyère au premier col, associée d'ailleurs à la variation de la section rectangulaire du second col. La différence de pression nécessaire à l'obtention de chaque Mach résulte du vannage adéquat des tuyères d'injection.

A ce sujet on doit rappeler l'originalité du système énergétique. L'aspiration de l'air dans la veine est faite à l'aide de quatre trompes à induction alimentées par de l'eau chaude sous pression (9). Les tuyères d'injection pénètrent dans la chambre d'induction qui est placée immédiatement en aval du diffuseur.

3.2. Variation continue du Mach - Association premier - second cols (7,8)

3.2.1. Le collecteur est constitué par deux parois verticales planes et parallèles dans le prolongement de celles de la veine d'essais (Fig.1). Les deux autres parois se rapprochent progressivement l'une de l'autre de façon à permettre le rétrécissement de la section jusqu'à la section de la veine proprement dite.

Deux demi-corps profilés sont appliqués par leur surface plane contre les parois verticales du collecteur. Leur grand axe est parallèle à l'axe horizontal de celui-ci et leur face convexe est tournée vers l'intérieur de la tuyère. Ces bulbes et le collecteur forment le premier col (Fig.9) (Système Ménard).

3.2.2. En écoulement subsonique et transsonique inférieur ($0,4 < M_0 \leqslant 1$), les deux bulbes situés en position extrême amont, demeurent fixes (Fig.9a).

Les parois pleines horizontales du second col prolongent celles de la veine, alors que ses parois verticales sont mobiles. En amont, elles sont pourvues de perforations que l'on peut obstruer à l'aide de portes pivotantes (Fig.1). Ce second col est entouré d'un caisson étanche qui continue celui qui se trouve tout autour de la veine.

L'ouverture du deuxième col est réduite au maximum de façon à provoquer un col sonique - Mo = 0,4 est obtenu. La variation progressive de son ouverture permet d'augmenter la valeur du Mach (Fig. 10). Mach 1 est atteint lorsque les parois verticales du second col se trouvent sensiblement dans le prolongement des parois verticales de la veine.

Mais à partir de Mach 0,8/0,9 les portes auxiliaires du second col doivent être ouvertes de façon à augmenter le débit d'air aspiré par l'auto-aspiration du diffuseur à travers les parois perforées de la veine (Fig. 10).

3.2.3. Ecoulement transsonique supérieur et supersonique

Au-delà de Mach 1, de façon à transférer le col sonique vers le premier col, l'ouverture du second col continue à croître jusqu'à Mach 1,2 (Fig. 10). Il en résulte ainsi une augmentation de l'aspiration auxiliaire du diffuseur supersonique.

Mais par suite du nouvel emplacement du col sonique, à partir de Mach 1 en théorie, en fait à partir de Mach 1,1 , à cause des écoulements visqueux, les deux bulbes se déplacent alors de leur position amont vers l'aval de façon continue (Fig. 9b).

La section de passage offerte au fluide diminue et le col sonique qui prend naissance entre les bulbes au minimum de section va en diminuant. Le nombre de Mach dans la veine, dont la section demeure constante, augmente donc continûment jusqu'à une valeur légèrement inférieure à 2,8 qui correspond à la position extrême aval des bulbes.

Revenons au second col (Fig.10).

A partir de Mach 1,2 , le diffuseur supersonique de la soufflerie est refermé progressivement au fur et à mesure de l'augmentation du nombre de Mach de l'essai. Le Mach dans le diffuseur diminue donc progressivement et la recompression par choc droit a lieu à un nombre de Mach beaucoup plus faible que celui de la veine. La perte de charge par choc droit est donc réduite, ce qui a pour effet d'augmenter le rendement énergétique de la soufflerie.

Vers Mach 1,7/1,8 , les portes auxiliaires sont fermées.

Le fonctionnement en supersonique s'établit. C'est d'ailleurs cet écoulement qui conditionne la grande longueur ($l \cong 5H$) de la section constante du second col. En effet, elle correspond à la distance entre la position du choc de recompression et l'entrée du diffuseur subsonique nécessaire pour stabiliser la couche limite de paroi après l'interaction du système de choc de recompression sur cette dernière (7).

3.3. Veine d'essais (6, 11)

La veine de section carrée (Fig.1) a pour dimensions effectives aérodynamiques : 0,85 x 0,85 m.
Soit $C = H^2 = 0,723$ m2.

En effet les épaisseurs des couches limites qui se développent sur les parois sont compensées par une légère divergence longitudinale des parois horizontales. Ces couches limites pariétales jouent d'ailleurs un rôle auto-régulateur de la veine fluide et contribuent à diminuer l'intensité du blocage (10).

Les parois verticales sont pleines. Les deux parois horizontales comportent des surfaces rectangulaires, perforées, de perméabilité géométrique égale à 29,7%, délimitées par deux bandes latérales pleines placées dans les angles de la veine (Fig.12). Chaque surface rectangulaire est précédée d'un triangle perforé (perméabilité 14,85 %) dont la pointe est dirigée vers l'amont du courant d'air pour assurer son uniformité.

Les parois ont pour épaisseur 10 mm. Les perforations dont les axes sont normaux aux parois ont un diamètre égal à 4,2 mm.

A l'extérieur des parois perforées et placées dans les caissons étanches qui les entourent se trouvent des tôles pleines, flexibles et longitudinalement déformables à l'aide de trois vérins électriques dont les courses sont de 60 mm environ (Fig.11). Leur déplacement contribue à modifier la perte de charge de l'écoulement auxiliaire qui traverse les parois perforées. Il est ainsi possible de faire varier et contrôler la porosité de ces dernières, lors des écoulements subsoniques et transsoniques (Fig.11). A noter que les porosités des parois supérieure et inférieure peuvent être éventuellement modulées de façon différente, car la mobilité des parois flexibles est indépendante l'une de l'autre.

Les tôles flexibles sont équipées sur la partie interne d'un coussin de caoutchouc mousse qui permet, lorsqu'elles sont plaquées contre les parois perforées de la veine, de réaliser une veine guidée parfaite pour les essais en supersonique élevé et aussi en faible subsonique (Fig.11).

Ainsi grâce à son dispositif de parois mobiles, et flexibles, une veine unique permet d'assurer les essais en écoulement sub/trans/supersonique.

3.4. Mesure des pressions - Détermination expérimentale de la porosité R (11)

3.4.1. Des prises de pression statique sont disposées longitudinalement sur les quatre bandes latérales non perforées des parois horizontales (Fig.12). Le contrôle du champ des vitesses et des gradients de pressions longitudinaux, en présence ou non de maquettes, qui se développent dans la veine en fonction de ses diverses configurations, associées à celles du second col, est ainsi possible (11). Le choix de l'emplacement de la prise de pression statique p_o de référence en a été déduit (11).

3.4.2. En outre, des prises de pression p_c sont placées au droit du centre de rotation du modèle sur la face des parois perforées extérieure à la veine. La mesure des différences de pression de part et d'autre de la paroi en présence de la maquette est ainsi aisée. Les parois flexibles peuvent donc être adaptées de façon à obtenir des différences de pression correspondant aux valeurs théoriques de la porosité R imposée, comme il va être montré.

Au préalable un échantillon de paroi perforée du type de celle utilisée dans SIGMA 4 a été étalonné.

Le dispositif expérimental utilisé est reproduit ci-contre. L'échantillon est caractérisé par un coefficient de perte de charge :

$$K = \frac{\Delta p_n}{\frac{\rho_o}{2} v_n^2} = 13$$

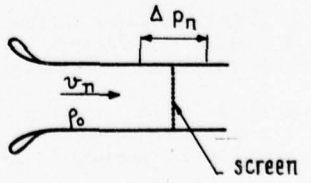

pour des vitesses uniformes v_n comprises entre 6 et 20 m/s.

Maintenant, $\Delta p_p = p_n - p_c$ désigne la différence de pression entre la veine dans laquelle se trouve la maquette et le caisson étanche. Par définition, le paramètre de porosité R :

$$R = \frac{\rho V v_n}{\Delta p_p}$$

où v_n désigne la composante normale à la paroi de la vitesse de l'écoulement auxiliaire, et V la vitesse de l'écoulement principal de masse spécifique ρ.

Avec : $$K_p = \frac{\Delta p_p}{\frac{\rho}{2} V^2} ,$$

et en admettant que $\Delta p_n = \Delta p_p$, il vient :

$$\frac{V}{v_n} = \sqrt{\frac{K}{K_p} \frac{\rho_o}{\rho}}$$

soit :

$$R = \frac{\rho V v_n}{K \frac{\rho_o}{2} v_n^2} = 2\sqrt{\frac{\rho}{\rho_o}} \sqrt{\frac{1}{K K_p}} = 2\sqrt{\frac{\rho}{\rho_o}} \sqrt{\frac{q}{13.\Delta p_p}} ,$$

Un exemple de courbes expérimentales R = f(Mach) déterminées en présence de maquettes pour une position fixe des parois flexibles est donné Fig.8. Il confirme le tracé des courbes théoriques R = f(M_o), donc la possibilité d'adapter la porosité des parois perforées à une valeur qui annule les corrections de moments de tangage, comme il a été expliqué en 2.4.

3.5. Gradients de pression statique longitudinaux

Certaines configurations de la soufflerie introduisent des gradients parasites. Il en est ainsi lorsqu'à faible Mach, les portes du second col sont ouvertes. La Fig.13 traduit cet effet en donnant l'évolution du coefficient de traînée C_D d'une maquette en fonction de M_o. Ces portes d'ailleurs ne sont ouvertes que pour des Mach élevés. L'influence du gradient diminue lorsque M_o croît et l'on sait en tenir compte par une correction connue (H.Ludwieg Drag corrections in high-speed wind tunnels NACA TM 1163 - Göttingen 1944).

La Fig.13 montre aussi que lorsque le gradient de pression statique dans la veine avec maquette est nul, les résultats bruts obtenus sont exempts d'effet de blocage : ils sont confondus avec les résultats corrigés acquis avec la même maquette en présence de parois guidées.

Les nombreuses prises de pressions disposées longitudinalement et reliées à un multimanomètre permettent constamment le contrôle du gradient. L'expérience montre qu'une légère correction de la forme des parties amont et aval des parois flexibles autour de la position privilégiée qui donne à R la valeur nécessaire pour avoir $\delta_1 = 0$ est suffisante pour obtenir un gradient nul.

Cette correction est d'autant plus faible voire négligeable que la porosité R est élevée ($\geqslant 4$) ce qui est le cas pour la plupart des essais. On aboutit ainsi à donner aux parois flexibles le profil reproduit sur la Fig.11, imposé par l'action des vérins, fonction des pressions statiques.

4. ORDINATEUR/SOUFFLERIE - RESULTATS OBTENUS

4.1. Soufflerie SIGMA 4 (12)

La soufflerie SIGMA 4 est pilotée par son propre ordinateur, Télémécanique T 1600, pendant toute la durée d'un essai à partir du moment où l'ordre lui en est donné (Fig.14).

Au cours d'un essai en régime continu, n - 1 paramètres de soufflerie sont tenus constants. L'ordinateur assure la double fonction d'une part, de faire varier régulièrement, suivant une loi programmée, le nième paramètre qui peut être l'incidence ou le Mach selon le mode d'utilisation de la soufflerie et d'autre part, de mettre en oeuvre en "temps réel" l'acquisition de signaux émis par les appareillages de mesure au cours de la variation du nième paramètre (12).

L'ordinateur possède aussi des lignes de sorties qui permettent des commandes diverses numériques ou analogiques. La conjugaison acquisition/commandes donne à l'ordinateur des fonctions de régulation. Il en est ainsi de celle du Mach en écoulement subsonique (Fig.15).

En effet, dans ce cas, la vitesse dans la veine dépend du rapport de la section fluide de cette dernière à celle du second col sonique.

Pour une même position des parois de ce col, la vitesse obtenue dépend donc de la taille de la maquette, ainsi que de son incidence ou de son angle de dérapage. Comme ces angles varient au cours d'une rafale, l'ordinateur rattrape les écarts en Mach à partir des acquisitions de la pression statique de la veine en modifiant l'écartement des parois mobiles du second col. Cette régulation fournit une stabilisation :
$\Delta M = \pm 0{,}001$.

Un essai réalisé à $M_o = 0{,}5$, avec une maquette d'avion AMDBA, dans les conditions qui viennent d'être

décrites, en s'imposant une valeur de la porosité R destinée à annuler les corrections de moments de tangage, a donné les résultats présentés Fig.16. La durée de l'essai qui comporte l'acquisition des données dépend du Mach. En effet la vitesse de déroulement d'incidence $\alpha°$ est donnée par la loi établie expérimentalement :

$$\Delta\alpha°/s = 0{,}375 + 0{,}75 \cdot |M_o - 1| ,$$

soit pour $M_o = 0{,}5$: $\Delta\alpha°/s = 0°{,}75/\text{seconde}$.

Pour diminuer le temps de rafale, le dépouillement, qui tient compte des effets du dard et des pressions de culot, n'intervient qu'après l'essai. Dépouillement et tracé des courbes représentatives des résultats demandent environ 11 secondes/degré.

La précision de la chaîne de mesure est de $\pm$ 1 bit soit environ 6.10^{-5} de la pleine échelle et pour une cadence de 50.000 points/seconde (50 K hertz).

4.2. Remarques

L'introduction des ordinateurs dans les essais aérodynamiques, associés aux chaînes de mesures est récente et liée aux progrès réalisés dans leurs performances. Leur utilisation dans les souffleries à grande vitesse munies de parois ventilées devint opérationnelle vers 1967 aussi bien à l'IAT St-Cyr qui utilisait alors un ordinateur C.I.I.90.10 (12,13) qu'à l'O.N.E.R.A. (Modane) - (13,14) - Le but recherché était d'acquérir les données et de dépouiller les résultats en temps réel, sans se préoccuper de l'effet des parois supposé négligeable. Il est vrai qu'à cette époque, le problème de la connaissance théorique de l'effet des parois ventilées était loin d'être résolu.

4.3. Souffleries basse vitesse

4.3.1. Cette technique d'essais fut appliquée aux souffleries basse vitesse généralement équipées de veines guidées ou libres. Mais, grâce à l'ordinateur, un programme complet de corrections de parois put enfin être appliqué, pour la première fois, en France, aux résultats donnés par la veine guidée (de section circulaire : $\emptyset$ = 4,25 m) de la Soufflerie S5 du Centre d'Essais Aéronautiques de Toulouse, en 1967 (15).

Des résultats acquis et dépouillés dans ces conditions, à 40 m/s, sont reproduits Fig.16. Les maquettes essayées à S5 Toulouse et à SIGMA 4, représentatives d'un même avion, ne diffèrent que par leurs échelles.

Les valeurs corrigées des coefficients C_L , C_D , C_M en fonction de l'incidence corrigée ainsi que le tracé des courbes sont obtenues à partir de l'ordinateur I.B.M. 370-135 en 6 minutes dans le cas où quarante points d'incidence sont imposés.

4.3.2. La soufflerie basse vitesse A.M.D.B.A., de Vélizy, qui s'intéressa aux dépouillements automatiques et aux ordinateurs, dès 1959 (Bull, Electromécanique, EMD 848), fut refondue en 1974/75 tout en conservant sa veine rectangulaire (3,80 x 3,10 m) semi-guidée par plancher et plafond dans laquelle les effets de parois sont négligeables (16 et 17). En fait, une excellente qualité d'écoulement du courant d'air fut recherchée et obtenue en vue de son utilisation en liaison avec un ordinateur TEXAS 980A qui pilote entièrement l'essai au cours duquel les dépouillements sont effectués et la vitesse de variation continue de l'incidence est de l'ordre de 0°,20/s. A la fin de l'essai, les coefficients C_D , C_L , C_M sont fournis en fonction de l'incidence sous forme de tableaux de chiffres et les courbes correspondantes tracées en 4 minutes pour une variation totale d'incidence égale à 30°.

La Fig.16 donne les résultats obtenus dans ces conditions d'essais avec la maquette déjà soufflée à S5 Toulouse.

5. CONCLUSIONS

5.1. La soufflerie Sigma 4 (IAT St Cyr), dont le Mach varie de façon continue de 0,4 à 2,8, a été décrite. Son tunnel aérodynamique se présente sous la forme d'une tuyère à deux cols réglables placés en amont et en aval de la veine d'essais de section carrée (0,85 x 0,85 m). Chacune de ces trois parties est mobile ou possède des éléments mobiles.

CETTE SOUFFLERIE RESPIRE .....

En particulier, les parois horizontales perforées de la veine sont à porosité adaptable grâce au déplacement de parois flexibles placées dans les caissons étanches. Une veine unique permet donc les essais en écoulements sub/trans/supersonique. En régime subsonique ou transonique, la mesure du facteur de porosité est possible tout au long d'un essai en présence de la maquette.

5.2. En écoulement sub/transsonique, une méthode a été proposée qui a pour but d'annuler les effets des parois sur les moments de tangage en adaptant leur porosité à une valeur théorique imposée par le calcul numérique des corrections (V.L.M.).

La Vortex Lattice Method tient compte de la géométrie réelle de la veine. Celle de la maquette intervient par l'envergure et la flèche de l'aile ainsi que par sa longueur de queue. La porosité dépend des dimensions du modèle et croit avec sa taille.

L'adaptation de la porosité associée à des procédés expérimentaux - tels que la réalisation de gradients de pression statique longitudinaux nuls dans la veine avec maquette - conduit à obtenir des résultats d'essais pratiquement exempts d'effets de parois.

5.3. Comme Sigma 4 possède de nombreux éléments mobiles ou adaptables, un ordinateur propre à la soufflerie est indispensable pour la piloter en temps réel : soit pour figer dans une position optimale chacune des parties de sa tuyère, soit pour faire varier de façon continue cette position correspondant à l'essai en cours. Cette association ordinateur/soufflerie est effective depuis plusieurs années.
Ainsi de façon continue, en temps réel, l'ordinateur commande soit la variation du Mach, soit la position angulaire de la maquette et permet l'acquisition des données. Il commande aussi les vérins, des scanivalves ... Par combinaison des acquisitions et des commandes, il assure aussi des fonctions de régulation, telle que celle de la pression cinétique, par exemple, en écoulement inférieur à Mach 1.
En outre, il permet également, en temps réel, le dépouillement et le tracé des courbes représentatives des résultats avec une très grande précision.

5.4. Des résultats obtenus dans ces conditions avec une maquette d'avion A.M.D.B.A., à Mach = 0,5, ont été présentés. Pour un débattement d'incidence égal à 20°, la durée de l'essai est inférieure à 30 secondes. Dépouillement et tracé des courbes demandent moins de quatre minutes.
Ces résultats ont été comparés à ceux obtenus dans des souffleries basse vitesse qui font également appel à l'ordinateur. On peut remarquer leur grande homogénéité.

La soufflerie basse vitesse A.M.D.B.A. (40 m/s - 3,80 x 3,10 m), de Vélizy, dont la technique s'inspire de celle de Sigma 4, est pilotée par son propre ordinateur. Pour un débattement d'incidence de 20°, l'essai au cours duquel se font les dépouillements, dure un peu plus d'une minute. Tableaux de chiffres et courbes tracées sont fournis en moins de quatre minutes après la fin de l'essai.

5.5. En conclusion, il faut souligner le rôle de plus en plus important imparti à l'ordinateur qui est maintenant devenu indispensable à la soufflerie. D'abord pour calculer de façon réaliste, grâce à la méthode des singularités , les contraintes de parois. Ensuite pour la piloter et en assurer les fonctions annexes, en temps réel.
L'ordinateur ne peut plus être considéré comme son auxiliaire, mais doit faire corps avec celle-ci.

Aussi bien dans la modernisation d'une soufflerie existante que dans la conception future d'un laboratoire d'essais, il faut penser ensemble ordinateur/soufflerie, associés dans leurs actions réciproques.

Cette action réciproque appelle deux remarques :

i) L'intégration du personnel de la soufflerie doit être totale. Dans le cadre d'une modernisation, les expérimentateurs doivent être à même de définir les caractéristiques des ordinateurs, en liaison avec les chaînes de mesures, dont ils ont besoin. Inversement, le personnel qui a la charge des ordinateurs doit posséder des connaissances d'aérodynamique expérimentale étendues pour satisfaire des impératifs précis. Les ingénieurs responsables de Sigma 4 et de la soufflerie A.M.D.B.A. répondent à ces critères. Leur intervention est alors immédiate dans le cas - fort rare - où l'ordinateur tombe en panne et arrête totalement ou partiellement le fonctionnement de la soufflerie.

ii) En prévision de cette panne, on peut doter la soufflerie d'un second ordinateur de secours. C'est ainsi que Sigma 4 équipée maintenant d'un Télémécanique T 1600 a conservé son précédent ordinateur C.I.I.90-10 en ordre de marche. Il est possible encore d'envisager de relier la soufflerie à un autre ordinateur du centre dans lequel elle est implantée.

Quoiqu'il en soit, la taille de l'ordinateur propre à la soufflerie sera modérée et son prix aussi bien à l'achat qu'en exploitation sera inférieur à celui d'un grand centre de calculs d'ailleurs d'un emploi beaucoup moins souple.

REMERCIEMENTS

Le soutien du Service Technique de l'Aéronautique (S.T.Aé) du Gouvernement Français a permis :

- à l'Institut Aérotechnique de Saint-Cyr, de construire la Soufflerie Sigma 4 et d'assurer son fonctionnement en liaison avec les ordinateurs C.I.I. 90-10 puis Télémécanique T.1600,

- aux Avions Marcel Dassault-Bréguet Aviation, d'entreprendre et de poursuivre des études théoriques et expérimentales d'effets de parois.

Pour la rédaction de cet exposé, nous avons été grandement aidés par MM. J.MAS et F.REBMANN, ingénieurs IAT St-Cyr, et M. H.GIRARD, ingénieur AMD-BA.

6 REFERENCES

1 - R.G. JOPPA - A method of calculating wind-tunnel interference factors for tunnels of arbitrary cross-section.
NASA CR 845 (1967).

2 - R.G. JOPPA - Wind tunnel interference factors for high-lift wings in closed wind tunnels.
NASA CR 2191 (1973).

3 - Y. BOROVIK - F. WASSERSTROM - J. ROM - Wind tunnel boundary interference corrections - Part I : theoretical calculation
Aeronautical Research Center - Report 0 - 124 Technion Israël - Institute of Technology Haïfa (1972).

4 - Y. VAUCHERET - J.C.VAYSSAIRE - Corrections de parois en écoulement tridimensionnel transsonique dans des veines à parois ventilées.
Symposium FDP AGARD - CP 174 Londres - (Oct. 1975).

5 - J.C.VAYSSAIRE - Methodes de corrections de parois avec applications expérimentales
12è Colloque d'Aérodynamique Appliquée - A.A.A.F. Poitiers (Nov. 1975).

6 - J. BROCARD - Une soufflerie transsonique et supersonique de conception moderne. La soufflerie Sigma 4 de l'Institut Aérotechnique de Saint-Cyr
Association Technique Maritime et Aéronautique Paris - 1962 -

7 - M. MENARD - Tuyères supersoniques à Mach variable
Technique et Sciences Aéronautiques - Tome 2 Paris 1954.

8 - F GRUSON - M. MENARD - O. MONOD - Tuyères supersoniques à col réglable
Publications Scientifiques et Techniques du Ministère de l'Air - I.A.T. St-Cyr - N.T. N° 51 - Paris 1955.

9 - O. FRENZL - Nouveaux progrès dans les souffleries à trompe d'induction par eau chaude
DOC - AIR - ESPACE N° 81 - Paris - Juillet 1963.

10- M. LANGOT - R. LACHAIZE - M. MENARD - Influence des couches limites des parois de souffleries sur les phénomènes de blocage.
A.A.A.F. 9è Colloque d'Aérodynamique Appliquée Paris - St-Cyr Nov. 1972.

11- M. MENARD - J.C. VAYSSAIRE - Un exemple d'utilisation de soufflerie munie de parois perforées à géométrie variable
A.A.A.F. 9è Colloque d'Aérodynamique Appliquée Paris - St-Cyr Nov. 1972.

12- M. LANGOT - Dépouillements par ordinateur d'essais en soufflerie
Publication I.A.T. St-Cyr A.A.A.F. 202è réunion de la Commission d'Aérodynamique - Paris - 24 Sept. 1969.

13- S. SCHNEIDER - M. MENARD - Cadences de mesures dans les essais en soufflerie
A.A.A.F. 199è réunion de la Commission d'Aérodynamique - Paris 26 Mars 1969.

14- J.M.CHRISTOPHE - Mesures continues d'un paramètre dans les souffleries
ONERA - T.P. N° 828 (1970).

15- J.C.VAYSSAIRE - Nouvelle méthode de calculs de correction des résultats d'essais en soufflerie basse vitesse
L'Aéronautique et l'Astronautique N° 15 et 16 - Paris 1969.

16- A. TOUSSAINT - Influence of the dimensions of the air-stream
Aerodynamic Theory W.F. Durand - Vol 3.p. 295 - Springer Berlin 1935.

17- C.WIESELSBERGER - Uber den Einfluss der Windkanalbegrenzung auf den Wider-stand insbesondere im Bereiche der kompressiblen Strömung.
Luftfahrtforschung, Vol. 19, 6 mai 1942.
Traduction française : L'influence des parois de la soufflerie sur la résistance aérodynamique notamment dans le domaine de l'écoulement compressible.
Traduction technique G.R.A. N° 403 - Paris

Fig. 3 - VORTEX LATTICE METHOD - LIFT (WALL) INTERFERENCE AMD-BA
HALF MODEL - SQUARE WORKING SECTION

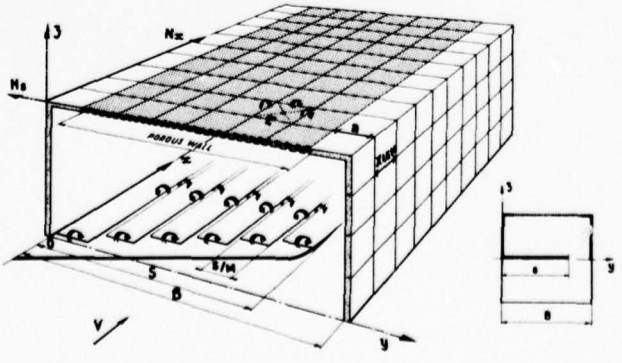

_ Fig. 1 _

SIGMA 4 WIND TUNNEL

0,4 < continuous test Mach number range < 2,8

Square working section: 0,85m X 0,85m.

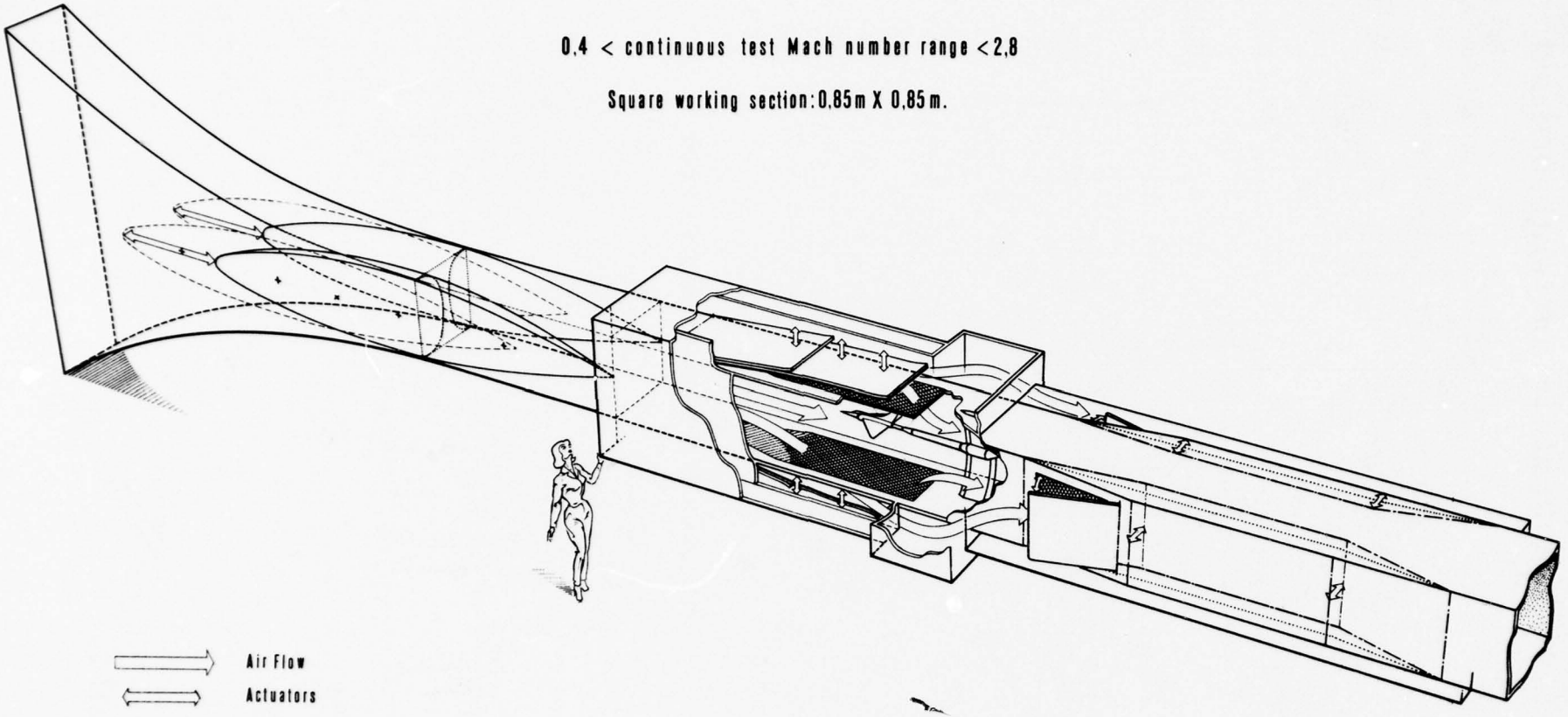

— INSTITUT AEROTECHNIQUE DE ST-CYR —

AMD-BA

Fig. 2 _ VORTEX LATTICE METHOD _ LIFT (WALL) INTERFERENCE

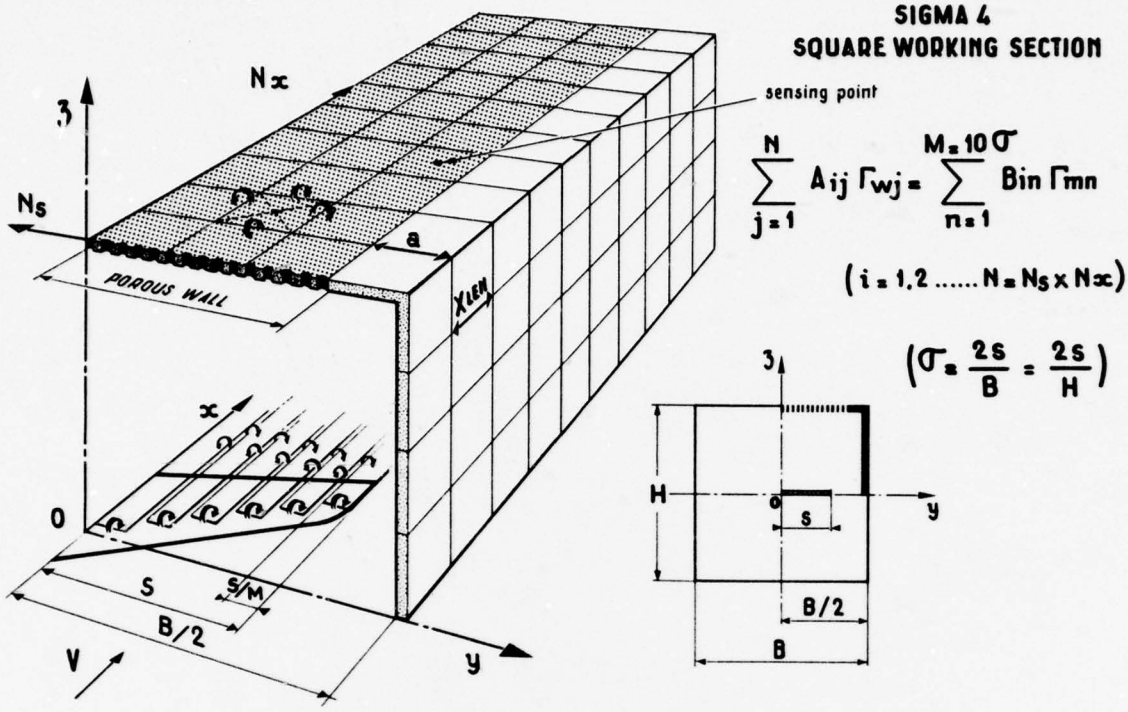

AMD.BA

Fig 4 _ INFLUENCE OF THE WORKING SECTION GEOMETRY

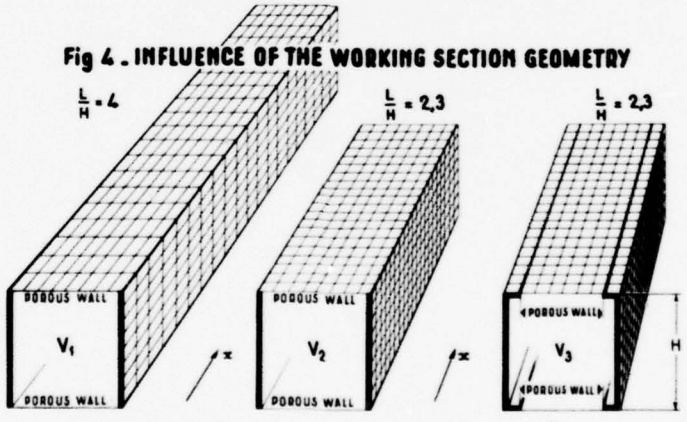

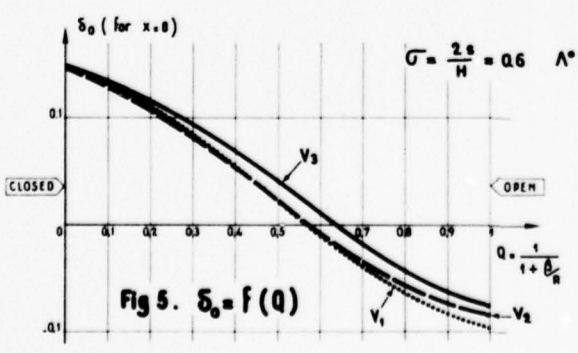

Fig 5. $\delta_0 = f(Q)$

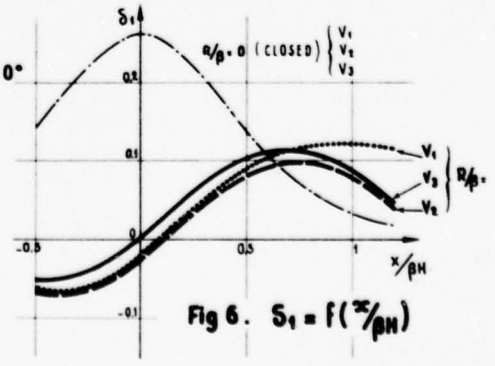

Fig 6. $\delta_1 = f(x/\beta H)$

AMD-BA

Fig 7. ZERO PITCHING MOMENT CORRECTION

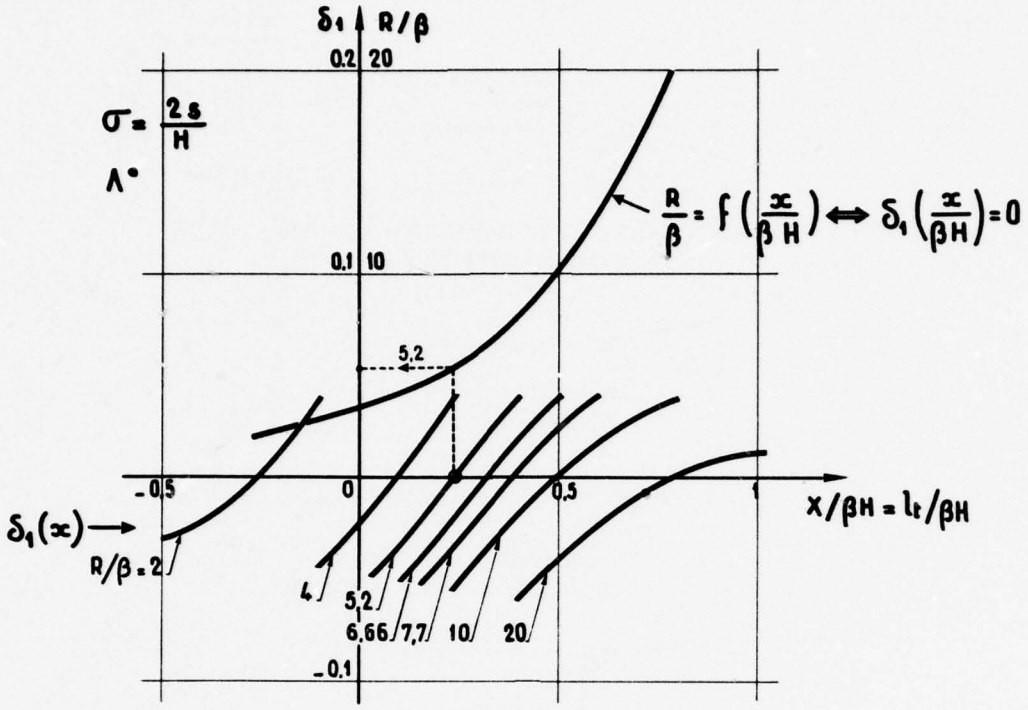

AMD.BA

Fig.8 - THEORETICAL POROSITY FACTOR R FOR $\delta_1 = 0$

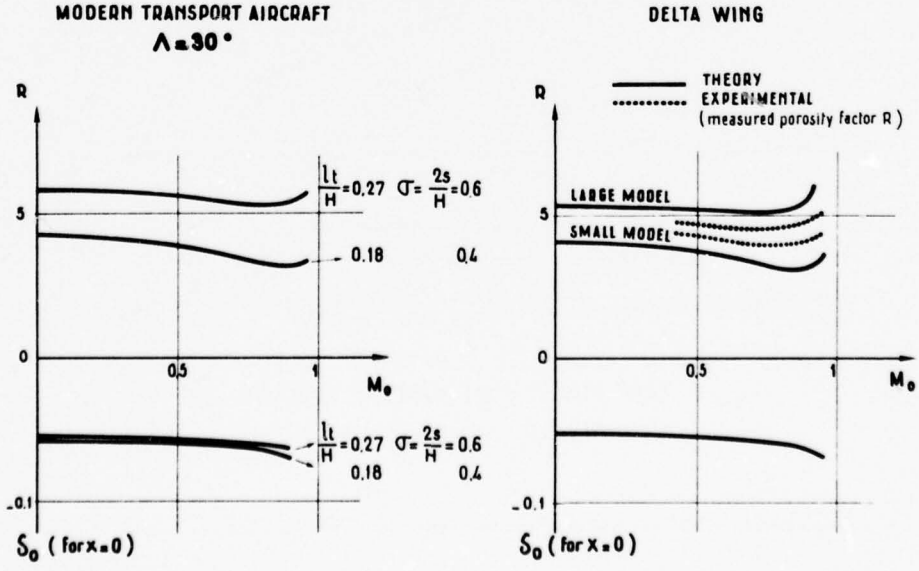

Σ 4 - IAT S'CYR

Fig.9 a. STATIONARY BUBBLES

$M_0 < 1$

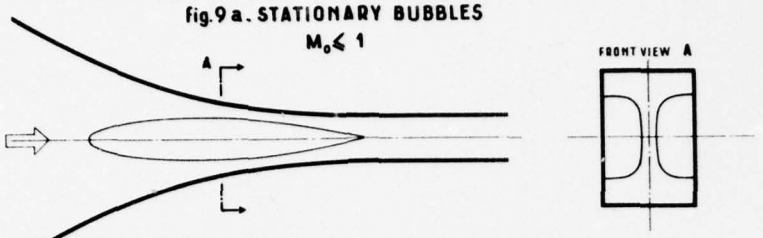

Fig.9 b - CONTINUOUS NOZZLE CROSS SECTION VARIATION

(1ST THROAT WITH STREAMLINED BUBBLES)

$1 < M_0 < 2,8$

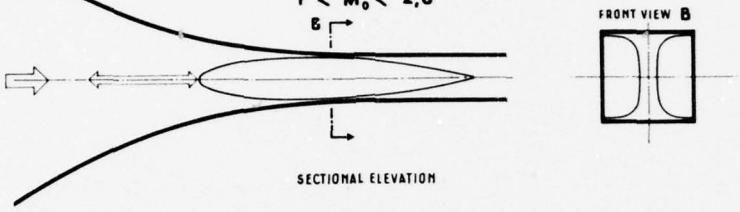

Fig.10 - CONTINUOUS DIFFUSER VARIATION

2nd SONIC / SUPERSONIC THROAT (With re-entry door)

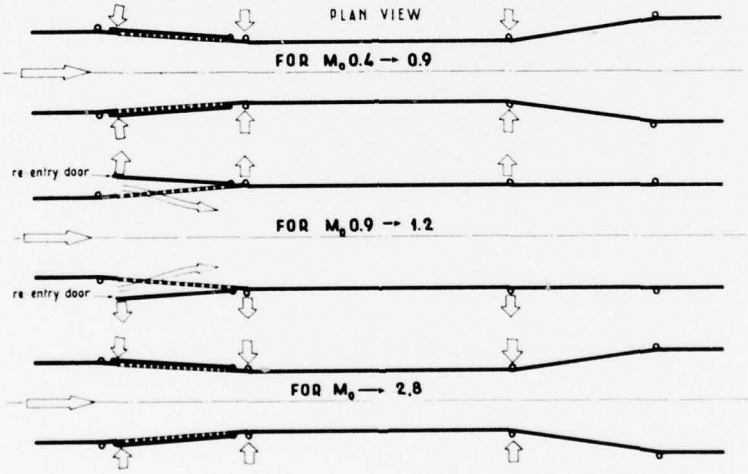

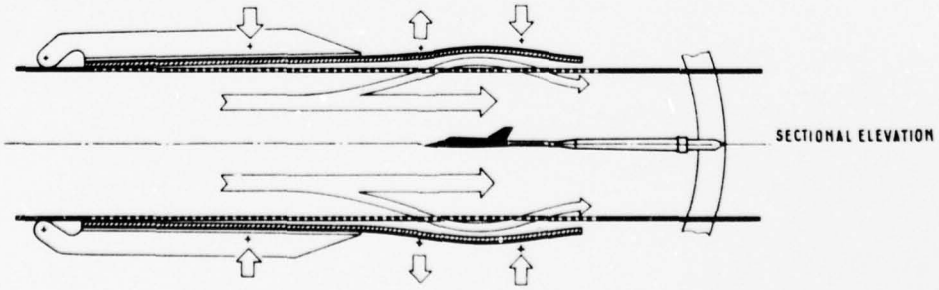

Fig. 11 - CONTINUOUS WALL POROSITY VARIATION

VARIABLE WORKING SECTION MACH NUMBER

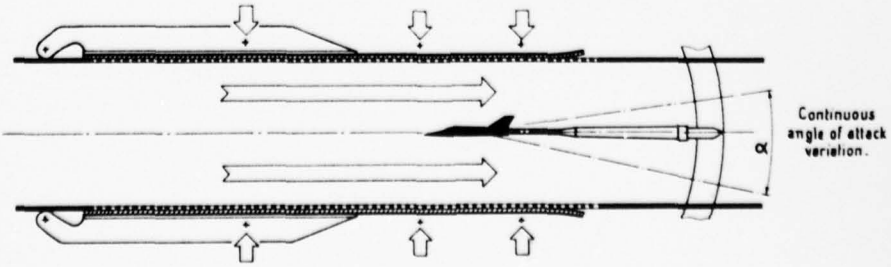

Fig. 12 - STATIC PRESSURE HOLES
WORKING SECTION / Σ 4

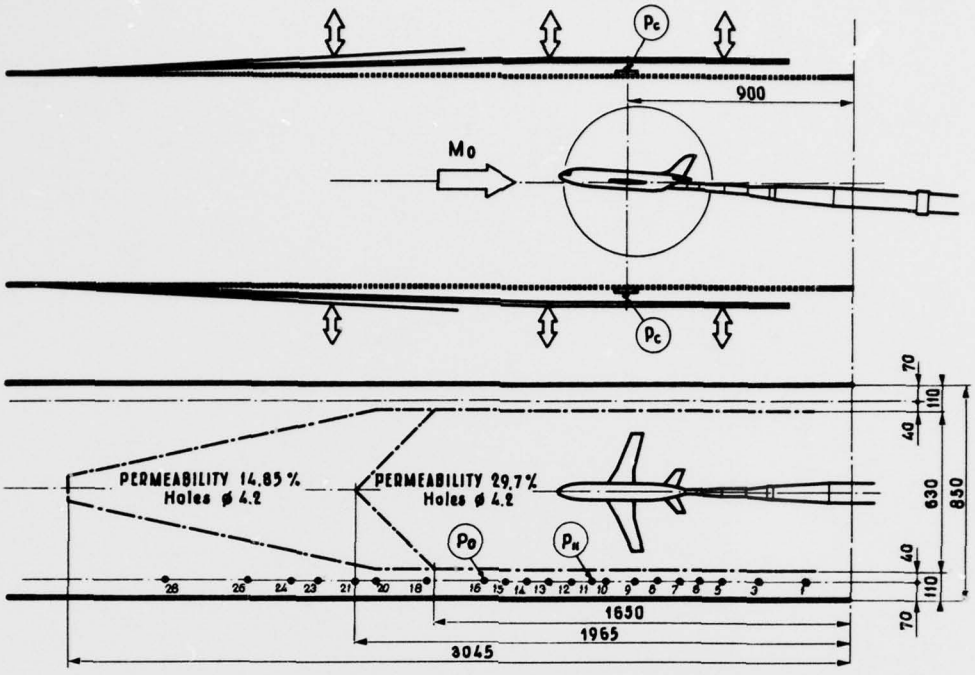

Fig 13 - EFFECT OF WORKING SECTION AND 2ND THROAT GEOMETRY UPON PRESSURE GRADIENT

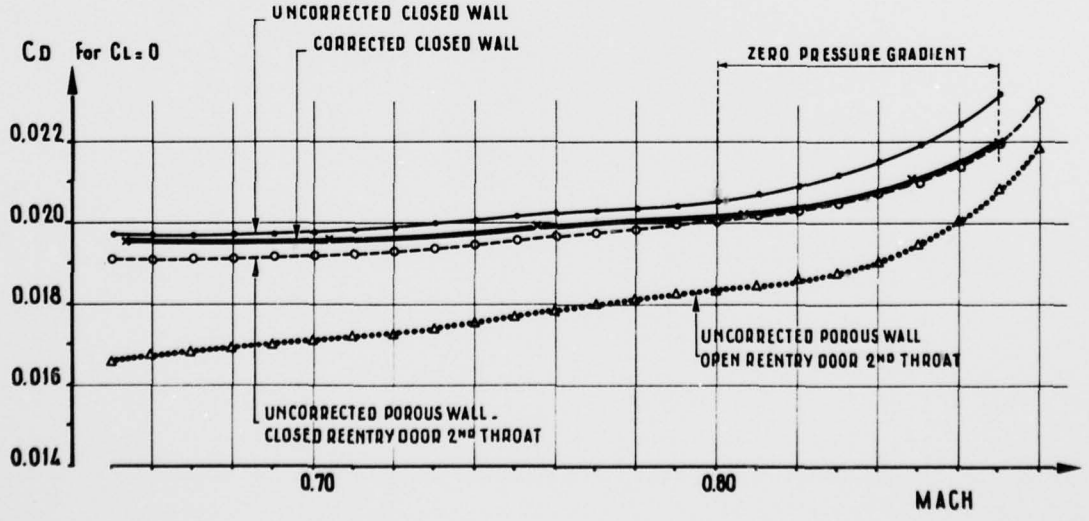

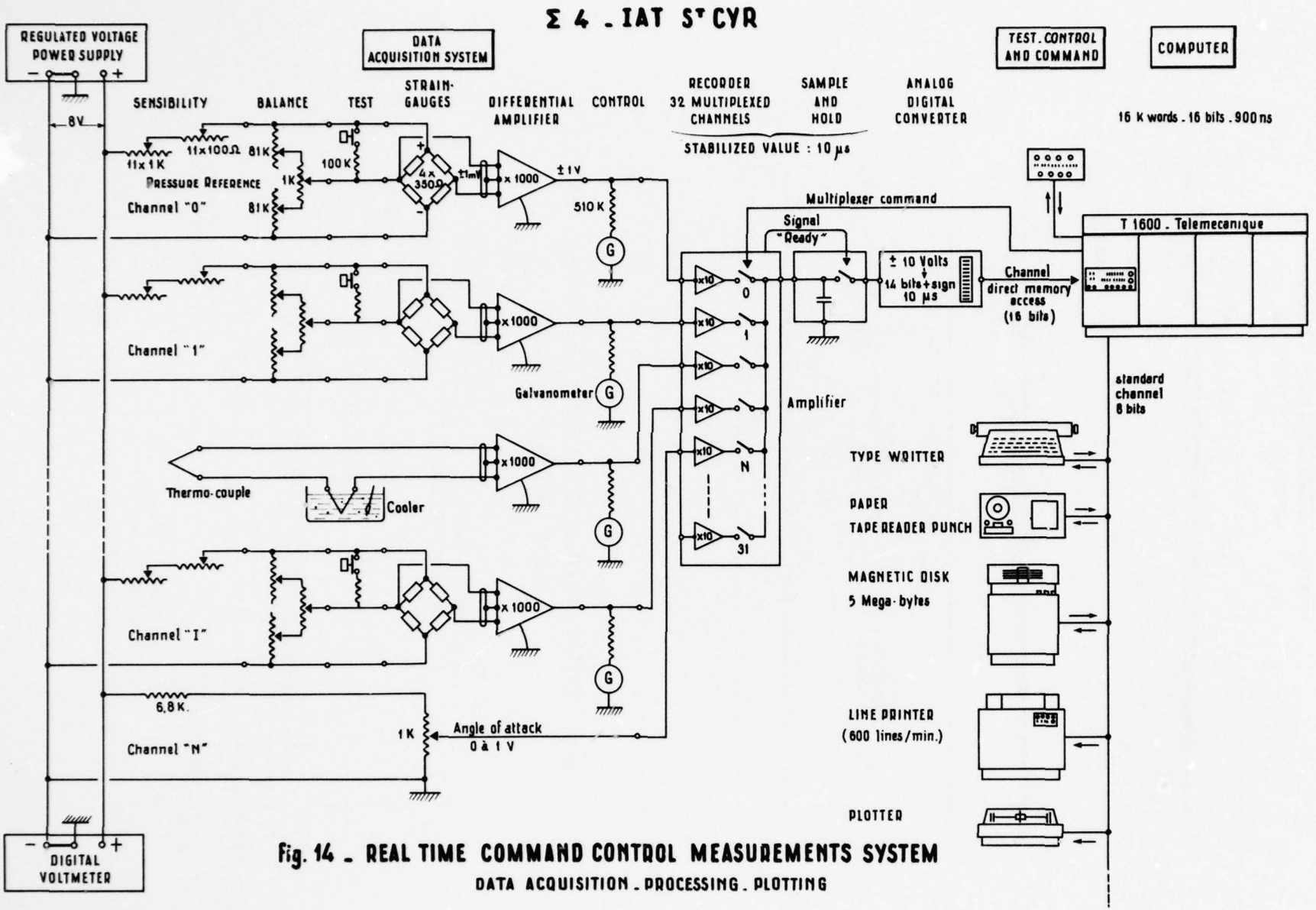

Fig. 14 - REAL TIME COMMAND CONTROL MEASUREMENTS SYSTEM

DATA ACQUISITION - PROCESSING - PLOTTING

Fig. 15 _ REGULATION SYSTEM/Σ 4

SUB/TRANSONIC FLOW

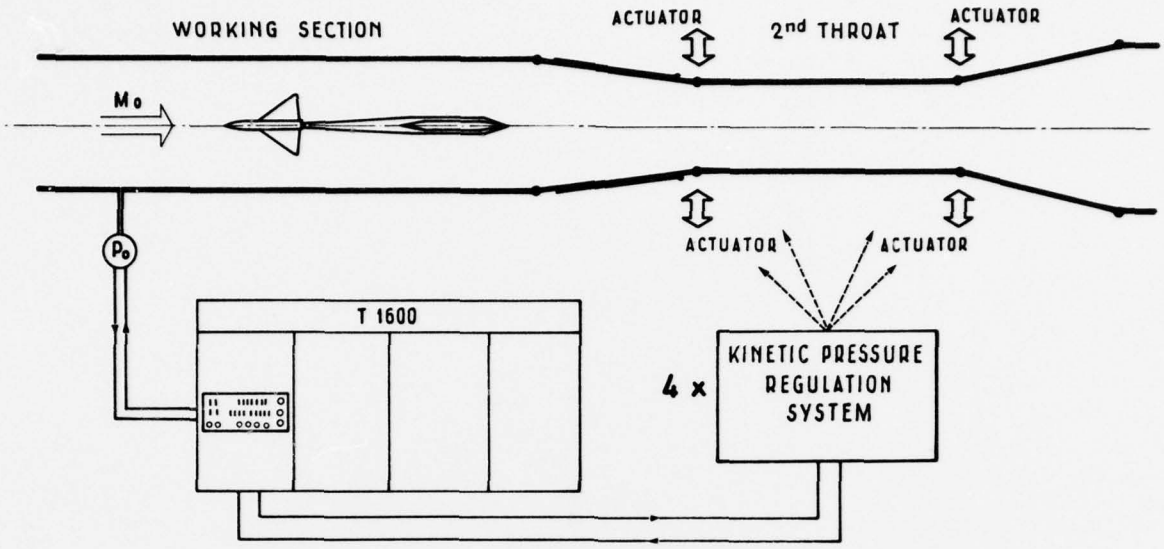

Fig. 16 _ TEST RESULTS

AMD-BA AIRCRAFT MODELS

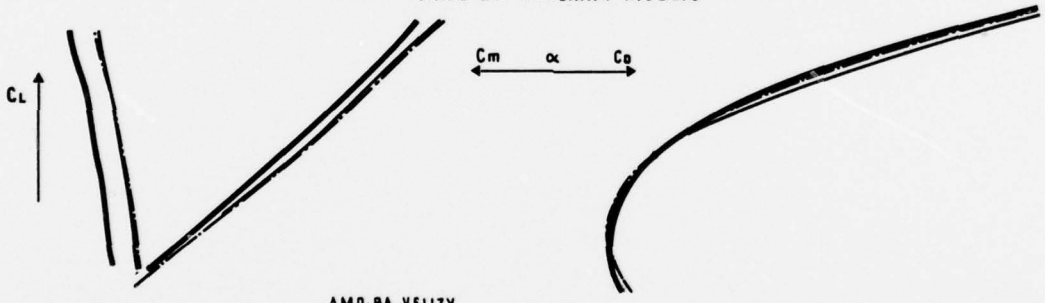

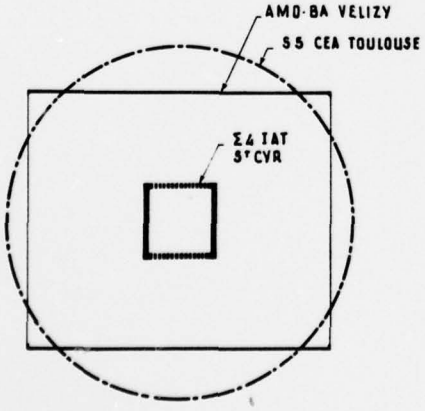

	Σ4 IAT S°CYR M_o = 0.50	AMD-BA VELIZY 40 m/s	S5 CEA TOULOUSE 40 m/s
WALL INTERFERENCE	ZERO *	ZERO	CORRECTED
Δα °/s	0°.75	0°.20	0°.11
PROCESSING PLOTTING	AFTER TEST 11 s./degree	DURING TEST 8 s./degree	AFTER TEST 9 s./degree
COMPUTER	TELEMECANIQUE T 1600	TEXAS 980 A	IBM 370/135

* with AMD-BA IBM 370/168

AUTOMATIC CONTROL OF A TRANSONIC WIND TUNNEL WITH A REAL-TIME COMPUTER SYSTEM*

by
J. A. Gunn and J. P. Christopher, Jr.
ARO, Inc.
Arnold Engineering Development Center
Arnold Air Force Station, Tennessee 37389

SUMMARY

The Aerodynamic Wind Tunnel (4T) Real-Time Control and Display System is a computerized system which has increased the productivity of the Tunnel 4T tests by providing real-time displays of test conditions, test condition monitoring, and automatic control. The system is built around a Digital Equipment Corporation PDP 8/E minicomputer which has a 16K word memory and a hardware floating point processor. The system uses standard tunnel measurements to calculate stream and plant parameters. The program, which is written in the FORTRAN IV language, is executed three times per second. Computer-driven video displays provide tunnel operators and other control room personnel with test conditions such as Mach number, Reynolds number, and dynamic pressure. The real-time system monitors all test parameters, continually checks to determine if test conditions are as requested, and informs the operators of the current plant and test conditions status via the status panel. The real-time system automatically controls the test section wall porosity, ejector flaps, wall angle, the tunnel stagnation pressure for most conditions, and the Mach number in the range from 0.2 to 0.9. In the future, the system will provide automatic Mach number and pressure level control for the full range of 4T operations. The system is also capable of keeping tunnel operating records which can be used to determine tunnel productivity.

1.0 INTRODUCTION

During the past four years the price of minicomputers suitable for wind tunnel automatic control systems has steadily decreased while the unit cost of electrical energy required for wind tunnel operation has doubled. This situation has generated a strong economic inducement to increase wind tunnel productivity by making capital expenditures for control computers in order to offset higher wind tunnel direct-operating costs. A minicomputer is now being used in Tunnel 4T to increase productivity by providing test conditions displays, monitoring and displaying the test condition status, and automatically controlling test parameters. The Tunnel 4T Real-Time Control and Display System (RTCDS) has increased productivity for all types of testing while also improving test data quality. This paper describes the Tunnel 4T RTCDS, the factors considered in the system design, and the productivity and data-quality gains obtained from the system.

2.0 TUNNEL 4T

Tunnel 4T is a 4-ft closed-loop, continuous-flow, transonic wind tunnel which has a usable continuous Mach number range from 0.10 to 1.3. In addition, Mach numbers 1.6 and 2.0 can be obtained by the use of nozzle inserts. Tunnel stagnation pressure can be varied from 0.075 to 1.6 atm, and the stagnation temperature can be controlled to a limited extent between approximately 25 to 55°C.

Tunnel 4T is normally powered by the second increment of the Propulsion Wind Tunnel Facility (PWT) Plenum Evacuation System (PES). The general arrangement of the Tunnel 4T ducting is illustrated in Fig. 1. Mach number in the subsonic range is set by adjusting the pressure ratio across the test region and the movable side wall ejector-flap region located just downstream of the test region. Supersonic Mach numbers are generated by control of auxiliary plenum suction rate.

The Tunnel 4T wall characteristics can be altered by changes in wall angle or wall porosity. The top and bottom test section walls may be converged or diverged by 0.5 deg. The variable wall porosity feature of Tunnel 4T is obtained by utilizing a sliding cutoff plate behind the airside plate. The wall porosity, which can be changed during testing, ranges from 0 to 10 percent open area on each wall.

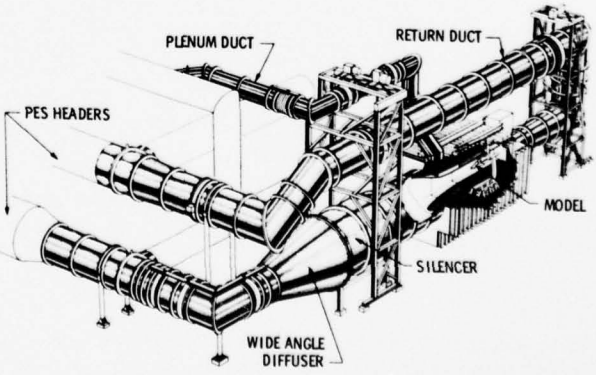

Figure 1 Tunnel 4T General Arrangement

*The research reported herein was conducted by the Arnold Engineering Development Center, Air Force Systems Command. Research results were obtained by personnel of ARO, Inc., contract operator at AEDC. Further reproduction is authorized to satisfy needs of the U. S. Government.

3.0 OBJECTIVES

The general design philosophy for the Tunnel 4T RTCDS was to use the computer to the greatest extent possible. This included providing displays of all test condition parameters, making every reasonable check on the test status, and eliminating manual operations.

The primary objective of the Tunnel 4T RTCDS effort is to increase productivity by increasing the ratio of "on-conditions" time to "air-on" time, i.e., decrease the nonproductive air-on time. This increase in productivity has the effect of reducing the total tunnel energy consumption if the annual number of on-conditions hours are held constant or to increase the data output if the annual number of air-on hours is maintained. In either case the net result is to reduce the energy consumed per data point. It was also an objective of the RTCDS design to improve data quality by maintaining a consistent operational procedure and by reducing the deviation in test conditions.

The system was designed (1) to establish test conditions as soon as possible after bringing the tunnel air on, (2) to maintain Mach number during model attitude excursion, and (3) to move rapidly from one test condition requirement to the next.

4.0 COMPUTER HARDWARE

The Tunnel 4T Real-Time Control and Display System is built around the Digital Equipment Corporation (DEC) PDP 8/E minicomputer. The system is illustrated in Fig. 2. The minicomputer includes a central processor, 16,384-12 bit words of core memory, input/output interfaces, and a floating-point processor. The memory is expandable to 32K words. The input/output interfaces include digital input channel, analog to digital (A/D) converters, digital output channels, and digital to analog (D/A) converters. The floating-point processor (FPP) in combination with the central processor unit (CPU) gives the computer a dual-processor capability. Since the FPP makes floating-point calculations with hardware rather than software, the computational speed of the computer is approximately 10 times faster with the FPP.

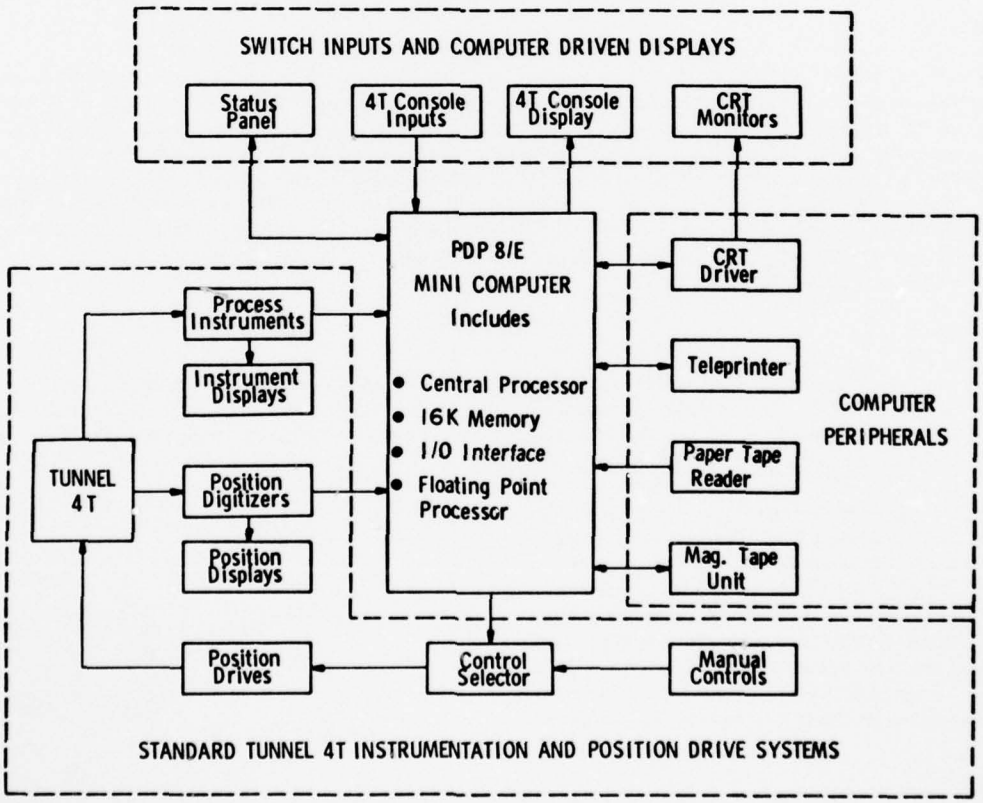

Figure 2 The Tunnel 4T Real Time Control and Display System Computer

Computer peripheral equipment includes a cathode ray tube (CRT) display driver, a teleprinter, a high-speed paper-tape reader, and a magnetic tape (DEC tape) unit. The CRT driver provides video displays on closed-circuit television (CCTV) monitors. Commands to the computer operating system are given through the teleprinter which also includes a low-speed paper-tape punch and reader. Programs are loaded into the computer through the dual-drive DEC tape unit which is also the computer system device.

4.1 Computer Inputs and Outputs

Inputs for the 4T RTCDS are obtained from the standard tunnel instrumentation and position drive systems and from special valve position devices required for the automatic controls. The process inputs are the temperature and

pressures required to calculate stream parameters. The position digitizers provide test section wall angle, wall porosity, and diffuser flap position. Switches and constants boxes on the tunnel control room operating console are manually set to provide the computer with the desired Mach number and stagnation pressure or Reynolds number. Computer outputs include switch closures and analog signals in addition to the CCTV displays. Through switch closures the computer activates light-emitting diode displays, incandescent status lights, and relays which energize electric drive motors. Computer-generated analog signals (voltage) are used to provide setpoints for servo-controlled valves.

4.2 Software

Computer system software was purchased as a package from the manufacturer. This included both the programs needed to operate the peripherals and a FORTRAN IV language. Some machine language routines, primarily handlers, were developed to expand the FORTRAN IV capabilities.

5.0 TUNNEL 4T RTCDS OPERATION

Figure 3 illustrates the relationship between the three components of the Tunnel 4T operation: the tunnel, which includes the operating machinery; the computer and associated peripheral equipment; and the tunnel operating personnel. Data from the tunnel instrumentation and test condition requirements from the operators are connected to an input interface peripheral. Computer output peripherals operate analog signals, switch closures, and CCTV displays. Once the program is loaded and started it is locked in an endless real-time loop which is executed three times per second. During each pass the program reads the input; makes calculations of test conditions, control, and logical parameters; and controls the output peripherals.

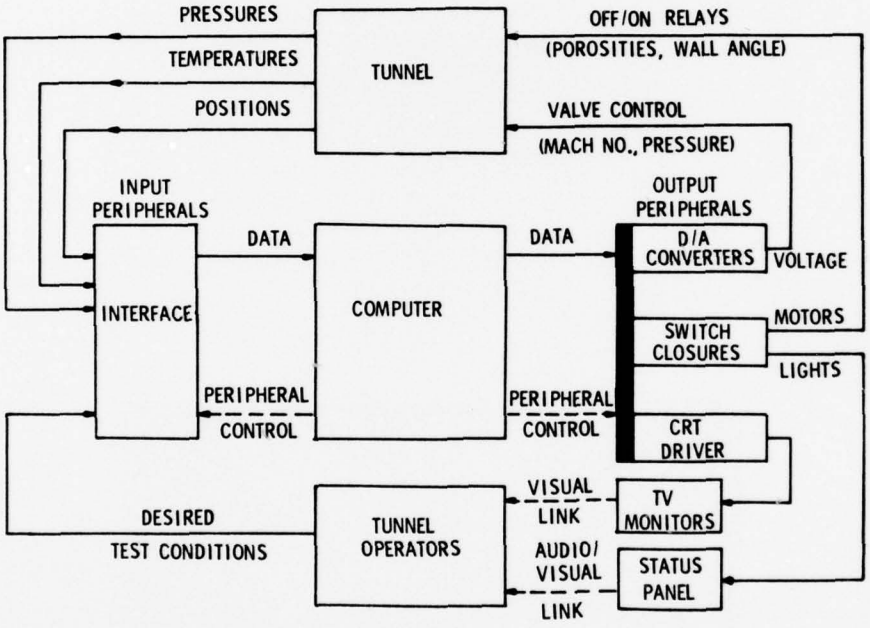

Figure 3 The Tunnel 4T Real Time Control and Display System

5.1 System Development

The Tunnel 4T RTCDS was developed in three phases as is illustrated in Fig. 4. The first phase was to provide the tunnel operators and others with a display of test conditions in engineering units using the CCTV monitors. In Phase II, the constant box and switch inputs from the tunnel operator were added along with the computer-driven light panel to indicate the tunnel status. The final phase, which is still in progress, includes development of the hardware and software for complete automatic control of test conditions.

5.2 Test Conditions Display

The test condition displays using remote CCTV monitors are provided for the tunnel operators and for personnel in any test or operation area which will benefit from the displays. Mach number, Reynolds number, dynamic pressure, other test parameters, time of day, and time-on conditions (a bookkeeping parameter) are displayed on the CCTV monitor (Fig. 5). The CRT display is updated once each second.

The test conditions displays have improved Tunnel 4T data quality and productivity by allowing the tunnel operators to set test conditions with the actual control parameters rather than with displays of parameters which are functionally related to the controlled parameter. In addition, the CCTV displays unified the 4T operations and reduced communication requirements. Improvement in the consistency of test conditions and data quality were intangible benefits of the engineering unit displays. It is estimated that the computer-driven displays increased the Tunnel 4T productivity by 7 to 10 percent.

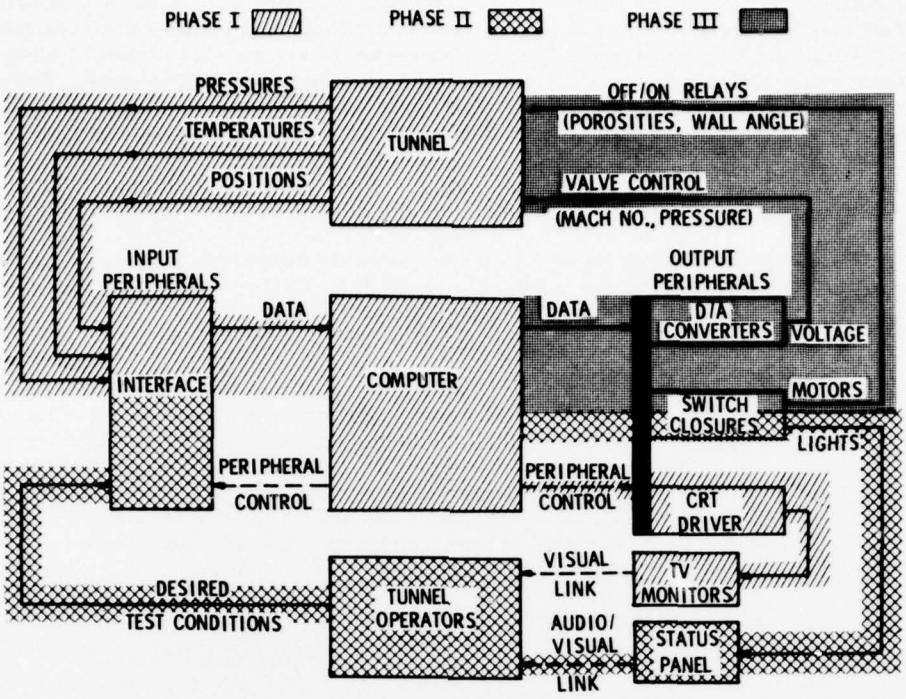

Figure 4 The Tunnel 4T Real Time Control and Display System Development

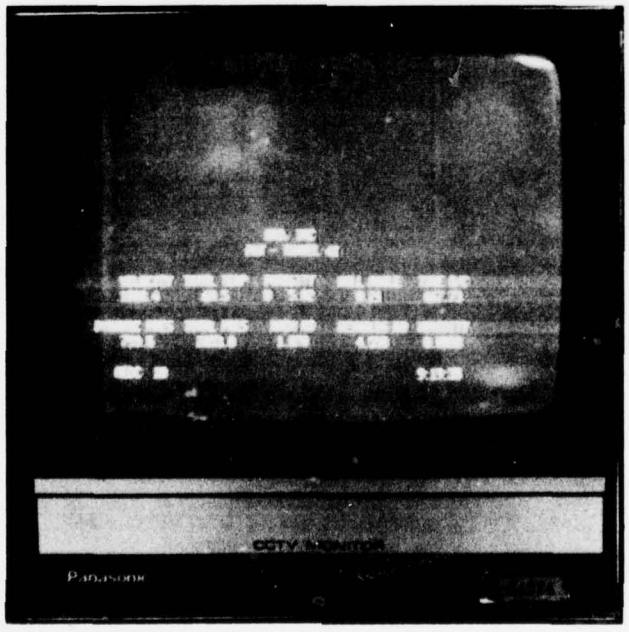

Figure 5 Closed Circuit Television Monitor Test Conditions Display

5.3 Test Conditions Monitoring

One of the most difficult and time-consuming tasks for tunnel operators is to determine when the tunnel is on test conditions. Normal operation requires that 14 parameters be within specified tolerances. Test conditions monitoring, i. e., having the computer assume the task of determining when the tunnel is "on conditions" and testing can begin, significantly improved the 4T operations. In the past, the on-conditions decision was made by the tunnel operator and the time required to reach the decision was subject to wide variation, depending on the tunnel operator's experience. The computer now monitors all test conditions and determines logically from preselected tolerances whether or not the tunnel is on test conditions.

Operators are informed of the test conditions status by a computer-driven display of lights, as shown in Fig. 6, and by audible tones. Status checks are made on tunnel configurations, instrumentation, and test conditions. An in-limit parameter will have a green light, whereas an out-of-limit parameter will be signified with a red light. Checks can be deleted by override switches on the status panel and an override is denoted with a white display light. Checks are made on the four wall porosities, and the two diffuser flap positions, wall angle, primary instrumentation agreement, wall porosity schedule, tunnel pressure ratio, Mach number, and stagnation pressure level. When all of the individual parameters are in limits the on-conditions light is switched to green and a momentary audible tone is sounded. If a parameter exceeds tolerances during testing the on-conditions light is switched to red and a different audible tone is sounded to attract the tunnel operator's attention. Initiation of the computer monitoring of test conditions has increased the Tunnel 4T productivity by an estimated five percent.

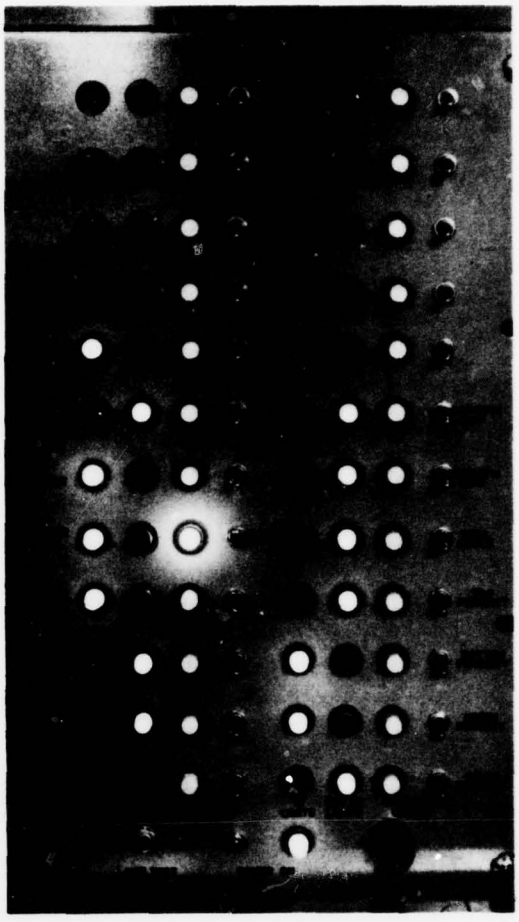

Figure 6 Status Display

5.4 Automatic Controls

Computer controls for the tunnel fall into two categories: position controls and process controls. The relative location of the controlled variables are shown in Fig. 7. In the test region, seven parameters - the four wall porosities, the two diffuser flaps, and the wall angle - are controlled as a function of the set point Mach number. Downstream of the test region, Valve 92 and the vernier Valve 92A are used to set Mach number in the subsonic range. Valve 93 is used to adjust plenum suction for supersonic Mach number control. Pressure level control for most conditions is controlled with Valve 8Q which is both an in-draft and blowoff valve. Valve 65 is used to control pressure level at some conditions.

The positioning of the four wall porosities and the wall angle is done through an adaptive bump control technique. Large moves are made by closing the drive motor contacts and driving toward the desired position. The motor relays are opened at a point which will allow the controlled parameter to coast to the controlled position. Small adjustments which arise from overshoot, undershoot, or drift are made by bumping the motor relays for a calculated time interval proportional to the error. The adaptive bump procedure is not required for diffuser flap control because flap positioning is not critical. The process controls of Mach number and stagnation pressure are not presently complete; however, the system automatically maintains Mach number between 0.2 to 0.9 and pressure level for most conditions. As more inputs are connected to the computer, the automatic controls will be extended for all Mach numbers and pressure levels. Automatic controls have increased productivity by an estimated 10 percent.

The Tunnel 4T automatic process controls utilize the proportional plus integral plus deviation (PID) control algorithm. The general form of the PID control equation (Ref. 1) is

$$m(t) = K_c\left[e(t) + \frac{1}{T_i}\int_0^t e(t)\,dt + T_d\frac{de(t)}{dt}\right] + mr$$

where

$m(t)$ = output signal to the control valve
mr = reference value at which control action is initialized
$e(t)$ = error signal
t = time
K_c = controller gain
T_i = integral constant
T_d = derivative constant

The computer implementation employs the discrete form of this PID control equation. The critical phase of control implementation is controller tuning, i.e., the selection of the controller constants, K_c, T_i, and T_d, which gives the response which most nearly satisfies the desired control criteria.

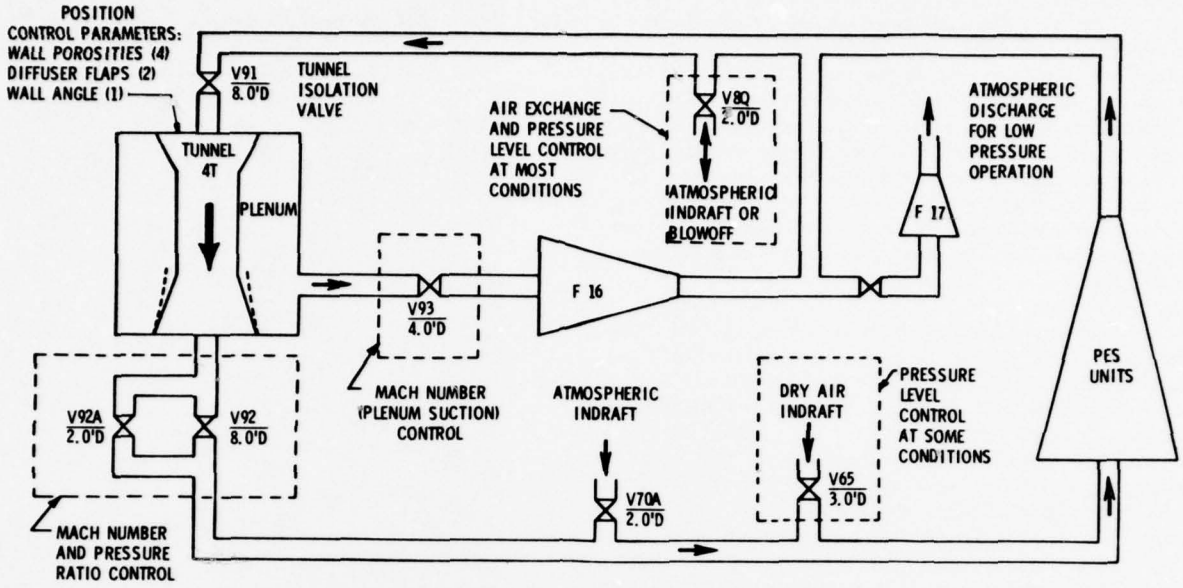

Figure 7 Ducting and Valves Used in the Operation of Tunnel 4T

5.5 Record Keeping

In addition to productivity gains through automation, the Tunnel 4T RTCDS has the potential for generating operating records which can be used as a management tool. These records can be used to pinpoint areas of low productivity and to improve the accuracy of required test time estimates. The real-time program now provides accounting of the time on test conditions, and this parameter is presently being used as one factor in the evaluation of test performance.

6.0 HUMAN FACTORS IN SYSTEM DESIGN

The interface between the tunnel console operator and the computer have been of prime concern throughout this project. Emphasis was placed on reducing the operators' present manual workload without adding extra buttons to push or sequences to remember during automatic operation. Since the computer was being integrated into an existing system, efforts were made to keep the operation in its natural state. As the system was developed, the computer began doing jobs that were a part of the manual operations. This eliminated operator retraining and enhanced operator acceptance of the system. Every attempt was made to keep operator confidence in the system by thoroughly checking out new features before making them a part of the system.

REFERENCE

1. Smith, Cecil L. Digital Computer Process Control, Intext Educational Publishers, Scranton, Pa., 1972.

ACKNOWLEDGEMENT

The authors wish to acknowledge the effort of A. M. Crowe, G. W. Allen, and S. B. Cowan, ARO, Inc., who were responsible for the installation, maintenance, and interface design.

RÉDUCTION DES CORRECTIONS DE PAROIS EN VEINES D'ESSAIS TRANSSONIQUES CLASSIQUES A L'AIDE D'ÉTUDES PARAMÉTRIQUES SUR ORDINATEUR

par Xavier VAUCHERET

Office National d'Etudes et de Recherches Aérospatiales (ONERA)
92320 Châtillon - France

RESUME

Des études paramétriques sur ordinateur, utilisant les programmes de calcul des coefficients de correction de parois en veine transsonique à parois perforées, permettent de définir des conditions optimales d'emploi des veines existantes associées à des tailles de maquettes telles que les corrections de parois soient négligeables.

En écoulement tridimensionnel les paramètres considérés sont : les rapports entre hauteur et largeur de veine, envergure de maquette et largeur de veine, la flèche de voilure et la porosité, supposée uniforme et égale, des deux parois horizontales de la veine. Des règles de schématisation des maquettes sont précisées pour les coefficients de correction de portance. Des recommandations de dimensionnement de maquettes sont formulées pour obtenir des corrections tolérables. Une veine optimale associée à une taille de maquette peut être définie en transsonique pour s'affranchir des corrections de parois alors négligeables.

En écoulement bidimensionnel, l'introduction d'un paramètre supplémentaire : la différence de porosité des deux parois, conduit à la définition d'une veine optimale. Une telle veine, à paroi basse pleine et à porosité de paroi haute faible permet de négliger les corrections de parois dans des domaines corde-épaisseur relative qui sont précisés.

MINIMIZING WALL INTERFERENCE IN CONVENTIONAL TRANSONIC TEST SECTIONS BY USING COMPUTER PARAMETRIC STUDIES

Parametric studies by computer, using the programmes for the calculation of the wall interference by the analytic method, for perforated wall transonic test sections, allow the determination of using of present test sections, with associated model sizing, so that the wall constraints can be negligible.

For tridimensional flow, the following parameters are investigated : test section height/width ratio, model span/test section width ratio, wing sweep and horizontal wall porosity ; this porosity is assumed to be uniform and the same for floor and ceiling. The model schématization rules, necessary and sufficient to calculate the lift interference coefficients, are given. Model sizing can be recommended to obtain reasonably low correction. An optimal test section, with an associated model size, can be determined to neglect the lift and drag interferences.

For two dimensional flow, an additional parameter, due to distinct porosities for floor and ceiling, allows the definition of an optimal test section. Such a section with closed floor, and slightly porous ceiling allows the neglecting of the wall constraints, in a domain of chord and relative thickness which is given.

NOTATIONS

AR	allongement
B	largeur de veine
c	corde d'un profil
$\bar{c}$	corde aérodynamique moyenne
c_R	corde de référence
C	section de veine
C_D	coefficient de traînée
C_L	coefficient de portance
C_M	coefficient de moment de tangage
C_{L_α}	gradient de portance
H	hauteur de veine
k_u	coefficient caractéristique d'un profil
k_v	facteur de volume apparent
l_e	distance du point à 25 % $\bar{c}$ au point à 25 % de la corde moyenne d'empennage
l_G	distance du centrage au point à 50 % de la corde moyenne d'empennage
M	nombre de Mach
q	{sans indice : variable intermédiaire {avec indice : pression dynamique
Q	facteur de porosité $\quad Q = 1/(1+\beta/R)$
R	paramètre de porosité
s	demi-envergure
S	surface de référence
u_i	vitesse de perturbation axiale
U_∞	vitesse à l'infini amont
V	volume de maquette

w_i vitesse de perturbation verticale

x abscisse (origine à 25 % de c ou $\bar{c}$)

x_G distance entre centre de réduction des efforts et point à 25 % de $\bar{c}$

X abscisse réduite : $X = 2x/\beta B$

α incidence

$\beta = \sqrt{1-M^2}$

Γ circulation

δ coefficient de correction de portance

δ_1 coefficient de correction de courbure de champ

$\Delta\alpha$ correction d'incidence

ΔM correction de Mach

$\epsilon = u_i / U_\infty$

$\lambda = H/B$

Λ flèche à 25 % de profondeur des cordes de l'aile

$\tau = 2s/B$

τ_v coefficient de blocage de volume apparent

φ potentiel

$\xi = tg\Lambda$

Ω coefficient de correction de blocage

Indices relatifs à

a aile

b terme corrigé des effets de blocage

B paroi basse

c terme corrigé des effets de blocage et de portance

d décollement

e empennage

H paroi haute

L correction de portance

m mesuré

s blocage de volume

u non corrigé des effets de parois

w blocage de sillage

$'$ dérivée par rapport à X

$\bar{}$ coefficient moyen de correction (intégré en envergure)

INTRODUCTION

Les résultats bruts d'essais de maquettes en soufflerie, après corrections inhérentes à la qualité de l'écoulement de la veine vide (ascendance de veine, gradient longitudinal de pression statique) doivent être corrigés des interactions entraînées par la présence des parois. Ces corrections ont pour but de rétablir, en grandeur et direction, les vitesses modifiées par la présence des parois de manière à déterminer leur champ autour de la maquette, comme si celle-ci était placée dans un écoulement en atmosphère illimitée. Le but de telles corrections n'est pas de donner des résultats identiques à ceux du vol, par suite des différences de nombres de Reynolds, mais de rendre homogènes les résultats de soufflerie obtenus à partir de maquettes d'un même avion réalisées à différentes échelles et essayées dans des veines différentes par la forme et le type de ventilation des parois [1]

Depuis les premiers calculs de correction datant de 1919 [2] , pour des veines guidées, ouvertes ou semi-guidées de nombreuses formules [3], [4] ont été successivement fournies pour ce type de veines avec des schématisations de plus en plus raffinées des maquettes et pour des formes variées de section d'essais. L'utilisation de veines transsoniques à parois ventilées (parois perforées ou à fentes) conduisit en 1950 [5] puis 1954 [6] à généraliser les conditions limites au cas des parois ventilées. Après des calculs fragmentaires [3] de certains coefficients de correction et des schématisations d'envergure finie [7] des formulaires furent établis en 1969 [8 , 9 , 10] à l'aide de la méthode analytique des petites perturbations pour la totalité des coefficients obtenus avec des schématisations de maquettes par singularités uniques en veines circulaires et rectangulaires à 2 ou 4 parois perforées. Les méthodes analytiques de calcul des coefficients de parois développées depuis 1973 sont examinées au paragraphe I.1. En 1967 [11] une méthode plus universelle dite méthode des petits pavés (vortex lattice method) fut proposée en veine guidée puis généralisée en 1972 [12] au cas des parois ventilées. Cette méthode a été particulièrement développée par AMD.BA [13] pour juger, a priori, de l'influence de la forme des sections de veine et de la répartition des ventilations.

Dans l'état actuel des parois ventilées des souffleries transsoniques et des dimensions couramment utilisées de maquettes en essais industriels, les méthodes de calcul théorique des coefficients de correction et de détermination expérimentale de la perméabilité aérodynamique moyenne des parois [13] , malgré certaines hypothèses simplificatrices utilisées, ont été portées à un stade de développement satisfaisant en ce sens que les erreurs commises sur les corrections n'excèdent pas les dispersions de mesures.

A ce jour, il n'apparaît pas que toutes les possibilités des souffleries existantes aient été mises à profit. Le propos de cette note est de montrer que, par des études paramètriques sur ordinateur, il est possible non seulement d'énoncer des recommandations pour dimensionner les maquettes en soufflerie de telle sorte que les corrections de parois puissent être appliquées avec confiance, mais encore de définir des conditions optimales

d'emploi des veines d'essais, associées à des dimensions de maquettes, selon leur type, de façon à ce que les corrections soient faibles ou négligeables.

Sans vouloir prétendre à un écoulement autour de la maquette strictement équivalent à celui régnant en atmosphère illimitée, ainsi que de nouveaux concepts de parois le proposent [14, 15 , 16 , 17] , il est proposé de rechercher des conditions d'utilisation des veines d'essais en service adaptées à un point moyen d'un programme d'essais de manière à ce que pour l'ensemble du programme les corrections de parois puissent être considérées comme faibles ou négligeables vis à vis des dispersions de mesure. Cette adaptation ou "conformation" de la veine à un point particulier d'utilisation doit être bien distinguée de l'"auto adaptation" des parois qui prétend à l'annulation stricte de toutes les corrections en nécessitant un remaniement profond des parois. Il s'agit donc ici de l'utilisation la plus rationnelle possible des concepts classiques de soufflerie à parois perforées.

Par la suite une veine sera appelée "idéale" si elle permet l'annulation des corrections de parois au sens global de ces corrections ; une veine sera appelée "optimale" si elle permet de rendre les corrections de parois négligeables c'est à dire si les corrections sont du même ordre de grandeur que les dispersions de mesure.

1 - SCHEMATISATION DES MAQUETTES EN ECOULEMENT TRIDIMENSIONNEL

1.1 - Méthode analytique des petites perturbations

La méthode analytique des petites perturbations a été particulièrement développée à l' ONERA car spécialement adaptée au cas des souffleries transsoniques industrielles de Modane dont les veines, de forme rectangulaire, possèdent deux parois horizontales perforées. Cette méthode consiste à rechercher une formulation mathématique directe des coefficients de correction de parois.

Le calcul des coefficients de corrections est basé sur la détermination du potentiel φ_i des vitesses complémentaires induites par la présence des parois. Ce potentiel φ_i est déduit, d'une part du potentiel φ_m des vitesses de l'écoulement règnant autour de la maquette en atmosphère illimitée, d'autre part des conditions aux limites imposées par les parois de la veine. La perméabilité des parois est supposée constante et égale de l'infini amont à l'infini aval. Les dérivées du potentiel de perturbation φ_i par rapport à x, y, z sont les vitesses de perturbations axiales u_i , transversales v_i et verticales w_i . Les vitesses de perturbations transversales, très petites, sont négligées.

Dans le cas de veine possèdent des parois verticales pleines, la méthode des images remplace la condition limite sur ces parois. Des transformées de FOURIER sont nécessaires pour tenir compte des conditions aux limites sur les parois horizontales. En prenant une condition de vitesse nulle, et non de potentiel nul, à l'infini aval, les transformées de FOURIER effectuées sur les vitesses [18] permettent de lever les paradoxes de discontinuité des corrections de blocage de sillage en veine guidée [19] et de portance en parois horizontales ouvertes. Ces discontinuités apparaissent alors comme des limites de fonctions lorsque x tend vers $-\infty$.

Lorsque la veine possède un plan horizontal de symétrie, c'est à dire que les perméabilités des deux parois sont égales, les corrections appliquées aux maquettes, calculées dans le plan de symétrie de la veine (z nul) sont simplifiées :

- les vitesses axiales de pertubation u_{is} , u_{iw} ne sont dues qu'aux singularités utilisées pour schématiser le volume apparent et le sillage de la maquette qui conduisent aux corrections de blocage de volume et de sillage

- les vitesses verticales de perturbations w_{iL} ne dépendent que des singularités représentant la surface portante de la maquette qui conduisent aux corrections dites de portance.

Les vitesses de perturbation sont présentées sous forme de coefficients sans dimensions :

- les vitesses axiales normées à celles obtenues au centre maquette (x nul) en veine guidée donnent les coefficients de corrections de blocage

$$\Omega_{s,w}(x) = \frac{u_{is,w}(x)}{u_{is,w_c}(0)}$$

- la vitesse verticale normée à $C/C_z S$ donne le coefficient de correction de portance

$$\delta(x,y) = \frac{w_{iL}}{U_\infty} \frac{C}{C_z S}$$

et le coefficient moyen de cette correction est

$$\bar{\delta}(x) = \frac{1}{S}\int_0^S \delta(x,y)\, dy$$

Les formules de Ω_s , Ω_w et $\bar{\delta}$ sont données en annexe 1. Ces coefficients sont calculés une fois pour toute en fonction des paramètres définissant la veine d'essais (x , Q et λ) et la maquette (τ, Λ). Des tables complètes de coefficients ont été ainsi établies dans le cas de maquettes complètes et demi-maquettes à la paroi en fonction de leurs envergures et flèche pour les souffleries transsoniques industrielles de Modane en fonction de la perméabilité des parois.

En principe il n'existe pas de limitations dans l'emploi de la méthode analytique mais elle risque de conduire à des formules compliquées nécessitant l'emploi de fonctions spéciales. Tel est le cas de répartitions elliptiques de portance en veines rectangulaires conduisant à des intégrales elliptiques, ou le cas des veines circulaires conduisant à des fonctions modifiées de BESSEL d'ordre élevé. Ceci ne constitue pas un handicap sérieux, car les coefficients sont calculés une fois pour toutes, donc les durées de calcul sur ordinateur seront amorties par l'utilisation des tables des coefficients de correction. Il n'en reste pas moins vrai qu'il est inutile de raffiner trop les schématisations de maquettes si les écarts engendrés sur les corrections par ces raffinements ne sont pas perçus de manière significative au niveau des corrections elles-mêmes.

1.2 - Schématisation des maquettes

Dans le cas des corrections de blocage de volume et de sillage, des singularités uniques: doublet et source, sont suffisantes pour représenter le volume apparent de la maquette et son sillage proportionnel à la traînée.

Dans le cas des corrections de portance, partant d'une singularité unique constituée par un tourbillon en fer à cheval, de circulation proportionnelle à la portance, la schématisation de la maquette peut être progressivement affinée pour tenir compte de :

- l'envergure finie de la voilure
- la flèche
- le type de répartition de circulation en envergure
- la déflexion de la nappe tourbillonnaire

Le type de modélisation de la maquette dépend essentiellement de la taille de la maquette vis à vis des dimensions de la veine d'essais. Lorsque celle-ci augmentera, il sera de plus en plus nécessaire de tenir compte des paramètres énoncés ci-dessus. Le seul moyen de s'assurer qu'une schématisation est suffisante est de vérifier qu'un raffinement supplémentaire ne modifie pas de manière sensible les corrections de parois c'est à dire que les écarts de corrections dus à la schématisation maquette restent inférieurs à la dispersion des mesures.

En référence de la valeur du coefficient de portance $\bar{\delta}$ obtenu à l'aide d'une singularité unique ($\tau = 0$), le coefficient $\bar{\delta}$ croît rapidement avec l'augmentation du rapport $\tau = 2s/B$ (figure 1) et ceci d'autant plus que la porosité est élevée. Cette évolution est plus modérée lorsqu'une répartition elliptique de circulation en envergure remplace une répartition uniforme. Enfin, lorsque la flèche Λ de l'aile croît, l'augmentation de $\bar{\delta}$ avec τ est nettement réduite.

Les évolutions du coefficient $\bar{\delta}_1$ de courbure de champ sont données figure 2 en fonction de l'abscisse X pour deux valeurs élevées de Q :

Pour une aile droite uniformément chargée l'augmentation de l'envergure réduit de manière importante la courbure de champ au voisinage de la maquette. Au delà de $x = \frac{3}{2}B$ la courbure de champ est pratiquement indépendante de la taille de la maquette. Il y a lieu de bien remarquer que, <u>à perméabilité maximale</u> ($Q = 1$), <u>plus la maquette sera grande, plus les corrections de courbure de champ seront faibles</u>. Sous cet aspect, il y a donc tout intérêt à accroître la taille des maquettes : une valeur $\tau = 0{,}80$ est nettement moins sujette à correction qu'une valeur égale ou inférieure à 0,60. Ce point est à retenir car intuitivement on pourrait penser le contraire.

Pour un rapport $\tau = 0{,}6$, l'influence de la flèche est nette à perméabilité maximale au voisinage de la maquette : l'accroissement de la flèche, à même envergure, contribue à réduire $\bar{\delta}_1$, en valeur absolue. Comme précédemment, au delà de $x = \frac{3}{2}B$, la modélisation de la maquette est sans importance.

Les évolutions de la correction d'incidence, normée au coefficient de portance $\Delta\alpha/C_L$ en fonction du rapport $\tau = 2s/B$ et du type de répartition de circulation en envergure sont données figure 3 pour une aile droite. Considérant que l'écart entre deux types de modélisation ne doit pas excéder la dispersion des mesures, soit 0,03° d'incidence, il apparaît qu'une singularité unique est suffisante si τ reste inférieur à 0,4. Le type de répartition de circulation en envergure doit être pris en considération au delà de $\tau = 0{,}6$ pour $Q = 0{,}6$ mais seulement de $\tau = 0{,}75$ pour $Q = 1$.

La correction d'incidence :

$$\frac{\Delta\alpha}{C_L} = \frac{\bar{c}}{2s} \cdot \frac{\tau^2}{\lambda} \left(\bar{\delta}(0) + \frac{\bar{c}}{2s} \tau \frac{\partial \bar{\delta}\left(\frac{\bar{c}}{2}\right)}{\partial \frac{x}{\frac{3}{2}B}} \right)$$

où $\quad \frac{\bar{c}}{2s} = AR^{-1} \sim \frac{tg\Lambda}{3} \quad (si\ \Lambda \neq 0)$

calculée, pour trois flèches Λ à 25 % des cordes, à Mach 0,9 fait ressortir (figure 4) l'importance de la schématisation de la voilure. Les écarts entre les corrections croissent avec τ et Λ ainsi que le montrent les trois courbes calculées pour :

- une envergure nulle ($\tau = 0$)
- une envergure finie, sans flèche ($\tau \neq 0$, $\Lambda = 0$)
- une envergure finie, avec flèche ($\tau \neq 0$, $\Lambda \neq 0$)

Les écarts sont notables, même pour les tailles couramment utilisées de maquettes ($\tau \sim 0{,}6$). Dans le plan (Λ, τ) (figure 5), il est possible de définir des domaines de modélisation, tels que les erreurs entraînées par le type de modélisation n'excèdent pas 0,03° d'incidence.

Ainsi à Mach 0,9 pour une soufflerie carrée à parois horizontales perforées, dans le cas d'une maquette d'avion de transport transsonique, il y a lieu de tenir compte de l'envergure puis de la flèche quand τ dépasse respectivement 0,5 et 0,65. Pour un chasseur ces limites deviennent

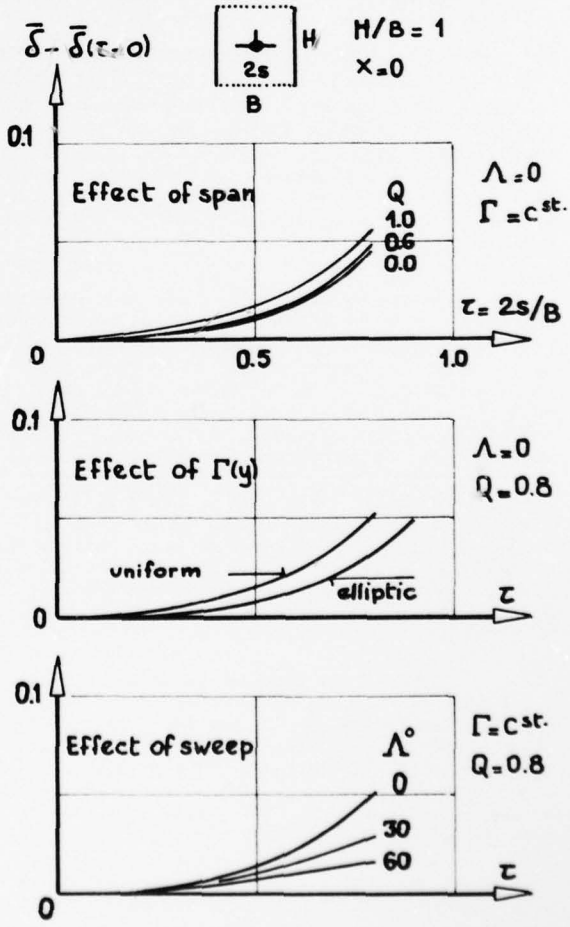

FIGURE 1 Influence de la modélisation de la maquette sur le coefficient de correction de portance

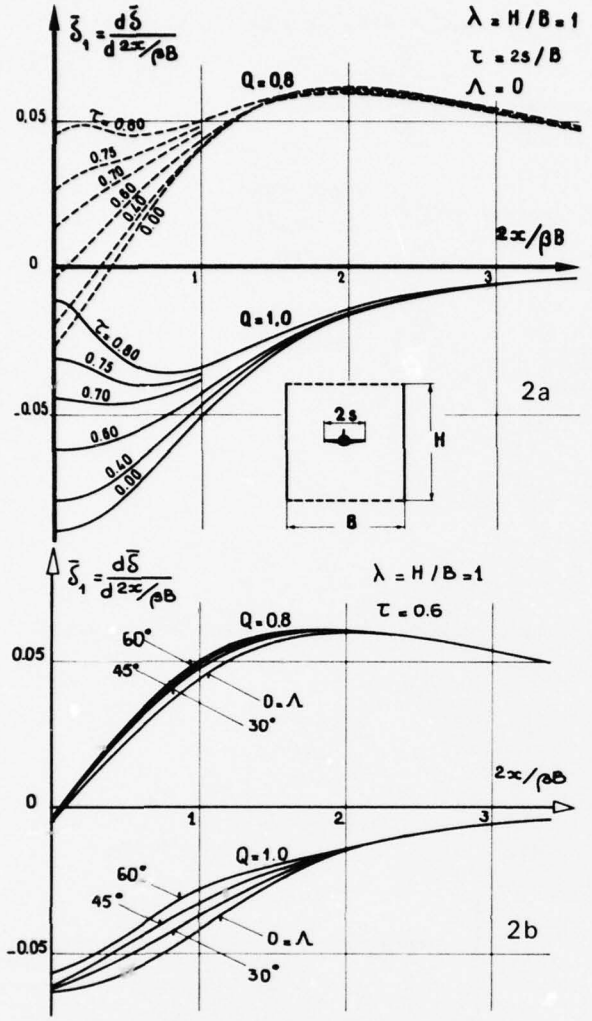

FIGURE 2 Influence de la modélisation de la maquette sur le coefficient de correction de courbure de champ. Aile uniformément chargée.

2a - Influence de l'envergure réduite τ à flèche nulle

2b - Influence de la flèche à τ = 0,6

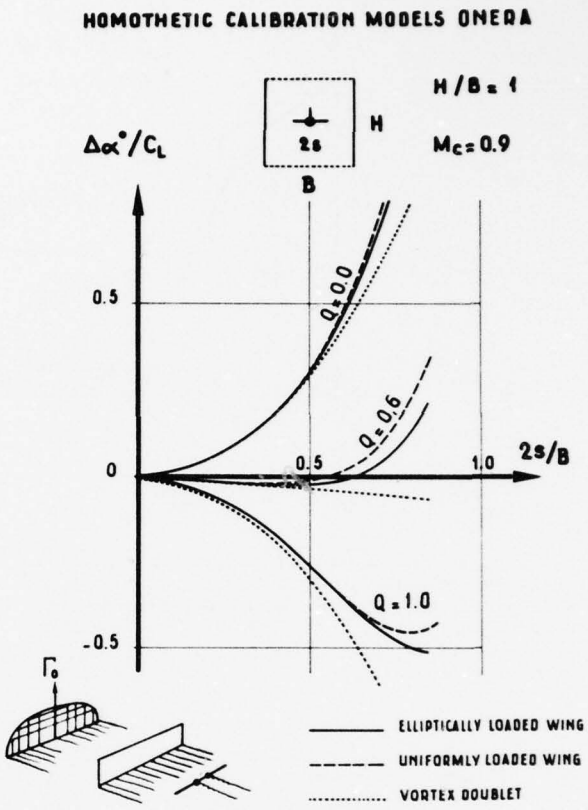

FIGURE 3 Influence de la répartition de circulation en envergure sur la correction d'incidence

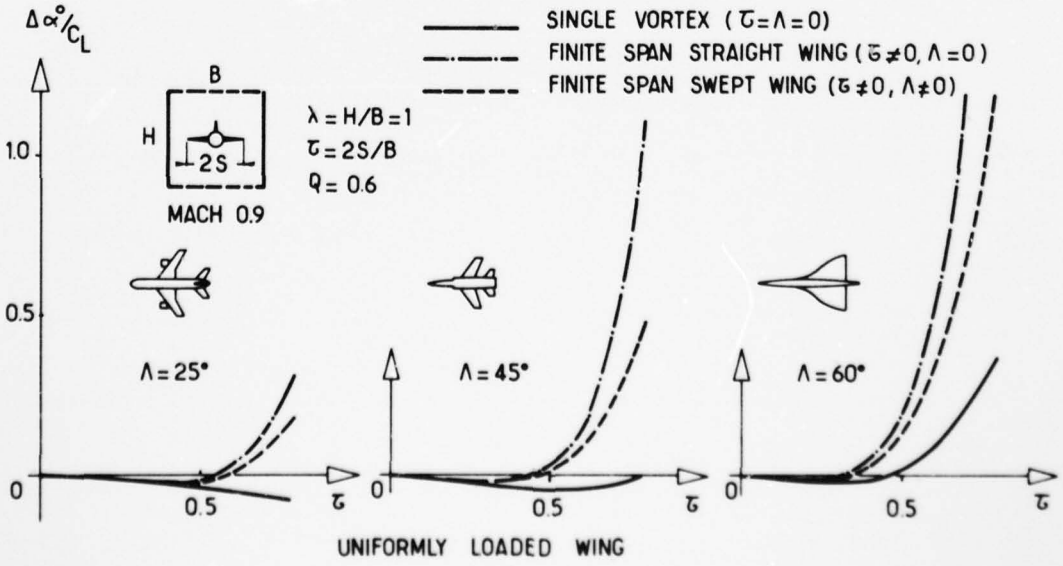

FIGURE 4 Influence de la schématisation de la maquette sur la correction d'incidence

AD-A034 324 ADVISORY GROUP FOR AEROSPACE RESEARCH AND DEVELOPMENT--ETC F/G 14/2
NUMERICAL METHODS AND WINDTUNNEL TESTING.(U)
OCT 76

UNCLASSIFIED AGARD-CP-210 NL

2 OF 3
AD-A
034 324

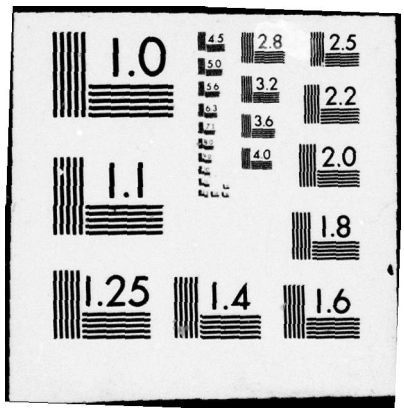
1.0
1.1
1.25
1.4
1.6
1.8
2.0
2.2
2.5
2.8
3.2
3.6
4.0
4.5
5.0
5.6
6.3
7.1
8.0
9.0
10.0

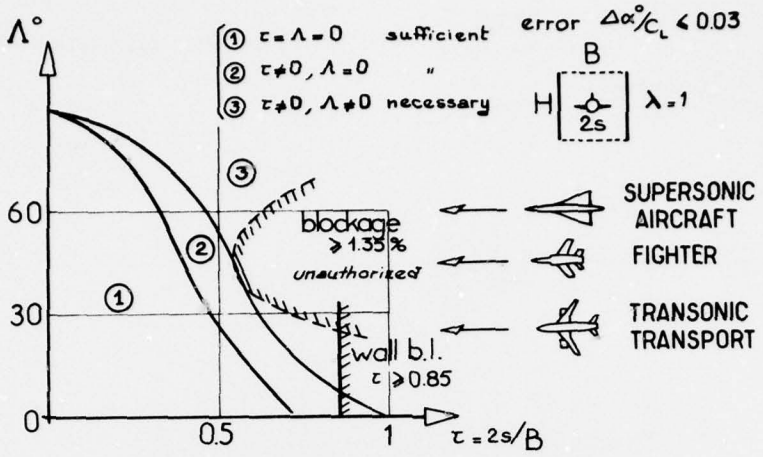

FIGURE 5 Limites de schématisation des maquettes

0,4 et 0,55. Comme dans ce dernier cas on verra qu'il est prudent de ne pas dépasser une obstruction de 1,35 % , il n'est pas nécessaire de tenir compte de la flèche. Pour un avion de transport supersonique, à flèche accusée, les deux limites sont plus restrictives (τ = 0,33 et 0,46).

Bien entendu, les coefficients calculés pour la schématisation la plus poussée peuvent être utilisés mais ceci n'est pas toujours nécessaire et permet d'éviter de longs calculs pour établir des tables de coefficients plus volumineuses.

2 - LIMITES D'EMPLOI DES CORRECTIONS CLASSIQUES EN ECOULEMENT TRIDIMENSIONNEL

Une étude des corrections de parois avec porosité uniforme en veine de section constante a été effectuée en fonction des divers paramètres intervenant dans les différentes corrections (annexe 2). Une telle étude permet d'énoncer des recommandations pour dimensionner les maquettes en soufflerie. Il apparaît en effet utile de préciser jusqu'à quelle taille raisonnable de maquettes, les corrections de parois peuvent être appliquées avec confiance.

2.1 - Limitations dues à la formule de corrections du Mach

La formule de corrections des nombres de Mach est du 8ème degré en Mach corrigé Mc. Dans le cas de veines guidées ou à faible perméabilité il existe des limites en Mach (figure 6) qui ne sauraient être transgressées par manque de solution de l'équation. En veine guidée, la limite obtenue correspond de manière satisfaisante au nombre de Mach de blocage obtenu en essais, ce qui valide la formule utilisée et fournit une limite d'emploi des des veines guidées. Aux fortes perméabilités des parois, la formule du Mach corrigé possède toujours une solution quel que soit le nombre de Mach d'essai ; il est alors raisonnable de limiter ce dernier Mu à 1 (figure 6).

Les paramètres intervenant dans ces limitations en Mach sont :
- les caractéristiques de la veine d'essais et la perméabilité des parois
- le volume de la maquette et la surface de voilure
- le coefficient de traînée inclus dans la correction due au blocage de sillage.

Un exemple d'abaque des Mc limites est présenté (figure 6) pour des maquettes homothétiques des maquettes étalon ONERA dans une soufflerie carrée à parois horizontales perforées telle que S2 Modane.

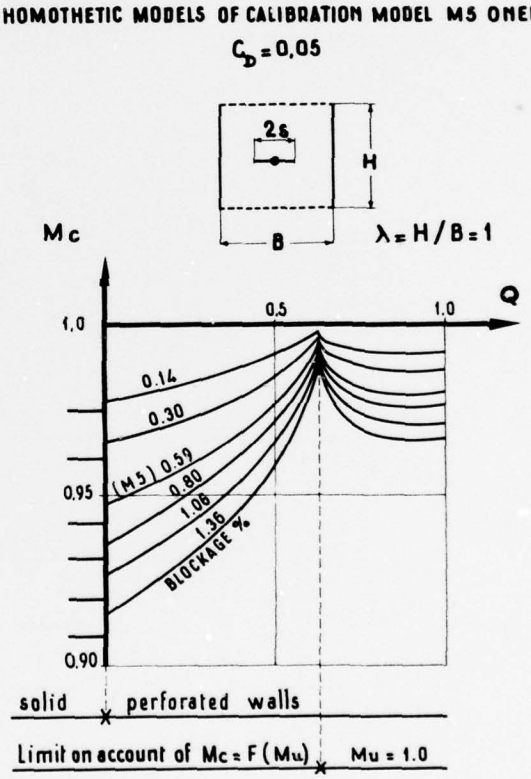

FIGURE 6 Limitation en nombre de Mach corrigé

Bien qu'une très faible perméabilité débloque la veine d'essais, et que les Mach d'essais Mu soient très différents, les limites Mc sont seulement un peu plus élevées en veine très faiblement perméable qu'en veine guidée. Heureusement, la limite Mc croît rapidement avec le facteur de porosité Q , libérant un domaine de Mach maximal pour Q = 0,65. Il est cependant illusoire de se tenir au maximum du domaine très susceptible à certains paramètres. Il est préférable d'utiliser des perméabilités élevées en écou-

lement tridimensionnel (Q de 0,8 à 1,0). Cependant, il y a lieu de noter que pour des nombres de Mach élevés, supérieurs à 0,90, les parois perforées tendent à se comporter comme des parois optimales ($Q \sim 0{,}65$) réduisant d'elles-mêmes les corrections de Mach.

Les courbes Mc limite = F (Q) sont peu sensibles à la forme des maquettes ; ainsi entre des maquettes de grand allongement et des corps de révolution, les écarts de Mc limite ne dépassent pas 0,003 pour deux parois perforées. Par contre ces écarts atteignent 0,016 avec quatre parois perforées.

A perméabilité élevée, si le Mach limite Mc est identique en veines rectangulaires de rapport $\lambda = H/B = 0{,}5$ avec deux ou quatre parois perforées, il n'en va plus de même en veine carrée: dans ce cas une veine à deux parois perforées autorise un Mc supérieur de 0,015 à celui d'une veine à quatre parois perforées pour une obstruction de 1 %.

2.2 - Critères de dimensionnement de maquettes

Les critères proposés pour dimensionner des maquettes consistent à admettre que les corrections de parois resteront d'un niveau tolérable en regard des valeurs mesurées, c'est à dire qu'une erreur commise sur une correction sera compatible avec la dispersion de la mesure de la valeur corrigée. Le critère proposé ici consiste à admettre une erreur de 5 % sur les corrections ; compte tenu d'une dispersion de mesures de 1 % ceci signifie que les corrections pourront atteindre 20 % de la valeur corrigée. Pour le nombre de Mach et l'incidence les corrections ne devront pas excéder 0,04 et 0,6 degré en effet :

$0{,}05 \quad \Delta C_i \sim 0{,}01 \quad C_i \Longrightarrow \Delta C_i / C_i = 20\ \%$

$0{,}05 \quad \Delta M \sim 0{,}002 \Longrightarrow \Delta M = 0{,}04$

$0{,}05 \quad \Delta\alpha^\circ \sim 0{,}03^\circ \Longrightarrow \Delta\alpha = 0{,}6^\circ$

En fait les limitations les plus restrictives sont dues à la correction ΔC_{D_S} engendrée par le gradient longitudinal de vitesse de perturbation créé par le blocage de volume. Dans le plan obstruction-Mach (figure 7) les deux limitations sont celles dues d'une part à la formule de Mach corrigé M_C (paragraphe 2.1), d'autre part à la correction ΔC_{D_S}. La première, en référence de la veine guidée (Q = 0) libère un domaine maximal à Q = 0,63, dans le cas considéré de veine d'essais, puis légèrement plus restreint en parois horizontales ouvertes (Q = 1).

La correction ΔC_{D_S}, nulle en parois pleines ou ouvertes, devient très restrictive pour Q = 0,4. Le plus large domaine (Mc, obstruction) est libéré, en regard du domaine obtenu en veine guidée, (courbe en trait interrompu) pour une perméabilité maximale Q = 1. Une réduction de perméabilité vers Q = 0,63 ne libèrera qu'une écaille de Mach élevé et restreindra l'obstruction aux Mach inférieurs à 0,98.

Le diagramme présenté figure 7 peut en fait se lire en :
- obstruction pour une maquette de chasseur
- rapport envergure/largeur de veine pour une maquette d'avion de transport transsonique.

Le choix d'une très grande perméabilité autorise donc une limite en Mach de 0,965 pour :
- $\tau = 0{,}85$ pour une maquette de grand allongement
- obstruction = 1,35 % pour une maquette de chasseur

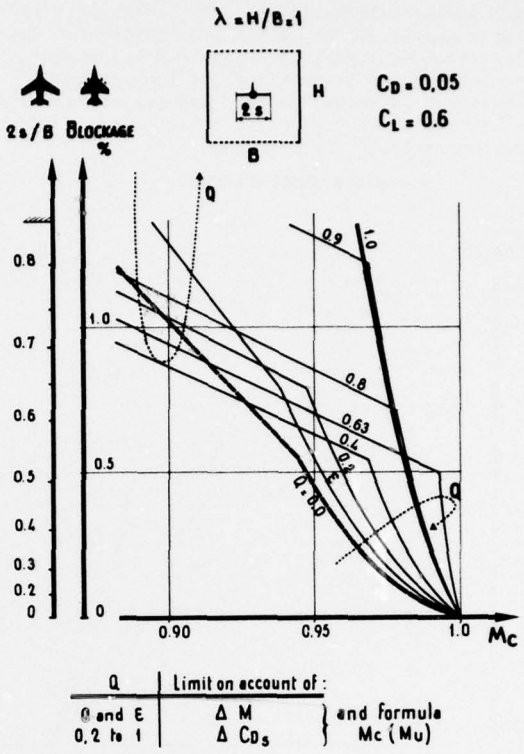

FIGURE 7 Abaque de dimensionnement des maquettes complètes

Dans le premier cas les dimensions de maquettes autorisées sont nettement supérieures à celles usitées ($\tau \sim 0{,}6$) et par suite permettraient un accroissement de Reynolds de 40 % qui peut être décisif si le nombre de Reynolds est voisin de 3 à 4 millions.

L'établissement d'abaque similaire pour le cas d'une veine carrée et d'une demi-maquette à la paroi (donc équivalent au cas d'une maquette complète en veine définie par $\lambda = 0{,}5$) montre (figure 8) que les corrections seront identiques si le rapport d'échelle entre maquette complète et demi-maquette est compris entre 0,8 et 1,1 selon la correction considérée. En outre pour une même échelle de maquettes et demi-maquettes, la limitation en Mach corrigé apparaît plus tôt pour la demi-maquette à forte perméabilité.

Sous le seul aspect des corrections de parois, il est illusoire de réaliser dans une veine carrée des essais sur demi-maquettes pour accroître le nombre de Reynolds. Bien entendu le cas d'une section définie par $\lambda = 0{,}7$ conduit aux mêmes limitations en maquette complète et demi-maquette mais, en référence d'une veine carrée, au détriment de la maquette complète et à l'avantage de la demi-maquette.

3 - RECHERCHE DE VEINES "IDEALE" ET "OPTIMALE" EN ECOULEMENT TRIDIMENSIONNEL

Le calcul des corrections de parois dans le cas des veines existantes ne pose pas de problème une fois les lois de perméabilité des parois définies [13] et des tables de coefficients de corrections établies. Il est cependant intéressant de rechercher si des conditions d'utilisation peuvent annuler les corrections ou les réduire à un niveau tel qu'elles puissent être négligées. Ce peut être en associant à une veine existante une maquette de taille bien définie ou en modi-

fiant les caractéristiques (λ , Q) de la veine d'essais. Cette utilisation meilleures des veines peut être définie à partir d'une étude paramétrique des corrections sur ordinateur en recherchant la veine "idéale" exempte de toutes corrections ou une veine "optimale" conduisant à des corrections négligeables.

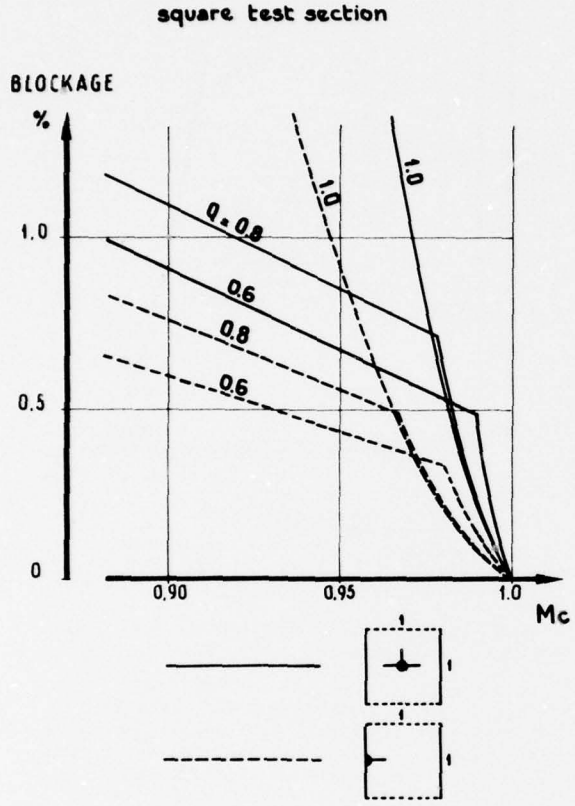

FIGURE 8 Dimensionnement de maquettes complètes et demi-maquettes

Les conditions d'annulation des diverses corrections sont examinées séparément puis simultanément.

3.1 - Annulation des corrections de blocage

La correction de nombre de Mach due aux blocages de volume et de sillage sera nulle (annexe 2) si les deux coefficients de correction correspondants Ω_S et Ω_W sont simultanément nuls. En outre les corrections de traînée dues aux gradients longitudinaux de vitesses induites dues aux mêmes blocages seront nulles si les coefficients Ω'_S et Ω_S (car $\Omega'_W = \Omega_S$) sont nuls.

Les trois coefficients Ω_S , Ω_W et Ω'_S dépendent de deux caractéristiques des veines : λ et Q . Quelle que soit la forme de la veine, donc λ , Ω'_S s'annule en parois pleines ($Q = 0$) et ouvertes ($Q = 1$). Le coefficient Ω_W ne peut s'annuler qu'en paroi ouverte ($Q = 1$). Le coefficient Ω_S s'annule pour une valeur de porosité dépendant de λ (figure 9) . *Les trois coefficients sont simultanément nuls dans le seul cas (figure 10)*

$$Q = 1 \qquad \lambda = 1{,}18$$

L'intérêt d'une telle veine a été souligné de longue date [20] ainsi que rappelé récemment [21] . Il y a lieu de noter en outre qu'ex-

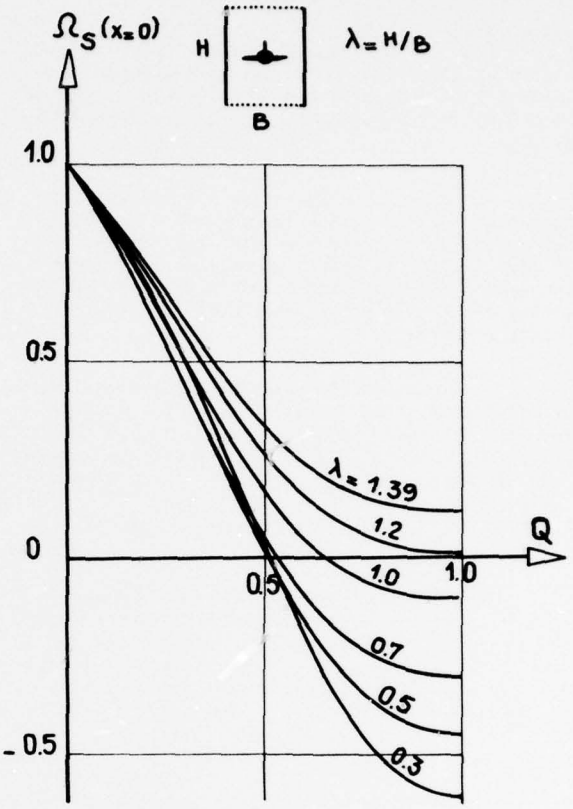

FIGURE 9 *Coefficient de correction de blocage de volume* Ω_S

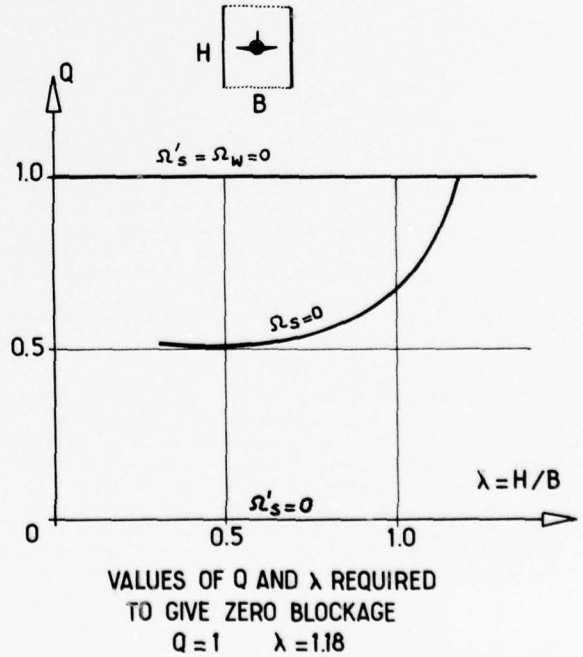

FIGURE 10 Annulation des coefficients de correction de blocage

périmentalement il a été constaté que la porosité Q = 1 conduisait à des corrections de décollement négligeables [13]

La condition Q = 1 signifie que la différence des pressions entre la veine d'essais et l'enveloppe étanche l'entourant est nulle. Cette condition peut être fortuitement satisfaite : tel est le cas de la soufflerie S2 de Modane [13] dont la veine équipée de parois conventionnelles perforées à trous inclinés à 60° au taux de 6 % est placée dans un caisson de très grandes dimensions. Cette condition pourrait également être utilement imposée par réglage du dispositif d'aspiration au travers des parois ventilées.

3.2 - Annulation des corrections de portance

En écoulement tridimensionnel, en reportant toute la correction de portance sur celle d'incidence (annexe 3) il suffit pour annuler celle-ci et la correction de traînée qui en découle, que

$$\bar{\delta}(x=0) + A \frac{\partial \bar{\delta}}{\partial x}(x=A) = 0$$

où $A = \frac{\tau}{\beta} \frac{tg\Lambda}{3}$ si $\Lambda \neq 0$ et $A = \frac{\tau}{7\beta}$

pour $\Lambda = 0$ et un allongement de 7.

A partir du programme de calcul des coefficients $\bar{\delta}$ et $\bar{\delta}_1$ (dérivée de $\bar{\delta}$ par rapport à X) les porosités Q annulant la correction d'incidence sont déterminées sur ordinateur en fonction des quatre paramètres M , τ , et λ, Λ.

Le réseau des courbes (Q, τ, λ) annulant la correction d'incidence à Mach 0,9 pour une aile droite d'allongement 7 (figure 11) peut ainsi être établi : il nécessite 15 minutes de calcul sur IRIS 80. Pour annuler la correction d'incidence sur une maquette donnée dans une soufflerie donnée il faudra ajuster la porosité des parois. Si cette porosité est fixée il faudra associer une dimension de maquette τ à la forme de la soufflerie λ . La forme rectangulaire définie par λ = 1,91 pour une soufflerie à parois horizontales ouvertes Q = 1 et une envergure faible τ = 0 est connue déjà de longue date [22] . A porosité maximale Q = 1, la correction d'incidence sera nulle si l'envergure relative τ de la maquette est d'autant plus élevée que la forme de la section tendra vers un carré (λ = 1).

L'influence du nombre de Mach sur les conditions (Q, τ, λ) rendant nulle la correction d'incidence (figure 12) est d'autant plus faible que la porosité est élevée. En particulier à Q = 1 les conditions requises sont indépendantes du nombre de Mach.

L'influence de la flèche Λ de voilure (figure 13) est de la même manière d'autant plus faible que la porosité est élevée. Toutefois à porosité maximale (Q = 1) l'influence de Λ subsiste et se manifeste d'autant plus que l'envergure relative τ de la maquette est grande.

3.3 - Veine "idéale" exempte de toutes corrections

Il a été vu au paragraphe 3.1 que les conditions requises pour annuler les corrections de blocage étaient Q = 1 , λ = 1,18 . A porosité maximale les conditions τ, λ, Λ requises pour annuler les corrections de portance (figure 14) sont insensibles au nombre de Mach. Il s'ensuit que pour annuler simultanément les corrections de blocage et de portance il faut associer à une veine (Q = 1 λ = 1,18) une maquette dont l'envergure relative τ dépend

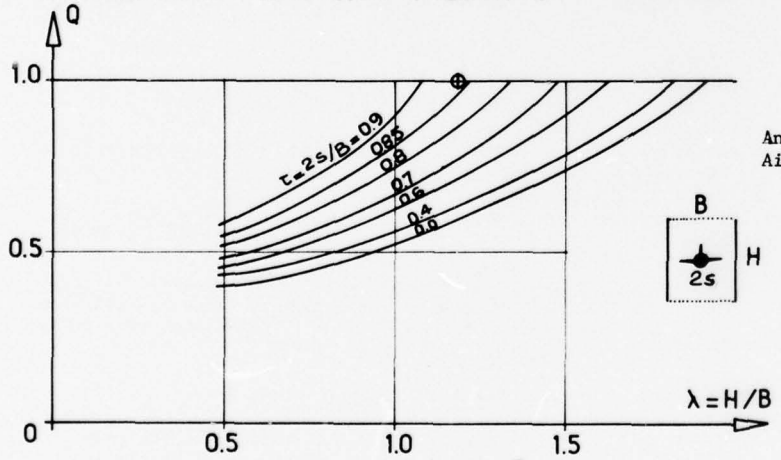

FIGURE 11

Annulation de la correction d'incidence
Aile droite - Mach 0,9

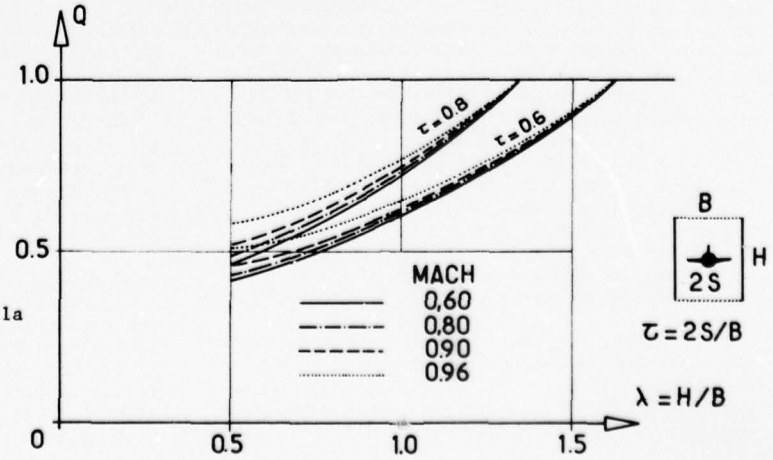

FIGURE 12

Influence du Mach sur l'annulation de la correction d'incidence - aile droite

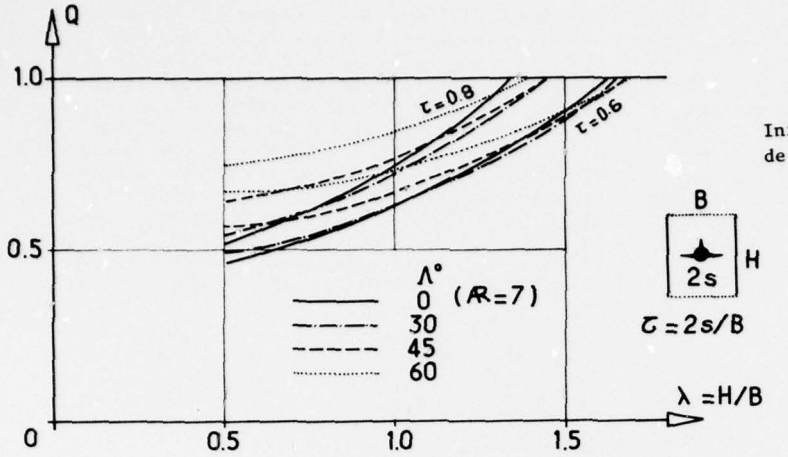

FIGURE 13

Influence de la flèche sur l'annulation de la correction d'incidence. Mach 0,9

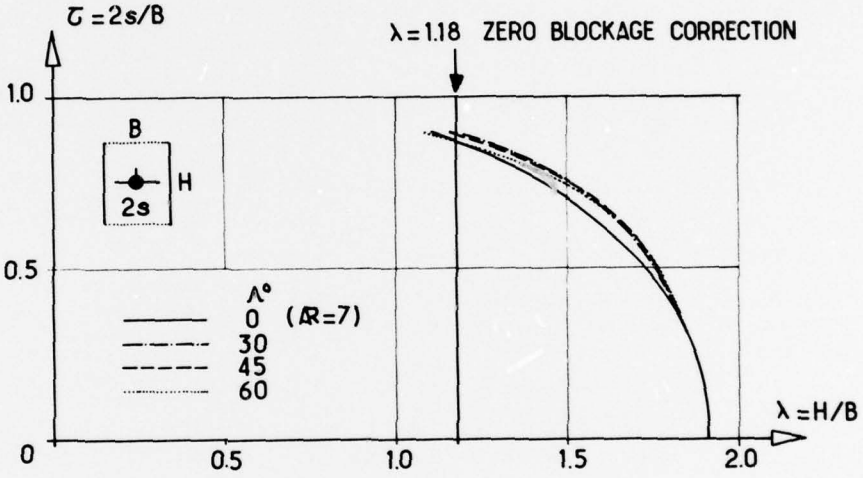

FIGURE 14

Annulation de la correction d'incidence à Q = 1

faiblement de la flèche : τ = 0,86 à 0,89 (figure 14). Une telle valeur de τ implique un nombre de Reynolds suffisamment élevé pour que les extrémités d'ailes ne soient pas dans la couche limite des parois latérales : A titre d'illustration les épaisseurs de couche limite δ des parois de la soufflerie S2 de Modane autoriseraient une valeur maximale τ = 0,91 à une pression génératrice de 1,8 bar.

3.4 - Veines "optimales" à corrections de portance négligeables

La veine définie ci-dessus ne peut être considérée comme "idéale" qu'en lui associant une envergure relative τ de maquette dont la valeur élevée (0,86 à 0,89) peut être redoutée. En fait, au lieu de rechercher les caractéristiques veine-maquette conduisant à la stricte annulation de toutes les corrections de parois, on peut se contenter de chercher dans quelles conditions les corrections peuvent être négligées c'est à dire qu'elles ne dépassent pas les dispersions de mesures : une telle veine sera considérée comme "optimale". Bien que les corrections soient utilisables avec confiance, dans la gamme de taille de maquettes, définie au paragraphe 2, une veine "optimale" permettra, en évitant les calculs de correction, de réduire les coûts et délais d'obtention des résultats d'essais industriels.

Dans un premier stade, une veine "optimale" au sens des corrections de portance est recherchée. Il est en effet loisible de contrer, par un réglage de la divergence des parois horizontales, la correction de traînée due au blocage par une correction due au gradient longitudinal de pression de la veine vide (buoyancy).

Avec les notations au paragraphe 3.2, la correction de portance, entièrement reportée sur celle d'incidence est :

$$\Delta\alpha^\circ/C_L = 57.3\,\frac{\tau\beta}{\lambda} A\left[\bar{\delta}(x=0) + A\frac{\partial\bar{\delta}}{\partial x}(x=A)\right]$$

Les courbes iso $\Delta\alpha/C_L$ sont obtenues sur ordinateur. De tels réseaux (figures 15 et 16) dépendent des paramètres M, Λ et Q ; ils nécessitent 20 minutes de calcul sur IRIS 80.

3.4.1 - Veine de porosité fixée Q = 1

Les réseaux iso $\Delta\alpha/C_L$ calculés pour M = 0,9 , Q = 1 et 2 flèches 0 et 45 degrés sont donnés figures 15 et 16. En tolérant une correction $|\Delta\alpha^\circ/C_L| \leq 0.1$ qui n'entraîne qu'une incertitude de 1 à 2 % du gradient de portance, et en se fixant une limite maximale raisonnable de τ = 0,85 , il est possible de définir des domaines (τ, λ) autorisés. Comme la correction d'incidence est proportionnelle à τ^2 , ces zones sont d'autant plus étendues que τ est réduit. Par contre de telles zones sont réduites par une augmentation de la flèche

Pour une flèche nulle (figure 15), selon λ , une ou deux plages de τ sont permises : une seule plage pour $\lambda \leq 1{,}16$ et $\lambda \geq 1{,}36$; Deux plages pour $1{,}16 \leq \lambda \leq 1{,}36$. Dans ce cas, de grandes valeurs de τ sont permises, mais les valeurs moyennes sont interdites. La plus forte valeur de τ = 0,85 n'est autorisée que si $1{,}16 \leq \lambda \leq 1{,}30$.

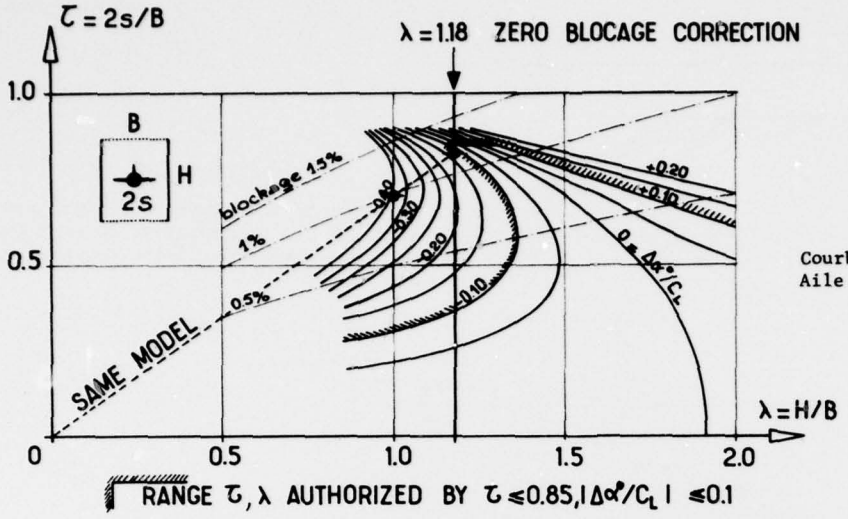

FIGURE 15

Courbes iso-correction d'incidence - Aile droite - Mach 0,9 - Q = 1

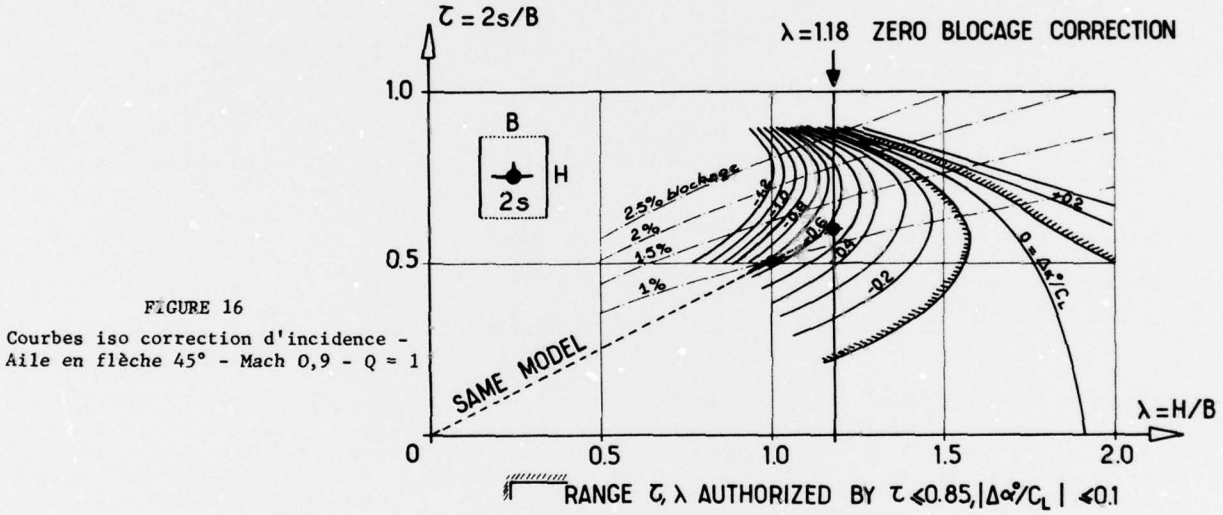

FIGURE 16

Courbes iso correction d'incidence - Aile en flèche 45° - Mach 0,9 - Q = 1

Pour une flèche de 45 degrés (figure 16) cas des maquettes de chasseurs, la zone autorisée s'est déplacée vers des valeurs plus élevées de λ . La plus grande envergure (τ = 0,85) n'est autorisée que si $1{,}26 \leq \lambda \leq 1{,}33$. Il n'existe pas de limite en envergures intermédiaires si λ dépasse 1,58.

Beaucoup de veines existantes sont carrées (λ = 1) et possèdent une porosité élevée de parois (Q = 1). Une règle communément admise pour fabriquer les maquettes est de ne pas dépasser τ = 0,7 ou une obstruction de 1 %. Fortuitement, à flèche nulle, ce choix est le plus défavorable (figure 15). Une diminution de largeur de veine pour porter λ à 1,18, possèderait dans ce cas, sans changer de maquette, l'avantage de

- annuler les corrections de blocage (paragraphe 3.3)
- s'affranchir des corrections de portance.

Un tel résultat n'était pas prévisible sans calcul du réseau iso $\Delta\alpha / C_L$ sur ordinateur; il démontre qu'un accroissement de τ et de l'obstruction réduit nettement les corrections au point de pouvoir les annuler ou les ignorer. Dans le cas d'une flèche de 45 degrés (figure 16) ce raisonnement n'est plus entièrement valable, lorsque λ passe de 1 à 1,18 sans modifier la maquette, les corrections de blocage sont encore annulées mais les corrections de portance sont seulement réduites de 15 % et ne peuvent être négligées.

3.4.2 - Veine de porosité réglable

Les zones (τ, λ) telles que $|\Delta\alpha^\circ/C_L| \leq 0.1$ obtenues pour deux flèches de 0 et 45 degrés (figures 17 et 18) se déplacent vers des valeurs plus faibles de λ lorsque Q diminue. Donc pour une veine, à porosité réglable, un ajustement de porosité Q à la valeur de τ permet d'annuler les corrections de portance, en ne se préoccupant pas des corrections de blocage. Les seules restrictions existent à τ d'autant plus élevé que λ est faible (d'environ λ = 1,32 à τ = 0,85 jusqu'à λ = 2,0 à τ = 0,5).

3.5 - Veines "optimales" à corrections de portance et de traînée négligeables

En rejetant le procédé de réglage de divergence des parois pour annuler la correction de traînée due au blocage, on peut rechercher une veine optimale qui permettra de négliger simultanément les corrections de portance et de blocage:

$$|\Delta\alpha^\circ/C_L| \leq 0{,}1 \quad \text{et} \quad |\Delta C_{D_b}| \leq 0{,}02\, C_{D_{(C_L=0)}}$$

La correction de traînée due aux blocages de volume et de sillage est (annexe 2) :

$$\Delta C_{D_b} = -\frac{4\tau^4 A R\, K_Y \tau_V}{\beta^4 \lambda^{3/2}} \nu^2 \left[\Omega_S' + \Omega_S \frac{C_{D_0}\beta^2(1+0{,}4M^2)}{4\tau A R \nu}\right]$$

où

$$\nu = 0{,}45 \frac{L D^2}{(2s)^3} + 0{,}7 \frac{e}{c} \cdot \frac{1}{(AR)^2}$$

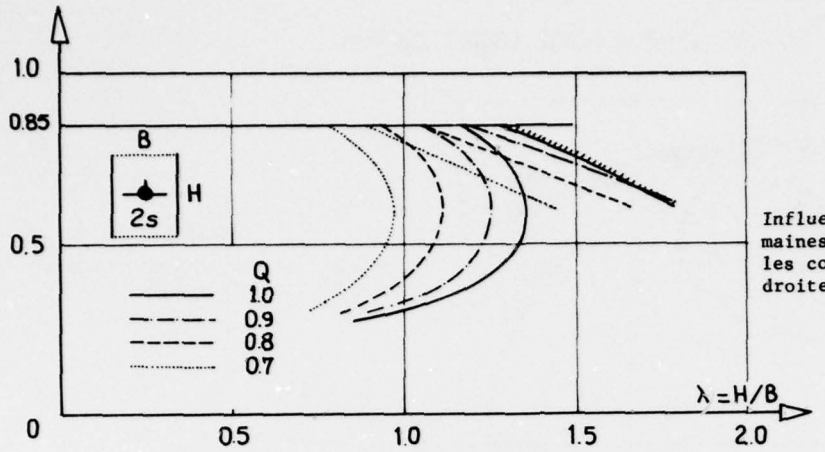

FIGURE 17

Influence de la porosité Q sur les domaines τ , λ permettant de négliger les corrections d'incidence - aile droite

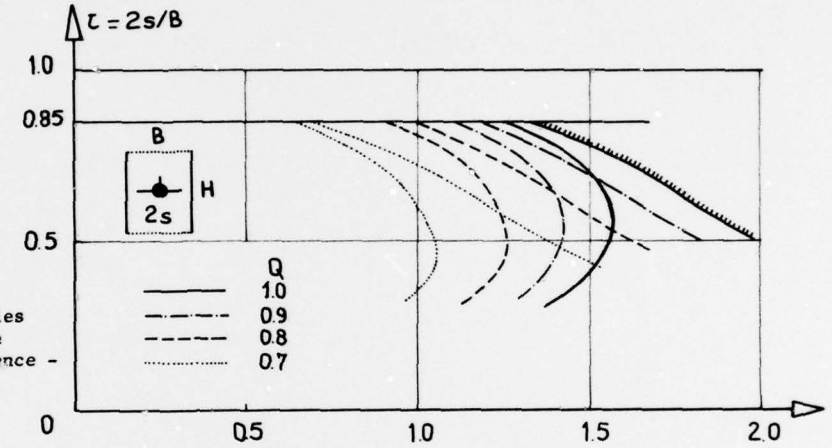

FIGURE 18

Influence de la porosité Q sur les domaines τ , λ permettant de négliger les corrections d'incidence - aile en flèche Λ = 45 degrés

dépend du type de maquette. A titre d'exemple, pour des maquettes d'avion de transport transsonique et de chasseurs, ν est respectivement égal à 0,0091 et 0.035. La limitation en traînée dépend des 5 paramètres λ , τ , Q , M et Λ . Le nombre de Mach est un paramètre décisif car il intervient par β à la puissance 4.

Les limitations correspondant aux conditions, dans lesquelles les corrections d'incidence et de traînée sont négligeables, sont reportées dans le plan (Q, τ) pour 4 formes de veine λ = 1,0 - 1,18 - 1,39 et 1,60 dans le cas de maquettes de flèche nulle (figure 19) et 45 degrés (figure 20).

A flèche nulle (figure 19, et pour une veine carrée, la condition d'incidence n'autorise à τ supérieur à 0,5 qu'une gamme envergure τ de plus en plus étroite lorsque la porosité Q augmente. Si de plus la condition de traînée est superposée à celle d'incidence, la plus grande envergure autorisée est τ = 0,45 pour Q = 0,75 à Mach 0,9 (en exceptant les valeurs de τ supérieures à 0,85). A plus faible Mach, la condition de traînée est moins restrictive et cesse d'intervenir au dessous de Mach 0,5, quelle que soit la porosité. Lorsque λ croît, les conditions de traînée sont moins contraignantes : elles sont couvertes par les conditions d'incidence, pour toute valeur de Q à Mach 0,9 lorsque λ dépasse 1,53. La condition $\Delta\alpha^\circ/C_L > -0,1$ cesse d'intervenir au delà de λ = 1,36 : dans ce cas toute envergure inférieure à τ = 0,83 est permise à Q = 1. Selon la valeur de λ , l'envergure maximale τ sera obtenue a une porosité Q croissant avec λ et τ. Lorsque $\lambda \geq$ 1,16 , l'envergure maximale est obtenue pour Q= 1 , elle décroît alors avec λ (figure 15).

Pour la flèche de 45 degrés (figure 20) les envergures sont plus réduites qu'à flèche nulle. La condition $\Delta\alpha^\circ/C_L > -0,1$ cesse d'exister pour $\lambda \geq$ 1,58. La condition de traînée est couverte par celle d'incidence à toute porosité, pour Mach 0,9, si $\lambda \geq$ 1,18. Comme à flèche nulle, l'envergure maximale est obtenue à Q croissant lorsque λ augmente. Au delà de λ = 1,26, l'envergure maximale à lieu à Q = 1 et diminue lorsque λ croît (figure 16).

La figure 21 résume l'ensemble des conditions optimales de forme de veine, envergure relative en fonction de Q et λ requises pour négliger les corrections d'incidence et de traînée.

Pour qu'une veine permette des essais de maquettes de même envergure maximale de τ pour des flèches de 0 à 45 degrés il faut que ses caractéristiques soient les suivantes selon le cas de porosité :

3.5.1 - Porosité fixée Q = 1

τ maxi.	λ
0,85	de 1,26 à 1,30
0,80	1,36 1,45
0,75	1,44 1,58
0,70	1,50 1,68
0,60	1,57 1,80
0,50	1,56 2,00

3.5.2 - Porosité appropriée ajustable

Le domaine ci-dessus s'agrandit uniquement au-dessous de τ = 0,7 et requiert de réduire la porosité légèrement aux valeurs suivantes pour la flèche de 45 degrés.

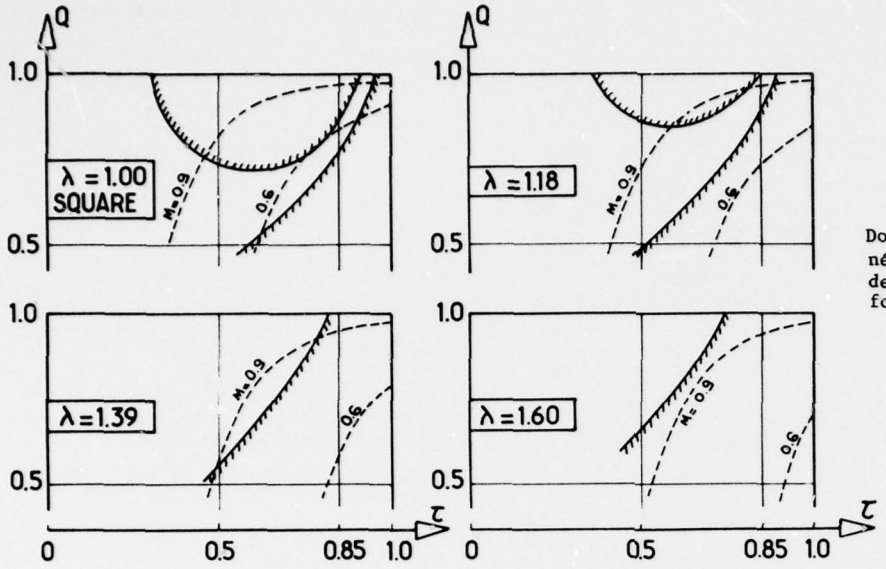

FIGURE 19

Domaines Q , τ permettant de négliger les corrections d'incidence et de traînée pour diverses formes de veine aile droite.

LIMITATIONS REQUIRED TO NEGLECT : STRAIGHT WING $\Lambda = 0°$

$\Delta\alpha°/C_L = -0.1$

$\Delta\alpha°/C_L = +0.1$

$\Delta C_{D_b} = -0.02\, C_D$

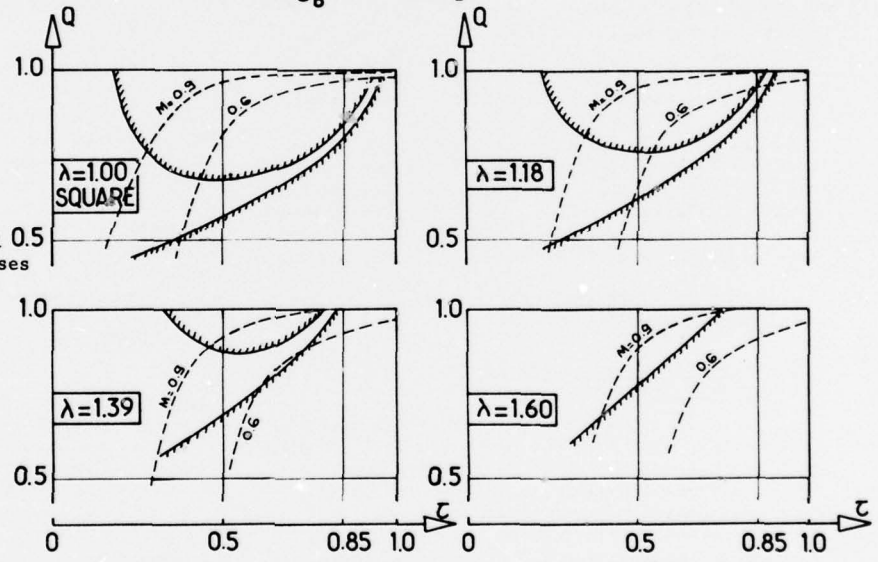

FIGURE 20

Domaines Q , τ permettant de négliger les corrections d'incidence et de trainée pour diverses formes de veine aile en flèche Λ = 45 degrés

LIMITATIONS REQUIRED TO NEGLECT : SWEPT WING $\Lambda = 45°$

$\Delta\alpha°/C_L = -0.1$

$\Delta\alpha°/C_L = +0.1$

$\Delta C_{D_b} = -0.02\, C_D$

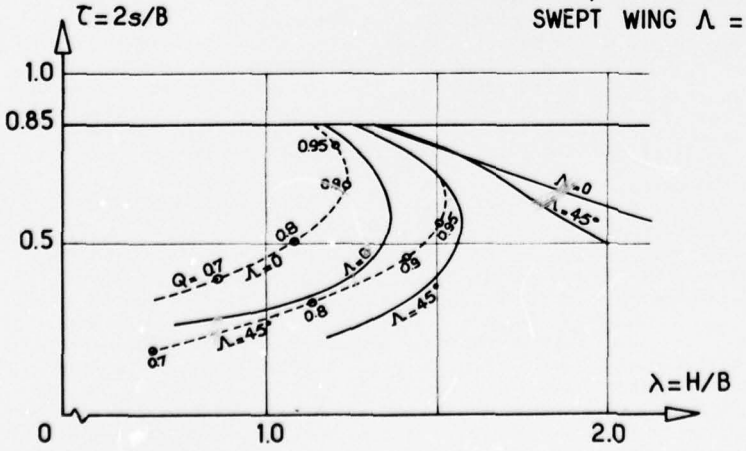

FIGURE 21

Envergures extrémales en fonction de λ , Λ permettant de négliger les corrections d'incidence et de traînée.

EXTREMAL RELATIVE SPANS τ VERSUS λ , Λ
TO NEGLECT $\Delta\alpha$, ΔC_{D_b}

——— AT Q = 1.0

------ AT APPROPRIATE Q

τ maxi.	λ	Q
0,70	1,50	1,00
0,60	1,52	0,97
0,50	1,46	0,92

L'examen de la figure 21 montre également qu'une veine caractérisée par λ = 1,58 et Q = 1 permet de négliger les corrections $\Delta\alpha$, ΔC_D de maquettes de flèche quelconque pour toute envergure inférieure à 0,75. Si la porosité peut être ajustée entre 0,97 et 1,00 l'intérêt est médiocre car τ maximale passe de 0,75 à 0,77 seulement pour une faible réduction de λ de 1,58 à 1,53.

La veine optimale est donc ainsi définie :

$$\lambda = 1{,}58 \qquad Q = 1 \qquad \tau \leqslant 0{,}75$$

L'intérêt d'une telle veine, par rapport aux caractéristiques indiquées dans les deux tableaux ci-dessus, est de permettre toute envergure plus faible, alors que dans les cas autorisant des valeurs plus élevées de τ , des restrictions existent : ainsi à titre d'exemple pour λ = 1,36, une envergure τ = 0,83 peut être atteinte, mais les valeurs $0{,}42 \leqslant \tau \leqslant 0{,}79$ ne sont pas autorisées, même avec une porosité appropriée.

Il y a lieu de noter que quatre paramètres ont ici été considérés dans la recherche d'une veine optimale : λ, τ, Λ, Q et que d'autres paramètres pourraient être ajoutés, telles que : longueur de perméabilité et dissymétrie de porosités des parois haute et basse.
Leur introduction possible en écoulement bidimensionnel, compliquerait considérablement les calculs en écoulement tridimensionnel par la méthode analytique. En particulier l'étude d'une étendue restrictive de la zone poreuse pourrait être effectuée avec la méthode des petits pavés.

4 - RECHERCHE D'UNE CONFIGURATION OPTIMALE DE VEINE COURANT PLAN

4.1 - Corrections de parois en écoulement bidimensionnel

Si en écoulement tridimensionnel, les obstructions sont modérées par suite de l'envergure limitée des maquettes, par contre en écoulement bidimensionnel il est courant de considérer des obstructions élevées, supérieurs à 3%. De ce fait les corrections de parois sont plus élevées que celles rencontrées en tridimensionnel. Comme par ailleurs les formules conduisant aux coefficients de corrections sont nettement moins compliquées qu'en tridimensionnel, des schématisations plus raffinées des profils et des parois peuvent être apportées.

Ainsi, des singularités d'ordre élevé ont été introduites [23] pour représenter le potentiel maquette φ_m alors qu'en théorie classique l'ordre est limité à 2. Ceci conduit à l'apparition dans les termes de blocage de volume de puissances de c/H supérieures à 2 [3] . En fait cette schématisation est nécessaire seulement si c/H dépasse 0,3. Dans le cas des essais effectués dans la soufflerie S3 de Modane c/H ne dépasse pas 0,27 et une valeur de 0,23 est recommandée.

En ce qui concerne les parois, les coefficients de corrections ont été calculés au centre maquette (x, z nuls) en fonction de la longueur d de perméabilité de la veine. L'influence est négligeable sur les coefficients de corrections de portance dès que d/H dépasse 2 [24] ; elle est plus importante sur les coefficients de correction de blocage [25] si la perméabilité des parois est faible.

La détermination de la porosité des parois peut être recherchée expérimentalement à partir des gradients de portance en référence d'essais réalisés en veine guidée. Cette méthode nécessite des essais supplémentaires en veine guidée et des comparaisons qui peuvent être mises en doute par suite de l'introduction de paramètres éventuels tels que le niveau de bruit dépendant de l'état des parois. La porosité Q des parois peut aussi être recherchée directement, sans essais de référence, en ajustant à l'aide d'un balayage en Q des répartitions de pressions sur les parois calculées théoriquement sur celles mesurées en essais. Ces deux méthodes supposent q'une seule inconnue est à déterminer : la porosité Q égale sur les deux parois.

Il est également possible de rechercher N inconnues en se fixant N données. Pour N = 2 , les deux inconnues peuvent être :

- les 2 porosités Q_H et Q_B des deux parois supposées constantes tout le long des parois [26]
- une loi , identique pour les deux parois, contenant deux paramètres [27]

$$Q = Q_0\, e^{-\alpha x^2}$$

tenant compte d'une variation longitudinale de la porosité.

Bien entendu, plus le nombre d'inconnues sera élevé, plus on aura de chance de faire coïncider l'ensemble des résultats obtenus sur profils homothétiques avec divers types de parois mais on accroîtra alors d'autant plus l'imprécision sur chaque paramètre. Le système d'équations à résoudre, résultant des conditions aux limites sur les parois, est non linéaire et peut contenir des intégrales de forme compliquée. Si à partir des données il n'est pas pensable de déterminer directement les inconnues, la résolution du système peut être effectuée par un balayage des paramètres cherchés et la recherche du meilleur compromis par optimisation.

4.2 - Corrections de parois en veine dissymétrique

Dans les hypothèses suivantes :

- singularités d'ordre 2 : doublet, source et tourbillon, représentant le profil
- porosité constante mais différente sur les deux parois haute et basse : Q_H et Q_B

les vitesses de perturbations au centre veine (z nul), données en annexe 2, sont au nombre de 6 et non 3 comme en veine symétrique. Aux vitesses axiales dues aux deux termes de blocage et à la vitesse verticale due au terme de portance se superposent une vitesse axiale due au terme de portance et deux vitesses verticales dues aux termes de blocage. Les termes IAA à INN (annexe 3) contenus dans les intégrandes des vitesses de perturbations sont les solutions du système de quatre équations correspondant aux conditions limites sur les deux parois (au lieu de deux équations à deux inconnues en veine symétrique).

4.3 - Recherche de la configuration optimale de veine dissymétrique

Le programme de calcul des corrections de parois établi pour une veine dissymétrique a été complété de manière à obtenir dans le plan (Q_H, Q_B) les courbes isocorrection de Mach ΔM d'incidence $\Delta\alpha$ et de traînée ΔC_D . Chaque correction est prise indépendamment en ce sens que la correction de traînée ne contient pas les termes dus à ΔM et $\Delta\alpha$ et que la correction de portance ne contenant pas la correction due à ΔM est reportée sur l'incidence :

$$\Delta\alpha = \Sigma \left(\frac{w_i}{U_\infty}\right)_{x=0} + \frac{c}{2} \Sigma \frac{1}{U_\infty} \left(\frac{\partial w_i}{\partial x}\right)_{x=\frac{c}{2}}$$

où $\Sigma = S+W+L$

La durée d'obtention d'un réseau iso correction, obtenu par interpolation à partir des corrections calculées pour 121 couples (Q_H, Q_B) nécessite 3 minutes de calcul sur ordinateur IRIS 80. Un tel réseau dépend de 5 paramètres c/H, e/c M, C_L, C_D. L'influence de chaque paramètre pris isolément est loin d'être évidente ainsi que les exemples suivants le montrent. On verra en particulier que la généralisation hâtive et l'intuition sont à prohiber et que seuls des calculs sur ordinateur permettent de définir une configuration optimale de parois.

L'influence du niveau de portance (figure 22) est importante : les réseaux de courbes sont altérés profondément, tant en allure qu'en espacement. L'obtention d'une veine exempte de corrections $\Delta\alpha$, ΔM n'est réalisable qu'à portance nulle et pour C_L supérieur à 0,5. C'est pourquoi une veine "optimale", telle que les corrections puissent être négligées en regard des dispersions de mesure, c'est à dire telle que

$$|\Delta M| \leqslant 0{,}004 \qquad |\Delta\alpha^\circ| \leqslant 0{,}05$$

est recherchée. Les domaines (Q_H, Q_B) remplissant simultanément ces deux conditions sont délimités figure 23. Dans le cas de portance nulle ou

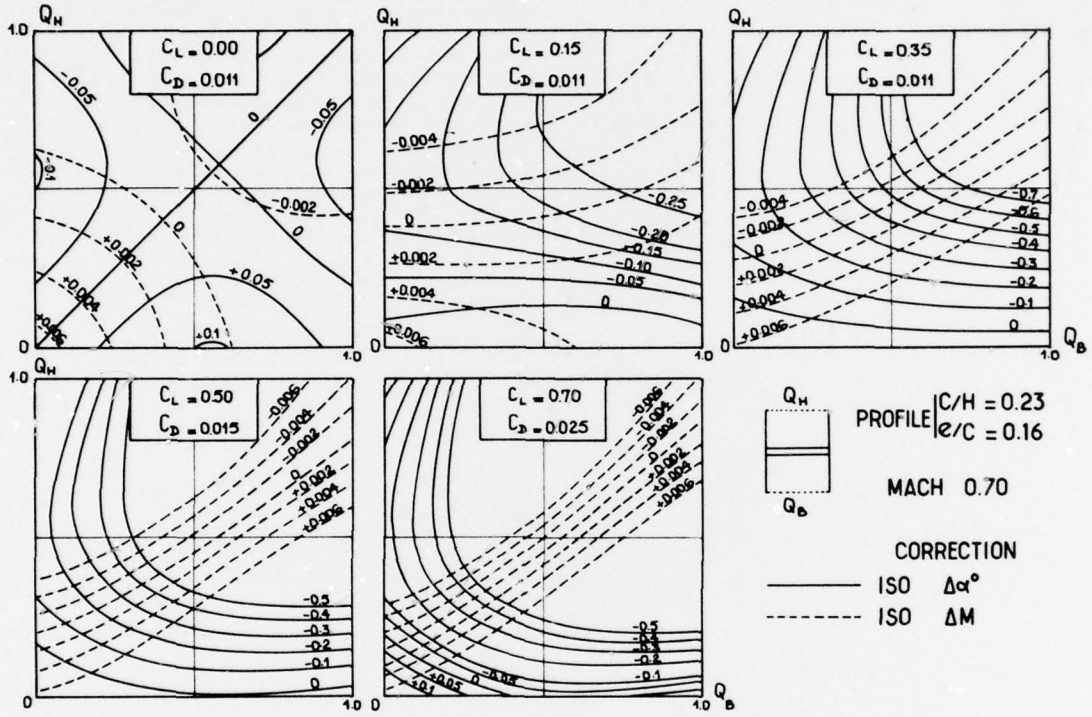

FIGURE 22 Réseaux iso $\Delta\alpha$, ΔM en veine courant plan dissymétrique

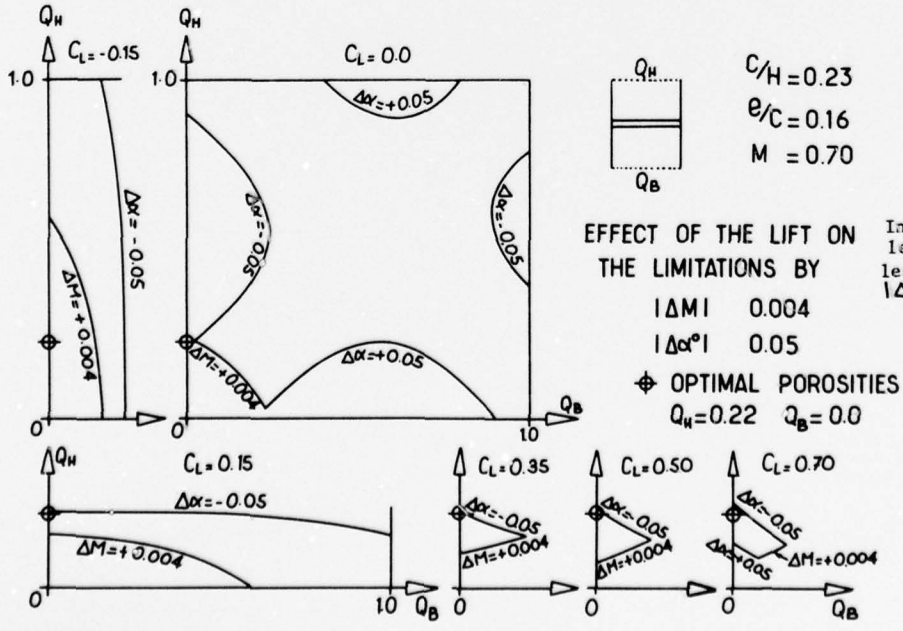

FIGURE 23

Influence de la portance sur les porosités autorisées par les limitations $|\Delta M| \leqslant 0{,}004$ - $|\Delta\alpha^\circ| \leqslant 0{,}05$.

positive le couple ($Q_H = 0,22$, $Q_B = 0,00$) permet de satisfaire aux conditions imposées : Pour un C_L variant de 0 à 0,70, les corrections ΔM et $\Delta\alpha$ sont respectivement de + 0,004 à - 0,002 et - 0,05° à - 0,03°. Au C_L négatif, le domaine autorisé est symétrique de celui obtenu en C_L positif. Comme de faibles C_L négatifs sont étudiés, le couple ($Q_H = 0,22$, $Q_B = 0,00$) est encore correct car à $C_L = - 0,15$, les corrections sont ΔM : + 0,005 et $\Delta\alpha$ = + 0,04°.

Lorsque le nombre de Mach augmente, à portance moyenne $C_L = 0,35$ (figure 24) le domaine (Q_H , Q_B) autorisé se rétrécit. La gamme de Q_H autorisée en paroi basse pleine ($Q_B = 0$) s'amenuise mais contient toujours la porosité $Q_H = 0,22$, même à nombre de Mach élevé.

L'intérêt d'une veine courant plan à paroi basse pleine et à parois haute de faible perméabilité est manifeste. Il reste cependant à rechercher pour quelles dimensions de profil une telle veine reste optimale.

Dans le plan (Q_H , C/H) les courbes correspondant aux limitations imposées en $\Delta\alpha$ et ΔM sont tracées pour diverses épaisseurs relatives e/C (figure 25). Les contours ombrés délimitent les zones autorisées (Q_H , C/H). Les deux exemples données figure 23 montrent la nécessité de calcul sur ordinateur. En effet on peut penser que moins le profil sera épais, plus le domaine autorisé s'agrandira. Il n'en est pas ainsi car les domaines autorisés par les conditions sur $\Delta\alpha$ et ΔM se déplacent de telle sorte que le domaine autorisé est borné par des limitations différentes (figure 25). Ainsi pour $e/C = 0,16$, partant de $Q_H = 0$ on trouve des limitations successivement dues à ΔM $\Delta\alpha$ puis ΔM alors que pour $e/C = 0,04$ elles sont dues à $\Delta\alpha$ puis ΔM .

En outre si une limitation due à ΔC_D est ajoutée, elle restreint le domaine (Q_H, C/H) pour $e/C = 0,16$ mais n'intervient pas pour $e/C = 0,04$. La plus grande corde est obtenue pour une perméabilité de paroi haute Q_H voisine de 0,22. Les cordes et épaisseurs relatives répondant aux conditions imposées sur ΔM et $\Delta\alpha$ sont optimales pour ($Q_H = 0,22$ - $Q_B = 0,0$) (figure 26). Les dimensions de profil permises sont limitées par deux courbes dues à la limitation $\Delta\alpha° = \pm 0,05°$ et une courbe correspondant à $\Delta M = \pm 0,004$. Le domaine obtenu est ensuite

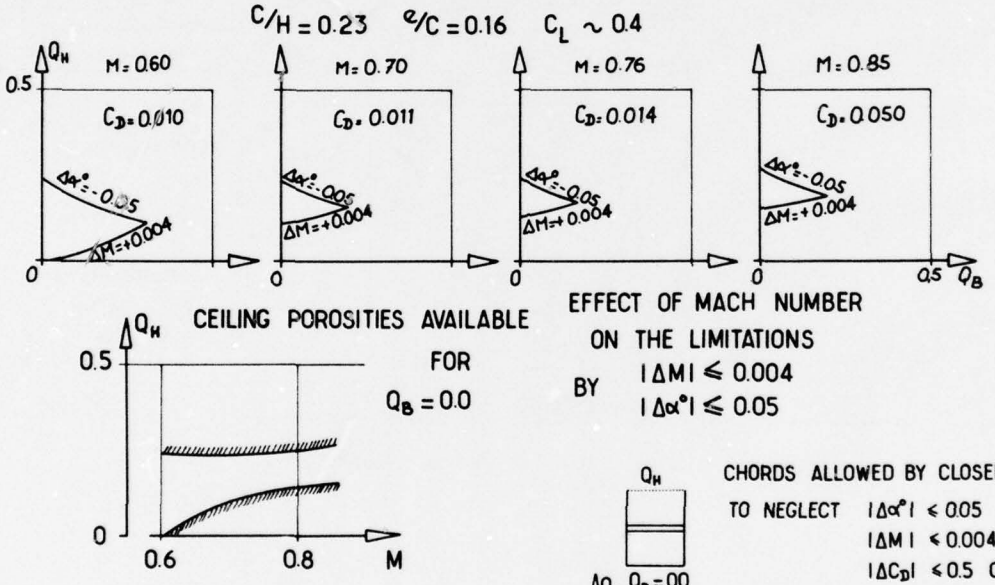

EFFECT OF MACH NUMBER ON THE LIMITATIONS BY $|\Delta M| \leq 0.004$ $|\Delta\alpha°| \leq 0.05$

FIGURE 24

Influence du nombre de Mach sur les porosités autorisées par les limitations $|\Delta M| \leq 0,004$ - $|\Delta\alpha°| \leq 0,05$

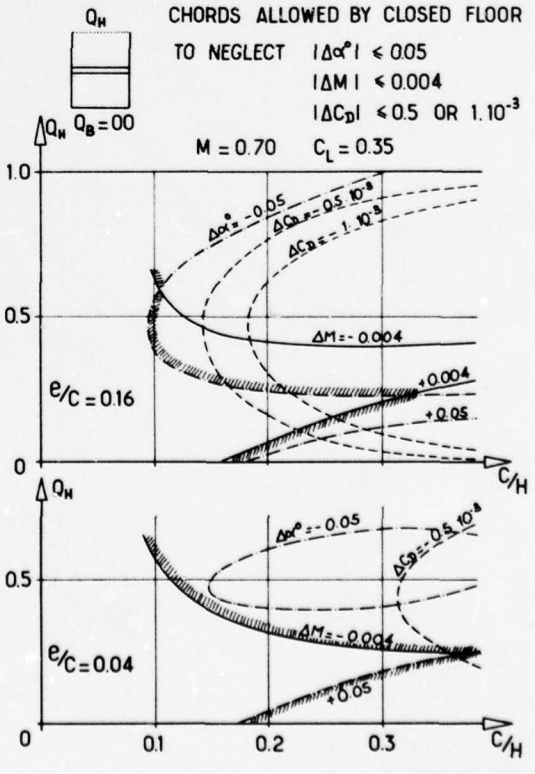

FIGURE 25

Veine à paroi basse pleine - Domaines Q_H , C/H autorisés

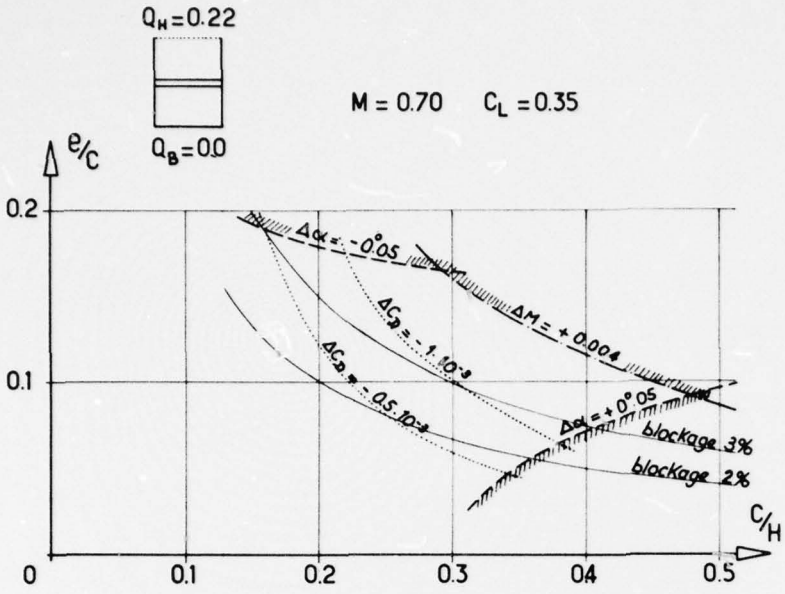

FIGURE 26

Veine optimale en courant plan (Q_H = 0,22 - Q_B = 0,00) c/H autorisés en fonction de e/c

restreint par une condition supplémentaire sur la correction de traînée. Si par exemple cette condition est fixée à 1.10^{-3} , la corde maxima - maximorum c/H = 0,378 doit être associée à une épaisseur e/c = 0,065. Pour une épaisseur relative plus faible, ou plus élevée, la corde devra être réduite; ainsi un profil de 16 % ne devra pas être plus grand que c/H = 0,228. Il y a lieu de remarquer que pour cette valeur, des singularités d'ordre 2 suffisent pour représenter le profil (paragraphe 4.1). Bien entendu des cordes plus grandes peuvent être utilisées dans la veine optimale : dans ce cas les corrections devront être calculées car dépassant les dispersions de mesure.

4.4 - Intérêt d'une paroi basse pleine

La configuration optimale des parois permettant de négliger les corrections (Q_H = 0,22 - Q_B = 0,0) possède un avantage intéressant du fait de l'utilisation d'une paroi basse pleine : l'inconnue Q_B disparaît et par suite la détermination de la porosité Q_H est beaucoup plus aisée si les corrections, même négligeables, sont calculées. Ce résultat peut être généralisé au cas d'une veine dissymétrique à paroi basse pleine, même si la porosité de la paroi haute n'est pas optimale.

L'intérêt d'une paroi basse pleine est confirmé en cherchant les domaines (Q_H , c/H) pour lesquels les corrections sont négligeables à diverses porosités Q_B (figure 27). Lorsque Q_B augmente, le domaine autorisé s'amenuise très rapidement. La corde maximale peut être obtenue pour une porosité Q_H de plus en plus faible lorsque la porosité Q_B croît; cette corde diminue très rapidement si Q_B augmente. De toute manière l'intérêt de la porosité nulle sur paroi basse est manifeste et une porosité réduite de paroi haute ne peut qu'être favorable. Une veine totalement guidée est moins bonne et n'autoriserait qu'une corde plus faible que celle permise par la veine optimale proposée (c/H = 0,23 contre 0,16 en veine guidée).

Il y a lieu de bien distinguer l'effet favorable d'une veine dissymétrique avec un profil placé au centre de la veine de l'effet d'un profil excentré en veine guidée où les corrections doivent être majorées en blocage [28] alors qu'il est possible d'obtenir des corrections de portance nulles en décalant vers le bas le profil d'une quantité dépendant de l'incidence [29] .

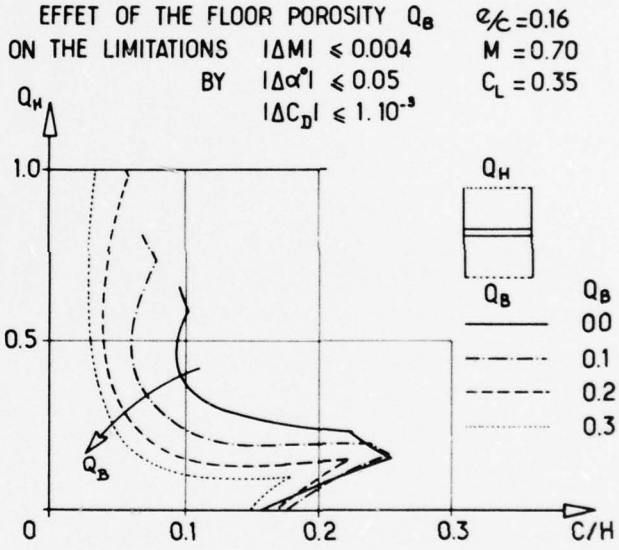

FIGURE 27

Influence de la porosité de paroi basse Q_B sur les cordes autorisées par les limitations $\Delta M \leq 0{,}004$, $|\Delta\alpha°| \leq 0{,}05$

4.5 - Validité de la veine optimale au sens local

La configuration optimale de veine, définie au paragraphe 4.3, a été déterminée dans le but de s'affranchir des corrections de parois au sens global. Il est intéressant de regarder si, au sens local des répartitions de pressions, les corrections sont également négligeables c'est à dire si les répartitions de pressions sur le profil ne s'écartent pas trop de celles qui seraient obtenues en atmosphère illimitée. A cet effet les répartitions de nombre de Mach sur l'extrados et l'intrados d'un profil NACA 0012, dont le rapport c/H = 0,23, ont été calculés théoriquement en fluide parfait. Le calcul a été effectué à Mach 0,70, α = 2,5 degrés d'une part en atmosphère illimitée et d'autre part pour trois configurations de veine :

- veine de porosité symétrique $Q_H = Q_B = 0{,}5$
- veine guidée
- veine optimale Q_H = 0,22 - Q_B = 0,00

Les différences entre les nombres de Mach calculés pour une veine donnée et en atmosphère illimitée sont portées en fonction de la profondeur

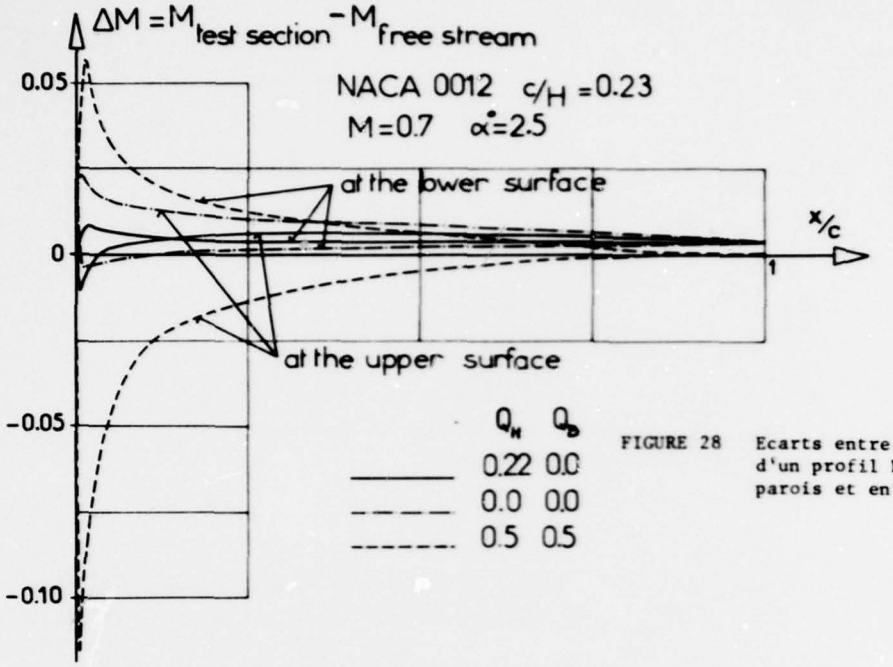

FIGURE 28 Ecarts entre nombres de Mach locaux d'un profil NACA 0012 en présence de parois et en atmosphère illimitée.

figure 28. Le nombre de Mach local calculé en atmosphère illimitée est respecté à ± 0,006 en présence de parois aux profondeurs de corde suivantes :

veine	extrados	intrados
porosité symétrique	50 à 100 %	50 à 100 %
guidée	90 à 100 %	0 à 100 %
optimale	1 à 100 %	10 à 100 %

Les écarts maximaux de nombre de Mach sont les suivants :

veine	extrados	intrados
porosité symétrique	- 0,116	+ 0,057
guidée	+ 0,024	- 0,004
optimale	- 0,011	+ 0,010

ils sont atteints au voisinage du bord d'attaque. En veine à porosité symétrique, seule la moitié aval du profil possède une répartition de Mach correcte ; près du bord d'attaque les Mach diffèrent énormément de ceux calculés sans parois. En veine guidée, si les nombres de Mach sont bien respectés sur tout l'intrados, par contre sur l'extrados ils sont trop élevés sauf au bord de fuite. C'est en veine optimale que le nombre de Mach local est le mieux respecté sur les 2 côtés du profil ; Seule une région restreinte de bord d'attaque n'est pas correcte. Une correction globale de Mach de 0,004 à 0,006 sur tout le profil correspond, dans le seul cas de la veine optimale, à la correction de Mach calculée au sens global.

L'intégration des répartitions de pressions conduit à des coefficients de portance s'écartant de celui obtenu en atmosphère illimitée de + 0,7 % + 4,7 % et - 17 % respectivement en veine optimale, guidée et symétrique.

Il apparaît donc que la veine optimale obtenue à partir de corrections au sens global est également correcte au sens local, en dehors d'une zone très restreinte de bord d'attaque où les écarts de pressions, par rapport à l'atmosphère illimitée, existant dans une zone de fort gradient de vitesse n'entraînent sur le coefficient de portance qu'une erreur inférieure à 1 %.

CONCLUSIONS

Des études paramétriques sur ordinateur, utilisant les programmes de calcul des coefficients *de correction de parois en veine transsonique* à parois perforées ont été menées dans un double but :

- formuler des recommandations sur le dimensionnement des maquettes pour que les corrections de parois d'un niveau tolérable puissent être appliquées avec un degré de confiance satisfaisant

- rechercher les meilleures conditions d'emploi des veines existantes associées à certaines tailles de maquettes de telle sorte que les corrections de parois soient idéalement nulles (veine idéale) ou négligeables c'est à dire n'excédant pas les dispersions de mesures (veine optimale).

En écoulement tridimensionnel, l'intérêt d'une veine de rapport hauteur/largeur de 1,18 possédant des parois horizontales à perméabilité maximale est d'annuler strictement les corrections de blocage. Pour annuler simultanément les corrections de portance il faut associer à cette veine des maquettes dont le rapport envergure /largeur veine, selon la flèche, est de 0,86 à 0,89, ce qui peut paraître excessif du fait de la proximité des extrémités d'ailes et de la couche limite des parois verticales. En considérant que des corrections d'incidence $|\Delta\alpha^\circ/c_L| \leq 0{,}1$ sont négligeables ces rapports peuvent être abaissés légèrement

Dans le cas de maquettes à aile droite, l'utilisation de maquettes d'envergure égale à 0,7 fois la largeur de veine en veine carrée constitue le cas le plus défavorable sous l'aspect des corrections de portance. En conservant la même maquette et en réduisant la largeur de veine pour que le rapport hauteur/largeur de veine soit 1,18 les corrections de parois peuvent être négligées.

Il apparaît donc que, dans ce cas, un moyen simple de s'affranchir des corrections consiste à accroître l'obstruction de la maquette en veine et son rapport envergure/largeur de veine. Cette conclusion assez paradoxale va à l'encontre du réflexe habituel de dimensionnement des maquettes.

Lorsque la flèche des voilures augmente, les rapports hauteur/largeur de veine requis pour négliger les corrections de portance augmentent au détriment des corrections de blocage. Les caractéristiques d'une veine "optimale" permettant de s'affranchir des corrections de portance et de traînée pour toute envergure relative inférieure à 0,75 sont :
hauteur/largeur = 1,58, porosité maximale Q = 1

En écoulement bidimensionnel, l'introduction d'un paramètre supplémentaire : la différence de porosité des deux parois, conduit à la définition d'une veine optimale permettant de négliger les corrections de parois. Cette veine est constituée d'une paroi basse pleine et d'une paroi haute de faible perméabilité. Sa validité, pour une gamme étendue en Mach et portance, requiert de ne pas dépasser des rapports cordes/hauteur de veine dépendant de l'épaisseur relative du profil. A titre d'illustration pour des profils de 10 % et 16 % les rapports autorisés vont respectivement jusqu'à 0,30 et 0,23. La veine optimale, établie à partir de calcul de corrections de parois au sens global est démontrée être valable au sens local des répartitions de pressions à l'aide d'un calcul théorique en référence de l'atmosphère illimitée.

Des exemples cités ci-dessus il ressort que toutes les possibilités des veines actuelles n'ont pas encore été mises à profit, soit pour augmenter la taille des maquettes tout en conservant des corrections de parois raisonnables, soit pour rechercher des configurations permettant de s'affranchir de ces corrections. L'introduction de paramètres supplémentaires tels que la différence de porosité volontaire des parois, l'étendue des zones perforées, l'excentrement des maquettes, permet des utilisations fructueuses des veines déjà existantes, en ne considérant que des veines cylindriques.

REFERENCES

(1) VAUCHERET X - BAZIN M. - ARMAND C
Comparaison d'essais transsoniques bi et tridimensionnels effectués dans diverses grandes souffleries
Symposium AGARD/FMP Valloire (juin 1975)
ONERA TP n° 1975-61

(2) PRANDTL L.
Tragflügeltheorie, Part II, Nachrichten der K.Gesellschaft der Wrissenschaften zu Göttingen (1919)

(3) GARNER H - ROGERS E - ACUM W. - MASKELL E.
Subsonic wind tunnel wall corrections
AGARDOGRAPH 109 (1966)

(4) RIEGELS F.W
Wind tunnel corrections for incompressible flow
AVA Monograph - section D3 - 4 - I
Göttingen (1947)

(5) GOODMAN TR
The porous wall wind tunnel - PART II
Interference effect on a cylindrical body in a two-dimensional tunnel at subsonic speed.CAL - Rep n° AD-594-A-3 (1950)

(6) BALDWIN B.S. - TURNER J.B. - KNECHTEL E.D.
Wall interference in wind tunnels with slotted and porous boundaries at subsonic speeds
NACA TN 3176 (1954)

(7) HOLDER D.R.
Upwash interference on wings of finite span in a rectangular wind tunnel with closed side walls and porous slotted floor and roof
ARC R & M 3395 (1965)

(8) PINDZOLA M. - LO C.F.
Boundary interference at subsonic speeds in wind tunnels with ventilated walls
AEDC TR 69.47 (1969)

(9) OLIVER R.H.
Determination of blockage and lift interference for rectangular wind tunnels with perforated walls
MASTER'S thesis - University of Tennessee (1969)

(10) LO C.F. - OLIVER R.H.
Boundary interference in a rectangular wind-tunnel with perforated walls
AEDC TR 70-67 (1970)

(11) JOPPA R.G.
A method of calculating wind tunnel interference factors for tunnels of arbitrary cross-section.
NASA CR 845 (1967)

(12) BOROVIK Y. - WASSERSTROM E.- ROM J.
Wind tunnel boundary interference corrections - Part. I : theoretical calculation
A R C Report O-124 - Technion Israël Intitute of technology - Haïfa (1972)

(13) VAUCHERET X. - VAYSSAIRE J.C
Corrections de parois en écoulement tridimensionnel transsonique dans des veines à parois ventilées
Symposium AGARD/FDP Londres (oct. 1975)
ONERA TP n° 1975-117

(14) FERRI A - BARONTI P.
A method for transsonic wind-tunnel corrections
AIAA Journal Vol 11 n°1 (janvier 1973)

(15) SEARS W.R.
Self correcting wind tunnels
Aero. Journal vol 78 n° 758/759 (Feb., march, 1974)

(16) GOODYER M.J.
The self streamlining wind tunnel
AGARD/FDP Londres (Oct. 1975)

(17) CHEVALLIER J.P.
Soufflerie transsonique à parois auto-adaptables
AGARD/FDP Londres (octobre 1975)
ONERA TP n° 1975-119

(18) KRAFT E.M.
Upwash interference on a symetrical wing in a rectangular ventilated wind-tunnel - Part I - Development of theory
AEDC TR 72-187 (1973)

(19) MOKRY M.
A wake blockage paradox in a perforated wall wind tunnel
AIAA Journal vol 9 n°12 (1971)

(20) WIESELSBERGER C.
Über den einfluss der windkanal-begrenzung auf den widerstand insbesondere in bereiche der kompressiblen strömung
Luftfahrtforschung - Vol 19 p.124 (1942)

[21] VAYSSAIRE J.C.
Survey of methods for correcting wall constraints in transonic wind tunnels
AGARD Report n° 601 (avril 1973)

[22] TOUSSAINT A.
Experimental methods wind tunnels, Influence of the air stream , Aerodynamic theory
Ed W.F. DURAND Vol III Div.1 chapter III
J SPRINGER Berlin (1935)

[23] MOKRY M.
Higher-order theory of two dimensional subsonic wall interference in a perforated wall wind tunnel
NRC Aeronautical Report LR 553 (October 1971)

[24] PARKINSON G.V. - LIM A.K.
On the use of slotted walls in two-dimensional testing of lowspeed airfoils
ICAS Paper n° 70 08 - (1970)

[25] WOODS L.C.
On the theory of two dimensional wind-tunnels with porous wall
Proc. Roy. Society - Series A Vol 233
(P. 74/90) (1955)

[26] MOKRY M. - PEAKE D.T. - BOWKER A.J
Wall interference on two dimensional supercritical airfoils using wall pressure measurements to determine the porosity factors for tunnel floor and ceiling
NAE Aeronautical Report LR575 (Fev. 1974)

[27] LO C.F.
Wind tunnel wall Interference reduction by streamwise porosity distribution
AIAA Journal Vol.10 n°4 (avril 1972)

[28] BATCHELOR G.K.
Interference on wings, bodies and airscrews in a closed tunnel of octogonal section
Report ACA 5 (Australia) (1944)

[29] HAVELOCK T.H
The lift and moment on a flat plate in a stream of finite width
Proc. Roy Soc. Series A Vol 166
p 178/196 (1938)

ANNEXE - 1 -

WALL CONSTRAINTS – ANALYTIC METHOD

$\lambda = H/B$

$\tau = 2s/B \qquad \xi = \tan\Lambda$

$X = 2x/\beta B$

BLOCKAGE $\quad \Omega = \varepsilon(X,Q)/\varepsilon(0,0)$

solid : $$\varepsilon_s(X,Q) = \left\{ \frac{1}{\lambda^2} \int_0^\infty \sum_{m=0}^{\infty} {}' j \left(I_G \cos\frac{qX}{\lambda} - I_E \sin\frac{qX}{\lambda} \right) \frac{q^2}{\alpha_m} dq - 4 \sum_{k=1}^{\infty} (X^2 - 2k^2)(X^2 + 4k^2)^{-5/2} \right\} \frac{2V}{\pi \beta^3 B^3}$$

wake : $$\varepsilon_w(X,Q) = \left\{ \frac{1}{\lambda} \int_0^\infty \sum_{m=0}^{\infty} {}' j \left(I_E \cos\frac{qX}{\lambda} + I_G \sin\frac{qX}{\lambda} \right) \frac{q}{\alpha_m} dq + 2 \sum_{k=1}^{\infty} X (X^2 + 4k^2)^{-3/2} + 1 \ (\text{if } Q=0) \right\} \frac{C_x S_a}{2\pi \beta^2 B^2}$$

with: $I_E = -\alpha_m q Q(1-Q)/\Delta_\Omega$

$I_G = e^{-\alpha_m} [\alpha_m^2 \operatorname{sh}\alpha_m (1-Q)^2 - q^2 \operatorname{ch}\alpha_m Q^2]/\Delta_\Omega$

$\Delta_\Omega = \alpha_m^2 \operatorname{sh}^2\alpha_m (1-Q)^2 + q^2 \operatorname{ch}^2\alpha_m Q^2$

LIFT : uniformly loaded swept wing

$$\bar{\delta}(x) = \frac{1}{4\pi} \int_0^\infty \sum_{m=0}^{\infty} {}' j \left(I_F \cos\frac{qX}{\lambda} + I_H \sin\frac{qX}{\lambda} \right) \left\{ \frac{\sin\tau(m\pi + q\frac{\xi}{\lambda})}{\tau(m\pi + q\xi/\lambda)} + \frac{\sin\tau(m\pi - q\frac{\xi}{\lambda})}{\tau(m\pi - q\xi/\lambda)} \right\} \cdot \frac{\sin m\pi\tau}{m\pi\tau} \frac{\alpha_m}{q} dq \pm \pi\lambda \sum_{m=1}^{\infty} \frac{m}{e^{2m\pi\lambda} \pm 1} \left(\frac{\sin m\pi\tau}{m\pi\tau} \right)^2 \left(\begin{matrix} + \text{ if } Q<1 \\ - \text{ if } Q=1 \end{matrix} \right) - \frac{1}{4} \ (\text{if } Q=1)$$

$$+ \frac{\lambda}{4\pi\tau^2} \left\{ \log\frac{\pi\tau}{\sin\pi\tau} + \sum_{k=1}^{\infty} \left[\log \left| \frac{B_{11}B_{21}}{B_{31}B_{41}} \right| + \frac{1}{\xi} \log \left| \frac{B_{12}B_{22}}{B_{32}B_{42}} \right| - \frac{\sqrt{1+\xi^2}}{\xi} \log \left| \frac{B_{13}B_{23}}{B_{33}B_{43}} \right| \right] \right\}$$

with: $I_F = -\alpha_m q Q(1-Q)\Delta_\delta$

$I_H = e^{-\alpha_m} [\alpha_m^2 \operatorname{ch}\alpha_m (1-Q)^2 - q^2 \operatorname{sh}\alpha_m Q^2]/\Delta_\delta$

$\Delta_\delta = \alpha_m^2 \operatorname{ch}^2\alpha_m (1-Q)^2 + q^2 \operatorname{sh}^2\alpha_m Q^2$

and: $\alpha_m^2 = q^2 + (m\pi\lambda)^2 \qquad j = 1,2 \text{ for } m =, \neq 0$

l	B_{il}
1	$Z_i + \sqrt{1+Z_i^2}$
2	$(1+\sqrt{1+Z_i^2})/Z_i$
3	$\dfrac{1+\xi Z_i + \sqrt{1+\xi^2}\sqrt{1+Z_i^2}}{Z_i - \xi}$

i	Z_i
1	$(X+\xi\tau)/2(k+\tau)$
2	$(X-\xi\tau)/2(k-\tau)$
3	$(X+\xi\tau)/2k$
4	$(X-\xi\tau)/2k$

ANNEXE -2-

INTERACTIVE CORRECTIONS

THREE DIMENSIONAL FLOW

<u>data</u> $M_m \; q_m \; \alpha_m \; C_{i_m}$ $(i = D, L, M \ldots)$

<u>model effect on static pressure</u> $(x = x_m) \longrightarrow M_u \; q_u \; C_{i_u}$

$$M_m = M_u \left[1 + (1 + 0.2 M_u^2)\, \varepsilon_m\right], \quad q_m = q_u \left[1 + (2 - M_u^2)\, \varepsilon_m\right]$$

<u>blockage interference</u> $(x = 0) \longrightarrow M_b \; q_b \; C_{i_b}$

$$M_b = M_u \left[1 + (1 + 0.2 M_u^2)\, \varepsilon_b\right], \quad q_b = q_u \left[1 + (2 - M_u^2)\, \varepsilon_b\right]$$

where

$$\varepsilon = \frac{K_T V}{C^{3/2}}\, \Omega_s(x)\, \beta^{-3} \qquad \text{solid}$$

$$+ \frac{S_a}{4C}\, C_D\, \Omega_w(x)\, \beta^{-2}(1 + 0.4 M^2) \qquad \text{wake}$$

$$+ (1.4 - 0.034\, \beta\, AR_a)\, \frac{S_a}{C}\, C_{D_d}\, \beta^{-3} \qquad \text{stall (if } Q = 0)$$

<u>buoyancy interference</u> $(x = 0)$

$$\Delta C_{D_b} = -\frac{K_T V}{C^{3/2}}\, \beta_b^{-3} \left[\frac{4V}{S_a B}\, \beta_b^{-1}\, \Omega_s'(x = 0) \right. \qquad \text{solid}$$

$$\left. + C_{D_u}\, \Omega_s(x = 0)\, (1 + 0.4 M_b^2) \right] \qquad \text{wake}$$

<u>Lift interference</u>

$$\alpha_c = \alpha_m + \frac{S_a}{C}\, C_{L_b} \left[\delta(x = 0) + \frac{\bar{c}}{\beta_b B}\, \delta_1\left(x = \frac{\bar{c}}{2}\right) \right]$$

$$C_{D_c} = C_{D_b} + \Delta C_{D_b} + C_{L_b}(\alpha_c - \alpha_m)$$

$$C_{M_c} = C_{M_b} + \Delta C_{M_a} + \Delta C_{M_e}$$

where

$$\Delta C_{M_a} = \frac{S_a}{C}\left(\frac{1}{4} - \frac{x_a}{c_R}\right) C_L\, C_{L_{\alpha_c}}\, \frac{\bar{c}}{2\beta_b B}\, \delta_1\left(x = \frac{\bar{c}}{4}\right)$$

$$\Delta C_{M_e} = \frac{S_e}{C}\, l_e\, \frac{l_e}{c_R}\, C_L\, \frac{4.58\, AR_e}{\beta_b AR_e + 2}\, \cos\varphi_{M_e}\, \frac{2}{\beta_b B}\, \delta_1(x = l_e)$$

with $\Omega_s' = \dfrac{\partial \Omega_s}{\partial \frac{2x}{\beta B}}$, $\delta_1 = \dfrac{\partial \delta}{\partial \frac{2x}{\beta B}}$

subscript: a for wing , e for tail

ANNEXE -3-

DISSYMMETRICAL 2D TEST SECTION

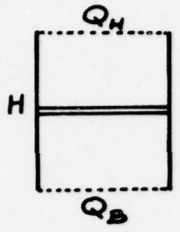

profile { c chord ; e thickness

perturbation due to:	axial velocities	vertical velocities
solid blockage	$\frac{u_{iS}}{U_\infty} = k_{u_S}\int_0^\infty I_{AA}\, q\, dq$	$\frac{W_{iS}}{U_\infty} = \rho k_{u_S}\int_0^\infty -I_{DD}\, q\, dq$
wake blockage	$\frac{u_{iW}}{U_\infty} = k_{u_W}\left[\int_0^\infty I_{BB}\, dq \;\; -\frac{\pi}{2}\ (\text{if } Q_H = Q_B = 0)\right]$	$\frac{W_{iW}}{U_\infty} = \rho k_{u_W}\int_0^\infty I_{CC}\, dq$
Lift interference	$\frac{u_{iL}}{U_\infty} = k_{u_L}\int_0^\infty I_{KK}\, dq$	$\frac{W_{iL}}{U_\infty} = \rho k_{u_L}\left[\int_0^\infty -I_{NN}\, dq \;\; -\frac{\pi}{2}\ (\text{if } Q_H = Q_B = 1)\right]$
	longitudinal gradients	
solid blockage	$\frac{u'_{iS}}{U_\infty} = k_{u_S}\int_0^\infty I_{BB} q^2 dq$	$\frac{W'_{iS}}{U_\infty} = \rho k_{u_S}\int_0^\infty I_{CC}\, q^2 dq$
wake blockage	$\frac{u'_{iW}}{U_\infty} = k_{u_W}\int_0^\infty -I_{AA}\, q\, dq$	$\frac{W'_{iW}}{U_\infty} = \rho k_{u_W}\int_0^\infty I_{DD}\, q\, dq$
Lift interference	$\frac{u'_{iL}}{U_\infty} = k_{u_L}\int_0^\infty I_{LL}\, q\, dq$	$\frac{W'_{iL}}{U_\infty} = \rho k_{u_L}\int_0^\infty I_{MM}\, q\, dq$

where:

$$\begin{cases} I_{AA} + i\, I_{BB} = (I_A + i\, I_B)\, e^{-iqX} \\ I_{CC} + i\, I_{DD} = (I_C + i\, I_D)\, e^{-iqX} \\ I_{KK} + i\, I_{LL} = (I_K + i\, I_L)\, e^{-iqX} \\ I_{MM} + i\, I_{NN} = (I_M + i\, I_N)\, e^{-iqX} \end{cases}$$

$$\begin{cases} (I_B - i\, I_A)[Q\,chq + i\,(1-Q)\,shq] \pm (I_D - i\, I_C)[Q\,shq + i\,(1-Q)\,chq] \\ \qquad = e^{-|q|}\left[(1-Q) + i\,\frac{q}{|q|}\,Q\right] \\ (I_L - i\, I_K)[Q\,chq + i\,(1-Q)\,shq] \pm (I_N - i\, I_M)[Q\,shq + i\,(1-Q)\,chq] \\ \qquad = \pm\, e^{-|q|}\left[\frac{q}{|q|}\,(1-Q) + iQ\right] \end{cases}$$

with + if $Q = Q_H$, − if $Q = Q_B$

and

$$\begin{cases} k_{u_S} = \frac{e}{c}\left(\frac{2c}{H}\right)^2 \frac{1 + 1{,}2\,e/c}{2\pi\beta^3}\ 0{,}65 \\ k_{u_W} = -\frac{2c}{H}\ \frac{C_{D_W}}{4\pi\beta^2}\ (1 + 0{,}4\,M^2) \\ k_{u_L} = \frac{2c}{H}\ \frac{C_L}{4\pi\beta} \end{cases}$$

WIND TUNNEL TESTS AND AERODYNAMIC COMPUTATIONS; THOUGHTS ON THEIR USE IN AERODYNAMIC DESIGN

by

J.W. Slooff
NATIONAL AEROSPACE LABORATORY (NLR)
Anthony Fokkerweg 2, Amsterdam-1017
The Netherlands

SUMMARY

In the past 10-15 years important developments have taken place in numerical methods for flow computations as well as in wind tunnel testing technology. Numerical methods in particular have provided the aerodynamic designer with a new set of tools.

After comparing the possibilities and limitations of numerical methods on the one hand and wind tunnel tests on the other, a discussion is given on their respective roles in aerodynamic design.

It is concluded from the discussion that the key problems of aerodynamic design are not solved by substituting numerical methods for the wind tunnel. The developing of numerical methods that produce optimized geometries on the basis of simplified physics deserves at least as much attention as the pursuit of full Navier-Stokes solutions for given geometries.

1. INTRODUCTION

Since the large-scale introduction of high-capacity digital computers in the early and mid-60's there have been tempestuous developments in numerical methods for flow computations. The achievements this has led to, are presently of great practical interest. They constitute what might be called a new scientific discipline: computational fluid dynamics.*)

Figure 1 illustrates the enormous gain in computational efficiency obtained over the last 10-15 years and the rapidly widening scope of computational airplane aerodynamics. Shown are the trends of computation times for the computational methods that are being used in today's design studies for tomorrow's generation of subsonic aircraft. It can be observed that singularity-type 2-d/3-d inviscid subsonic flow computations (Refs. 2-9) as well as 2-d inviscid transonic flow computations (Refs. 10-12) have become a routine matter. 3-d inviscid transonic flow computations (Refs. 13-16) seem to have reached the stage of practical applications, but with the exception of reference 16, have limited applicability due to the small perturbation assumptions (Ref. 17). Methods including boundary layer corrections are operational for 2-d flows but depend heavily on empiricism (Refs. 18-19, 12).

The developments in wind tunnel testing technology over the same period, are perhaps less spectacular in appearance but not necessarily less important. Due also to the computer, (at least to a large extent), the efficiency of data acquisition systems for both force and pressure measurements has increased significantly, and model manufacturing techniques have been improved. New evolving concepts, like cryogenic and self-correcting tunnels (Refs. 20, 21), when fully developed, could constitute major breaks-through in wind tunnel technology.

Although important achievements can be recorded for both the experimental and computational disciplines, it can, nevertheless, be noticed that, that there is a difference in the significance of these achievements. From the point of view of aerodynamic design the developments in wind tunnel technology have greatly improved existing possibilities for design development and verification, whereas new possibilities are being created through numerical methods.

The objective of the present paper is to, critically, consider the role of our new computational tools in relation to that of our classical tool the wind tunnel in the aerodynamic design process of flight vehicles. For that purpose we will first compare the possibilities and limitations of computational aerodynamics on the one hand and wind tunnel testing on the other. Having established the complementary aspects of the two, attention will be paid to the question of their combined use in aerodynamic design.

2. NUMERICAL METHODS AND WINDTUNNEL TESTS; POSSIBILITIES AND LIMITATIONS

Because of the large number of technical, structural and financial aspects of both wind tunnel testing and aerodynamic computations a complete assessment of their respective possibilities and limitations seems an impossible task. The summary contained by figure 2 is therefore necessarily crude and incomplete, but sufficiently detailed for the purpose of illustrating the complementary aspects.

The key value of wind tunnel testing is of course that, in the wind tunnel, we are dealing with complete physics. Although these are not always the required physics (e.g. in terms of Reynolds number, turbulence and noise levels etc), they do allow us to study most if not all phenomena that may occur in the flow about flight vehicle configurations. In contrast, numerical methods represent only part of the physics and, hence, can describe only a limited number of flow phenomena.

An attractive aspect of numerical methods is that flow computations do not need to suffer from wall and/or support interference. In fact, numerical methods can be used and are used in understanding the mechanism and establishing the magnitude of wall and model support interference in wind tunnel testing. This supplementary role of numerical methods, in design verification, is a subject on it's own and outside the scope of this paper.

A major advantage of numerical methods is the high flexibility with respect to changes in model configuration: we can compute in sequence, the (potential) flow around perhaps a dozen or more wings in the time-span needed for the manufacturing and testing of one wind tunnel model. The high level of accessibility of modern computer systems in relation to that of wind tunnels is one of the reasons for this situation.

An aspect related to cost is that once we have a wind tunnel model (and the wind tunnel) it takes relatively little time and effort to measure the aerodynamic characteristics for a large number of flow conditions; the cost per data point reduce rapidly with the number of data points. This is probably somewhat less the case with aerodynamic computations where the variable costs (actual computation costs) have the tendency to constitute a larger percentage of the total costs. However, there is often not much of a point in performing an exhaustive number of calculations for one configuration; becaure of the simple

*) The status and prospects of computational fluid dynamics have recently been summarized by Chapman (Ref. 1).

physics in the mathematical models the limits of useful application are easily exceeded.

Probably the most important and also unique aspect of computational methods is the ability to do not only the "direct" problem (i.e. the determination of the flow about a given shape) but also the "inverse" or "design" problem of determining the shape that produces a given pressure distribution. Oddly enough, it seems that this possibility, which should be of great interest to the aerodynamic designer, has received relatively little attention.

Having established the possibilities and limitations of wind tunnel testing on the one hand and numerical methods on the other we will next pay attention to the question of how to exploit the respective capabilities in the aerodynamic design process.

3. THE ROLE OF NUMERICAL METHODS AND WIND TUNNEL TESTING IN THE AERODYNAMIC DESIGN PROCESS

Prior to considering the aerodynamic design process itself it is useful to have a quick look at the goals of aerodynamic design. As an example we will consider the high speed requirements of subsonic transport type aircraft. In a crude sense, these requirements are summarized in figure 3. Subject to a large number of constructional and other constraints a (wing) geometry is sought that combines low drag properties in a limited region of the C_L-MA plane with acceptable off-design characteristics. To a certain extent the latter can be formulated in terms of sufficient margins ΔC_L and ΔMA between the cruise locus and boundaries for buffet onset, insufficient stability and control characteristics, etc.

Traditionally, one can distinguish two phases in the process that is used in pursuit of these design goals. The first phase (preliminary design, Fig. 4) consists of a parametric study in which the major design quantities such as wing loading (C_L), basic wing planform etc. are fixed *). During the second phase (design development) the geometry of the wing is worked out in detail. Numerical methods and wind tunnel tests are utilized primarily in phase II.

3.1 The classical situation

Historically, the task of the aerodynamic designer was to select a number of airfoil shapes and spanwise twist distributions and find out in the wind tunnel how his geometrical compositions behave aerodynamically. If the aerodynamic characteristics were not satisfactory he would, using his experience and physical intuition, change the geometry, test again etc. (Fig. 5a).

A most frustrating aspect of this kind of process is that the amount of parameters that, in principle, can be changed is overwhelming, while only a very limited number of possibilities can be investigated. Model manufacturing time is the factor that determines how many "iterations" can be performed within a given time span.

A characteristic feature of the process is further, that the designer is inclined to attempt direct correlation between aerodynamic characteristics like C_L, C_D, C_M -behaviour, stall etc. and geometrical properties as camber, thickness, twist, leading-edge radius, trailing-edge angle etc.. Within such an approach it is consistent that the majority of wind tunnel tests consists of force measurements only. The latter is also highly attractive from a model manufacturing point of view, because models intended for overall force measurements only are significantly easier to manufacture than pressure-plotting models.

Next, let us consider the situation that numerical methods are available for solving the direct problem.

3.2 With "direct" numerical methods available

At first sight it seems, that the possibility to calculate, in an approximate sense, the flow about a given complex configuration (Refs. 6-9) means an immense step ahead, and to a certain extent it is. As noticed in the preceding section numerical methods offer the possibility to "test" perhaps a dozen wings in the time span that is required for manufacturing and testing one wing in the wind tunnel. However, as illustrated by the upper part of figure 5b this does not solve the designer's key problem of selecting the shape-to-be-tested. It merely changes the question of "what shall I test in the wind tunnel?" into "what shall I compute?" This is irrespective of the degree of sophistication of the numerical method. It would be true even in the case that we could solve the full time-dependent Navier-Stokes equations!

One other aspect of the introduction of numerical methods into the aerodynamic design process is that they provide easy means of obtaining (potential flow) pressure distributions. The attractiveness of this aspect is in the fact that the pressure distribution, in a more direct sense than the geometry, determines the aerodynamic characteristics of a wing. This is of particular importance in the subtle shaping for transonic flow with low wave drag.

Optimal use of the pressure plotting facility of (direct) numerical methods requires, in a sense, a change of attitude of the aerodynamic designer; he will have to abandon the one-step (geometry→aerodynamics) correlation approach in favor of a more sophisticated two-step one (geometry→pressure distribution→aerodynamics). An implication of the latter for his wind tunnel testing is that there is a stronger need for combined force/pressure measurements. This, of course, is more time consuming and expensive. However, just because of the use of numerical methods, the total number of tests is reduced. In general terms the situation might be described as one in which the role of the wind tunnel as an analogue computer is taken over by numerical methods but the role as a tool for verification is emphasized.

3.3 "Inverse" methods available

Let us now consider the case that methods are available for solving the inverse problem of aerodynamics, i.e. that of determining the geometry of a wing with given pressure distribution (Refs. 2,3,6,22). As illustrated by figure 5c the key problem of the aerodynamic designer now has become a different one. The question of selection of geometry has been replaced by the question of the choice of a suitable "target" pressure distribution for a property selected combination of lift coefficient and Mach number (design condition). The target pressure distribution must be chosen such that the aerodynamic characteristics in both design and off-design conditions are acceptable. This requires establishing of a pressure distribution → aerodynamic characteristics correlation. The physics of (viscous) flows suggest that this should be more straight-forward than the classical geometry → aerodynamics correlation.

Although inverse numerical methods are of considerable interest to the aerodynamic designer, they also have their pitfalls. One well-known reason is, that an arbitrary selected pressure distribution may give rise to physically unrealistic shapes such as locally negative thickness (even if proper trailing

*) Expressing the aerodynamic design requirements in terms of figure 3 does, in fact, take place during this phase.

edge closure is enforced). More in general it may lead to shapes that are not acceptable from the point of view of full-scale wing construction and manufacturing. In other words, the designer has traded the direct control over the geometry that is typical of the processes represented by figures 5a, 5b for better control over the aerodynamics. A consequence of this is that he will also have to establish a pressure distribution→geometry correlation.

A second problem that appears to be associated with non-linear inverse methods is lack of convergence near the root of wings and of swept wings in particular. Recent experience obtained at NLR during the development and application of iterative methods for the design of wings with given pressure distribution has indicated that the inverse problem exhibits a certain "lack of uniqueness". It has been found, that near the root of a wing, several different, but carefully balanced three-dimensional shapes may generate approximately the same pressure distribution. Figure 6 presents an example of this phenomenon for a simple non-lifting wing (thickness problem only). Both results were obtained through the same iterative process (Fig. 7) involving a linear inverse (Ref. 23) and a non-planar, direct, "panel" type method (Ref. 7). The starting geometries for the two cases were different. Results like the one just shown suggest that the main reason for the lack of convergence near the root of wings is, that the inverse process cannot decide which of the related geometries it will select.

3.4 "Optimizing design methods"

The thought that several wing shapes may produce almost the same pressure distribution is a very exciting one for the aerodynamic designer because it offers an additional degree of freedom. The problem with direct as well as inverse numerical methods is how to utilize this freedom.

It would seem at present, that there are two ways out of this dilemma. One approach ("direct optimization", Fig. 8) has, for 2-d flow, been investigated by Van der Plaats, Hicks and Murman (Ref. 24). These authors have developed a numerical optimization design code by linking an optimization program based on the method of feasible directions with the analysis program of Garabedian et al (Ref. 12) for the compressible potential flow about given 2-d airfoils (direct method). The numerical optimization minimizes some specified parameter (e.g., the drag), for a set of design variables (polynomial coefficients) describing the airfoil geometry, while satisfying a number of specified constraints. These constraints may be aerodynamic (e.g. on lift and moment), geometric (e.g. airfoil thickness or volume) or related to the pressure distribution ($C_{p_{min}}$, max. pressure gradient). Figure 9 shows an example of application of this approach. A weak point of the method in it's present form is probably the polynomial contour representation. There is reason to believe that this severely limits the class of obtainable solutions.

A second approach ("constrained inverse method", Fig. 10) is to feed both a target pressure distribution and the geometrical constraints (or a target geometry) into the computer and solve the problem in a weighted least squares' sense. Figure 11 presents a first result of recently started NLR explorations along this line for the case of two-dimensional incompressible flow (Ref. 25). Starting from a given shape a functional of the type

$$F = \int \left\{ w_t (V_o - V_t)^2 + w_n V_n^2 + w_g (Z_o - Z)^2 \right\} dx \qquad (1)$$

is minimized by means of variation of the strenght γ of distributed surface vorticity and the airfoil ordinates Z. In (1) V_o represents the target velocity distribution and Z_o a "target geometry". V_t and V_n are the actual tangential and normal velocity components. w_t, w_n and w_g are suitably chosen weight functions. Note that for $w_t = o$ a Neumann-like (direct) problem is obtained and a Dirichlet-like problem for $w_n = o$. $w_g = o$ represents the "classical" (non-linear) inverse problem. In the simple example of figure 11 w_t, w_n and w_g were all set equal to 1. Convergence for this type of method is generally obtained within 2 to 4 iterations.

It is the author's opinion that the (potential) benefits of numerical methods are best exploited in optimization type methods like those outlined in the preceding paragraphs. Obviously such methods are still in it's infancy at present. However, from the point of view of the aerodynamic designer they deserve much attention. The need for extension to three dimensions in particular seems large.

4. CONCLUDING REMARKS

Having discussed the role of the wind tunnel and that of different types of numerical methods in the aerodynamic design process the conclusion proposes itself that we do not solve the key problems of aerodynamic design by substituting numerical methods for the wind tunnel. Rather than persuing full Navier-Stokes solutions for given geometries we should perhaps look for methods that produce optimized shapes even if such methods must, necessarily, be based on a simplified representation of the physics. We still have the wind tunnel for solving the full, unsteady Navier-Stokes equations!

5. REFERENCES

1. Chapman, Dean R. — Status and prospects of computational fluid dynamics. *von Karman Inst. for Fl. Dyn. LS.87, March 1976.* Also Astronautics and Aeronautics, Vol. 13, No. 4, April 1975.
2. Woodward, F.A. — Analysis and design of wing-body combinations at subsonic and supersonic speeds. Journal of Aircraft, Vol. 5, No. 6, Nov-Dec. 1968.
3. Carmichael, Ralph L., Castellano, Charles R. and Chen, Chuan F. — The use of finite element methods for predicting the aerodynamics of wing-body combinations. NASA SP-228, Analytical methods in aircraft aerodynamics, 1969.
4. Giesing, Joseph P. — Lifting surface theory for wing-fuselage combinations. Mc Donnel Douglas Rept. DAC-67212, 1968.
5. Hess, J.L. and Smith, A.M.O. — Calculation of non-lifting potential flow about arbitrary three-dimensional bodies. Douglas Aircraft Co. Rept. ES 40622, 1962.

6. Rubbert, P.E. and Saaris, G.R. — Review and evaluation of a three-dimensional lifting potential flow analysis method for arbitrary configurations. AIAA Paper 72-188, Jan. 1972.

7. Labrujère, Th.E., Loeve, W. and Slooff, J.W. — An approximate method for the calculation of the pressure distribution on wing-body combinations at subcritical speeds. AGARD CP. No. 71, paper 11, 1970.

8. Kraus, W. and Sacher, P. — Das Panelverfahren zur Berechnung der Druckverteilung von Flugkörpern im Unterschallbereich. Zfw., Heft 9, Sept. 1973, S.301-311.

9. Hess, J.L. — Calculation of potential flow about arbitrary three-dimensional lifting bodies. Douglas Aircr. Co. MDC J5679-11, Oct. 1972.

10. Bauer, F., Garabedian, P. and Korn, D. — Supercritical wing sections. Lecture notes in economics and mathematical systems, Vol. 66. Springer-Verlag, 1972.

11. Boerstoel, J.W. and Huizing, G.H. — Transonic shock-free aerofoil design by an analytic hodograph method. AIAA Paper 74-539, 1974.

12. Bauer, F., Garabedian, P., Korn, D. and Jameson, A. — Supercritical Wing sections II. Lecture notes in economics and mathematical systems, Vol. 108. Springer-Verlag, 1975.

13. Bailey, F.R. and Ballhaus, W.F. — Comparisons of computed and experimental pressures for transonic flow about isolated wings and wing-fuselage combinations. NASA SP-347, pp. 1213-1231, 1975.

14. Albone, C.M., Hall, M.G. and Joyce, G. — Numerical solutions for transonic flows past wing-body combinations. Symposium Transsonicum II, Sept. 1975, Springer-Verlag.

15. Schmidt, W. and Vanino, R. — The analysis of arbitrary wing-body combinations in transonic flow using a relaxation method. Symposium Transsonicum II, Sept. 1975, Springer-Verlag.

16. Jameson, A. — Transonic flow calculations. von Karman Inst. for Fl. Dyn. LS 87, 1976.

17. van der Vooren, J., Slooff, J.W., Huizing, G.H. and van Essen, A. — Remarks on the suitability of various transonic small-perturbation equations to describe three-dimensional flow; examples of computations using a fully-conservative rotated difference scheme. Symposium Transsonicum II, Sept. 1975, Springer-Verlag.

18. Stevens, W.A., Goradia, S.H. and Braden, J.A. — Mathematical model for two-dimensional multi-component airfoils in viscous flow. NASA CR-1843, July 1971.

19. Callaghan, J.G. and Beatty, T.D. — A theoretical method for the analysis and design of multi-element airfoils. AIAA Paper 72-3, Jan. 1972.

20. Vidal, R.J., Erickson Jr. J.C. and Catlin, P.A. — Experiments with a self-correcting wind tunnel. AGARD CP. No. 174, Paper 11, Oct. 1975.

21. Kilgore, R.A., Adcock, J.B. and Ray, E.J. — The cryogenic transonic wind tunnel for high Reynolds number research. AGARD CP. No. 174, Paper 1, Oct. 1975.

22. Bristow, D.R. — A new surface singularity method for multi-element airfoil analysis and design. AIAA Paper 76-20, Jan. 1976.

23. Fray, J.M.J. — A source lattice method for wing thickness design. Unpublished paper presented at Euromech Colloquium 75 on the Calculation of Flow Fields by means of Panel Methods, May 1976.

24. van der Plaats, G.N., Hicks, R.M. and Murman, E.M. — Application of numerical optimization techniques to airfoil design. NASA SP-347, part II, pp. 749-768, March 1975.

25. Labrujère, Th.E. — Airfoil design by means of an optimizing least-squares singularity method. NLR report to be published.

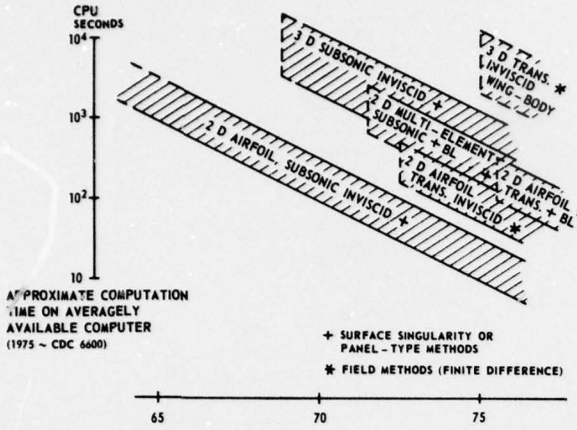

FIG. 1 TREND OF COMPUTATION TIMES FOR TODAY'S SUBSONIC AERODYNAMIC ANALYSIS TOOLS

WINDTUNNEL TESTING	NUMERICAL METHODS
COMPLETE PHYSICS (FULL EQS. OF MOTION)	APPROX. FLOW EQS. (PART OF PHYSICS)
WRONG GEOMETRICAL ENVIRONMENT (WALLS, STINGS ETC.)	CORRECT GEOMETRICAL ENVIRONMENT POSSIBLE
MODEL TIME CONSUMING AND EXPENSIVE	MODEL GEOMETRY EASILY CHANGED
EASY CHANGE OF FLOW CONDITIONS (α, MACH)	CHANGE OF FLOW CONDITIONS EASY, NOT ALWAYS CHEAP
FLOW ABOUT GIVEN BODY ONLY	TYPE OF B.C. CAN BE CHANGED (DIRECT / INVERSE)
LIMITED ACCESSIBILITY	HIGH ACCESSIBILITY

FIG. 2 MAIN POSSIBILITIES AND LIMITATIONS OF NUMERICAL METHODS AND WINDTUNNEL TESTING

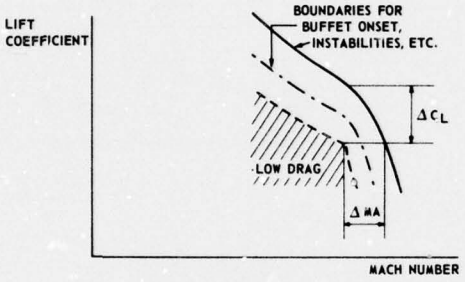

FIG. 3 SUMMARY OF HIGH SPEED DESIGN REQUIREMENTS FOR TRANSPORT AIRCRAFT

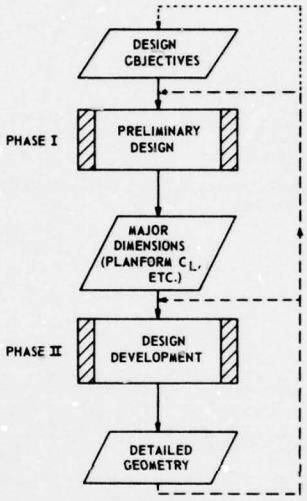

FIG. 4 MAJOR PHASES OF AERODYNAMIC DESIGN PROCESS

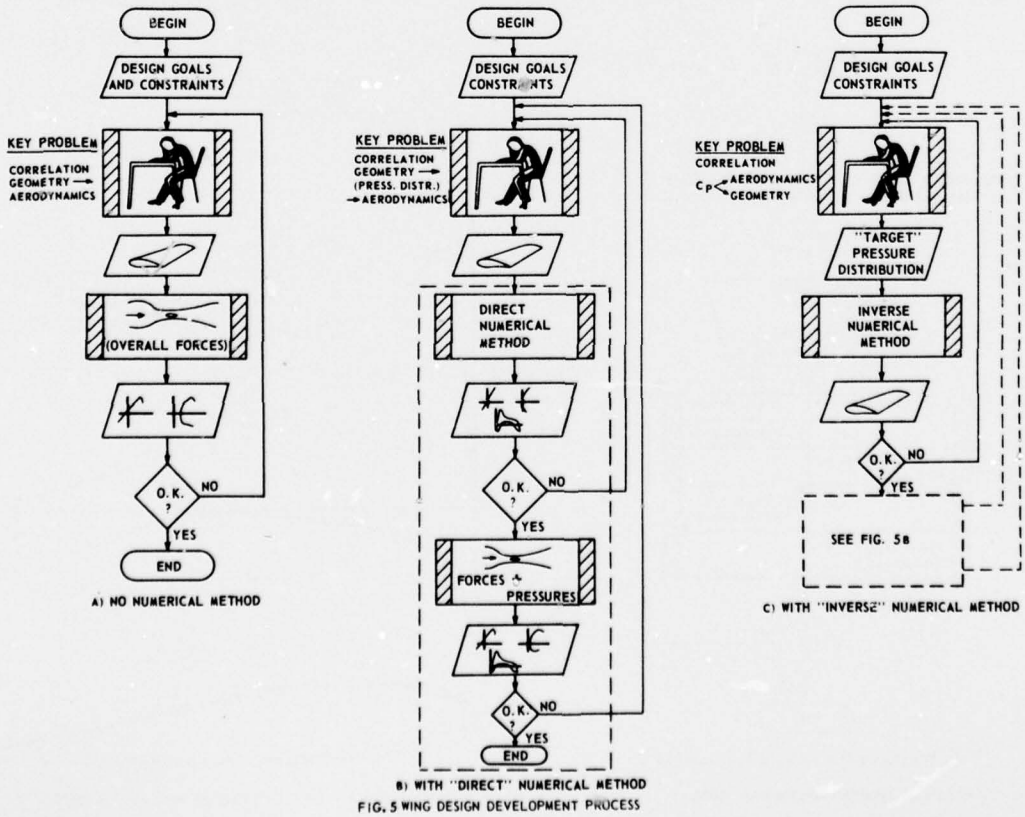

FIG. 5 WING DESIGN DEVELOPMENT PROCESS

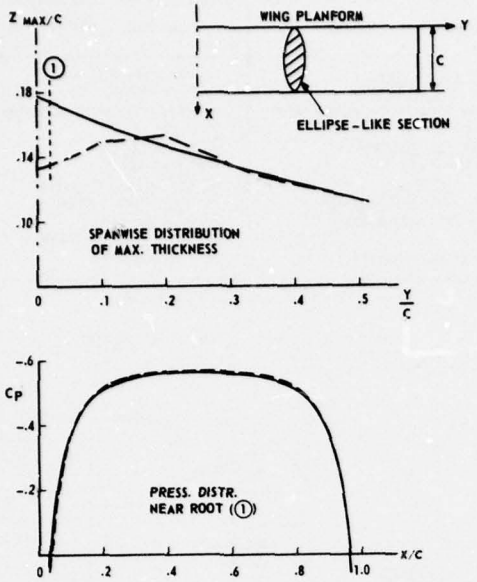

FIG. 6 EXAMPLE (NON-LIFTING) ILLUSTRATING "LACK OF UNIQUENESS" OF INVERSE PROBLEM

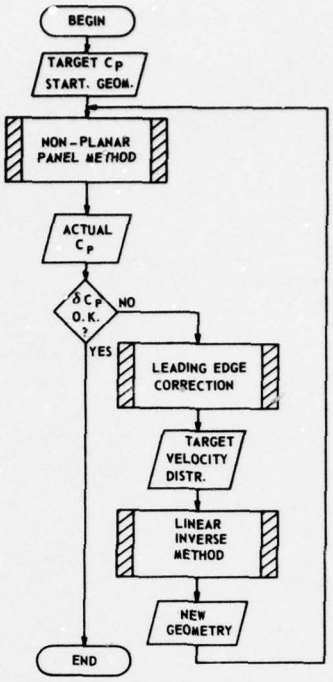

FIG. 7 FLOW DIAGRAM OF ITERATIVE INVERSE METHOD

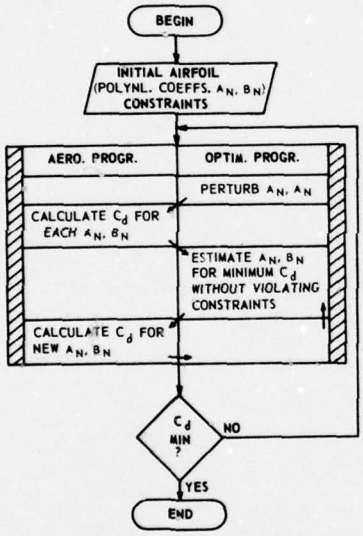

FIG. 8 DIRECT NUMERICAL OPTIMIZATION PROCEDURE
(drag minimization, v.d. Ploats et. al.)

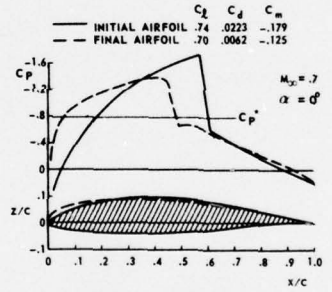

FIG. 9 EXAMPLE OF DIRECT OPTIMIZATION METHOD
Inviscid drag minimization, upper surface mod. only, constraint on area (v.d. Ploats et al.)

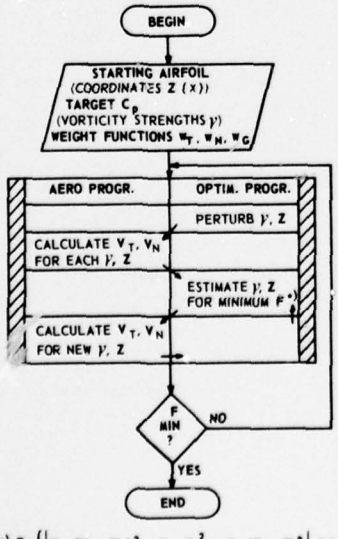

*) $F = \int \left| w_T (V_0 - V_T)^2 + w_N V_N^2 + w_G (Z_0 - Z)^2 \right| dx$

FIG. 10 CONSTRAINED INVERSE PROCEDURE

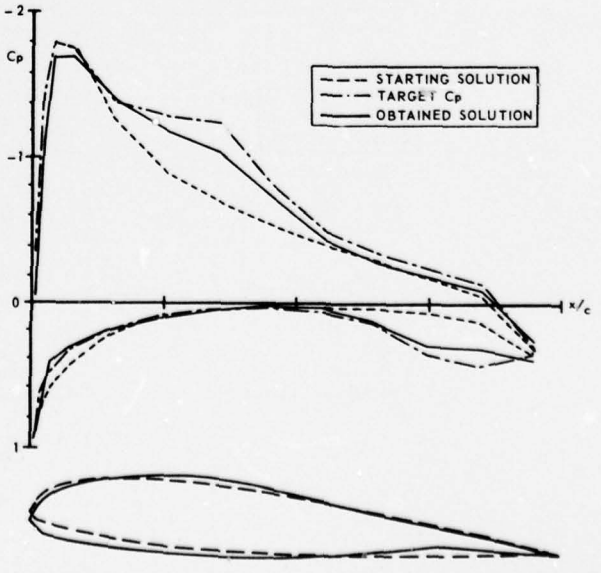

FIG. 11 EXAMPLE OF CONSTRAINED INVERSE METHOD

Application of Computed Shock Standoff Distances for Windtunnel Calibration at Supersonic Mach Numbers less than 1.2

D.J. Jones,
National Aeronautical Establishment, Montreal Road,
Ottawa, Canada.

SUMMARY

Calibration of the National Aeronautical Establishment (NAE) wind tunnel in the Mach number range $1 < M < 1.1$ has been carried out by taking Schlieren photos of the bow shock in front of a sphere. A theory has been developed to calculate this bow shock for flows about axisymmetric bodies. Thus, correlating the experimental and theoretical shock waves, a calibration of the wind tunnel was made.

INTRODUCTION

First, the NAE wind tunnel which required calibration in the transonic-supersonic range will be described (see ref. 1 for more details). It is a 5 ft × 5 ft blowdown wind tunnel and can achieve Reynolds numbers up to about 20 million/ft (70 million/metre). It can operate at subsonic speeds of around $M = 0.25$ up to Mach numbers of 4.5. A working section with porous walls is inserted for use in the transonic range. Surrounding the porous walls is the plenum chamber. The pressure is measured in this chamber and from this pressure and the stagnation pressure we determine a Mach number called M_p. For calibration purposes we have to correlate M_p to the free stream Mach number and hence find a correction, ΔM, to M_p. This is usually done by pressure probes but it was felt that the probe method may disturb the flow too much and so give inaccurate measurements.

The main purpose of our work on shock standoff location for flow about axisymmetric bodies was to provide an alternative method of calibrating the wind tunnel in the transonic range $1 < M < 1.1$. Our aim was to provide a Mach number calibration accurate to $\Delta M < 0.002$.

Previous calibration had been made at Mach numbers greater than 1.1 and less than 1.3 by inserting a cone at zero incidence in the wind tunnel and measuring the shock angle on the Schlieren photo. By correlating this data with the theoretical prediction of the shock angle it was possible to correct the Mach number M_p. For supersonic Mach numbers less than 1.1 we previously used a semi-empirical approach which involved the use of a modification to Serbin's formula for shock standoff from a flat ended cylinder (ref. 2). However it was felt that a more accurate method was needed. A suitable method seemed to be that of measuring from Schlieren photos the shock standoff distance from a sphere. In our experiments we covered a range of Mach numbers from 1 to 1.3 and it is felt that the present method would be suitable for wind tunnel calibration from 1 to about 1.2 because, in this range, the variation of shock standoff is quite sensitive to changes in Mach number.

To do the above calibration we needed a suitable theory for calculating the bow shock in front of a sphere and this is where the main difficulty lay as previous theoretical methods were not accurate. The method finally derived was also suitable for other blunt axisymmetric bodies besides spheres and it could also be used for two dimensional bodies.

THEORETICAL DIFFICULTIES

Figure 1 shows a plot of standoff distance versus Mach number for flow about a sphere. This figure is taken from an AEDC report of 1969 (ref 3) except that also added are the theory of Belotserkovskiy (ref 4) and the experiments of Stilp (ref 5). It can be seen that there is a huge scatter in theoretical and experimental data. Also shown on this figure with the symbol I is the accuracy to which we require our standoff distance so that we achieve $\Delta M < 0.002$. It seems clear that the theories quoted in the figure are not sufficiently accurate and so our objective here is to develop an accurate, efficient scheme.

Several methods were attempted before finally selecting the relaxation method mentioned later. Firstly Belotserkovskiy's Schemes I and II we unsuitable at low supersonic Mach numbers and Scheme III had to be used; however it can be seen from fig 1 that these results (taken from ref 4) differ considerably from other results especially in our Mach number range of interest ($M < 1.2$). A method of lines solution was attempted but this gave convergence difficulties for Mach numbers less than 1.3. Next a collocation method was used and this gave reasonable results down to $M = 1.15$ but below this convergence was difficult. Then a time dependent method (ref 6) was used but produced 'kinky' shocks at $M = 1.2$ and also the convergence was very slow. A second time dependent method, due to Aungier, and run by Hsieh at AEDC (ref 7) required 22 hours computer time on an IBM 370/155 at $M = 1.05$. Thus a new approach was attempted.

PRESENT THEORY

The present theory, which uses a finite difference approach, is fully reported in refs 8 and 9. Basically it consists of estimating the shock shape and applying the Rankine-Hugoniot relations across it. From quantities at the shock we can extrapolate by Taylor series the disturbance potential ϕ ($q = q_\infty + \nabla\phi$) to the line of mesh points adjacent to the shock. We then fix this line of ϕ's and iterate, using Jameson's rotated difference scheme, the rest of the flow field between shock and body until the residuals are sufficiently small. However non-zero residuals now remain at the line of points adjacent to the shock; these are driven towards zero by a Newton scheme which changes the shock shape. The rest of the flow field is then re-iterated and so the process continues.

RESULTS

The results of our computation showing shock standoff versus Mach number for flow about a sphere are given on fig 2. It can be seen that Hsieh's time dependent method gives practically identical results to ours (see M = 1.3, 1.17, 1.10 and 1.05). At the latter Mach number there is a very slight difference but this is believed to be due to Hsieh's extrapolation to infinite time from the smaller time at which the computation was stopped. Because of this agreement between the two completely different theories it seems reasonable to suppose that the present results are accurate. Frank and Zierep (ref 10) results are also included for completeness - it can be seen that their approximation is reasonably good even though they use a semi-empirical approach with a modification of a formula derived for slender bodies of revolution.

Also shown on fig 2 are several experimental results. The NACA 2000 results agree with our theory (see M = 1.3 and 1.17) while Stilp's results are consistently low at Mach numbers less than 1.10 (perhaps due to Stilp's wind tunnel calibration). Our NAE data are given for three different values of Reynolds' number but are plotted against M_p and as such show the correction ΔM that must be applied. Only some of the low Reynolds number NAE data has been corrected by using the cone Schlieren shock angle as mentioned earlier - these are represented by the full circle and it can be seen that these points now straddle our theoretical prediction.

The effect of Reynolds number should be mentioned here. It is estimated that the displacement thickness upstream of the maximum sphere diameter is negligible at $Re > 6 \times 10^6$/ft - thus inviscid flow can be assumed. Now to change Reynolds number in our wind tunnel we change the stagnation pressure but to keep the same M_p we alter slightly the tunnel configuration (diffuser re-entry flap setting). It is thought that these two changes then give a different Mach number at the tunnel centre line, M_C. Thus there is a different relation between M_p and M_C (as indicated on fig 2) depending on Re.

The remaining experimental data on fig 2 show the ballistic range results obtained at AEDC by Starr et al (ref 11) and by Bailey and Hiatt (ref 12). It can be seen that very good agreement with the present theory is obtained particularly when one remembers that the lag effects in a ballistic range would tend to increase their standoff prediction.

Finally fig 3 shows our wind tunnel correction, ΔM, to be applied to M_p.

CONCLUSIONS

It has been shown that wind tunnel calibration can be made in the Mach number range $1 < M < 1.2$ by measuring shock standoff distances from a sphere. The NAE 5 ft × 5 ft blow-down wind tunnel will be calibrated in this manner.

REFERENCES

1. Brown, D. Information for Users of the National Research Council's 5 ft × 5 ft Blowdown Wind Tunnel. NRC Report LTR-HA-6, Sept 1970.

2. Galway, R. Centreline Mach Number Calibration, Transonic Working Section ($1.0 < M < 1.16$). NRC Lab Memo HSA-46, Jan 1971.

3. Buzyna, G. and Wegener, P. Experiments on Non-Equilibrium Supersonic Flow Shock Standoff Distance of Spheres Carried Out in a New Type of Intermittent Wind Tunnel. AEDC-TR-69-81, May 1969.

4. Belovtserkovskiy, O.M. Supersonic Gas Flows around Blunt Bodies. NASA TT.F-453, June 1967.

5. Stilp, A. Strömungsuntersuchungen an Kugeln mit Transonishen und Supersonischen Geschwindigkeiten in Luft und Frigen-Luftgemischen. Ernst Mach Institute Bericht Nr. 10/65.

6. Barnwell, R.W. and Davis, R.M. A computer Program for Calculating Inviscid Adiabatic Flow about Blunt Bodies Travelling at Supersonic and Hypersonic Speeds at Angle of Attack. NASA TM X-2334, Sept 1971.

7. Hsieh, T. Hemisphere-Cylinder in Low Supersonic Flow. AIAA Journal, 13, (1975) 1551-2.

8. Jones, D.J. and South, J.C. Jr. A Numerical Determination of the Bow Shock Wave in Transonic Axisymmetric Flow about Blunt Bodies. NRC Report LR-586, May 1975.

9. Jones, D.J. Computation of Bow Shocks in Transonic Flow. Proceedings V.th International Conference on Fluid Dynamics, Enschede. June 1976.

10. Frank, W. and Zierep, J. Transonic Supersonic Flow around Bodies of Revolution. Acta Mechanics, 19, 1974, 277-287.

11. Starr, R.F., Bailey, A.B. and Varner, M.O. Shock Detachment Distance at Near Sonic Speeds. AIAA Journal, 14 (1976), 537-9.

12. Bailey, A.B. and Hiatt, J. Free Flight Measurements of Sphere Drag at Subsonic, Transonic, Supersonic and Hypersonic Speeds for Continuum Transition, and Near-Free-Molecular Flow Conditions. AEDC-TR-70-291, March 1971.

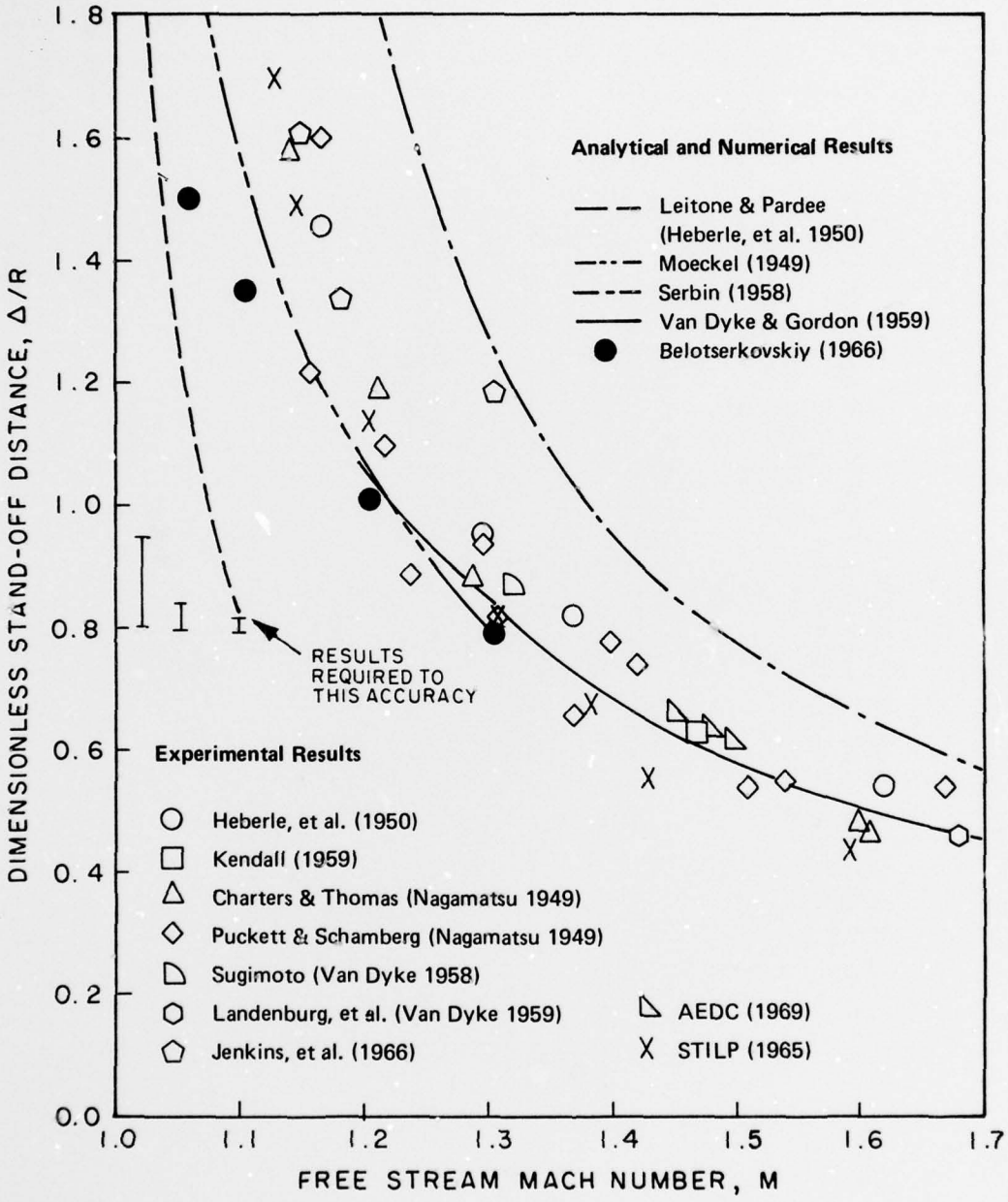

FIG 1. SHOCK STANDOFF VERSUS MACH NUMBER (SPHERE)

FIG 2.
SHOCK STANDOFF DISTANCES FOR SPHERE

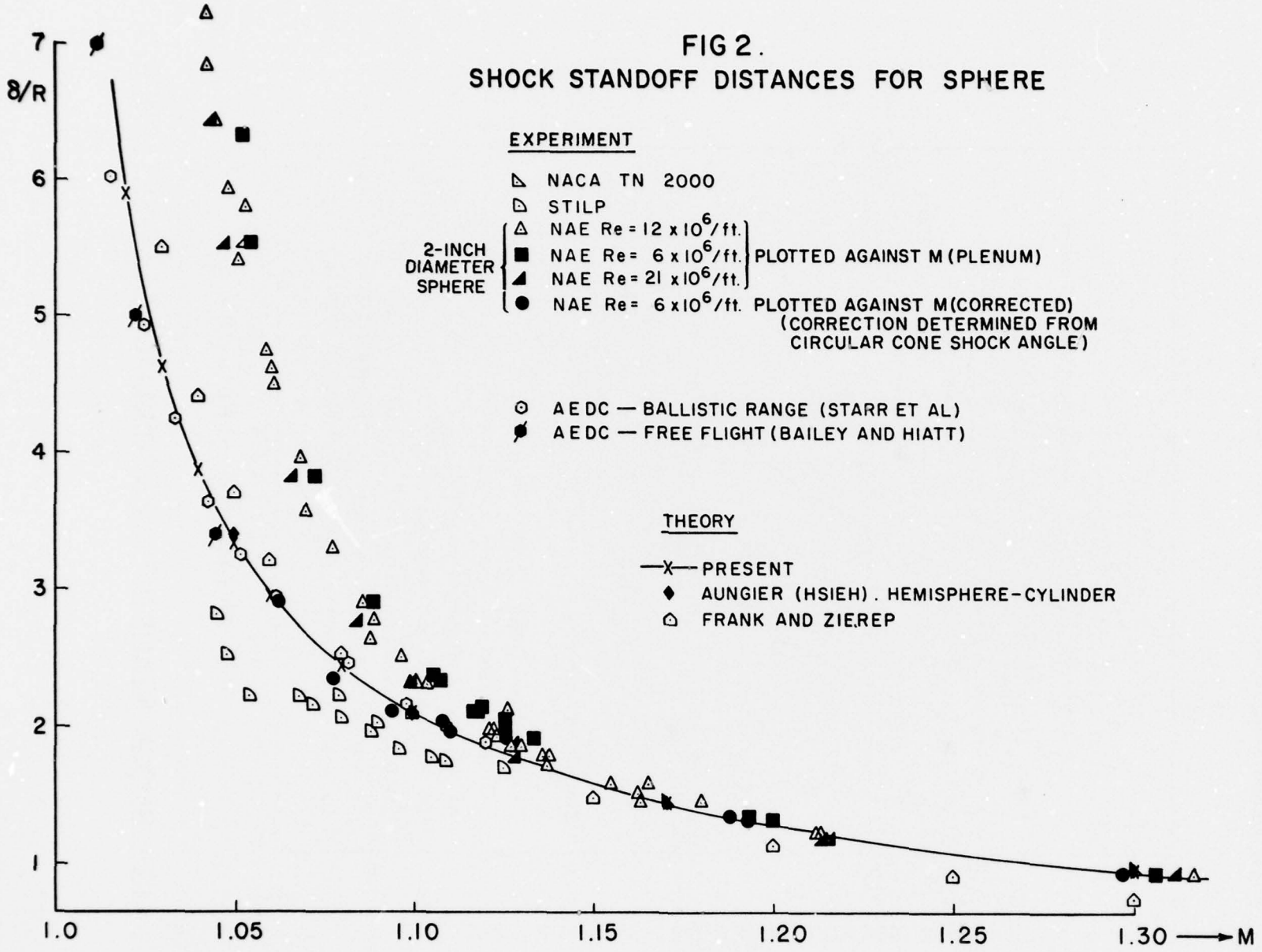

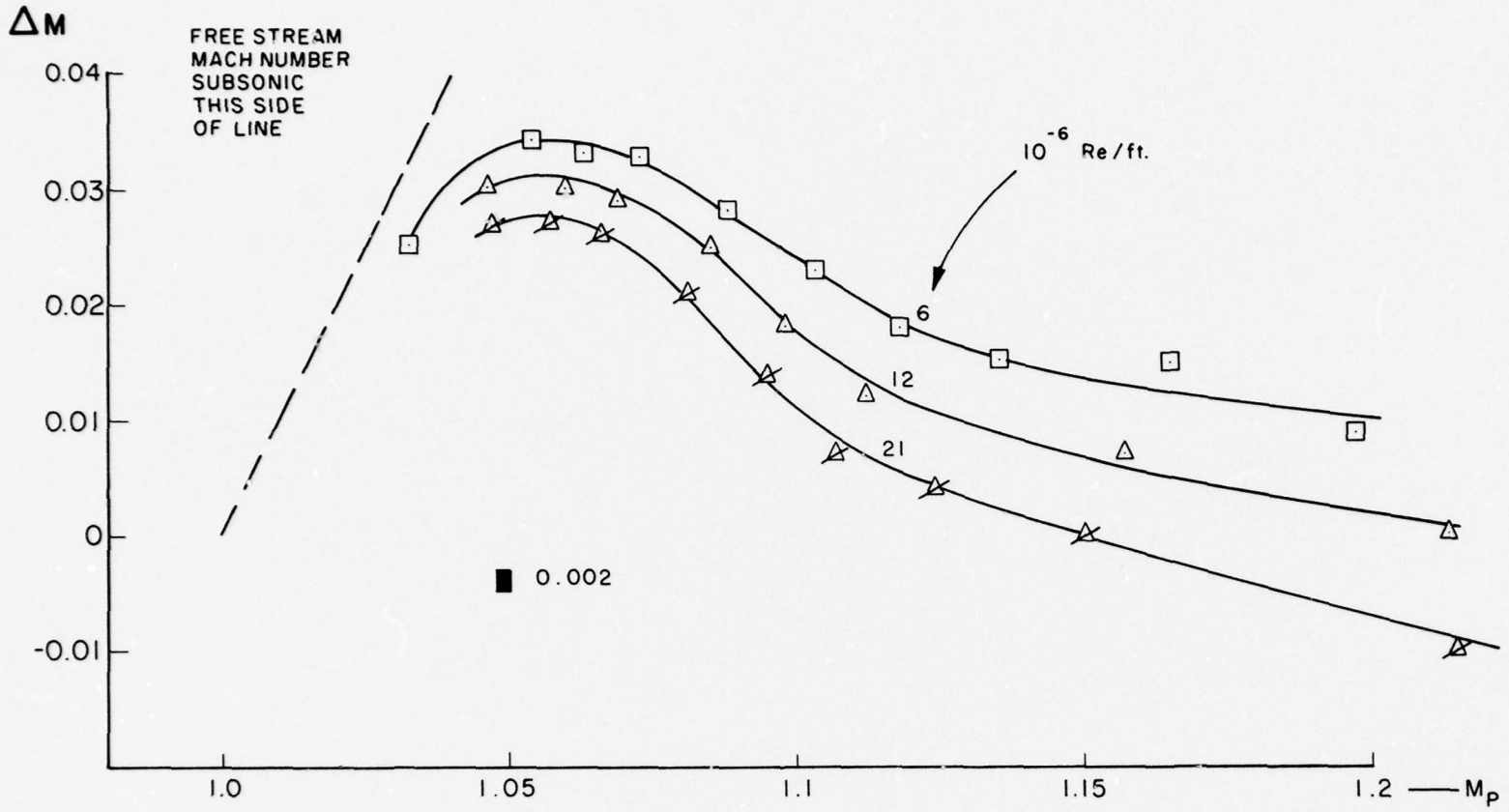

FIG 3. MACH NUMBER CORRECTION ΔM versus MACH NUMBER IN PLENUM ($M = M_p - \Delta M$)

THEORETICAL AND EXPERIMENTAL SIMULATION METHODS FOR EXTERNAL STORE SEPARATION TRAJECTORIES *

J. VON DER DECKEN, P. ESCH, W. FRITZ

DORNIER GMBH

FRIEDRICHSHAFEN, GERMANY

SUMMARY

A review of numerical methods and experimental techniques for the simulation of separation trajectories of external powered and unpowered stores at low and high speed is given.

For the theoretical simulation, potential flow methods are used to calculate the quasi-steady loadings on the store while the trajectory itself is determined by solving the equations of the 6-degree-of-freedom motion.

Based on the experience of numerous systematic experimental studies gained with the rigid loads and the freedrop technique for unpowered stores the advantages and limitations of different windtunnel techniques will be demonstrated including a critical discussion of scaling effects.

The experimental and theoretical simulation techniques have proven to be a satisfactory tool for the investigation of the separation characteristics of unpowered external stores. The on-line combination of windtunnel techniques and numerical methods including the thrust determination will provide an efficient trajectory simulation for powered air-launched missiles. This technique - known as captive trajectory technique - will be described.

RESUME

Une revue est présentée pour des méthodes numériques et expérimentales de simulation des trajectoires de séparation des charges externes autopropulsées ou non dans le régime des vitesses basses et élevées.

Pour la simulation théorique des méthodes pour écoulement potentiel sont utilisées pour calculer les forces quasi-stationaires sur les charges tandis que la trajectoire est déterminée en résolvant les équations des mouvement à six degrées de liberté.

En se basant sur de nombreuses études expérimentales systématiques obtenues par des techniques "rigid load" et "freedrop", les avantages et limitations des différentes techniques de soufflerie seront démontrées.

Les techniques de simulation theoriques et experimentales ont montré d'être un outil satisfaisant pour l'investigation des charactéristiques de séparation des charges non-autopropulsées. La combinaison "on line" des techniques de soufflerie et des méthodes numeriques, y compris la détermination de la poussée, va donné une simulation efficace des trajectoire des missiles lancés en air. Cette techniques - connue comme "captive trajectory technique" - sera décrite.

1. INTRODUCTION

Due to the high speed and the complexity of modern military aircraft the problems of aircraft/stores-compatibility have become of significant magnitude. Therefore, in the last few years new theoretical and experimental methods of simulating and predicting store separation trajectories have been developed and applied to present aircraft.

Modern hybrid fighter-bomber are laid out to perform multiple missions carrying as many external stores as possible in single, double, triple or multiple stations and racks respectively at the wing and at the fuselage. For logistic reasons the big arsenal of different weapons, fuel tanks, dispensers etc. (more than 100 different types within NATO) is required to fit on all current aircraft. This will generate a possible work load for flight certification of a few billion cases for 1 military aircraft and involves the expenditure of large sums of money.

We try to give a review of theoretical and wind tunnel methods for the simulation of store separation trajectories in a cheap and effective way. By help of such simulation methods the immense effort of flight testing and certification can be reduced considerably.

---

* This work was sponsored by the German Ministry of Defense under contract T/RF 41/RF 410/21244 and 51086.

2. THEORETICAL SIMULATION METHODS

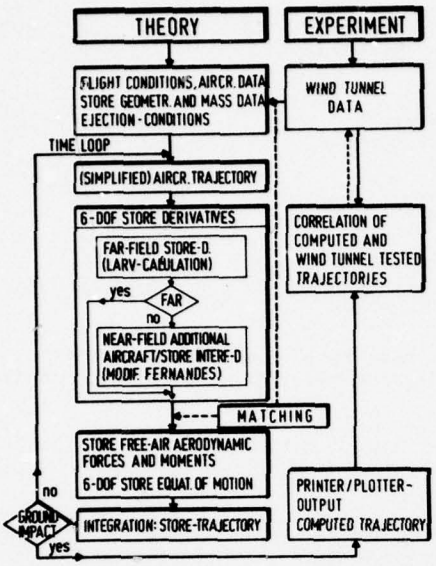

Fig. 1 Computer program flow chart for the theoretical simulation of external store separation trajectories

Fig. 1 shows a flow chart of the theoretical treatment of the problem with the possibility to adjust and improve the calculations by wind tunnel data. As input the parent aircraft data (geometry, flight conditions, maneuver simulation) and the store data (geometry, mass data, ejection and thrust forces) are fed into the computer program. The momentary position of the aircraft on its path is calculated in a simplified form only. The store derivatives are determined for the momentary position of the store on its trajectory by superimposing the far-field solution for the store in undisturbed flow (LARV-calculation) and a near-field additional due to store/aircraft interference effects calculated after a modified FERNANDES method. With these dimensionless aerodynamic coefficients the quasi-steady loadings acting on the store are determined which are input to the 6-degree-of-freedom equations of motion. Integration leads to translational and rotational increments of the store motion and thus to the new coordinates of the store trajectory for the time instant under consideration. The next time step starts again with the aircraft trajectory. If there is a bad correlation between computed and wind tunnel data it is possible to adjust the theoretical suppositions in the determination of the near-field additional derivatives.

The LARV-program (Low Aspect Ratio Vehicle) provides the store's aerodynamic derivatives in uniform potential flow for

- arbitrary store configurations with/without jet
- subsonic/transonic/supersonic flow
- angles of attack $-90^0 < \alpha < 90^0$
- angles of roll $-90^0 < \alpha < 90^0$.

The elements of LARV [1] are based on slender body theory with empirical correlations, base drag correlations and DATCOM analyses for wings. All relations are given in functional form to provide fast computation. The LARV-method has been proved by numerous comparisons with experimental data.

Fig. 2 and fig. 3 show examples of LARV-calculations in subsonic and supersonic flow. The agreement between theory and experiment is good including non-linear effects of lift, drag and pitch moment versus angle of attack.

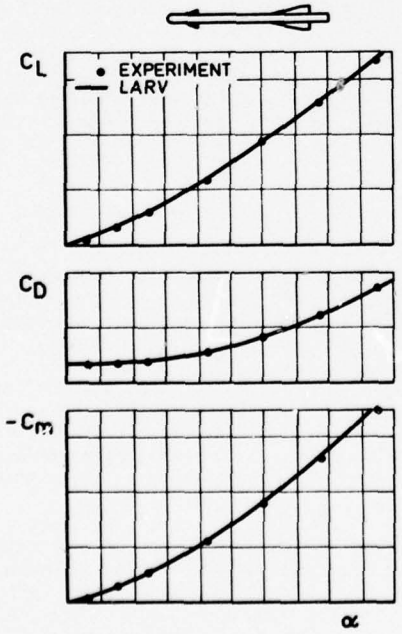

Fig. 2 Comparison LARV-theory/experiment for a missile. Lift, drag and pitch moment versus angle of at $M_\infty = 0.6$

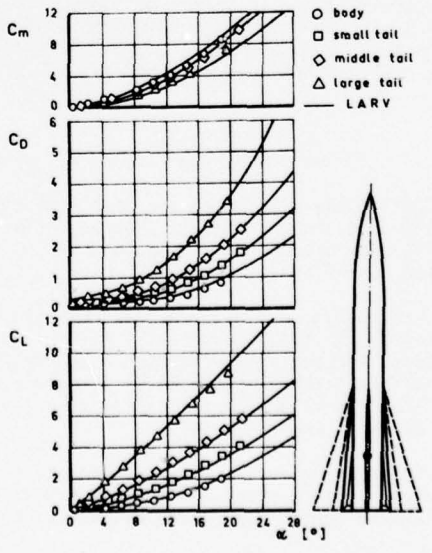

Fig. 3 Comparison LARV-theory/experiment for a tail/body combination at $M_\infty = 1.5$

The interference flow field and the interference loading coefficients acting on the store are calculated by the FERNANDES method [2], which has been modified in some aspects.

The disturbance flow field produced by the aircraft is predicted using the linear potential flow theory with source and vortex distributions. For a number of different positions on the store trajectory the disturbance velocities are calculated along the store axis. The force and moment coefficients of the store due to this variable flow field are determined giving the interference coefficients. To get the total store coefficients the free-air coefficients due to the store's angle of incidence and of yaw in undisturbed flow (result of LARV-method or experimental data) have to be added.

The geometric features producing the interference flow field about an aircraft are wing, body, engine inlet, pylons and further stores in the neighbourhood which will not be released. The prediction method [2] represents all these features for an aircraft of general geometric description, with no slender body assumptions and no two-dimensional approximations.

To obtain the disturbance flow field around the aircraft, the complete flow field is split into parts due to the different aircraft components. Each component is treated seperately and all effects are superimposed linearly. Compressibility effects are corrected for by the Prandtl-Glauert rule. The different aircraft components are represented by singularities in the following way:

Wing

The interference flow field due to the wing is split into one part due to wing lift and one due to wing thickness. Wing lift is represented by a spanwise and chordwise vortex lattice. The vortex strengths are found by solving the linear system of equations given by the influence coefficients matrix and the wing boundary conditions as right hand side. The wing thickness is represented by a spanwise and chordwise distribution of elementary source strips.

Pylon

The flow field produced by the plyon's thickness is described by use of source strips in the same manner as for the wing thickness. The pylon interference with the wing is simulated by representing the pylon with horseshoe vortices to match the boundary conditions of flow tangency at the pylon. Wing-pylon interference effects are accounted for by mirroring the pylon vortices above the wing plane. Alternatively the wing-pylon combination can be represented by one joined set of vortex-lattices.

Bodies

The aircraft fuselage (resp. further stores) is represented by a line source distribution for the axial flow and by a line doublet distribution for the crossflow. Engine inlets are either included in the body cross-sections or represented by additional line singularities. Further stores are represented in the same manner as the fuselage.

Wing-Body Interference

The components of mutual interference between wing and body are accounted for by mirroring the wing vortices at the body while the bodies are assumed to be circular cylinders.

To calculate the interference loading, the store is segmented axially into a number of small sections. The load on each section is computed from the local crossflow by use of a set of loading coefficients which describe the section aerodynamic properties. These loading coefficients may be obtained from test data in uniform flow or from theory. The interference coefficients are then calculated by integrating along these store sections. The total store loading is obtained by adding the free-air coefficients (calculated with LARV or known from experiments) linearly to the interference coefficients.

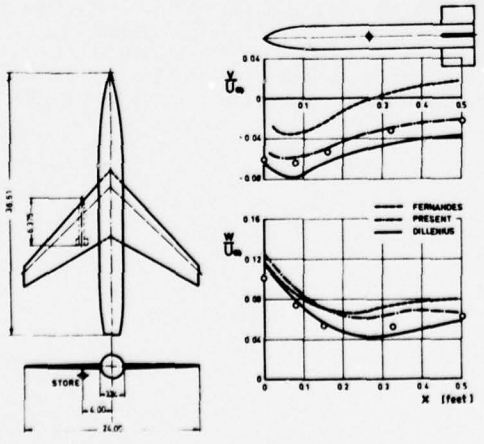

Fig. 4 Interference velocity distributions (sidewash v, upwash w) along store axis for a wing/body combination with external store. Comparison theory/experiment at $M_\infty = 0.4$ and $\alpha = 6^0$

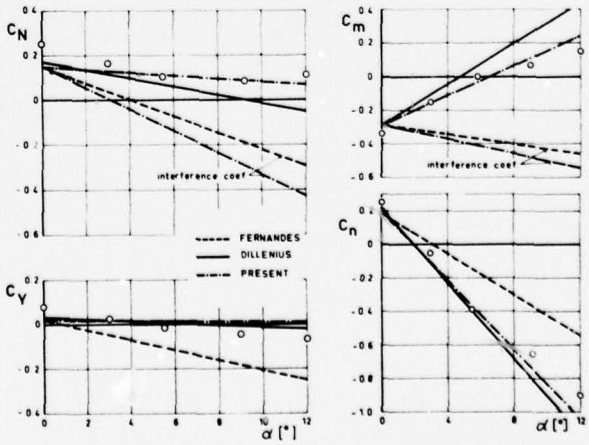

Fig. 5 Comparison theory/experiment for normal force C_N, side force C_Y, pitch moment C_m and yaw moment C_n versus angle of attack at $M_\infty = 0.4$ for the same configuration as in fig. 4

Fig. 4 shows the upwash and sidewash distribution due to the interference flow field along the store axis for a simple wing-body combination with an external store. X is the distance from the store nose. The results of the original FERNANDES [2], of the DILLENIUS [3] and of the present method are compared with experimental data.

Fig. 5 shows the total normal force, side force, pitch moment and yaw moment acting on the store mounted in the same configuration as shown in fig. 4. For the original FERNANDES method [2] and the present method the interference coefficients are compared, too.

Examples of complete separation trajectories calculated by the present simulation program after fig. 1 are not yet available. We look forward to presenting a comparison of theoretical results with wind tunnel test data obtained by the freedrop technique later this year.

3. EXPERIMENTAL SIMULATION TECHNIQUES

In addition to theoretical simulation methods for external store separation trajectories wind tunnel experiments are necessary because of the complexity of the aerodynamic flow fields generated by today's fighter-bomber aircraft carrying stores externally in multiple configurations, i.e.

- interacting pressure distributions
- interacting shock waves
- compressibility effects such as local supercritical zones
- self generated perturbations of the separating store

are virtually impossible to predict analytically without massive simplifications. Therefore, a basic supposition for wind tunnel tests is that the model should be as realistic as possible especially concerning the store loading configuration, i.e. all external stores should be correctly mounted at the different wing pylons or at the fuselage via

- single ejector rack (SER) or
- double ejector rack (DER) or
- triple ejector rack (TER) or
- multiple ejector rack (MER)

while the store attachment provisions are accurately simulated, i.e. crutch arms, adjustment screws etc. In addition the ejection characteristics are to be correctly simulated corresponding to the full scale jettison behaviour of the store measured in ground tests at the original ejector rack. Of course the common similarity rules (Reynolds, Mach) should be met, too, as close as possible. The following wind tunnel techniques will be discussed shortly:

3.1 Rigid Loads Technique (RLT)
3.2 Free Drop Technique (FDT)
3.3 Grid Testing Technique (GTT)
3.4 Captive Trajectory Technique (CTT)
3.5 Flow Field Angularity Technique (FAT).

3.1 Rigid Loads Technique

The aircraft is conventionally mounted in the wind tunnel via a internal balance on an operational rear sting. Integrated in the store of interest there is a 6-component strain gage balance rigidly mounted to the aircraft model and capable to measure forces and moments acting on the store alone or on the store plus adapter and pylon.

The result of the RLT is the aerodynamic 6-DOF-derivatives of the store in captive carriage position only. However, these derivatives are the predominant factor affecting the whole separation trajectory of the store as it includes already the maximum of interference effects and of the release disturbance. Therefore, the very simple RLT is generally adapted to contribute an essential part to the theoretical simulation of separation trajectories and serves as a check for the FERNANDES method. In addition the performance penalties of the aircraft due to the different external stores can be more accurately predicted by the results of the RLT.

3.2 Free Drop Technique

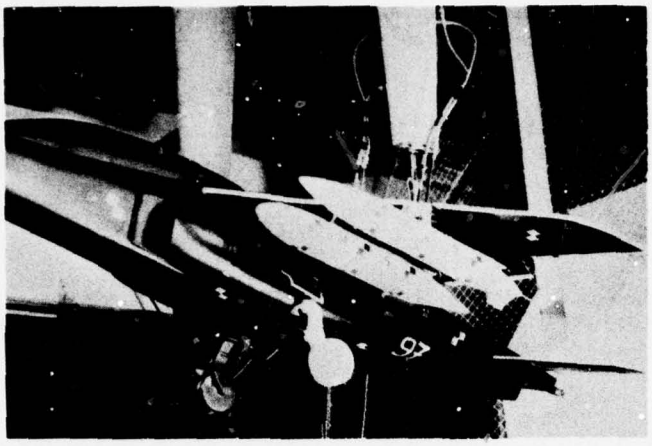

Fig. 6 Arrangement for freedrop technique in the DFVLR-wind tunnel in Cologne. Alpha Jet 1:5 with external stores

The FDT involves actually releasing store models in the wind tunnel from the aircraft model and requires already a rather big effort of unconventional experimental equipment for the model itself and also in the wind tunnel. First, the aircraft model should be mounted in the test section as rigidly as possible to avoid stochastic accelerations of the model which could produce an error in the required release acceleration of the store.

Fig. 6 shows a typical FDT-arrangement in a low speed (80 m/s) wind tunnel with open test section (3,2 m x 2,3 m). A fishing net for catching the dropped stores is to be seen beneath the 1:5 Alpha Jet aircraft model.

Second, a model release unit with two ejector pistons is needed for each store, i.e. in case of a DER or TER there are 2 or 3 release units necessary which provide the possibility to simulate pair, multiple or ripple releases.

Fig. 7 shows a release unit for external stores, scale 1:5 to the original ML AVIATION device. The two ejection pistons and a third piston working on a knife (a sort of guilotine) which cuts the suspension wire off are pneumatically driven.

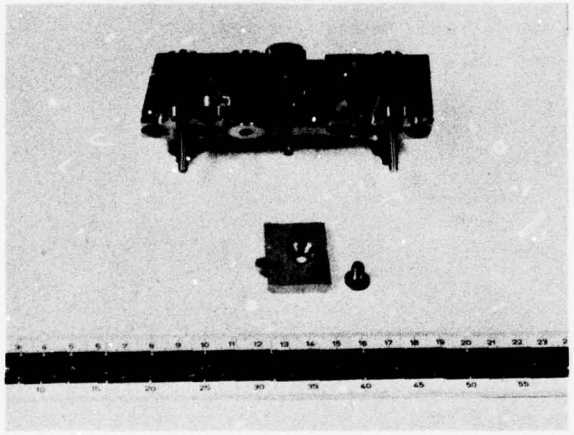

Fig. 7 Release unit for external stores scale 1:5

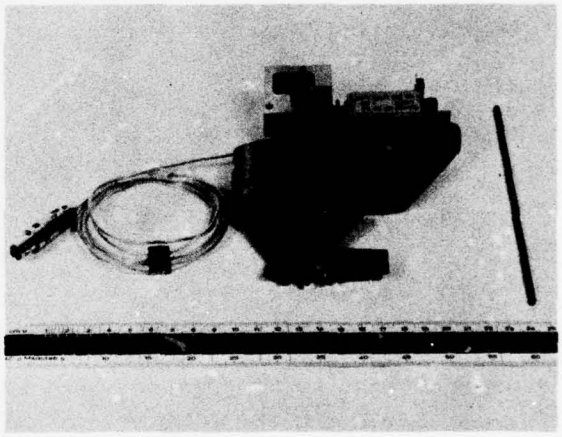

Fig. 8 Release unit for external stores scale 1:20

Fig. 8 shows a scale 1:20 release unit and illustrates that it is not possible to reduce the scale of the device to be able to integrate it into the wing pylon and resulting in a very large part of the release unit located above the wing generating an uncorrect flow disturbance. The ejector impulse is dependent on the driving pressure and must be carefully calibrated for each piston in advance of the tests to allow an adjustment of the correct acceleration during the store release in the wind tunnel.

Third, for jettison tests the store models have to be dynamically similar with respect to the full-scale store and must be extremely accurately scaled concerning the

- geometric properties
- dynamic mass properties (mass, center of gravity, moments of inertia).

The following similarity rules have to be fulfilled:

Flow Similarity

Derived out of the NAVIER-STOKES equations one obtains the wellknown similarity parameters

$$Re = \frac{v_\infty \cdot l}{\nu_\infty}$$ Reynolds

$$Fr = \frac{v^2_\infty}{g \cdot l}$$ Froude

$$Str = \frac{v_\infty \cdot t}{l}$$ Strouhal

$$M = \frac{v_\infty}{v_s}$$ Mach

v_∞ = velocity of onset flow
ν_∞ = kinematic viscosity
v_s = velocity of sound
g = gravitational acceleration
l = characteristic length of store
t = time in seconds

Similarity of Forces

The aerodynamic forces and the mass forces due to acceleration and gravity equilibrate each other as well in the full scale as in the model case which leads to the condition

$$\left(\frac{\rho_\infty \cdot v^2_\infty}{\rho_b \cdot l \cdot a}\right)_m = \left(\frac{\rho_\infty \cdot v^2_\infty}{\rho_b \cdot l \cdot a}\right)_f$$

m = model
f = full scale
ρ_b = body density
a = body acceleration

This condition may be fulfilled by different methods.

Froude-Method (FM)

The Mach-condition is neglected. Therefore, the Froude-Method is limited to *low speed tests*, where compressibility effects are unimportant. The following conditions are valid:

$$\left(\frac{v^2_\infty}{l}\right)_m = \left(\frac{v^2_\infty}{l}\right)_f$$

$$(a)_m = (a)_f \; ; \quad (g)_m = (g)_f$$

$$\left(\frac{\rho_\infty}{\rho_b}\right)_m = \left(\frac{\rho_\infty}{\rho_b}\right)_f$$

The body velocity as well as the onset flow velocity are both dependent to the square root of the scale factor. This means that the angle of attack for the model is identical with that one of the full scale store over the whole separation trajectory.

For jettison tests in the *high speed range* one of the two following methods are adapted.

Light-Model Method (LM)

$$(M)_m = (M)_f$$

$$\left(\frac{\rho_\infty \cdot v^2_\infty}{\rho_b}\right)_m = \left(\frac{\rho_\infty \cdot v^2_\infty}{\rho_b}\right)_f$$

$$(a \cdot l)_m = (a \cdot l)_f$$

As the acceleration of the store due to ejection and aerodynamic forces are joinded with the scale factor but the acceleration due to gravity obviously is *not*, leads the LM to different motion properties in axial (x) and normal (z) direction.

However, by a modification of the LM it is possible to adjust the ejection velocity in such a manner that for a choosen *single point* of the separation trajectory the relation of z/x is identical for model and *full scale*. That means for a complete trajectory several steps are required. But the so obtained trajectory is not correct, because

- the store travels through a different flow field in the wind tunnel and in the full scale flight test
- the normal velocities in model and full scale do not correspond which leads to different angles of attack, and different trajectories in the wind tunnel and flight test.

The error of the LM is the smaller the larger the ejection acceleration is.

Heavy-Model Method (HM)

$$(M)_m = (M)_f$$

$$\left(\frac{\rho_\infty \cdot v^2_\infty}{\rho_b \cdot l}\right)_m = \left(\frac{\rho_\infty \cdot v^2_\infty}{\rho_b \cdot l}\right)_f$$

$$(a)_m = (a)_f \; ; \quad (g)_m = (g)_f$$

Though in the HM the velocities in the wind tunnel and in the flight test are equal $(v_\infty)_m = (v_\infty)_f$ the relation of the normal velocities is joined with the square root of the scale $(v_z^2/l)_m = (v_z^2/l)_f$, that means the angles of attack are not the same in the model test and the full scale test; but the trajectory of the center of gravity (c.g.) will be essentially correct.

It should be pointed out especially that constructing the store models after HM is very difficult because the relation of the body density is a function of the scale $(\rho_b \cdot l)_m = (\rho_b \cdot l)_f$. It is not possible to fulfil this relationship for small-scale models of high density stores even when exotic metals such as tungsten, gold or platinum are used.

Finally, a precise kinematographic registration of the separation trajectory from 3 orthogonal directions (side, bottom, rear) is required for to provide a good qualitative illustration of the trajectory and an accurate quantitative analysis. This is done on the one hand by 3 remotely controlled cameras taking stroboscope pictures of the separation trajectory by means of stroboscope-flash illumination. Fig. 9 shows an example of such stroboscope pictures which are not quantitatively analysed.

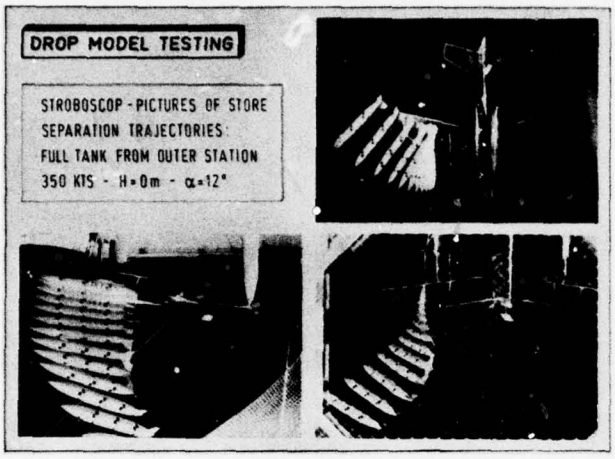

Fig. 9 Example of stroboscope photo pictures showing the separation trajectory of a full fuel tank releasing from 1:5 Alpha Jet model in the DFVLR wind tunnel, Cologne (photos by DFVLR)

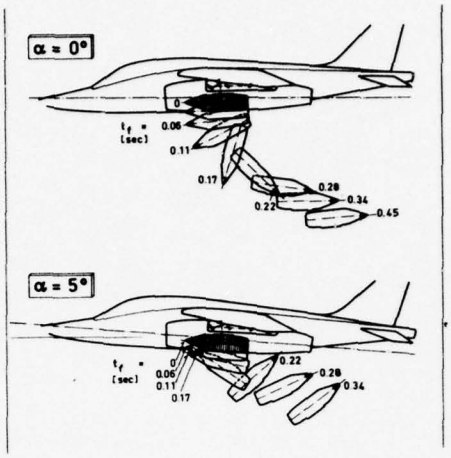

Fig. 10 Rocket launcher released from 1:5 Alpha Jet at simulated 350 KTS. Different store positions are copied from the high speed motion pictures film obtained by lateral camera. The time after release is given for full scale.

However, the main information is received from high speed motion picture films, taken by 3 remotely controlled 16 mm-cameras (1000 to 10000 frames per second) during a permanent powerful illumination (typical installation 30 to 100 KW). On one edge of each film there is written a precise time annotation (every 0.001 sec) generated by a single master clock and on the other edge the instant is marked when the store has moved the first little distance (0.05 mm). Later on the films are analysed frame by frame on a special projector and the operator measures the c.g.-positions and angles of the store in constant time-steps.

Fig. 10 illustrates different store positions which are copied from the high speed motion film seen by the lateral camera. The influence of the aircraft angles of attack on the motion characteristics of a rocket launcher is to be seen: nose down tendency for $\alpha = 0^0$, but nose up tendency for $\alpha = 5^0$.

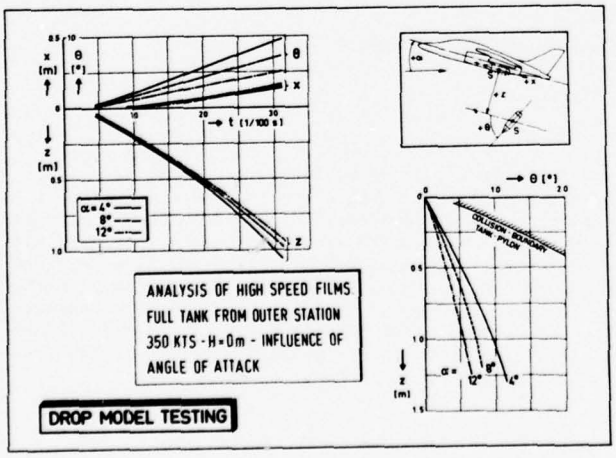

Fig. 11 Analysis of high speed motion films for the example of a full fuel tank released from 1:5 Alpha Jet at the same configuration as in fig. 9.

Fig. 11 shows the complete analysis of a set of 3 high speed motion films giving the separation trajectory of a full fuel tank in terms of the axial (x) and normal (z) c.g.-position and the pitch angle versus the time for 3 angles of attack. The yaw and roll angle is not plotted in this figure. In addition a z-diagram versus Θ illustrates the distance to the collision boundary.

Another more special kind for the FDT is the wind tunnel test of tow targets concerning the release, reeling out and reeling in behaviour. In fig. 12 and fig. 13 two examples of targets which recently have been tested in the DORNIER wind tunnel are given. In this case, besides the dynamic similarity of the target model and also the cable mechanism and the reeling speed must be simulated properly. In the case of the SK 5 towed by a FIAT G 91 aircraft (fig. 12) a flight velocity of 300 KTS at 3000 ft was simulated and in the case of the SK 10 towed by a MC DONNELL DOUGLAS F-4 aircraft (fig. 13) the simulated flight condition was 220 KTS at 10000 ft. In the photo picture of fig. 13 the cable connection between the target and the launcher system mounted on the wing of the aircraft model is to be seen.

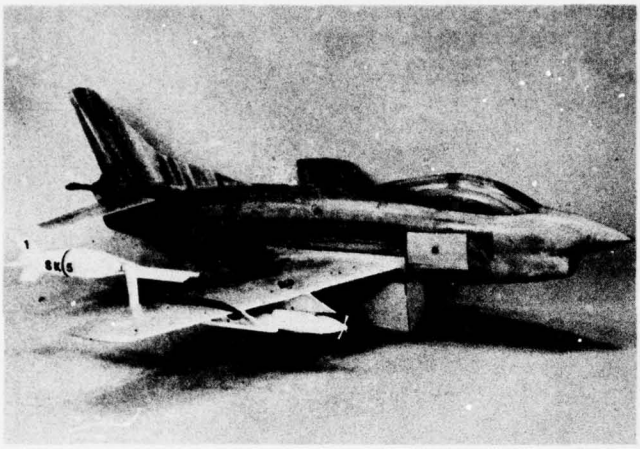

Fig. 12 Tow Target SK 5 with carrier aircraft FIAT G 91 scale 1:10, launcher system DEL MAR

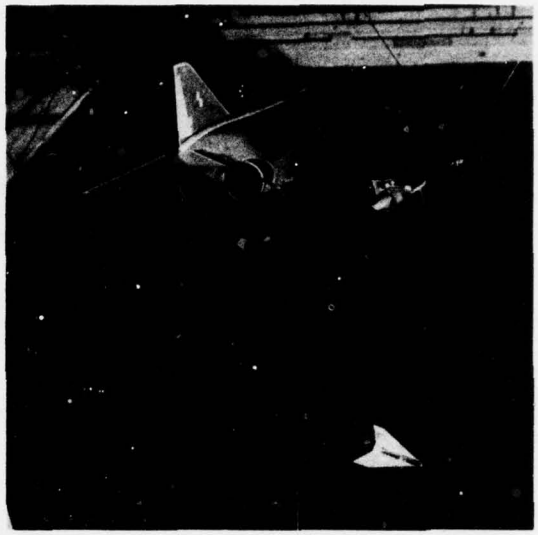

Fig. 13 Tow Target SK 10 with carrier aircraft F-4 scale 1:10, launcher system ANDERSON GREENWOOD, in the DORNIER low speed wind tunnel. Releasing, reeling out and reeling in behaviour is tested.

To summarize, the FDT offers the following advantages and disadvantages respectively.

Advantages of FDT

- Qualitative illustration of release behaviour including the simulation of collisions store-to-aircraft or store-to-store
- Complete quantitative separation trajectory including the distance to collision boundary
- Simulation of pair, multiple or ripple releases are possible
- Simulation of ill-conditioned trajectories due to unstable stores are possible, e.g. empty dispensers (pods, fuel tanks, rocket launchers) and stores without tail.

Disadvantages of FDT

- Complicated model release units due to small scale
- Difficult construction of dynamically similar store models, especially for high speed tests
- Store models are often destroyed after first release
- Risk of damaging wind tunnel equipment
- Considerable effort for analysing the high speed motion films frame by frame
- Off-line data reduction.

3.3 GRID Testing Technique (GTT)

Another method to simulate store separations in the wind tunnel is called grid testing technique. Here the aircraft model is conventionally mounted on an operational rear sting while the store model to be investigated is suspended on a second operational rear sting via its own internal balance. When the required flow conditions have been stabilized in the tunnel the store is moved to various discreet spatial positions and the forces and moments acting on the store are measured. These points are preselected by experience in a 3-dimensional box (GRID) below the aircraft model. GRID-runs are made for each configuration at different M. The interference forces and moments are computed for each GRID-point by subtracting the corresponding theoretical or experimental data in undistrubed flow. By interpolation functions the complete interference flow field in terms of aerodynamic coefficients is calculated. Feeding the proper interference and free-stream data into 6-DOF-equations of motion leads to the separation trajectory.

Advantages of GTT

- Conventional test technique with conventional store models
- With one set of test data the complete interference flow field is known. That means an arbitrary number of different store separation trajectories may be simulated theoretically changing parameters such as initial acceleration due to ejection forces, geometric properties of the store etc.

Disadvantages of GTT

- Separate operational sting rig for the store
- Difficult store manipulation in the wind tunnel
- No trajectory simulation in the wind tunnel
- No on-line results
- Considerable effort for data reduction.

3.4 Captive Trajectory Technique (CTT)

The CTT is based on the same wind tunnel equipment as GTT, but uses a much more advanced technique. It is an on-line simulation of the store separation trajectory in synchronous time steps in a pre-programmed computer running parallel to the experimental simulation in the wind tunnel and automatically activating the control system for the captive trajectory rig of the store model. In the simpliest form, a corrector/ predictor algorithm, based only on the measured store forces and moments, is used to predict theoretically step by step the separation trajectory by solving the 6-DOF-equations of motion with real time as independent variable and deminishing the choosen time increment if bad agreement occurs for the ckeck back. This means a kind of hybrid simulation where the windtunnel plays the role of the analog computer. However, it has proven to be more efficient to compute the separation trajectory completely in the digital computer using the windtunnel only to check the predicted store positions and loads and to adjust the theoretical assumptions if bad agreement occurs between the theoretical predicted and the measured loads in the new position. This last methods allow also to take account for secondary effects due to store thrust, dynamic derivatives of the store and aircraft manoeuver conditions.

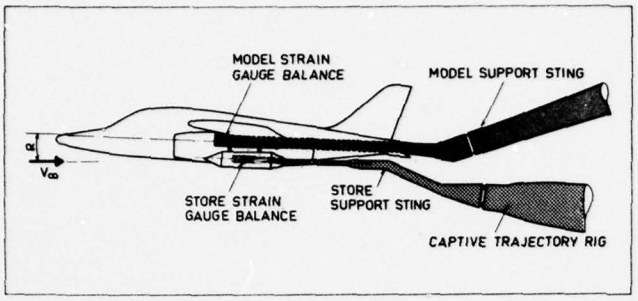

Fig. 14 Schematic arrangement of the captive trajectory technique

Advantages of CCT

- on-line graphs of the separation trajectory data
- simple store models (geometric similarity only)
- simulation of secondary effects
- fast simulation technique

Disadvantages of CCT

- big effort for captive support rig and control system
- mechanical limitations for store sting support
- it is not possible to simulate ill conditioned trajectories of unstable stores.

3.5 Flow Field Angularity Technique (FAT)

The experimental methods described above are based either on the measurement of the forces and moments acting on the store in the interference flow field or by actually releasing store models. The FAT is a direct approach to measure the interference flow field itself and has been worked out in the US AIR FORCE ARMAMENT LABORATORY [5]. In the FAT the aircraft model is conventionally mounted in the wind tunnel with the stores of interest loaded in the captive carrying position. The aircraft flow field below and beside the store is measured in a pre-selected GRID by means of a 3-dimensional pressure probe capable of determining velocity vectors. The result is a set of data giving the changes in angle of attack and angle of sideslip of the interference flow field. From this, the interference flow field in terms of isoclines, i.e. lines of constant change with respect to angle of attack or sideslip, may be plotted. The store interference aerodynamic coefficients are then calculated by using the store free-stream coefficients and the measured flow angularity values obtained from the wind tunnel. The interference coefficients are input to a 6-DOF-computer program solving the equations of motion for the store and resulting in the separation trajectory.

The main advantage of the FAT is that once the data set has been aquired large numbers of trajectories for arbitrary configurations are computed in short time and in a cheap effective way. Post-flight analysis of unusual occurences can be easyly studied by varying the input parameters for the computer program. The FAT has been sucessfully used in the US to predict store separation from F-4, F-15, A-10 and A-7D aircraft.

4. LITERATURE

[1] W.R. Schmidt, H.W. Stock: "Ein Verfahren zur Berechnung der aerodynamischen Beiwerte von Flugkörpern im Unter-, Trans-, Über- und Hyperschall"; Dornier Report 75/10 B (1975)

[2] F.D. Fernandes: "Theoretical Prediction of Interference Loading on Aircraft Stores"; NASA Rep. CR 112065-1 to 3 (June 1972)

[3] M.F.E. Dillenius, F.K. Goodwin, J.N. Nielsen: "Extensions to the Method for Predicting 6-DOF Store Separation Trajectories up to the Critical Speed to a Fuselage with Noncircular Cross Section"; Air Force Flight Dynamics Lab. Rep. AFFDL-TR-74-130 Vol. I and II (March 1974)

[4] L. H. Schindel: "Store Separation", AGARDograph No. 202 (June 1975)

[5] C.S. Epstein: "Aircraft/Stores Compatibility Analysis and Flight Testing", Unpublished Review. US Air Force Armament Laboratory, Eglin Air Force Base-Florida (1975)

EXPERIMENTS PLANNED SPECIFICALLY FOR DEVELOPING TURBULENCE MODELS IN COMPUTATIONS OF FLOW FIELDS AROUND AERODYNAMIC SHAPES

by
Joseph G. Marvin*
Ames Research Center, NASA, Moffett Field, Calif. 94035, USA

SUMMARY

Building-block experiments and companion numerical simulations intended to verify and guide turbulence modeling are described. Emphasis is given to a series of experiments and computations being used to enhance modeling development for the shock-wave turbulent-boundary-layer interaction problem. Experiments and computations for the exact experimental geometry are presented for Mach and Reynolds number ranges encompassing those associated with full-scale vehicles in transonic, supersonic, and hypersonic flight. Results are given for transonic flow over a circular-arc airfoil undergoing shock-wave-induced, boundary-layer separation, for supersonic flow along a tube wall undergoing a normal-shock-wave-induced, boundary-layer separation, and for supersonic and hypersonic flows undergoing oblique-shock-wave-induced, boundary-layer separation. The detailed experimental data and computations, which use the complete Navier-Stokes equations, are discussed with emphasis on their role in establishing the concept of turbulence modeling. The main conclusion established is that turbulence modeling progress can be achieved by combining numerical simulations with carefully controlled building-block experiments. Extending this concept to complete aircraft is the step to be achieved in the next decade.

NOTATIONS

A	Van Driest damping parameter, Eq. (5)
C_F	skin-friction coefficient
C_H	Stanton Number
C_p	pressure coefficient
c	chord length
d_k	distance from location of initial pressure rise to location of the knee in the pressure distribution curve
d_s	distance from location of initial pressure rise to location of separation point
e	internal energy
h	distance from wing centerline to upper or lower tunnel wall
L	relaxation length
ℓ_s	distance from initial pressure rise to location of reattachment point
M	Mach number
p	pressure
q	kinetic energy of turbulence
R	reattachment location
$\bar{R}$	radius of test section
Re	Reynolds number
S	separation location
T	temperature
t	wing maximum thickness
u	mass-averaged velocity parallel to wall in axial direction
v	mass-averaged velocity normal to wall
w	mass-averaged velocity parallel to wall normal to axial direction
x	axial distance
Δx	distance between mesh points
y	distance normal to surface
Z_s	distance of shock extent relative to wing centerline
γ	Klebenoff intermittency factor
δ	boundary-layer thickness
δ_o	boundary-layer thickness at first measuring station ahead of interaction
δ_u	boundary-layer thickness upstream of interaction ($x = 0$)
δ_i^*	kinematic displacement thickness
ε	eddy viscosity
ε_u	eddy viscosity immediately upstream of interaction
μ	molecular viscosity
ρ	density
$\rho\overline{v'u'}$	turbulent shear stress
τ, τ_{xr}	total shear stress
$<( )>$	root mean square

Subscripts

c	based on chord length
i,j	indices in tensor notation
k	value at the knee in the pressure curve
o	location of incident shock impingement on surface in absence of a boundary layer

* Chief, Experimental Fluid Dynamics Branch

s value at shock wave; also value of separation point

t total

u value upstream of interaction

w wall value

∞ free-stream value

Superscripts

$\bar{(\ )}$ time averaged

$(\ )'$ fluctuating value

1. INTRODUCTION

The rapid development of faster, larger computers has been paralleled by an equally rapid development of computational aerodynamics. Table 1 is a simplified summary of the status of computational aerodynamics that illustrates its rapid development, particularly since the start of this decade. The stage of approximation of the governing equations has been divided into four progressively more complex categories, culminating with the viscous time-dependent Navier-Stokes equations. Beginning in the 1930's and progressing through the 1960's, inviscid linearized theory in various refined stages has been used to design many of the current aircraft. Many limitations in this theory required that much of the configuration design be accomplished experimentally, however. In the 1970's, development of inviscid nonlinear theory advanced more rapidly and is nearing completion. Computations for transonic and hypersonic flight have been made for realistic aerospace vehicle geometries (notable examples are refs. 1-3). The major limitation of these computations is that they cannot handle separated flows. To provide that capability, the next stage of equation approximation requires utilization of the time-averaged Navier-Stokes equations or their approximation. Such computations for turbulent flows, which are ubiquitous and very important in most aerospace vehicle applications, are in the early stages of development. The limitation of these computations is the accuracy of the turbulence model used to complete the system of governing equations; this item now paces the development. Once this stage of approximation reaches the point of practical utility, it is expected that computations using the complete Navier-Stokes equations in time-dependent form will begin their development, but an advanced computer is essential before practical computations become available because the resolution scale for the smaller turbulent eddies precludes the use of any current computers. Thus, within the next decade, it could be possible to numerically simulate the flow about complete aircraft shapes including important viscous effects. Then, performing complimentary roles, the computer and the large wind tunnel can significantly reduce the time and cost required to develop new aerospace vehicles (ref. 4).

The Navier-Stokes equations are the basic governing equations used to describe most fluid mechanics phenomena. They apply to problems involving turbulent flow, but to avoid the difficulty of describing every discrete turbulent motion possible, they are usually time averaged. Time averaging eliminates some of the information contained in the equations and, moreover, results in more unknowns than governing equations through the introduction of apparent Reynolds stresses for the actual transfer of momentum by velocity fluctuations. Therefore, the extra unknowns must be represented by physically plausible combinations of quantities for which transport equations are expressed in terms of constants or empirical functions considered as known or expressible in terms of the mean variables. The problem of reducing the unknowns to equal the number of equations is referred to as the "closure problem"; the process of expressing the unknowns as transport equations in terms of empirical functions or constants is referred to as "turbulence modeling."

Historically, progress in turbulence modeling has been slow and deliberate, and has relied substantially on a few carefully controlled experiments performed over a range of test conditions. Such experiments could be called "building-block experiments" because they provided the gage for establishing the credibility of computational techniques, but, more importantly, because they provided physically meaningful concepts that were used to enhance heuristic modeling ideas. The conference on the computation of turbulent flows held at Stanford University in 1968 (ref. 5) used many of the classic experiments to assess progress in predicting incompressible, attached, turbulent flows. Later that same year, the conference on compressible turbulent flows held at Langley Research Center (ref. 6) concluded that very few, if any, compressible flow experiments in the building-block category were being performed.

Relying on historical perspective, if progress in modeling is to be made, it will come through combining a broad experimental effort with computational techniques and modeling ideas (ref. 5). However, for compressible flow, the problems are more complex because Mach number must be included in the list of variables. Figure 1 shows the Mach-Reynolds number domain for aerospace vehicles and it gives an indication of the range of conditions over which adequate turbulence modeling must be provided. The upper limit on Reynolds number based on vehicle length (ref. 7) is shown as well as the upper limit based on wing chord. Mach number varies between subsonic and hypersonic, encompassing the range encountered by commercial passenger vehicles and NASA's Space Shuttle Vehicle. Figure 2 compares the domain of available experiments that can be used to test turbulence modeling concepts with that for the vehicles. The shaded area represents partially documented experiments where zero- or mild-pressure gradients were impressed on the flow. Reference 8 summarizes available experiments and their measurements. Most of these earlier experiments were performed at lower Reynolds numbers, which made it difficult for the analysts to confidently predict Reynolds number trends for actual flight conditions and, in most cases, not enough meaningful data were available in any single experiment to assess modeling concepts confidently. Thus, the situation remains somewhat the same as for the development of linearized theory, where designers rely mainly on experiment for their vehicle development. The unshaded area in Fig. 2 represents the domain of more recent experiments where shock-induced separation was studied and where specific attempts to document the complete flow-field features have been made or are under way. These latter experiments and companion computations, which together are being used to establish adequate turbulence models for designers, are discussed subsequently. Another disturbing consideration is the lack of large-scale facilities that can operate at Reynolds numbers high enough to verify complete vehicle designs at the proper Reynolds number (ref. 7).

If the concept of numerical simulation of flow fields over complete aircraft is to become a reality, the ability to predict flow-field behaviors at flight Reynolds numbers and Mach numbers must be developed. This paper illustrates how the computer and the wind tunnel are being used to develop turbulence models for a complex class of fluid-dynamics problems, i.e., turbulent boundary-layer separation caused by the interaction of a shock wave with a boundary layer. Such a study can be viewed as an early predecessor of the larger problem of using the computer and the wind tunnel to develop real aircraft shapes at reduced cost and time. The first portion of this paper reviews the essential elements of turbulence modeling. Since experiments are an essential part of the concepts established, some recent developments in instrumentation are reviewed to establish confidence in our ability to measure quantities that can guide the modeling processes. Thereafter, the modeling concepts and experimental results are compared and conclusions drawn.

2. ELEMENTS OF TURBULENCE MODELING

Turbulence is a random, dissipative, three-dimensional phenomenon that involves many characteristic scales. While the Navier-Stokes equations contain all the necessary elements of the physics involved in the processes, practical solutions are possible only if approximate forms of the equations are used. Of the myriad of possible approximations, the Reynolds-averaged form (ref. 9) of these equations has proven the most fruitful and probably will continue to be so for some time. However, averaging introduces unknowns and, in order to close the equations, it is essential that certain terms be modeled.

The objective of turbulence modeling is to provide the designer with useful tools for confidently predicting the behavior of turbulent flows. The basic three elements leading to this objective — are experiments, intuitive modeling concepts, and the computer code — shown in Fig. 3. Each element is essential, and they are not easily separated. The process could start with the modeling concept or with the experiments. Historically, the process began with experimental observations that later led to modeling concepts. This trend is beginning to change in that model development and experiment are being performed in parallel and coordinated efforts. Once the modeling concepts are established, the computer code can be assembled. This particular sequence is essential for complicated equation systems because the modeling concepts can often alter the order of the equation system or method of solution. Once the code has been established, it can be compared with and verified by the experiments. If the experiments provide enough detail, they can guide changes in the modeling concepts and the process is continued until the predictive capability of the code can be established and provided to the designer. An important aspect of the computation code development is that it be directed specifically to the geometry of the experiment and that it use exact experimental initial conditions so that no doubt can be cast on the comparative results.

Experiments that support the modeling process can be classified according to the type of closure proposed. Bradshaw (ref. 10) broadly classified these closures as first and higher order, corresponding, respectively, to closures either where second-order correlations like the Reynolds stresses are expressed in terms of first-order correlations like the mean velocity, viz., algebraic mixing length or eddy viscosity formulations, or where third- and higher-order correlations are expressed in terms of second- and higher-order correlations by introducing additional appropriate transport equations. Table 2 gives the elements of the experiments required, depending on the type of equation closure. Verification experiments by their nature require documentation of mean and surface quantities over the practical ranges of flight Mach and Reynolds numbers. These experiments are useful for any closure technique used. First-order modeling experiments are those that require measurements of the shear stress and heat fluxes across the flow field because these quantities provide insight into concepts used to model these terms and provide closure. Such experiments can, but need not be, attempted over the complete Mach and Reynolds number ranges because the verification experiments can test the ability of the model to perform outside the domain where, e.g., the shear stresses have been measured. They must be performed at Reynolds numbers sufficiently high to establish fully developed turbulence. Higher-order modeling experiments require that fluctuating measurements be made across the flow field. Depending on the order of the closure, more and more information on the fluctuating field must be ascertained. As for any modeling experiment, data need not be acquired over the complete Mach and Reynolds number domain provided verification experiments are available. Ideally, one well-conceived experiment could suffice for all three types listed in Table 1. Moreover, the same experimental apparatus and instrumentation can be used to eliminate experimental uncertainties. Coles (ref. 11) emphasized this latter aspect when commenting on the flows used as the basis for the Stanford Conference. He also emphasized the need for redundancy of measurement, complete documentation for future reference, and the elimination of three-dimensional uncertainties by, for example, testing axisymmetric configurations.

3. INSTRUMENTATION DEVELOPMENTS

Verification and modeling experiments for incompressible flows have been available for some time. Compressibility introduces complexities into the modeling concepts as well as the experiments. The complexity in the experiments results from the hostile test environment of high Reynolds numbers and high Mach numbers as well as in the use and interpretation of fluctuating measurement devices. Recent instrumentation developments and techniques have made it possible to perform modeling experiments at high Reynolds numbers and Mach numbers. Results from two such experiments are given in Figs. 4 and 5.

Figure 4 shows the results from several experiments where shear stress measurements were made across turbulent boundary layers without pressure gradients. The boundary-layer-edge Mach number in these experiments ranged from subsonic through hypersonic. The solid line indicates the expected variation of the normalized total shear stress shown in ref. 12 to be independent of edge Mach number. The measurements, obtained with hot-wire and hot-film anemometers and a laser velocimeter, show the variation of the turbulent component of shear stress. Except for the decreases near the wall ($y/\delta < 0.3$) due mainly to the relatively large probe size and not the difference between the total and turbulent magnitudes of shear, the data agree reasonably well with the expected trends in shear distribution. Work is in progress to resolve the

differences near the wall and some success has been achieved (ref. 13, e.g., use of a split-film anemometer minimizes the probe scale effects and suppresses the decrease to a location much nearer the wall). From such data, mixing lengths or eddy viscosities in the outer regions of a turbulent boundary layer can be determined for use in first-order modeling concepts.

Figure 5 shows the results of measurements of the fluctuating velocities and densities across a high-speed subsonic turbulent boundary layer (ref. 14). These data were obtained with hot-wire and hot-film anemometers operating at high overheats so that the sensitivities to various fluctuations can be separated (ref. 14). The solid lines are the usual ratios 4:3:2 for $(\langle u' \rangle)^2 : (\langle w' \rangle)^2 : (\langle v' \rangle)^2$ in incompressible flows. The compressible measurements agree reasonably well with the ratios obtained for incompressible flow. Reasonably accurate measurements for the fluctuating components of the velocity field in compressible flows can be expected. Also, for modeling purposes, it might only be necessary to obtain trends in these quantities with parameter changes such as pressure gradient, Reynolds number, and Mach number rather rather than absolute magnitudes.

Recent advances in wall skin-friction measurements techniques have also been reported (ref. 15). Results obtained using these surface-mounted hot-wire gages of the Ludwig type are presented later. The advantage of these gages is that they can be used in either laminar or turbulent flows and they are insensitive to pressure-gradient effects.

4. EXPERIMENTS

Some of the building-block experiments now being used to predict the behavior of turbulent boundary layers undergoing separation after their interaction with an incident shock wave are described. Each experiment, in which there is a significant coupling of the viscous and inviscid flow fields, has a companion computer simulation that uses the complete time-averaged, Navier-Stokes equations and requires a large fast computer for their solution. The experiments, in various degrees of completeness at this time, cover a wide range of Mach number and Reynolds number.

4.1 Transonic Regime

The first two experiments involve transonic flows with particular interest directed toward shock-boundary-layer interactions on wings. Figure 6(a) shows the experimental arrangement for a verification experiment (ref. 16) being performed on a wing that spans the test section of a high Reynolds number channel recently built at Ames Research Center. The facility operates in a blow-down mode, and the free-stream Mach number can be adjusted before or during tests by a translating wedge that acts as a downstream choke. The upper and lower walls are contoured so that strong shocks would not extend to the walls and choke the flow. A thick circular-arc wing (Fig. 6(b)) was chosen to allow local airfoil Mach numbers to achieve values where shock-induced separation would occur, but without having the shock extend more than about 2/3 of the distance between the wing and the outer wall. Surface pressures for various Mach numbers and Reynolds numbers have been obtained (ref. 16) as well as surface skin friction at specific Reynolds numbers. Still to be obtained are mean velocity data and more skin-friction data.

The wing experiment resulted in both shock-induced and trailing-edge-induced separation, depending on the free-stream Mach number. Data were obtained to Reynolds numbers, based on chord length, of 17×10^6. At intermediate Mach numbers, some unsteadiness in the flow field occurred. The results are discussed in detail in ref. 16. Reynolds-number effects for both the trailing edge and shock-induced separation were not significant beyond Reynolds numbers of 10×10^6 based on wing chord. Some results obtained when shock-induced separation occurred are given in Fig. 7. Oil-flow patterns (lower portion of the figure) illustrate the two-dimensionality of the flow and the detail in the region downstream of separation. The shadowgraph view near the interaction clearly illustrates shock-induced separation. The pressure ratios downstream of the shock are below C_p^*, indicating that the flow is slightly supersonic and suggesting the presence of an oblique shock (also apparent in the shadowgraph). Figure 8 presents the airfoil pressures at several Reynolds numbers and the skin-friction measurements at a single Reynolds number. The skin-friction measurements were obtained recently by Rubesin and Okuno using surface-mounted wire gages specifically developed for this experiment (ref. 15). The location of separation, determined from the oil-flow photograph, is shown on the abscissa of the skin-friction plot. This location also corresponds to the location of the knee in the pressure curve downstream of the shock. The comparison with the computations is discussed subsequently.

Figure 9 shows the physical arrangement of another transonic flow experiment (ref. 17) being used for code verification and model concept development. These tests are also being conducted in the Ames high Reynolds number channel. Supersonic flow was developed at the entrance of an axisymmetric test section and a normal shock wave was positioned at a fixed location by adjusting the location of a downstream shock generator. The relative distance between the shock wave and the downstream shock generator was always about 1 m. Experimental verification data were obtained for Reynolds numbers, based on distance along the wall to the location of the shock wave, between 9×10^6 and 290×10^6. Over this range of Reynolds number, Mach number varied between 1.35 and 1.45 because of the differences in wall boundary-layer growth. With this arrangement, data are also being obtained at constant shock Mach number by allowing the shock position to vary along the tube surface when the Reynolds number is varied. A complete flow documentation, including turbulence measurements, has been performed at a Reynolds number of 37×10^6 where the corresponding Mach number ahead of the shock wave was 1.44.

Examples of the data are presented in Figs. 10 and 11. Additional results, including velocity profiles and velocity fluctuation data, are given in ref. 17. The shock position is located at $x/\delta_u = 0$. The pressure rises rapidly downstream of the shock wave and causes separation, after which it increases gradually. The corresponding skin friction is reduced ahead, reverses sign in the separated region, and then increases thereafter. The shear stress data (Fig. 11) were obtained with a supported cross-wire anemometer specially designed to withstand the high dynamic pressures encountered in this experiment (ref. 17). The maximum shear stress in the boundary layer shows a significant increase after the shock wave and then decreases

downstream toward the value expected for a mild adverse pressure gradient. Downstream of the shock wave beyond the effective boundary layer, some measurable shear was evident. It reverses sign because the mean velocity profiles are retarded, probably resulting from a coalescence of compression waves ahead of the shock wave (ref. 17). In this flow, the height of the separated zone was very small and no details were measured in the reversed-flow region.

Documentation of the mean flow over a wide range of Reynolds numbers is now under way. These data will be used to assess the ability of the turbulence model to predict Reynolds-number effects on quantities such as interaction lengths, pressure rise to separation, and the effects of Mach number on incipient separation. An example of this is shown in Fig. 12 wherein the pressure rise to separation, as determined from the location of the knee in the pressure curve (ref. 18), and the normalized interaction lengths, as determined by measuring the distances from the beginning of the pressure rise to the location of the knee in the pressure curve and to the point of reattachment, are plotted as a function of Reynolds number. For these data, the test Mach number varied somewhat because the shock was always at the same axial location in the test section. The normalized data indicate that the pressure rise to separation is unaffected by Reynolds number and that the length of the interaction scales with the initial boundary-layer thickness. Additional data of this type are being obtained for a constant shock Mach number by allowing the shock position to change along the tube surface when the Reynolds number is changed.

4.2 Supersonic Regime

One experiment being used to verify the computations in the supersonic regime is the adiabatic shock-impinging flow originally reported by Reda and Murphy (ref. 19). Figure 13 is a schematic of the test arrangement. Shock waves of varying strength were impinged on a M = 3 boundary layer developed along a tunnel wall. For some tests, the shocks were strong enough to separate the flow on the tunnel wall. Mean-flow profiles and surface-pressure data were reported originally. Since the original work was completed, skin-friction data have been inferred from the profile data (ref. 20) and shear distribution upstream and downstream of an interaction without separation were measured (ref. 21). Currently, measurements throughout a separated region, such as velocity fluctuations, shear distributions, and surface skin friction, are being documented.

The surface pressure, normalized by the upstream total pressure, and indirectly inferred wall shear stress for a separated flow case are shown in Fig. 14. Separation and reattachment points from oil-flow photographs are indicated. The pressure data have a plateau near the separation. Data for various shock strengths (ref. 19) will be used to assess the ability of the Navier-Stokes codes to predict the onset of separation.

4.3 Hypersonic Regime

At hypersonic speeds, the axisymmetric shock expansion boundary-layer interaction flow described in Ref. 22 is being used to guide turbulence modeling concepts. The experiment is sketched in Fig. 15. The leading edge of the shock generator was varied between 5° and 20°. Measurements in the axial direction were made in finely spaced steps by traversing the shock generator in the axial direction during the tests. Complete flow documentation, including turbulence measurements across the flow field, is available for shock generator angles of 7° and 15° where unseparated and fully separated interactions occurred, respectively. Surface pressure, skin friction, and heat transfer are available for other generator angles and will be used to verify the ability of the turbulence model to predict the effects of shock strength on separation at hypersonic speeds.

The surface pressure, skin friction, and heat transfer for separated flow are shown in Fig. 16. Separation and reattachment points obtained from pitot-pressure measurements on probes near the surface facing both upstream and downstream (ref. 22) are shown. The pressure increases through the interaction region to a plateau near separation and then rises farther after reattachment. The skin friction decreases, then rises downstream of reattachment. The heat transfer rises continually. The decay in pressure, skin friction, and heat transfer downstream of the interaction results from the expansion fan emanating from the corner of the generator.

Fluctuating turbulence properties to be used to guide modeling changes were measured across the boundary layer at four locations through the interaction (ref. 23). An example of the measurements is shown in Fig. 17, where the shear stresses at the four measurement locations are plotted. It was not possible to obtain shear measurements in the reversed-flow region of the separation bubble at the second measurement station so the expected trend has been sketched. The measurements show many of the same features as for the transonic test shown previously in Fig. 11. Through the interaction, the maximum level of shear stress near the separated region increases significantly. Downstream of reattachment, $(x - x_0)/\delta_0 > -1$, the shear profiles do not differ in shape from those usually found in zero or slightly favorable pressure gradients. Turbulence memory apparently persists only for about five boundary-layer thicknesses beyond the initial rise in pressure (ref. 23).

5. FLOW-FIELD SIMULATIONS

The flow fields experimentally investigated have each been programmed for numerical simulation on a CDC-7600 computer. Each program uses the mass-averaged form of the time-dependent Navier-Stokes equations (ref. 24) and solves them with the MacCormack time-marching explicit scheme with splitting (ref. 25). The complete Navier-Stokes equations were used because the viscous and inviscid flows interact significantly; use of approximate solution techniques would only introduce uncertainty when evaluating the ability of the turbulence models to predict measured trends with Mach number and Reynolds-number variations.

Each of the programs and solution techniques have been reported on separately and their details are not addressed here. Only the general form of the equations is presented and some of the terms in the equations affected by the turbulence assumptions are discussed briefly. Then the results are compared with experimental data.

Written in divergence form for the axisymmetric geometry shown in Fig. 9, the governing equations are (ref. 17):

$$\frac{\partial U}{\partial t} + \frac{\partial F}{\partial x} + \frac{1}{R - y}\frac{\partial G}{\partial y} = \frac{H}{R - y} \tag{1}$$

$$\left.\begin{aligned} U &= \begin{pmatrix} \rho \\ \rho u \\ \rho v \\ e \end{pmatrix} \quad ; \quad F = \begin{pmatrix} \rho u \\ \rho u^2 + \sigma_{xx} \\ \rho uv + \tau_{xr} \\ u(e + \sigma_{xx}) + v\tau_{xr} + q_x \end{pmatrix} \\ G &= (\bar{R} - y)\begin{pmatrix} \rho v \\ \rho uv + \tau_{xr} \\ \rho v^2 + \sigma_{rr} \\ r(e + \sigma_{rr}) + u\tau_{xr} + q_y \end{pmatrix} \quad ; \quad h = \begin{pmatrix} 0 \\ 0 \\ \sigma_{\theta\theta} \\ 0 \end{pmatrix} \end{aligned}\right\} \tag{2}$$

Solutions to the above equations are advanced in time until steady-state solutions are achieved. The turbulence terms to be modeled appear in the axial, radial, and azimuthal stress terms, σ_{xx}, σ_{rr}, and $\sigma_{\theta\theta}$, respectively, and in the heat-flux and shear-stress terms, q_x, q_y and τ_{xr}, respectively (ref. 17), e.g.,

$$-\tau_{xr} = \mu_T\left(\frac{\partial u}{\partial y} + \frac{\partial v}{\partial x}\right) \tag{3}$$

Turbulence effects are then introduced by using a scalar eddy viscosity coefficient,

$$\mu_T = \mu + \varepsilon \tag{4}$$

The turbulent thermal conductivity is related to the eddy viscosity by introducing a turbulent Prandtl number that is held constant for each computation. The choice of introducing an eddy viscosity description was dictated by two considerations. First, the initial objective of the computations was to simply assess the ability of the codes to compute a strong viscid-inviscid interaction such as that imposed when a shock wave separates a turbulent boundary layer and, to accomplish this within the numerical framework already established for laminar flows (ref. 26), the implementation of a Boussinesq effective viscosity (ref. 27) formulation was straightforward. Second, the economies of computation using a Navier-Stokes code required that the simplest turbulence model available be used, otherwise excessive computation times would make the assessment of even the first objective difficult. While the purpose of this paper is not to discuss recent advances in computation techniques, it can be reported that the basic MacCormack code has been speeded up by one order of magnitude (ref. 28) or more, depending on the problem under consideration. This was made possible by rearranging equation terms into inviscid and viscid combinations that allow further splitting into inviscid and viscid operators. The inviscid operators can be advanced in time steps larger than those dictated by CFL stability condition by introducing certain characteristics terms; the viscous terms are advanced implicitly. While the solutions may not be rigorously accurate in time, their steady-state solutions are. This major computational advance now makes it economically feasible to include higher-order modeling concepts into the codes for testing against the experimental data and this is now under way.

A baseline turbulence model has been used to determine whether the codes can predict the qualitative features of the flow fields. Essentially, the baseline model is a two-layer, eddy viscosity model that uses mixing length with Van Driest damping in the inner region and an eddy viscosity that scales on the incompressible displacement thickness in the outer region (ref. 22). In equation form, in the inner region:

$$\varepsilon_i = \rho(0.4y)^2\left[1 - \exp\frac{-y}{A}\right]^2\left|\frac{\partial u}{\partial y} + \frac{\partial v}{\partial x}\right| \tag{5}$$

where

$$\frac{1}{A} = \frac{[\rho_w\mu_w|\ (\partial u/\partial y)_w|\ ]^{1/2}}{26\mu_w}$$

and, in the outer region,

$$\varepsilon_o = 0.0168\ \rho u_e \delta_i^*/\gamma \tag{6}$$

In Eq. (6), δ_i^* and γ are the kinematic displacement thickness and the Klebenoff intermittency, respectively (ref. 22). As will be shown, solutions using the baseline model indicate that the computations can indeed predict all the qualitative features of the flow field, but improvements in the baseline model are required before quantitative features can be predicted.

Modifications to improve the predictions using the Boussinesq formulation have been guided by experiments in two separate approaches, both resulting in essentially the same findings. The first used experimental data to introduce an axial dependence on the baseline model constants throughout the interaction zone (ref. 22). Results with this technique showed improvement but the generalization to other

flows was limited. Essentially, the experimental results of ref. 22 showed that, in the separation zone, the effective mixing lengths in the wall region were smaller than those predicted by the baseline model and downstream they were higher. Both results seem to indicate that the corresponding effective eddy viscosities were lower and higher than the baseline values within and downstream of the interaction, respectively. The second approach introduced the concept of relaxation into the model (refs. 21 and 29). This relaxation concept was postulated on the basis of comparisons with experimental pressure data (as in ref. 29) or on the basis of interpretation of turbulence measurements (as in refs. 21 and 23). The latter measurements showed that the turbulence took a finite distance to equilibrate with the changes in mean flow through the interaction. This finite distance is somewhat different for each flow, and apparently depends on Mach and Reynolds numbers. In equation form, relaxation can be described either on a global or a point-by-point departure from the baseline model as follows:

$$\varepsilon = \varepsilon_u + (\varepsilon_{eq} - \varepsilon_u)\left[1 - \exp \frac{-x}{L}\right] \tag{7}$$

or

$$\varepsilon(x) = \varepsilon(x - \Delta x) + [\varepsilon_{eq}(x) - \varepsilon(x - \Delta x)]\left[1 - \exp\left(-\frac{\Delta x}{L}\right)\right] \tag{8}$$

where ε_{eq} is evaluated using the baseline formulation with locally determined mean flow properties and L is an arbitrary relaxation length.

Each of the experimentally determined flow fields has been computed using the baseline and relaxation models, then they are compared with the data in each of the figures introduced previously. In each application, the investigator introduced some differences in the details of applying the baseline and relaxation models described above. These details are discussed in the references cited. The observed trends of interest here are not thought to be affected by these differences, however.

5.1 Transonic Regime

The data from the transonic-wing experiment are compared with the computations in Fig. 8. With the baseline model, the overall features of the flow field are predicted reasonably well. For example, the trend of increasing airfoil peak Mach number with Reynolds number is predicted, as is separation due to shock interaction. Downstream of the shock, where the flow separates, the pressure recovery is overpredicted because the predicted shock wave is normal, whereas the experimental shock wave is oblique. A comparison of the predicted and measured skin friction at $Re = 10^7$ further illustrates the differences in that region as the location of predicted separation is downstream of that location determined from the oil-flow photographs. Use of the relaxation concept (ref. 30) with one boundary-layer thickness for L (relaxation length) tends to shift the location of the shock wave closer to the leading edge, reduces the peak Mach number and resulting shock strength, but the pressure recovery is still overpredicted. (Solutions using other choices for L did not improve the results (ref. 30).) Relaxation model solutions were not computed at the higher Reynolds number, but closer agreement with the separation location would be expected. For lower Mach numbers, where the flow is not separated but where viscous effects are still important, the computations using the baseline model compare vary favorably with the data, except at the trailing edge where extensive separation occurred (ref. 30).

Comparisons of the computations with the data from the normal shock-wave experiment are presented in Figs. 10 to 12. As mentioned in ref. 17, the height of the separation zone was fairly small, but the length of separation was large, perhaps 6-12 boundary-layer thicknesses, depending on the techniques of measurement. The pressure prediction agrees well with the data. The skin friction is underestimated downstream. Including local relaxation with a relaxation length, L, of 10 boundary-layer thicknesses in the turbulence model (i.e., Eq. (8)) resulted in poorer agreement in the skin friction downstream and no significant changes in the pressure rise. The shear distributions obtained using the global relaxation model are compared with the data in Fig. 11 at three locations downstream of the wave. Similar results were obtained with the baseline and local relaxation models. The computations fail to predict the significant increase in shear at the first station and, evidently, this continues to affect the prediction downstream. The effects of Reynolds number on the interaction are compared in Fig. 12. The predicted separation pressures and length of interaction to the separation point are compared with the experimental pressure and length evaluated at the knee in the pressure curve. The trends with Reynolds number are predicted reasonably well. The separation point from the computations occurs upstream of the knee in the pressure curve. The overall length of the interaction is underpredicted. All calculations shown in this figure were made recently by J. R. Viegas using the new faster version of the MacCormack code (ref. 28). These new calculations took less than 10 min on a CDC-7600, whereas the first computations (ref. 17) took about 5 hr on the same computer.

5.2 Supersonic Regime

Comparisons for the oblique-shock interaction using the baseline and relaxation turbulence models are shown in Fig. 14. For the oblique-shock interaction, the baseline model predicts the overall pressure rise reasonably well and also predicts separation. However, no appreciable upstream influence in the pressure and no plateau are indicated in the calculations because the size of the separation bubble is underpredicted. Introducing the relaxation concept with $L = 5$ boundary-layer thicknesses corrects this deficiency because it lowers the effective eddy viscosity near the separation, thus increasing the size of the separated zone, which in turn introduces a plateau in the pressure rise curve. The location of separation is predicted with the relaxation model, but the reattachment location is too far downstream. The comparison with the wall shear downstream of reattachment where the boundary layer thins may appear better than is the actual case because these computations were made with a relatively coarse grid, and in the downstream locations the first computation point away from the wall was in the logarithmic region of the turbulent boundary layer. Since the method used to obtain derivatives at the wall requires calculated points within the sublayer region, the predicted shear is expected to be lower than the measurements, and the results would be similar to those for the transonic normal-shock comparisons.

5.3 Hypersonic Regime

In Fig. 16, the predicted results and experimental data are compared. As with the supersonic oblique-shock interaction, the baseline model prediction reproduces the overall trends in the data but is deficient in the separated region. Recent calculations by T. J. Coakley using a relaxation model with L = 5 boundary-layer thicknesses (as indicated by the turbulence measurements from ref. 23) improve the situation somewhat. (See, e.g., Fig. 17 and the previous discussion of Fig. 17.) The height of the separation is greater and the resulting upstream influence leads to a plateau in the pressure. The location where skin friction begins to decrease is predicted, but the extent of the separation in the axial direction is overpredicted significantly, much as for the supersonic example. The heat transfer is underpredicted throughout the interaction region with either model.

From an examination of all the comparisons, general observations about the computations can be made. In most cases, the pressure rise can be predicted reasonably well with a simple eddy viscosity description for the turbulence. The exception is for the transonic wing where the shock-induced separation was very large and extended from the foot of the shock beyond the trailing edge. The eddy viscosity concept is deficient in providing the proper details within the separated zone and this, in turn, apparently affects the entire flow field when the separation zones are large, viz., the oblique-shock cases. Introducing relaxation tends to improve the situation somewhat because it decreases the eddy viscosity in the region of separation, resulting in an increase in the height of the separation. However, the net decrease in eddy viscosity persists beyond the separated zone even for short relaxation lengths, and the codes underpredict the skin friction downstream. Interpretation of the modeling experiments indicates the need for an increase in effective eddy viscosity downstream of reattachment. Therefore, improved turbulence models that more closely reflect the experimental findings must be introduced before realistic simulations can be made.

6. CONCLUDING REMARKS

Experiments of two types needed to achieve the objectives of numerically simulating, highly interacting turbulent flows were described. These experiments were classified as verification and modeling experiments: verification experiments that measure mean flow and surface quantities could suffice for checking the code's ability to predict correctly over a range of Mach and Reynolds numbers, whereas turbulence modeling experiments require, in addition to mean-flow measurements, that fluctuating measurements be made to the degree of complexity called for in the order of the modeling closure technique. From the numerical simulation viewpoint, the lowest-order closure technique is more desirable because the complexity of the numerical procedures and the computation times can be reduced.

Progress in modeling turbulence for the computer codes using the Navier-Stokes equations has been limited so far to modifications of the simple eddy viscosity descriptions because the computation times have been excessive. Recent developments in the method for solving the Navier-Stokes equations have altered that situation because the computations have been speeded up by several orders of magnitude. Computer simulations that use higher-order modeling concepts are forthcoming, and it is expected that these will more closely resemble the experimentally observed results.

REFERENCES

1. Bailey, F. R.; and Ballhaus, W. F.: Comparisons of Computed and Experimental Pressures for Transonic Flows About Isolated Wings and Wing-Fuselage Configurations. SP-347, Vol. II, 1975, pp. 1213-1232, NASA.

2. Rakich, J. V.; and Pegot, E. G.: Flow Field and Heating on the Windward Side of the Space Shuttle Orbiter. SP-347, Vol. II, 1975, pp. 1377-1394, NASA.

3. Marconi, F.; Yaeger, L.; and Hamilton, H. H.: Computation of High-Speed Inviscid Flows About Real Configurations. SP-347, Vol. II, 1975, pp. 1411-1456, NASA.

4. Chapman, D. R.; Mark, H.; and Pirtle, M. W.: Computers vs. Wind Tunnels for Aerodynamic Flow Simulation. Astronautics and Aeronautics, Vol. 13, No. 4, April 1975, pp. 22-30.

5. Kline, S. J.; Morkovin, M. V.; Sovran, G.; Cockrell, J. D.; Coles, D. E.; and Hirst, E. A., editors: Proceedings — Computation of Turbulent Boundary Layers — 1968 AFOSR-IFP-Stanford Conference, Vols. I and II. August 1968.

6. Anon: Compressible Turbulent Boundary Layers. SP-216, 1968, NASA.

7. Jones, J. Lloyd, Jr.: Problems of Flow Simulation in Wind Tunnels. AIAA Paper 69-660, 1969.

8. Waltrup, P. J.; and Schetz, J. A.: Supersonic Turbulent Boundary Layer Subjected to Adverse Pressure Gradients. AIAA Journal, Vol. 11, No. 1, Jan. 1973, pp. 50-57.

9. Reynolds, O.: On the Dynamical Theory of Incompressible Viscous Fluids and the Determination of the Criterion, Phil. Trans. A 186, pp. 123-161, or Papers 2, 535.

10. Bradshaw, P.: The Understanding and Prediction of Turbulent Flow. The Aeronautical Journal, Vol. 76, No. 739, July 1972.

11. Coles, D. E.: A Young Person's Guide to the Data, Proceedings — Computation of Turbulent Boundary Layers — 1968. AFOSR-IFP-Stanford Conference, Vol. II, 1968, pp. 1-45.

12. Sandborn, V. A.: A Review of Turbulence Measurements in Compressible Flow. TM X-62,337, March 1974, NASA.

13. Sandborn, V. A.; and Seegmiller, H. L.: Evaluation of Mean and Turbulent Velocity Measurement in Subsonic Accelerated Boundary Layers. TM X-62,488, Sept. 1975, NASA.

14. Horstman, C. C.; and Rose, W. C.: Hot-Wire Anemometry in Transonic Flow. TM X-62,495, Dec. 1975, NASA.

15. Rubesin, Morris, W.; Okuno, Arthur F.; Mateer, George G.; and Brosh, Aviel: A Hot-Wire Surface Gage for Skin Friction and Separation Detection Measurements. TM X-62,465, July 1975, NASA.

16. McDevitt, J. B.; Levy, L. L.; and Deiwert, G. S.: Transonic Flow About a Thick Circular-Arc Airfoil. AIAA Paper 75-878, 1975.

17. Mateer, G. G.; Brosh, A.; and Viegas, J. R.: A Normal Shock-Wave Turbulent Boundary-Layer Interaction at Transonic Speeds. AIAA Paper 76-161, 1976.

18. Seddon, J.: The Flow Produced by Interaction of a Turbulent Boundary Layer With a Normal Shock Wave of Strength Sufficient to Cause Separation. ARC R & M 3502, March 1960.

19. Reda, D. C.; and Murphy, J. D.: Shock-Wave Turbulent Boundary-Layer Interactions in Rectangular Channels, Part II: The Influence of Sidewall Boundary Layers on Incipient Separation and Scale of the Interaction. AIAA Paper 73-234, 1973.

20. Rubesin, M. W.; Murphy, J. D.; and Rose, W. O.: Wall Shear in Strongly Retarded and Separated Compressible Turbulent Boundary Layers. AIAA Journal, Vol. 12, No. 10, Oct. 1975, pp. 1442-1444.

21. Rose, W. C.; and Johnson, D. A.: A Study of Shock-Wave Turbulent Boundary-Layer Interaction Using Laser Velocimenter and Hot-Wire Anemometer Techniques. AIAA Paper 74-95, 1974.

22. Marvin, J. G.; Horstman, C. C.; Rubesin, M. W.; Coakley, T. J.; and Kussoy, M. I.: An Experimental and Numerical Investigation of Shock-Wave Induced Turbulent Boundary-Layer Separation at Hypersonic Speeds. AGARD Conference Proceedings No. 168 on Flow Separation, May 1975.

23. Mikulla, V.; and Horstman, C. C.: Turbulence Measurements in Hypersonic Shock-Wave Boundary-Layer Interaction Flows. AIAA Paper 76-162, Jan. 1976.

24. Rubesin, M. W.; and Rose, W. C.: The Turbulent Mean-Flow Reynolds-Stress, and Heat Flux Equations in Mass-Averaged Dependent Variables. TM X-62,248, March 1973, NASA.

25. MacCormack, R. W.; and Baldwin, B. S.: A Numerical Method for Solving the Navier-Stokes Equations with Application to Shock-Boundary Layer Interactions. AIAA Paper 75-1, 1975.

26. MacCormack, R. W.: Numerical Solution of the Interaction of a Shock Wave with a Laminar Boundary Layer. Lecture Notes in Physics, Vol. 8, Springer-Verlag, New York, 1971, pp. 151-163.

27. Boussinesq, J.: Theoríc de L'écoulement Tourbillant, Memoires Presentés Par Divers Savants Sciences Mathématique et Physiques, Académic Des Sciences, Paris, France, Vol. 23, 1877, p. 46.

28. MacCormack, R. W.: A Rapid Solver for Hyperbolic Systems of Equations. Paper to be presented at the 5th International Conference on Numerical Methods in Fluid Dynamics held at Twente University of Technology, Enschede, The Netherlands, June 28-July 2, 1976.

29. Shang, J. S.; and Hankey, W. L., Jr.: Numerical Solution of the Navier-Stokes Equations for Supersonic Turbulent Flow Over a Compression Corner. AIAA Paper 74-4, 1975.

30. Deiwert, G. S.: Computation of Separated Transonic Turbulent Flows. AIAA Paper 75-829, June 1975.

TABLE 1. STATUS OF COMPUTATIONAL AERODYNAMICS

STAGE OF APPROXIMATION	READINESS TIME PERIOD 2D AIRFOILS	3D WINGS	3D AIRCRAFT	LIMITATIONS	PACING ITEM
INVISCID LINEARIZED	1930's	1950's	1960's USED IN CURRENT AIRCRAFT DESIGN	SLENDER CONFIGURATIONS SMALL ANGLE OF ATTACK PERFECT GAS NO TRANSONIC FLOW NO HYPERSONIC FLOW NO FLOW SEPARATION	
INVISCID NONLINEAR	1971	1973	1976 ? DEVELOPMENT NEARING COMPLETION	NO FLOW SEPARATION	CODE DEVELOPMENT
VISCOUS TIME AVERAGED	1975	1977 ?	1979 ? EARLY STAGE OF DEVELOPMENT	ACCURACY OF TURBULENCE MODEL	TURBULENCE MODELING
VISCOUS TIME DEPENDENT	MID 1980's			ACCURACY OF NAVIER – STOKES EQS.	DEVELOPMENT OF ADVANCED COMPUTER

TABLE 2. ELEMENTS OF WELL-DOCUMENTED BUILDING-BLOCK EXPERIMENTS

TYPE OF EQUATION CLOSURE	TYPE OF EXPERIMENT	DOCUMENTED QUANTITIES	TEST CONDITIONS
FIRST ORDER OR HIGHER ORDER	VERIFICATION	C_F, C_H, p_w, $\bar{T}$, $\bar{u}$, $\bar{v}$, $\bar{w}$, $<q_\infty>$	TO FLIGHT MACH AND REYNOLDS NO.
FIRST ORDER	FIRST ORDER MODELING	C_F, C_H, p_w, $\bar{T}$, $\bar{u}$, $\bar{v}$, $\bar{w}$, $<q_\infty>$ $\rho\,\overline{v'u'}$, $\rho\,\overline{T'v'}$	REPRESENTATIVE FLIGHT MACH AND REYNOLDS NO.
HIGHER ORDER	HIGHER ORDER MODELING	C_F, C_H, p_w, $\bar{T}$, $\bar{u}$, $\bar{v}$, $\bar{w}$, $<q_\infty>$ $\rho\,\overline{v'u'}$, $\rho\,\overline{T'v'}$ u', v', w', q, $\overline{v'q'}$, $\overline{\frac{\partial u_i}{\partial x_j}}$, ...	REPRESENTATIVE FLIGHT MACH AND REYNOLDS NO.

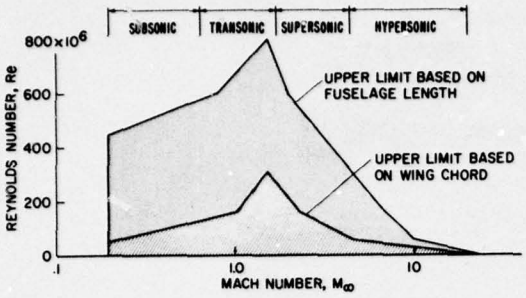

Fig. 1. Mach and Reynolds number domain for aerospace vehicles.

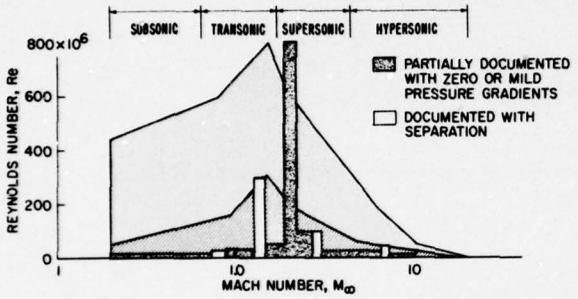

Fig. 2. Mach and Reynolds number domain for experiments compared with that for aerospace vehicles.

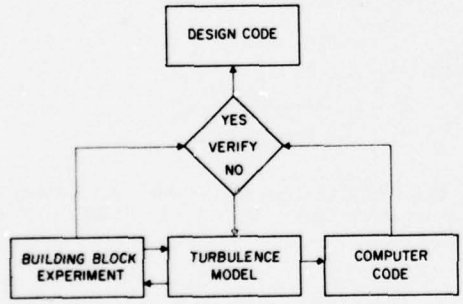

Fig. 3. Process of physical modeling for computer code development.

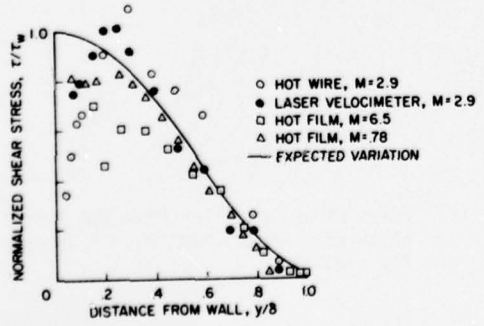

Fig. 4. Shear-stress measurements in compressible flows.

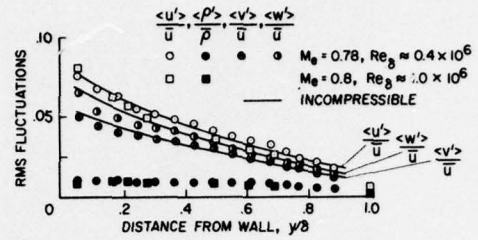

Fig. 5. Normalized rms velocity and density fluctuations across a compressible turbulent boundary layer.

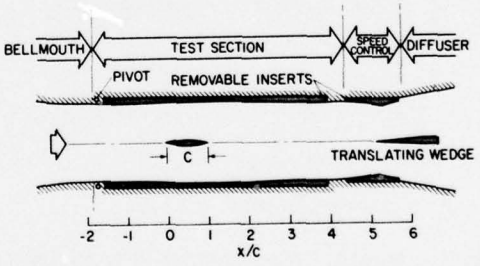

(a) Overall arrangement

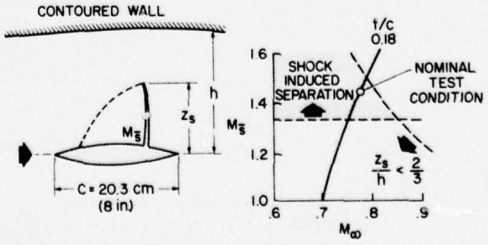

(b) Wing design

Fig. 6. Experimental arrangement for a transonic wing undergoing shock-induced separation.

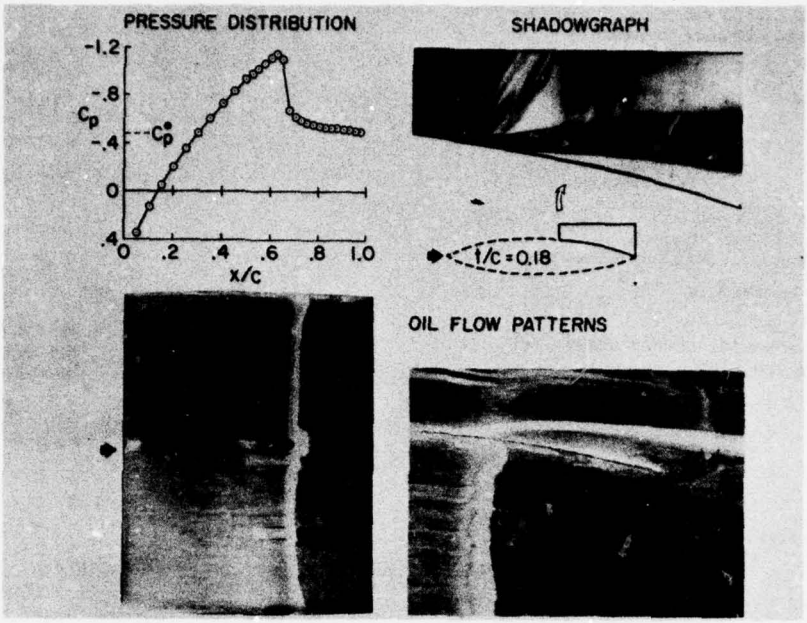

Fig. 7. Shock-induced boundary-layer separation experiment on a biconvex circular-arc airfoil; Re = 10.3×10^6, M_∞ = 0.786.

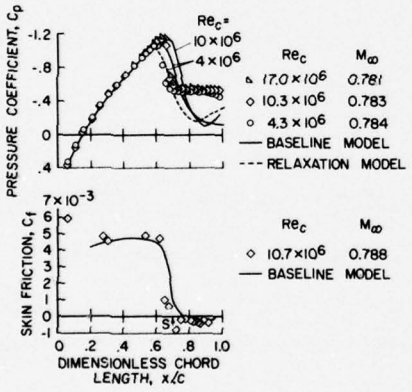

Fig. 8. Results from the shock-induced separation experiment on a biconvex circular-arc airfoil.

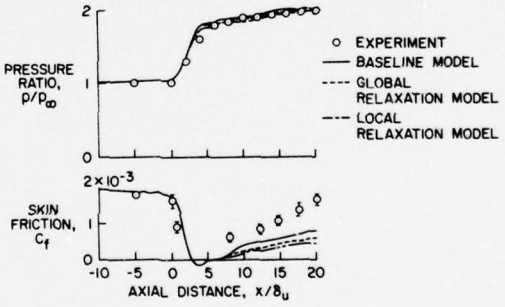

Fig. 10. Results from the normal-shock-wave experiment, M_∞ = 1.44 and $Re_x = 37\times10^6$.

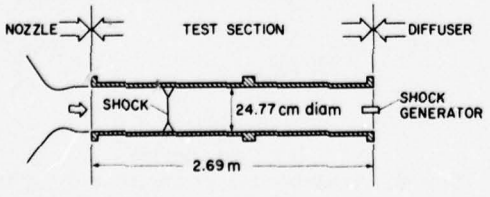

Fig. 9. Experimental arrangement for a normal-shock-wave, turbulent boundary-layer experiment with separation.

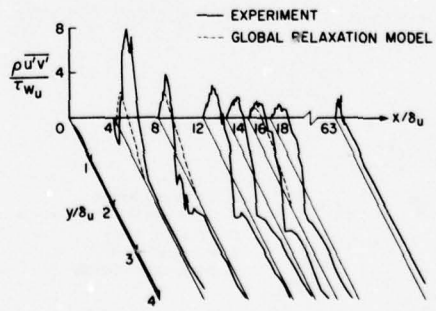

Fig. 11. Shear-stress profiles from the normal-shock-wave experiment, M_∞ = 1.44 and $Re_x = 37\times10^6$.

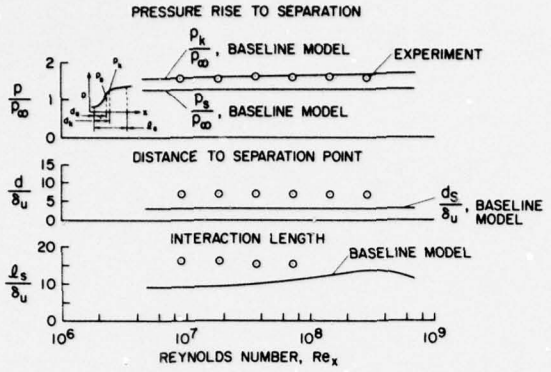

Fig. 12. Effect of Reynolds number on pressure rise to separation and on various interaction lengths.

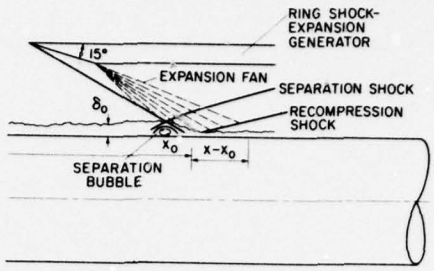

Fig. 15. Experimental arrangement for an axially symmetric hypersonic oblique shock-expansion, boundary-layer interaction experiment, $M_\infty = 6.9$ and $Re_X = 13\times10^6$.

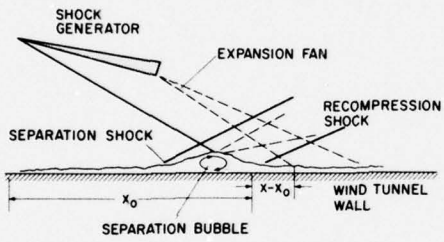

Fig. 13. Experimental arrangement for a supersonic oblique-shock-wave, boundary-layer interaction experiment, $M_\infty = 3.0$ and $Re_{\delta_0} = 9.73\times10^5$.

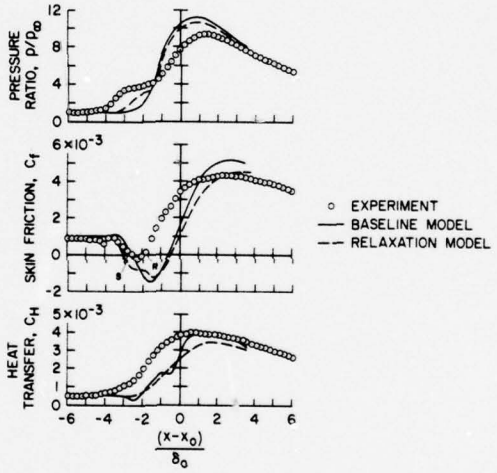

Fig. 16. Results from the hypersonic oblique-shock-expansion, boundary-layer interaction experiment, $M_\infty = 6.9$ and $Re_X = 13\times10^6$.

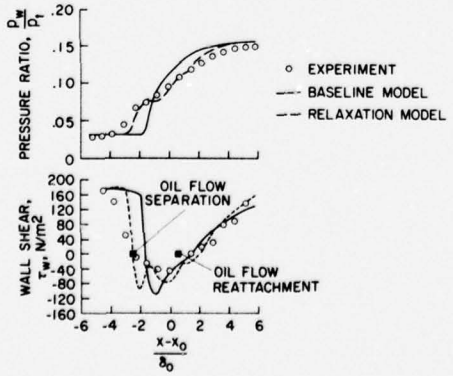

Fig. 14. Results from the supersonic oblique-shock-wave, boundary-layer interaction experiment, $M_\infty = 3.0$ and $Re_{\delta_0} = 9.73\times10^5$.

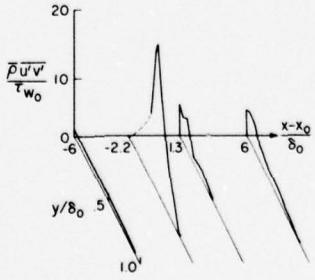

Fig. 17. Shear-stress distributions for the hypersonic oblique-shock-expansion, boundary-layer interaction experiment, $M_\infty = 6.9$ and $Re_X = 13\times10^6$.

THE IMPORTANCE OF EXPERIMENTALLY-DETERMINED CLOSURE CONDITIONS IN TRANSONIC BLADE-TO-BLADE FLOWS CALCULATED BY A TIME-DEPENDENT TECHNIQUE

by M. Couston

ABSTRACT

The use of a time-dependent technique to determine inviscid blade-to-blade flow in the transonic regime for axial turbomachines is faced with the problem of closure conditions. The importance of a Kutta condition in subsonic flow calculations is well known but for transonic blades the problem is still more complex. The quasi-discontinuous character of the flow through shock waves and Prandtl-Meyer expansions is then superimposed on the viscous effects which dominate near the trailing edge. In order to get more detailed information about the importance of this problem, a comparison between detailed measurements and calculations is presented herein. The calculations were performed for several trailing edge flow approximations including experimentally determined conditions.

RESUME

La solution numérique de l'écoulement non visqueux au travers d'aubages transsoniques utilisés dans les turbines axiales à l'aide d'une méthode instationnaire est liée au problème des conditions de cloture au bord de fuite. L'importance d'une condition de Kutta en régime soussonique est bien connue, toutefois, dans le cas d'aubages transsoniques, le problème est encore plus complexe. Le caractère quasiement discontinu de l'écoulement au travers des ondes de choc et des expensions se superpose dans ce cas au problème visqueux qui régit l'écoulement autour du bord de fuite. Dans le but d'avoir plus d'informations sur l'importance de ce problème, une comparaison entre des mesures détaillées et des calculs est présentée ici. Les calculs ont été faits en utilisant plusieurs approximations pour l'écoulement autour du bord de fuite ainsi que des conditions déterminées expérimentalement.

ACKNOWLEDGEMENTS

The author wishes to thank Professor Claus SIEVERDING and the Technical Staff of the von Karman Institute for their advice and valuable work concerning the experimental background of this paper. The author wishes also to express his thanks to the 'ANSALDO-MECCANICO-NUCLEARE' (Italy) for their financial support for the development of the basic time dependent program used throughout this paper.

LIST OF SYMBOLS

c	chord
e	internal total energy
g	pitch
h	height
i	spatial index in x-direction
$\vec{i}$	unit vector in x-direction
j	spatial index in y-direction
$\vec{j}$	unit vector in y-direction
l	length
M	Mach number
o	throat
p	static pressure
S	surface
t	time
TE	trailing edge diameter
u	velocity in x-direction
v	velocity in y-direction
V	volume
X	abscissa
β	flow direction
γ	specific heat ratio (Cp/Cv)
ρ	density

LIST OF SUBSCRIPTS

0	stagnation
1	inlet
2	exit
b	base
is	isentropic
l	local
p	pressure
s	suction or static

LIST OF FIGURES

I. INTRODUCTION

The problem of trailing edge flow conditions is very important for most of the calculations procedures. A lot of work has already been done for isolated airfoil or cascade flow operating in the subsonic range and the basic Kutta |1| - Joukowsky |2| condition has been interpretated in various manners. A review of such interpretations is presented by Gostelow |3| who shows the wide scatter between the various models presented. However, for transonic turbine blades, the problem appears to be different and if the transonic trailing edge flow has been studied experimentally by Sieverding and al |4,5| and Amana O.M. and al |6|, little is known about such conditions for transonic turbine flow calculations. The main reason for this is linked to the fact that transonic methods are not so developed as subsonic ones. The author developed at the von Karman Institute a transonic calculation procedure starting basically from the "Finite Area Method" proposed by Mac Donald P.W. |7|. Some improvements of the basic method are shown in references 8 and 9.

The present study is a tentative answer to questions which did arise with respect to the treatment of the trailing edge flow. In fact, the paper will in particular discuss the validity of the generally made assumption that the shock strength and flow direction are a strong function of the base pressure region and that a small error in this region will introduce a wide discrepancy between measurements and calculations.

As the transonic trailing edge flow is under experimental study at the von Karman Institute, references 4,5,11, it was possible to make carefull experimental investigations of both shock strength and flow direction and to compare these with the time dependent solution.

II. THE TRANSONIC NUMERICAL PROCEDURE

2.1. Basic Principle

The transonic calculation procedure used in this paper has first been suggested by Mac Donald |7|. This method follows the time dependent approach to overcome the basic difficulty of the mixed character of the flow equations in the transonic regime. The transient equations are of hyperbolic type whatever the Mach number is. But the numerical representation of the transient equations is done in an integral form applied to the conservation equations rather than using the usual finite difference technique. The advantages of this technique are described in more details in references 8 and 9. An important difference of the present method with respect to the one of reference 7 is the retention of the energy equation to avoid the hypothesis of isentropic flow. Such an hypothesis can lead to significant errors because the shock losses can be several times greater than the friction losses as shown by Meyer |10|, and there is no reason to neglect such losses. The basic volume elements used to solve the problem are presented in Fig.1. These elements of height h are six-sided and surround an interior point. For each of these elements, the four basic transient conservation equations are applied in the following manner :

- Mass

$$\frac{\partial \rho}{\partial t} + \frac{1}{dV} \int_{(s)} (\vec{i}\ \rho u + \vec{j}\ \rho v).h\ d\ \vec{l} = 0 \qquad (1)$$

- x Momentum

$$\frac{\partial \rho u}{\partial t} + \frac{1}{dV} \int_{(s)} (\vec{i}\ (\rho+\rho u^2) + \vec{j}\ (\rho uv)).h\ d\ \vec{l} = 0 \qquad (2)$$

- y Momentum

$$\frac{\partial \rho v}{\partial t} + \frac{1}{dV} \int_{(s)} (\vec{i}\ (\rho uv) + \vec{j}\ (p+\rho v^2)).h\ d\ \vec{l} = 0 \qquad (3)$$

- Energy

$$\frac{\partial e}{\partial t} + \frac{1}{dV} \int_{(s)} (\vec{i}\ (e+p)\ u + \vec{j}\ (e+p)v).h\ \ d\ \vec{l} = 0 \qquad (4)$$

where the internal total energy e is :

$$e = \frac{P}{\gamma-1} + \frac{1}{2}\ \rho\ (u^2+v^2) \qquad (5)$$

To evaluate the integrals, linear variations are assumed between the nodal points such that the integrals ($\int$) can simply be replaced by the sums (Σ) over the sides of the volume element. The time derivative is written as an upward derivative and is then used to update the solution through an iterative procedure. Stability, accuracy and convergence speed of this procedure are not of interest here and have already been treated previously in references 8 and 9.

Neverthelss, one of the main advantages of the method with respect to a finite difference technique lies in the fact that both physical and calculation plane are identical and so it is possible to have a direct sight into the calculation to applied experimental evidence.

2.2. Boundary Conditions

Upstream boundary

At the upstream boundary all variables are assumed to be uniform ; stagnation, pressure and density to be known and flow direction given. The static value of pressure and density and the velocity components are calculated to satisfy the continuity.

Downstream boundary

At the downstream boundary only one condition has to be retained. So the pressure is assumed uniform and constant throughout the iterative procedure.

Periodic boundary

The periodic boundary does not introduce any difficulty. Considering Fig.1, it is clear that the use of such mesh allows to treat periodic points as interior points.

Wall boundary

The wall boundary is calculated using a half-sided element as shown in Fig.1. This half-sided element is used to update the values of mass, momentum and energy, using equations (1) to (4). Here lies a fundamental difference with traditional methods in as far as no explicit tangency flow condition is applied at the wall. This will be used in the base region to calculate the pseudo-separation point. However, there is an equivalent tangency flow condition in the sense that mass and energy flow through the wall are explicitely set to zero. In such a way, the tangency condition is a result of the calculation.

III. THE TRAILING EDGE FLOW CONDITIONS

3.1. Experimental Base Flow Survey

Reference 11 provided the author with the experimental background of the base region problem. The detailed investigation of the flow through a turbine cascade as shown in Fig.2 is limited by the size of the cascade assembly. Hence, in order to obtain detailed data in the trailing edge region a model was developed at VKI which simulates the overhang section of a convergent cascade (as the one illustrated in Fig.2). A shadowgraph view of the flow around such enlarged model is shown in Fig.3. Here the principal flow features are clearly seen :

- the dead air region
- the two separation lines
- the two lip shocks (or separation shocks)
- the reattachment point (or zone)
- the two trailing edge shocks originating in the reattachment zone

In Fig.4, detailed pressure measurements around the model trailing edge are reported. This figure provided the following information : the pressure in the dead air region is constant, and the strength of the lip shock (introduced by the presence of a boundary layer in the real flow) is negligible with respect to the one of the trailing edge shocks.

In fact based on Fig.4, it is easy to show here that a condition like proposed by Wilkinson (Reference 12) of equal velocity on both side of the blade just before the trailing edge radius is in this particular case completely in contradiction with the real flow picture. Here Prandtl-Meyer expansions introduce almost a discontinuous

character of the flow in this region.

Moreover it can be seen in Figs.3 and 4 that the separation is close to the beginning of the trailing edge radius. So the flow around a truncated trailing edge with the same width will not be essentially different at the scale of the cascade.

3.2. The Numerical Trailing Edge Approximation

At this point several ways can be taken to approach the numerical problem of the trailing edge flow.

The first hypothesis is to transform the trailing edge of the blade in a manner presented in Fig.5a. In this case, two possibilities exist :

- either the pseudo-base-region defined in this manner is fixed during the calculation and then large error can be expected, if the correct base flow has not been selected, because the Prandtl-Meyer expansion will be limited by the wedge and not by the downstream pressure.

- or the base flow is updated at each iteration using a method like the one of references 13 and 14. This is probably the most suitable procedure but as shown in Fig.5b, the reattachment point will move from R1 to R2 and the mesh will have to be adapted after each updating of the base region. The calculations of both the base flow pattern and new mesh will introduce additional load in computer time and will make the numerical procedure less flexible.

The second way (the one the author has preferred) is presented in Fig.5c. The trailing edge is truncated, points A and B are assumed to be the separation point of the flow. The direction of the flow in these two points is free, this means that the flow takes a direction which satisfies the two momentum equations and not a direction imposed by external consideration. The location of the two separation points, as shown in Figs.3 and 4, is not very affected by the change in the base pressure value and can therefore be set a priori almost accurately. The next question is then what pressure has to be applied to the trailing edge between A and B. It appears to be a reasonable assumption that this pressure will set the trailing edge shock strength. The author has followed also here the usual assumption in the numerical procedure of a linear variation of quantities between points. Hence, the pressure at the trailing edge is the average of the pressures at points A and B.

One has to remember also that the flow in this region is very complicated and that it is not possible with a mesh like the one presented in Fig.5c to represent all the phenomenon correctly. So the trailing edge flow will be only an approximation of the real flow.

IV. CALCULATED RESULTS

4.1. Blade Definition

Two rotor blades with inlet angle of 60° and design outlet angle of 25° were selected for this investigation, they are called MIT-VKI I and II and are taken from reference 5. The very dense instrumentation of the blade allows an accurate determination of the shock strength. Moreover the major difference between these two blades was the trailing edge thickness and so an other important parameter was present in the comparison. In fact, MIT-VKI I has a trailing edge two times thicker than the one of the MIT-VKI II blade presented in Fig.2.

Detailed coordinates as well as velocity distributions are presented in reference 5 for these two blades. Therefore, only the main blades and cascades geometry are reported here :

	β_1	β_2	g/c	TE/c	TE γ	TE/o
MIT-VKI I	60°	25°	0.75	0.04	0°	0.145
MIT-VKI II	60°	25°	0.75	0.02	0°	0.075

The time-dependent program was applied to these two blades with a mesh using approximately one thousand nodal points (with 56 points on the blade surface). Fig.6 presents the calculation points on the blade surface near the trailing edge region.

Two samples of calculations are compared with experimental results in Fig.7. The comparison is only shown for one back pressure for both profiles to give an idea of the left running trailing edge shock definition. For this particular back pressure the left running trailing edge shock impinges at approximately 55% of the chord. But one can see ahead of this shock, between x/c=0.25 and 0.35, a velocity peak and a subsequent recompression which is better defined in the experimental results. This recompression is also seen on the schlieren picture presented in Fig.2. It is clear that this has nothing to do with the left running trailing edge shock. A detailed investigation of the manufactured blades has shown that there are here some "knobs" which were not expected. As in this region no shock was expected, only a relative coarse mesh was used, which explains why the method does not predict correctly this recompression.

4.2. Calculated versus Measured Trailing Edge Conditions

As already explained before, the trailing edge was truncated as shown in Fig.6. The points A and B are approximate separation points and the dotted-line represents the real trailing edge shape.

The pressure applied between points A and B for calculation purpose should represent the base pressure value P_b. This value of P_b can be expected to influence the calculated flow pattern. Hence Fig.6 presents a comparison of the measured pressure in the base flow region with the numerical one for both blades. Solid symbols correspond to the measurements and open symbols to the calculation. In order to check the influence of a change of the base pressure value, several test cases were calculated with different values of P_b.

Instead of

$$P_b = \frac{P(A)+P(B)}{2} \qquad (6)$$

which was the usual value,

$$P_b = P(B) \qquad (7)$$

was used, and these cases correspond to the symbols ⊡ ⊙ in Figs.8 to 10. However, it is clear that P(B) is not the same in equations (6) and (7) because the flow adapts itself locally due to the change in pressure. The adaptation of the pressure in this region when a change is made of the calculation of P_b is shown by the following example. Using equation (6) for blade I and for $M_{2,is}$=1.20+, the isentropic Mach number at point B was 1.40, using equation (7) the isentropic Mach number is then 1.52 and the flow direction changes by approximately 3°. One can see in Fig.6 that for the thin trailing edge the value obtained by equation (6) is in very good agreement with the measured one, but for the thick trailing edge such an agreement is not obtained. This discrepancy is easily understood looking at Fig.6 where point A is already located on the trailing edge radius and so the pressure obtained using (6) is too low. This corresponds to a situation where the pseudo separation point A is not correctly set and corresponds to a too large expansion. In fact if the pseudo-base pressure has the importance expected it is evident that for VKI-MIT I blade the calculated strength should be quite different than the measured one due to the observed discrepancy.

4.3. Shock Strength

To evaluate the possible effect of the base pressure on the shock strength, the right running trailing edge shock was selected. This choice is made because the right running shock strength affects the suction side boundary layer and is therefore of primary importance for the blade performance. In any case, the right running shock is the only which can be measured accurately. However, if there is any influence of the base pressure value, the strength of both shocks will be affected.

To characterize the shock strength the Mach numbers just ahead and just after the shock have been plotted in Fig.9 versus the downstream isentropic Mach number M_{2is}. The symbols to differentiate experiments and calculations are consistent with the one of Fig.8. From Fig.9, it seems that the measured shock strengths of blades I and II are nearly identical in the range of outlet Mach numbers under consideration. For higher exit Mach number it should be pointed out that the measurements indicate a shock slightly stronger for blade I than for blade II. The predicted shock intensity agrees quite well with the measured values, however, contrary to the experiments the theoretical calculation already indicates slightly stronger shocks for the blade with the thick trailing edge. The fact already mentionned before that for the VKI-MIT I blade, the pseudo-separation point A is probably not the real one, does not at all affect the right running trailing edge shock strength which appears to be correctly predicted. Nevertheless the

---

+ The isentropic Mach number is derived from the ratio of the local static pressure to total inlet pressure.

Mach number behind the shock seems to be better predicted than the one ahead of it. This is attributed to the fact that the Mach number is almost constant after the shock and therefore better defined.

The variation of the base pressure itself, already shown in Fig.8, does not change in a noticeable manner the calculated shock strengths. The small difference which can be observed between ◘ and ◘ or ● and ● for a same back pressure is introduced by the author to differentiate the calculations. This apparently indicates that for the present method the base pressure is not as important as expected. Nevertheless, one should not conclude that there is no influence at all, but rather that the importance of P_b introduced in the program has only a local influence on the channel Mach number.

The next step is to check a possible influence of a base pressure variation on the outlet flow direction.

4.4. Flow Direction

Another important parameter for cascade turbine flow is the exit flow direction which has been measured at the von Karman Institute (reference 11) for both the blades presented herein. A comparison is shown in Fig.10 between the measured and calculated outlet angle β_2 (referred to the tangential direction), for blades I and II. Here also the agreement is reasonably good for both blades. The difference between calculated and measured value does not exceed 1.5° for MIT-VKI I and something like 0.5° for MIT-VKI II.

For comparison purpose, the value arc sin o/g (known as sinus-rule) has been added as dotted line. It has been shown in reference 15 that this value agrees very closely with the outlet flow angle for M_2=1.0 and zero trailing edge thickness. It is therefore not surprising that the agreement is better for MIT-VKI II which has the smaller trailing edge thickness. The solid line corresponds to a semi-empirical correction of the preceeding rule, proposed by Bammert and Sonnenschein (reference 16), which takes into account the trailing edge thickness. This modified sin-rule improved the comparison especially for blade I.

The variation of the base pressure applied in the calculation is almost without influence on the outlet flow direction as shown in the Fig.10. So, if the exit flow direction appears to be practically not influenced by the base pressure value in the range investigated, the reason for the better predicted values for VKI-MIT II has to be searched perhaps in the fact that viscous phenomenon are less important for a thin trailing edge than for a thick one.

A simple example in Fig.11 demonstrates the absolute independance of the flow angle from the base pressure for a wedged trailing edge. It is assumed that the Mach number on one side of the trailing edge is unity and on the other side 1.5 a variation of the base pressure from M=1.5 to 3.0 shows a large displacement of the confluence point but not of the overall direction.

V. CONCLUSIONS

This study was stimulated by the analysis of the experimental results concerning the trailing edge flow in transonic turbine cascades. A theoretical investigation has been undertaken in order to clarify the importance of the correct formulation of the trailing edge flow.

Rather than going to the complex calculation of the base flow region, pseudo-separation points are assumed. This has the advantage of avoiding to define a variable dead-air region which will introduce additional calculations and make the program less flexible.

Herein, it has been shown that the present method is not sensitive to the way in which the trailing edge region is treated. It is demonstrated that both the trailing edge shock strength and the exit flow direction are not strong functions of the base pressure. In fact the influence is limited to a small region around the trailing edge and does not affect the overall calculated performances. However, it is evident that this procedure will probably fail if too thick trailing edges are used because in this case a large region is affected by the viscous flow. Then it will probably soon be necessary to have a base pressure and dead air region calculation to separate the inviscid region from the viscous one. However, for turbine calculations purposes, a trailing edge thickness to chord ratio of 4% (the one of MIT-VKI I) lies in the upper limit of trailing edge thickness. For most of the cases the present method is then sufficient.

Of course improvements of the present method of treating the trailing edge flow are probably still possible, but the author believe that such improvements will probably be, for most cases, not appreciable. This remark is based on the experience which the author gathered with his method in the calculation of a large number of very different turbine blade profiles over a wide range of Mach number. Reference 9 demonstrates with a few examples the good agreement between theoretical and experimental results.

REFERENCES

1. KUTTA W.M. "Lift Forces in Fluid Flow"
Illustrierte Aeronautische Mitteilungen, 1902, p.133

2. JOUKOWSKY N.E. "Collected Works" (Vol.6
Ogiz, State Publ. House of Tech. Theo. Lit., Moscow (1950)

3. GOSTELOW J.P. "Trailing Edge Flows over Turbomachine Blades and the Kutta-Joukowsky Condition"
ASME Paper no 75-GT-94

4. SIEVERDING C., DECUYPER M., COLPIN J., AMANA O. "Model Test for the Detailed Investigation of the Trailing Edge Flow in Convergent Transonic Turbine Cascades"
ASME Paper No 76-GT-30

5. SIEVERDING C. "Base Pressure Measurements in Transonic Turbine Cascades"
Part I and II
VKI L.S. 84 Transonic Flow in Axial Turbomachinery (February 2-6,1976)

References (continued)

6. AMANA O.M., DEMUREN H.O., LOUIS J.F., SIEVERDING C., CHAUVIN J. "Aerodynamics and Heat Transfer at the Trailing Edge of Transonic Blades"
ASME Paper No 76-GT-95

7. MAC DONALD P.W. "The Computation of Transonic Flow Through Two-Dimensional Gas Turbine Cascades"
ASME Paper No 71-GT-89

8. COUSTON M., MAC DONALD P.W., SMOLDEREN J. "The Damping Surface Technique for Time-Dependent Solutions to Fluid Dynamic Problems"
VKI TN 109 (March 1975)

9. COUSTON M. "Time-Marching Finite Area Method"
VKI L.S. 84 Transonic Flow in Axial Turbomachinery (February 2-6,1976)

10. MEYER J.B. "Theoretical and Experimental Investigations of Flow Downstream of Two-Dimensional Transonic Turbine Cascades"
ASME 72-GT-43

11. SIEVERDING C. Unpublished Data. Private Communication.

12. WILKINSON D.H. "A Numerical Solution of the Analysis and Design Problems for the Flow Past One or More Aerofoils or Cascades"
ARC R&M 3545 (1968)

13. CARRIERE P. "Recherches Récentes sur le Problème de la Pression de Culot"
Paper presented at the Conference on Fluid Mechanics, Paris (February 18,1963)

14. CARRIERE P., SIRIEIX M. "Facteurs d'Influence du Recollement d'un Ecoulement Supersonique"
Paper presented at the Xth International Conference on Applied Mechanics, Stresa (August 1960)

15. TRAUPEL W. "Thermische Turbomaschinen"
Springer-Verlag (1968)

16. BAMMERT K., SONNENSCHEIN H. "Der Einfluss Verdickter und Verdünnter Turbinenschaufeln auf die Gittereigenschaften"
Archiv für das Eisenhüttenwesen
38 Jahrgang, Heft 4, pp. 287-299 (April 1967)

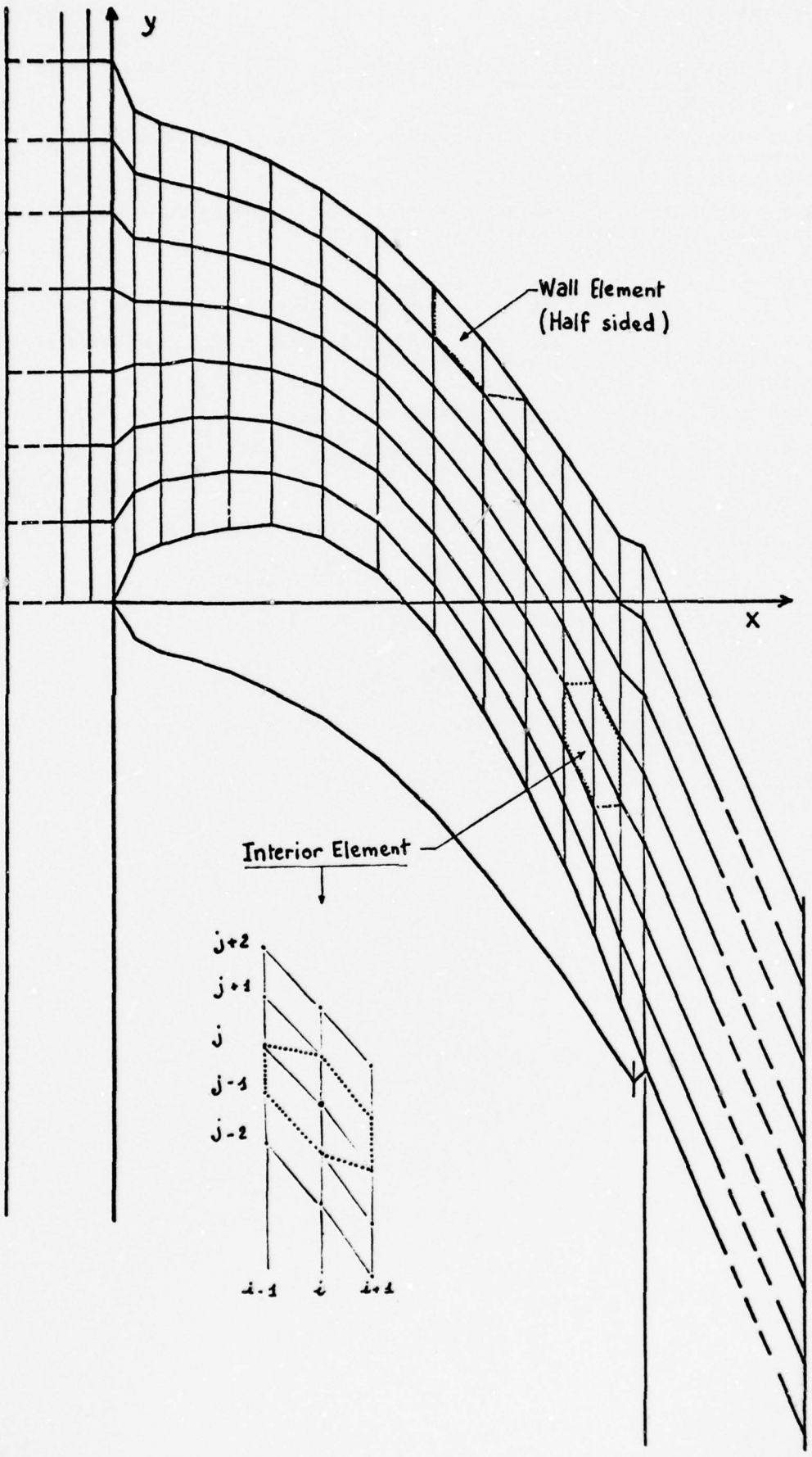

Fig.1 Mesh definition

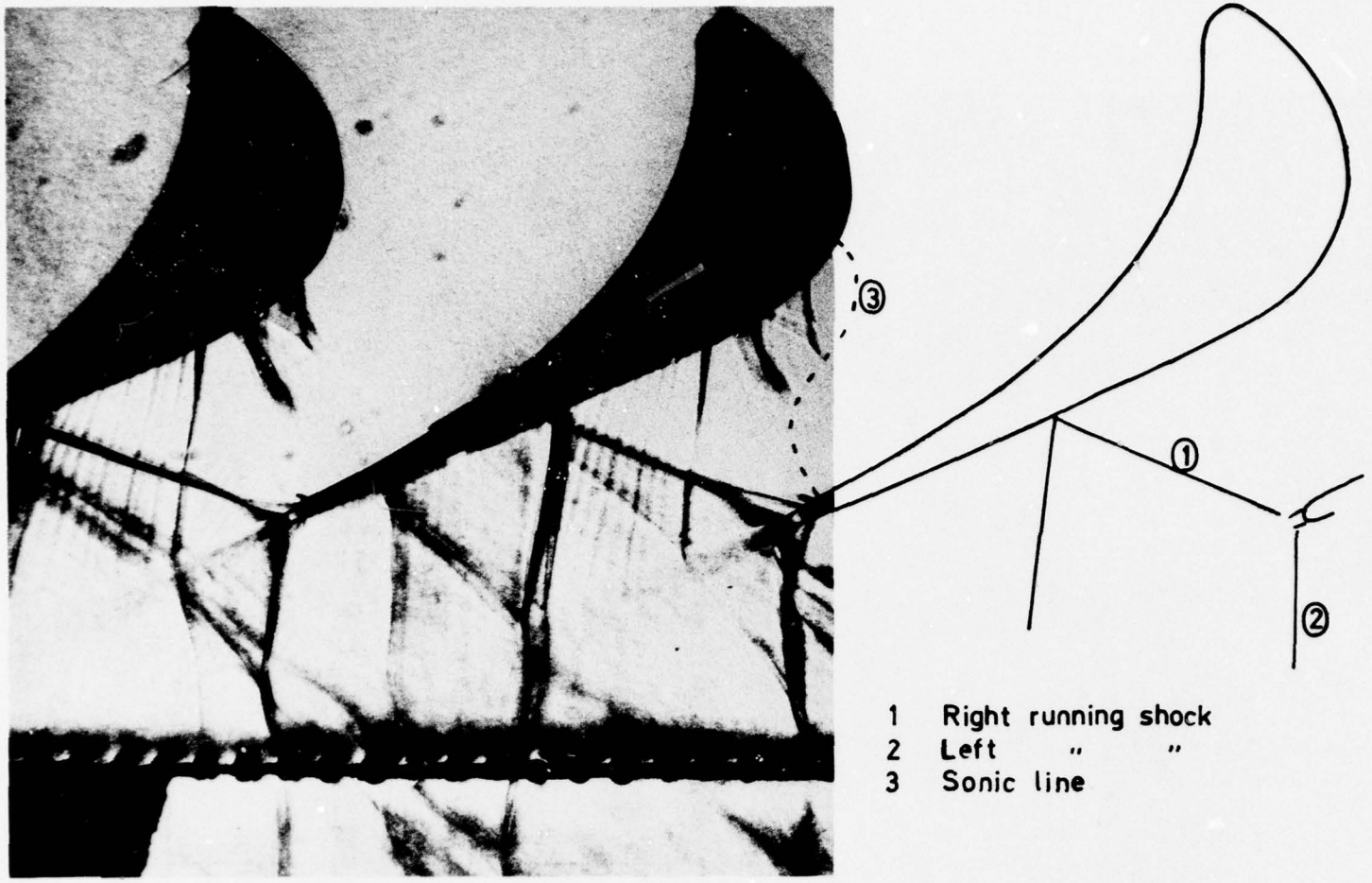

Fig.2 Schlieren picture of flow pattern in the transonic regime ($M_{2is} \simeq 1.2$) for MIT–VKI II blade.

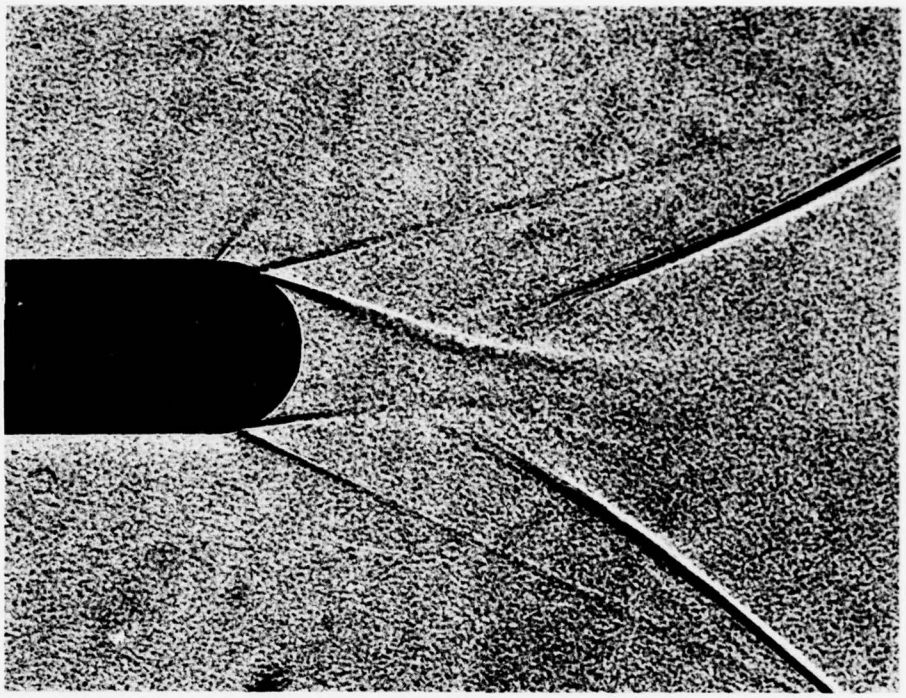

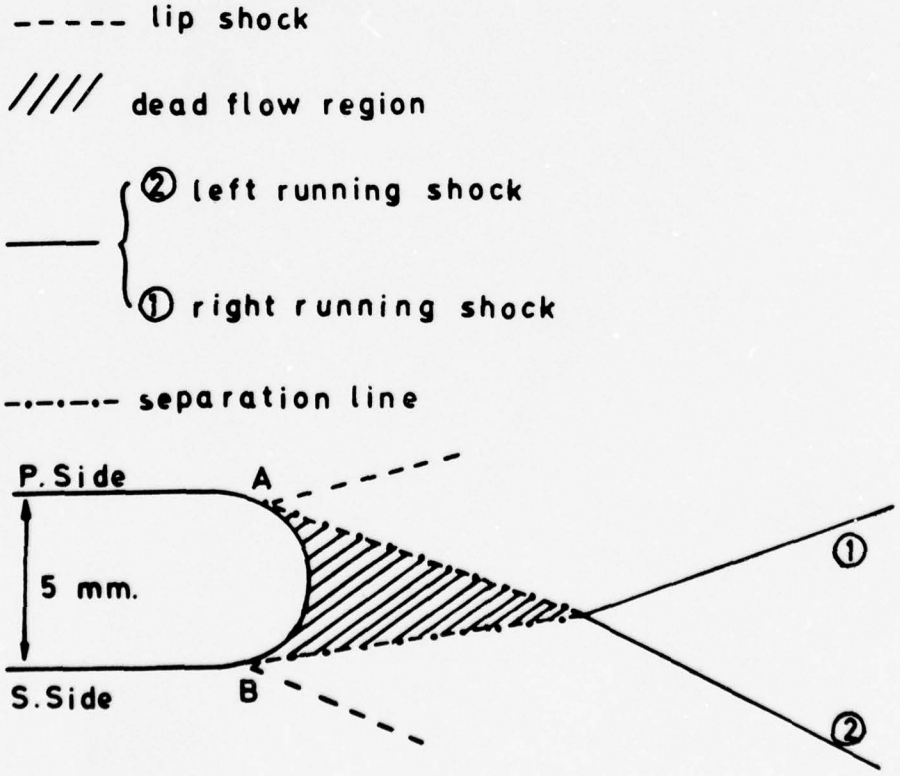

Fig.3 Shadowgraphs of the trailing edge flow (Ref.11).

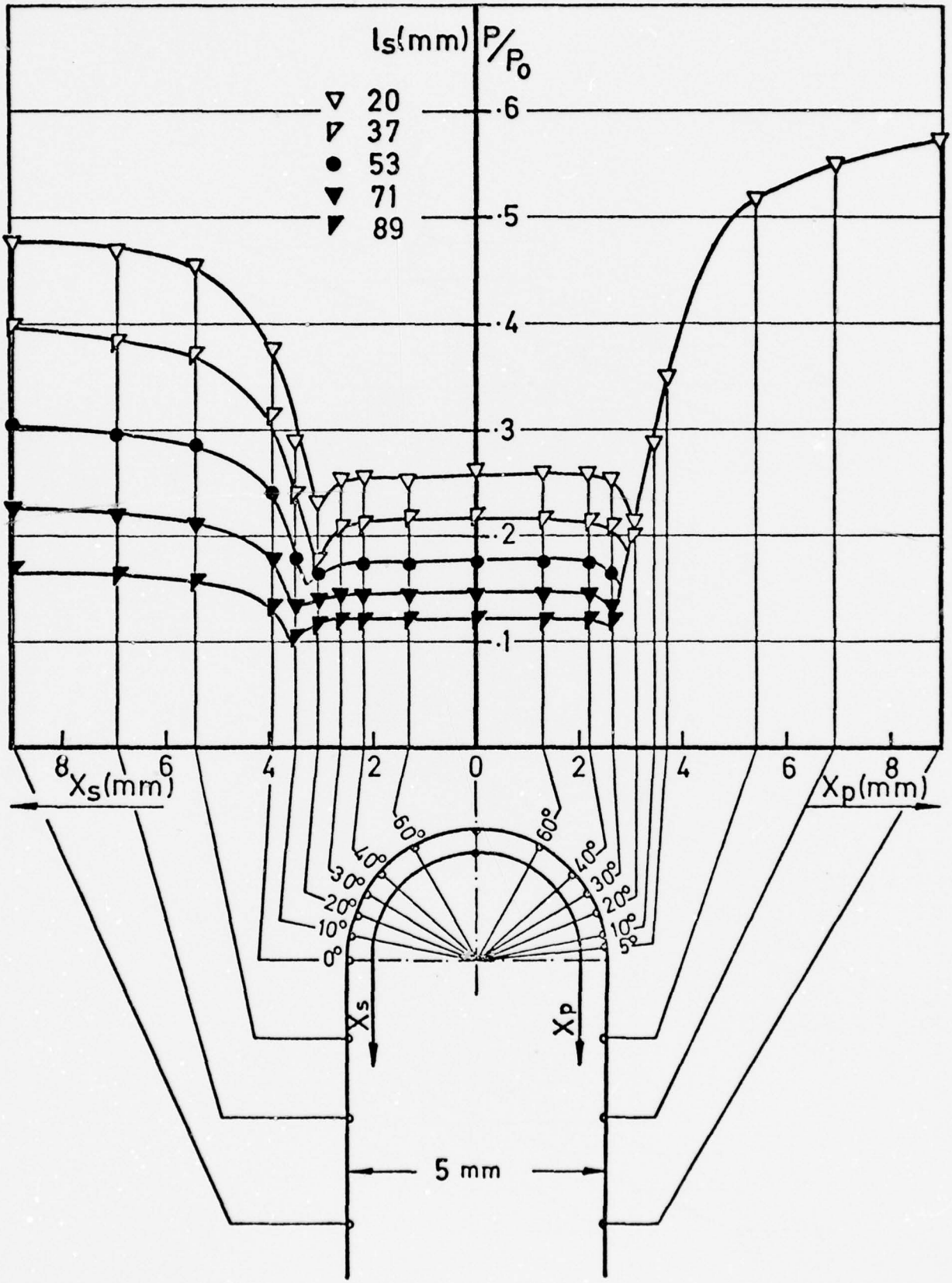

Fig.4 Detailed pressure distribution around trailing edge (Ref.4).

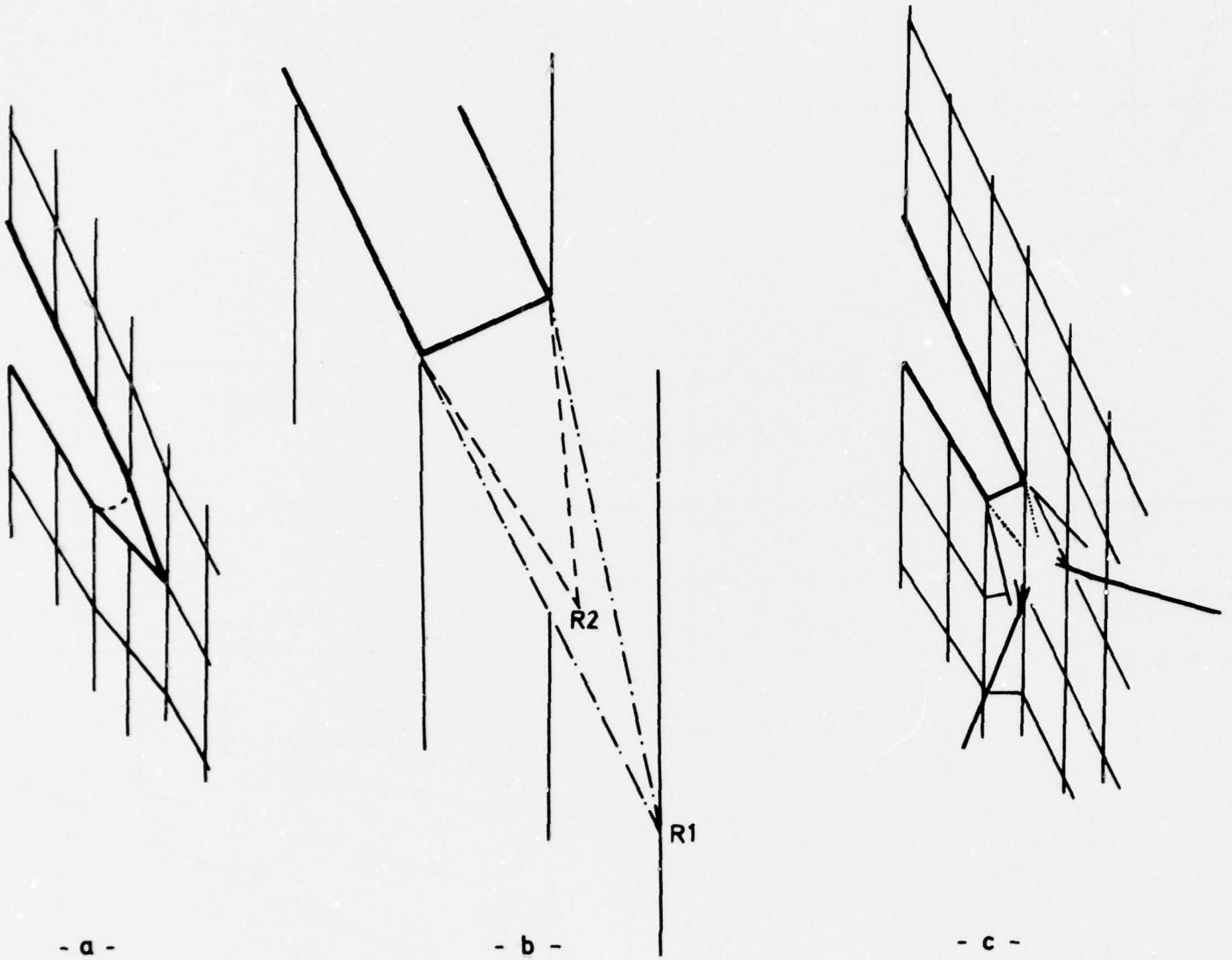

Fig.5 Trailing edge approximations

Fig.6 Trailing edge calculation points

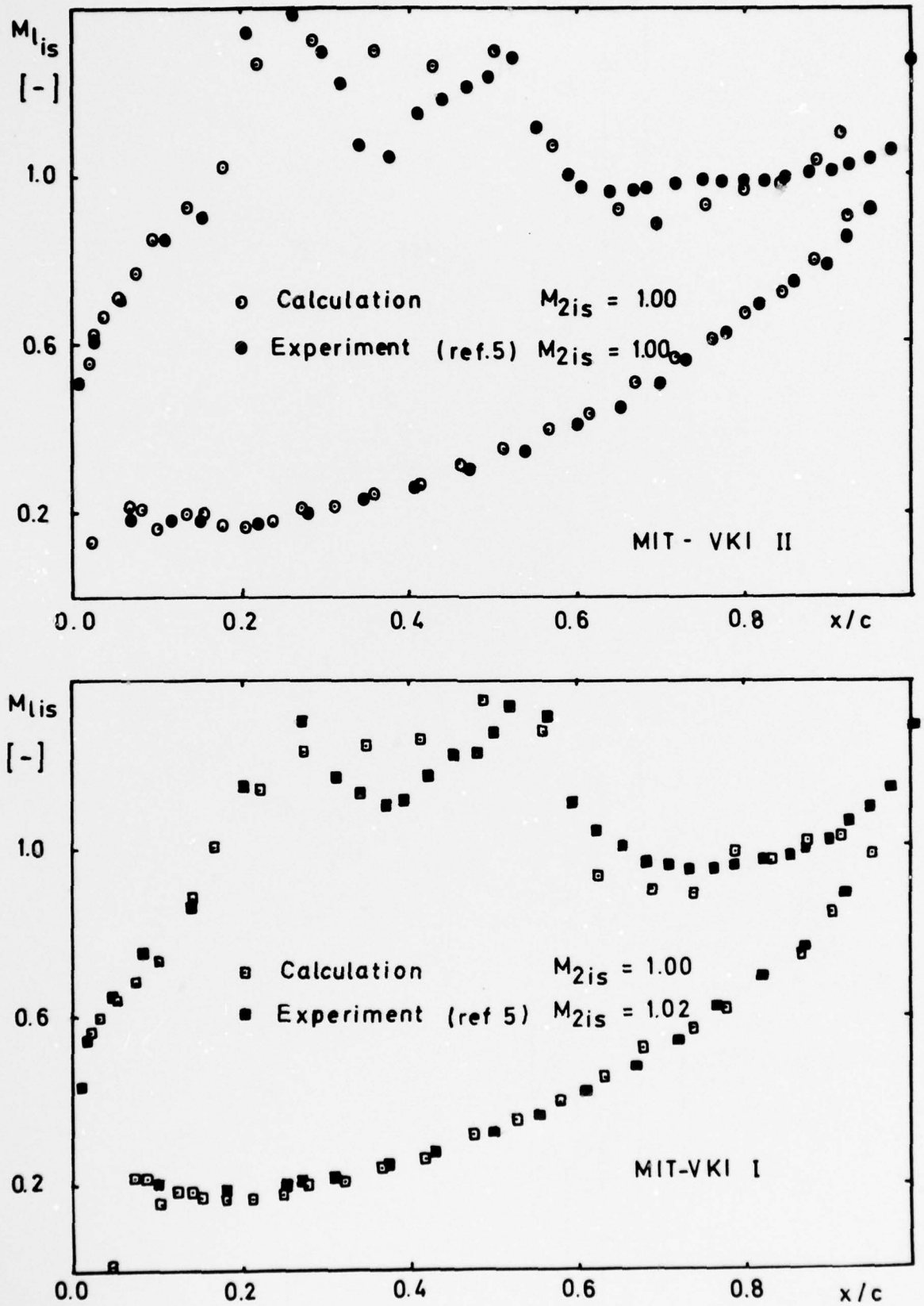

Fig.7 Sample of velocity distributions

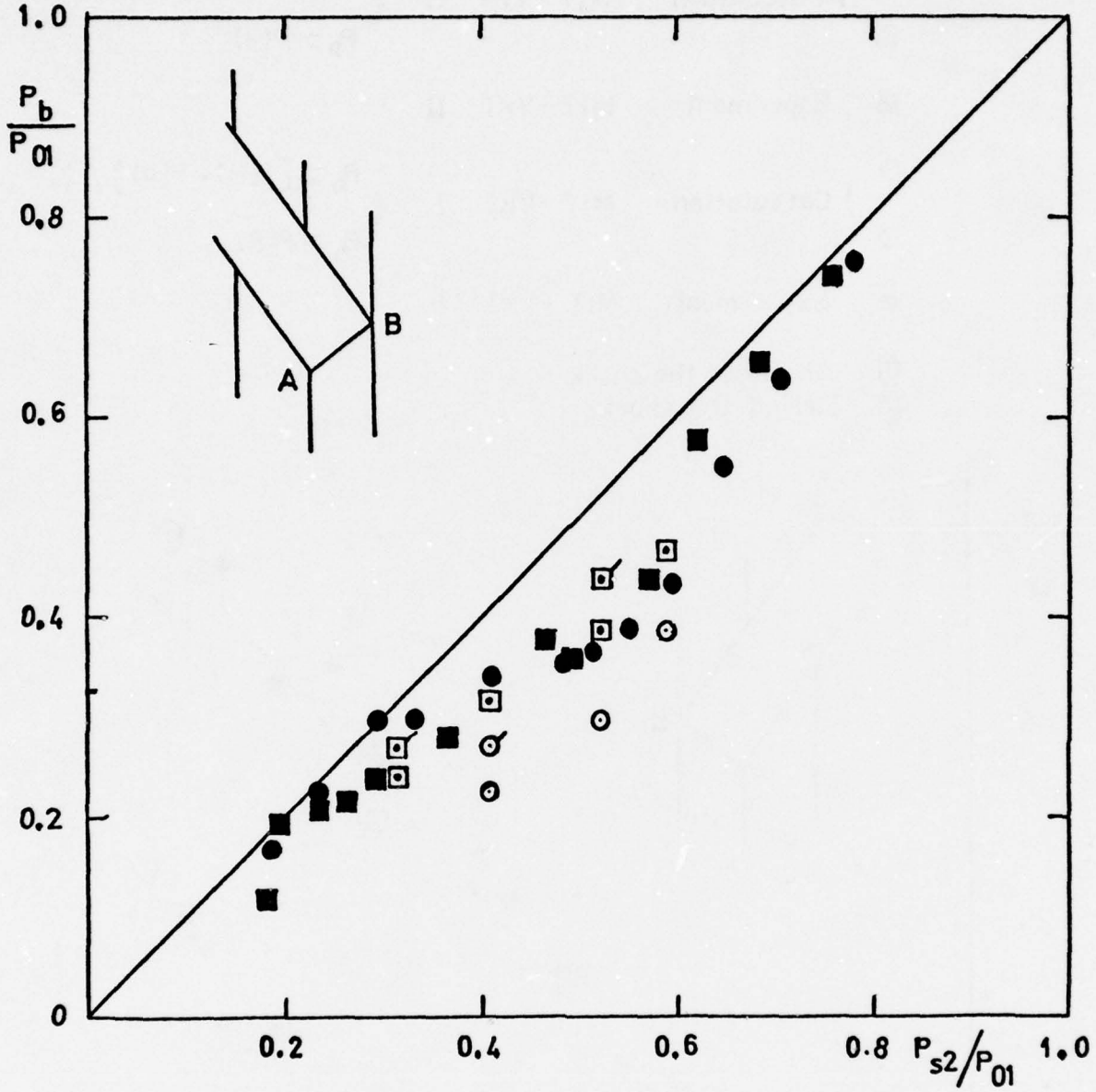

⊡ ⊡ } Calculation MIT - VKI II { $P_b = [P(B) + P(A)]/2$. ; $P_b = P(B)$

■ Experiment MIT - VKI II

⊙ ⊙ } Calculation MIT - VKI I { $P_b = [P(B) + P(A)]/2$. ; $P_b = P(B)$

● Experiment MIT - VKI I

Fig.8 Base pressure versus downstream pressure

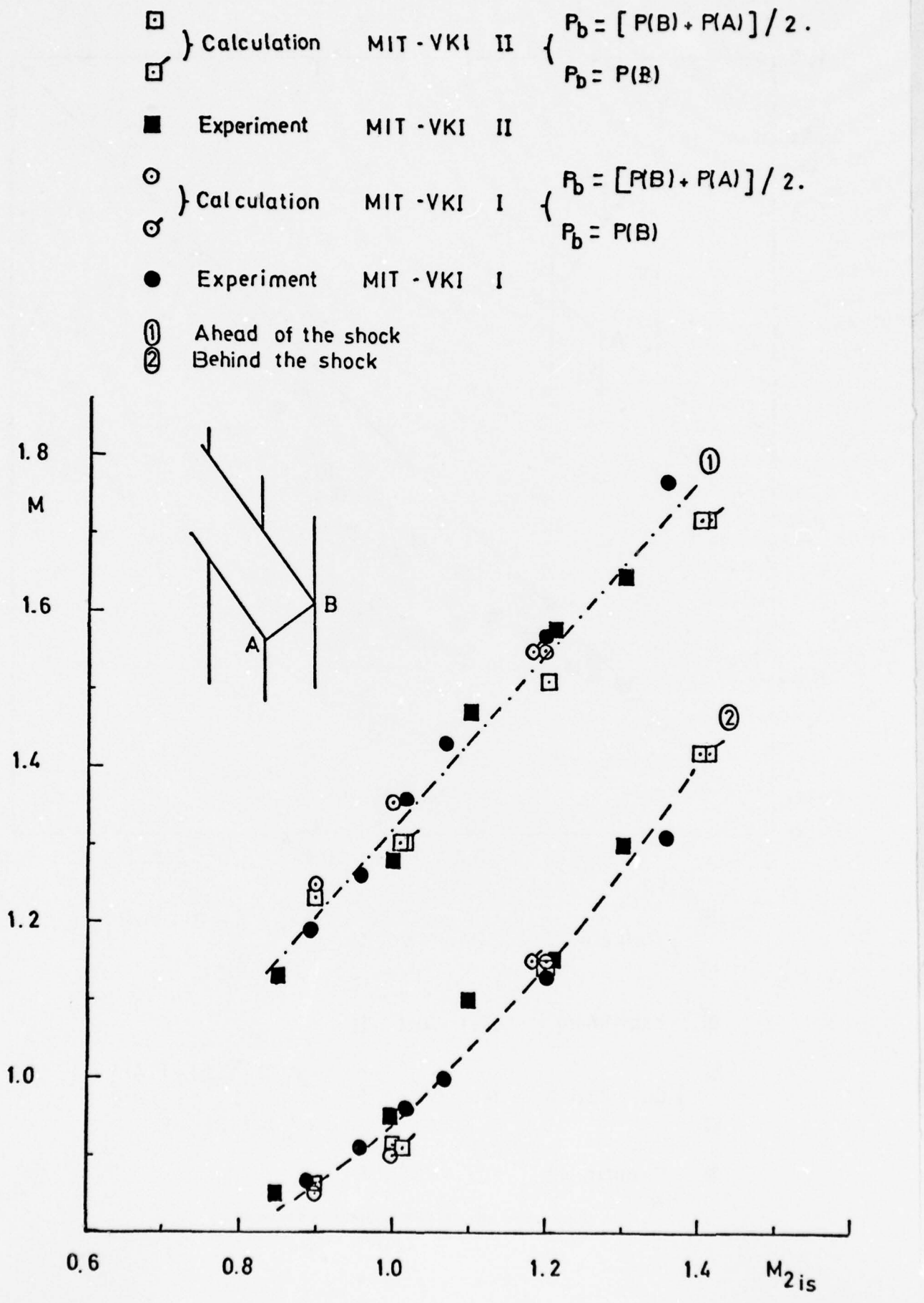

Fig.9 Mach number in front and after the right running trailing edge shock

MIT – VKI – I

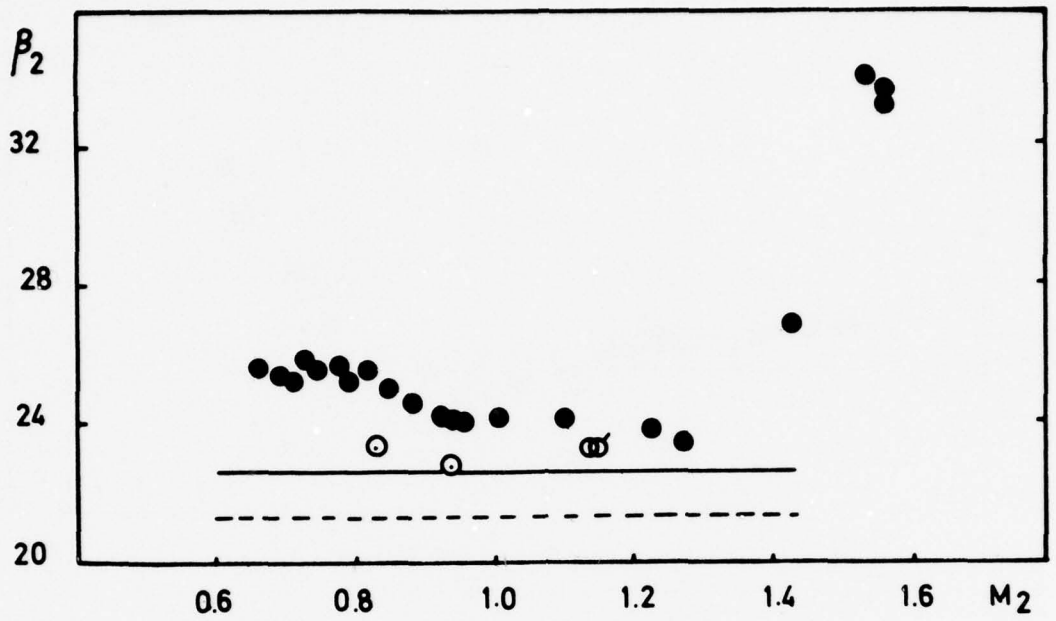

---- Sin^{-1} (o/g) (ref. 15)

——— Bammert (ref. 16)

● Experiment VKI (ref. 11)

⊙ $P_b = [\ P(B) + P(A)\ ] / 2.$

Calculation

⊙ $P_b = P(B)$

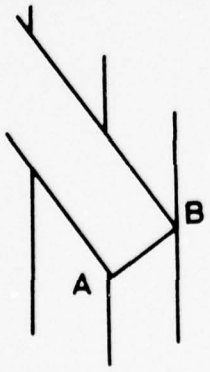

Fig.10a Exit flow direction

MIT - VKI - II

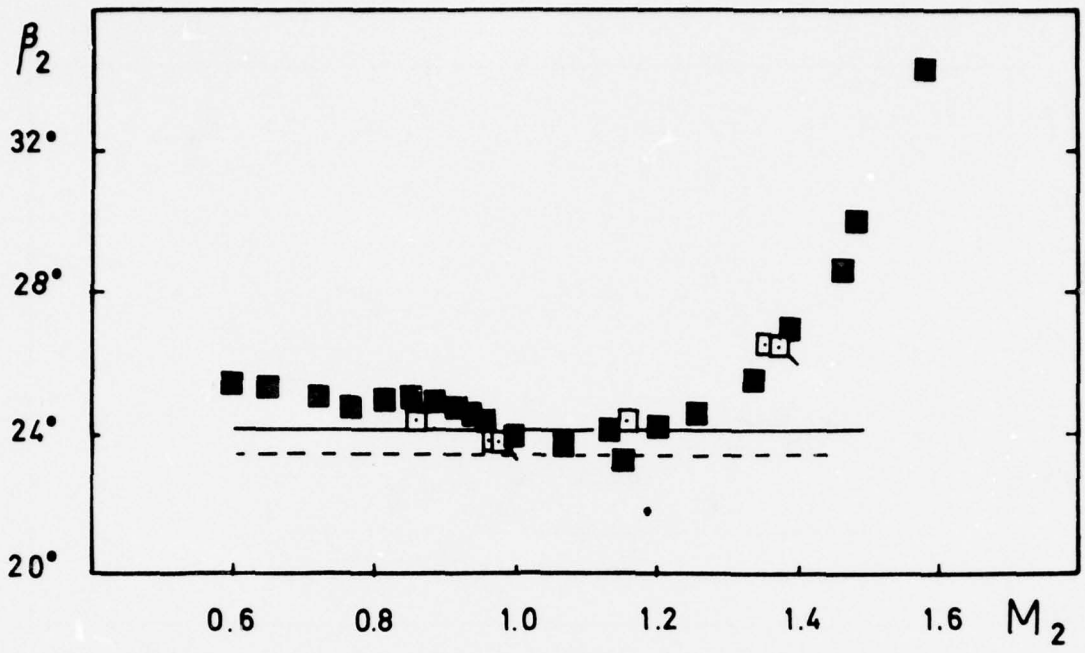

--- Sin^{-1} (o/9) (ref. 15)

—— Bammert (ref. 16)

■ Experiment VKI (ref. 11)

⊡ Calculation $P_b = [\ P(B) + P(A)\ ] / 2.$

⊡ $P_b = P(B)$

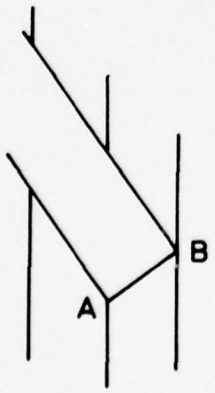

Fig.10b Exit flow direction

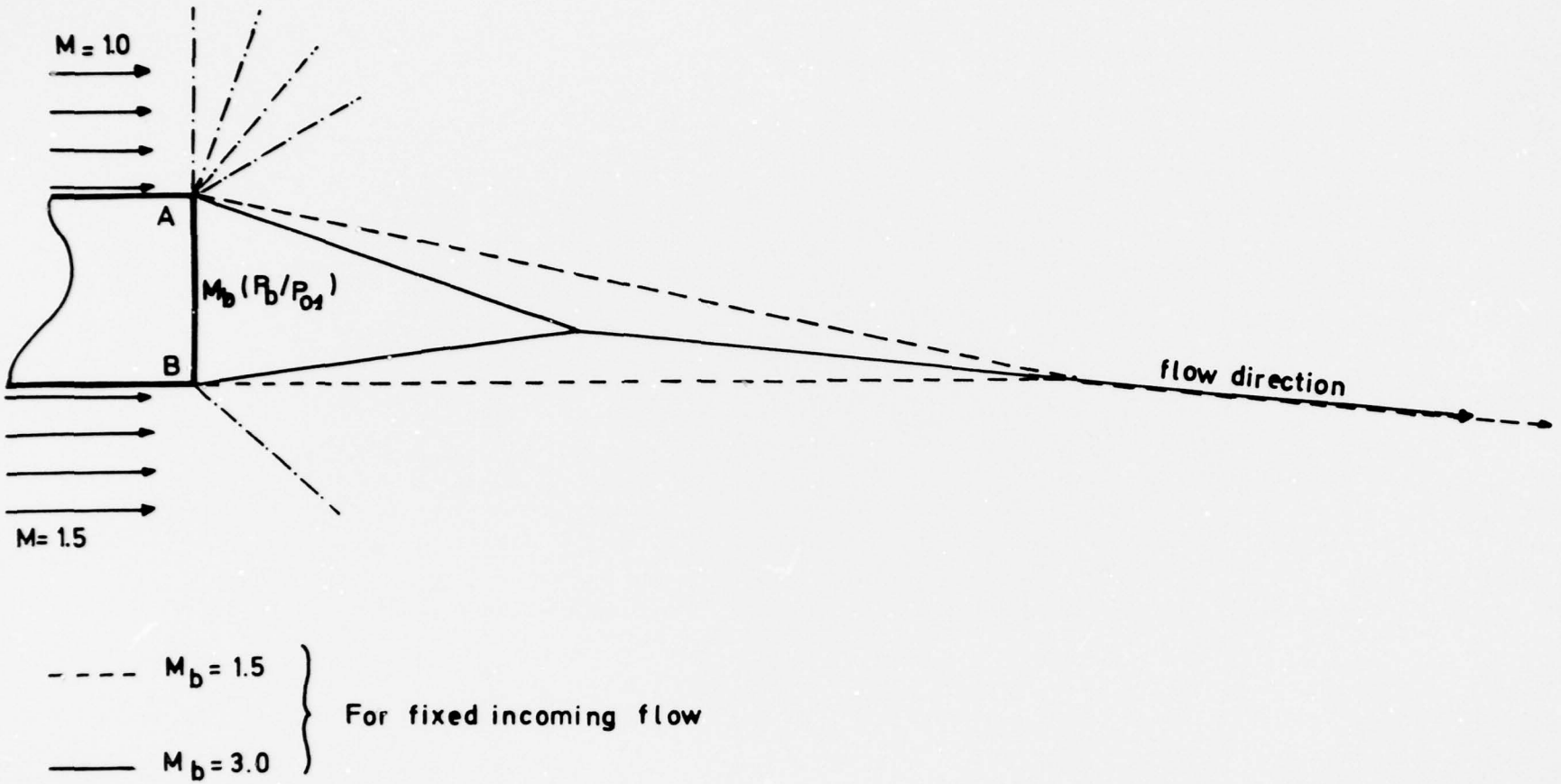

Fig.11 Influence of the base Mach number on the flow direction

NUMERICAL SIMULATION OF THREEDIMENSIONAL TRANSONIC FLOW INCLUDING WIND TUNNEL WALL EFFECTS *

W. SCHMIDT, H.-W. STOCK, W. FRITZ

DORNIER GMBH

THEORETICAL AERODYNAMICS GROUP

D-7990 FRIEDRICHSHAFEN, GERMANY

SUMMARY

This paper presents the numerical methods and their practical implementation to compute steady transonic flow fields about wings and wing-body combinations in transonic flow including viscous effects as well as wind tunnel wall effects.

The transonic small disturbance potential equation is solved by a mixed finite difference scheme as known from previous publications. Wind tunnel wall boundary conditions are incorporated in the relaxation procedure by use of the classical wall condition equations.

The threedimensional boundary layer equation is solved by an integral prediction method. Solving potential equation and boundary layer equation iteratively, viscous effects are accounted for by means of the displacement thickness concept.

Results showing the influence of Reynolds-number and Mach-number on pressure distribution and shock position are shown. The influence of the wall conditions compared with the numerical free flight results are shown as well as some results showing the necessary wall contouring, resp. porosity parameter distribution to adjust the windtunnel to free flight conditions.

RESUME

Ce travail présente les méthodes numériques et leur introduction pratique pour le calcul des écoulements transoniques stationnaires autour d'ailes et de combinations aile-fuselage en transonique y compris les effets visqueux et les effets de parois en soufflerie.

L'équation potentielle transonique aux petites perturbations est résolue par un schéma mixte de différences finies qui est connu par des publications précédentes. Les conditions de parois en soufflerie sont introduites dans le procédé de relaxation par les équations classiques de condition de parois.

L'équation tridimensionelle de la couche limite est résolue par une méthode intégrale de prédiction. En résolvant l'équation potentielle et celle de la couche limite itérativement, les effets visqueux sont pris en considération au moyen du concept d'épaisseur de déplacement. Des résultats présentés montrent l'influence des nombres de Reynolds et de Mach sur la distribution de pression et la position du choc. L'influence des conditions de parois est comparée avec les résultats numériques du vol libre et d'autres résultats montrent la forme nécessaire des parois ou la distribution du paramètre de porosité pour régler la soufflerie selon les conditions du vol libre.

* This work was sponsored by the German Ministry of Defense under ZTL contract T/R 720/R 7600/42009 and RüFo 4 contract T/RF 41/RF 410/51 154

1. INTRODUCTION

Aerodynamicists are confronted with the problem of designing more and more efficient aircraft as well for transport as combat purposes. Part of such design work is done on computers by flow computations using numerical methods, part by wind tunnel testing. Figure 1 illustrates these two tasks to simulate the behaviour of a full scale aircraft in free flight.

The wind tunnel testing provides us with the complete physics although due to limited tunnel size and thus lower Reynolds-number, finite distance walls, free stream turbulence, noise, these physics can differ significantly from the required. While the error sources model shape and test equipment can be kept very small in general, those scaling effects form the basic limitations for the accuracy of wind tunnel results.

In contrast, numerical methods represent only physical models which are part of the full physics. Additional sources of errors are included by the use of mathematical models and special numerical procedures as well as by the numerical discretization of the aircraft in the computer.

It should always be kept in mind that comparing wind tunnel results and computed flow fields the errors of both sides will be included, unless either the wind tunnel test itself is simulated or both results are compared with free flight data.

At the present time there is no aim to replace the wind tunnel but to use numerical methods to

- o reduce total wind tunnel running time

by providing better design. Numerical methods are well suited to show the influences of different configuration parameters because computations can be done very fast and unexpensive compared with wind tunnel tests. Furthermore numerical methods can be used to

- o correct for unadequate wind tunnel walls effects

by either computing the wall effects and thus correcting the flow field or by adjusting the wind tunnel walls to give the same conditions along the wall as along the corresponding streamline at free flight conditions. Boundary layer methods can be used to show the influence of the different Reynolds numbers at free flight and in the wind tunnel, i.e.

- o extrapolate viscous effects to free flight Reynolds number.

On the other hand computational fluid mechanics suffer from the lack of good experimental data to

- o improve physical models
- o have reliable data to compare with.

The present paper particularly shall give some ideas of the use of a threedimensional transonic potential flow method and a boundary layer method to

- o simulate viscous effects on threedimensional wings
- o simulate wind tunnel wall boundary conditions
- o adjust wind tunnel wall conditions to simulate free flight conditions.

The last item especially is of some interest because of the possibility to estimate the efforts we have to undertake to simulate free flight conditions in a wind tunnel. Time optimal iteration procedures for wall adjusting can be established by numerical simulation.

The computational methods used will be

- o TSP transonic relaxation method
- o classical wind tunnel wall conditions
- o boundary layer integral method.

2. TRANSONIC SMALL PERTURBATION POTENTIAL FLOW METHOD

The threedimensional relaxation method used is well known from previous publications [1], [2], [3]. Similar to the methods of Bailey [4], Albone [5] and v.d. Vooren [6] the TSP equation is solved by means of Murman's finite difference scheme and his line relaxation algorithm. In contrast to the others no transformation is used and the modified small perturbation equation is solved in the threedimensional cartesian coordinate system. To get unique results a fully conservative scheme is used including Murman's shock point operator.

The wing boundary conditions are linearized while on bodies exact boundary conditions are fulfilled. A straight wake is assumed to leave the wing trailing edge in the wing mean plane $z = o$ with jumps in the potential equal to the local section circulation $\Gamma(y)$.

Similar to Bailey's method farfield solutions on finite boundaries are used, i.e. solution of Laplace-equation at $x = \pm \infty$, and either Klunker's expression [7] for the potential or normal velocity components calculated by means of a vortex lattice method [8] along the planes $z = \pm \infty$ and $y = + \infty$. The figure 2 gives a schematic view of the grid arrangement.

Finally, pressures are calculated from the first or second order isentropic equation.

One great advantage of the present method is its flexibility in treating as well analysis as design or mixed problems. Figure 3 shows the basic arrangement of the computer program which allows calculations by interactive means.

3. WIND TUNNEL WALL BOUNDARY CONDITIONS

The equation derived by Baldwin, Turner, and Knechtel [9] is used to model a longitudinally slotted perforated wind tunnel wall. Their derivation assumes that both the slot flow velocities and the perturbations from the mean flow are small compared to the undisturbed tunnel velocity. The pressure is constant across the open portions and the slot spacing is small compared to the tunnel dimensions. In addition it is assumed that the plenum pressure equals the undisturbed free stream pressure and the walls are taken to be straight and parallel with constant width slots.

Relating the pressure drop at the wall ($c_p = -2\,\phi_x$) to the local flow inclination (ϕ_n) and the longitudinal gradient of the flow inclination (ϕ_{xn}) the wall boundary condition reads

$$A\,\phi_x + BH\,\phi_{xn} + C\,\phi_n = 0 \qquad \text{at } n = +H \tag{1}$$

Adding one inhomogeneous term to account for contoured walls finally the equation used in the present paper is

$$A\,\phi_x + BH\,\phi_{xn} + C\,\phi_n + D = 0 \tag{2}$$

The three dimensionality of the flow at the wall is replaced by a relationship between two-dimensional velocity components and geometric parameters. No explicit account is taken of the tunnel boundary layers, although some of these effects may implicitly be included in determining P. Equation (2) contains the boundary conditions for different tunnel walls as limiting forms, i.e.

straight solid: $A = B = D = 0,\ C \neq 0,\ \phi_n = 0$

contoured solid: $A = B = 0,\ -D/C = \text{wall slope},\ \phi_n = -D/C$

free jet: $B = C = D = 0,\ A \neq 0,\ \phi_x = 0$

ideal slotted: $C = D = 0,\ B/A = \text{slot parameter},\ \phi_x + B/A + \phi_{xn} = 0$

porous or perforated: $B = D = 0,\ A/C = \text{porosity parameter},\ A/C\ \phi_x + \phi_n = 0$

Several recent papers have included tunnel wall boundary conditions in nonlinear transonic relaxation procedures for two dimensional [10, 11] and axisymmetric problems [12, 13]. Newman and Klunker [14] show three-dimensional results for a rectangular wing with tunnel walls. The present paper is using a numerical scheme similar to that used by Murman [10] but having the wall conditions included in the line relaxation. To guarantee better convergence different schemes are used for the different conditions.

The wall conditions enter the transonic potential equation via the derivatives ϕ_{zz} at the upper and lower wall and ϕ_{yy} at the side wall. The following difference formulas show the wall expressions used for ϕ_{zz} at the upper wall depending upon the wall conditions.

Scheme for solid, ideal slotted, slightly porous walls

The wall plane z = z (JMP) is included in the relaxation procedure. The second derivative ϕ_{zz} is built using the potential at the points JMP - 1, JMP and the first derivative ϕ_z at the point JMP.

$$\phi^{n+1}_{zz_{I,JMP,K}} = \frac{2}{z(JMP) - z(JMP-1)} \left\{ \phi^{n+1}_{z_{I,JMP,K}} - \frac{\phi^{n+1}_{I,JMP,K} - \phi^{n+1}_{I,JMP-1,K}}{z(JMP) - z(JMP-1)} \right\}$$

ϕ_z being estimated from the wall conditions

solid wall: $$\phi^{n+1}_{z_{I,JPM,K}} = -\,\varepsilon \left.\frac{n_x}{n_z}\right|_{I,K}$$

ideal slotted: $$\phi^{n+1}_{z_{I,JMP,K}} = \phi^{n+1}_{z_{1,JMP,K}} - \frac{1}{FH} \left\{ \phi^{n+1}_{I,JMP,K} - \phi^{n+1}_{1,JMP,K} \right\}$$

slightly porous P < P*: $$\phi^{n+1}_{z_{I,JMP,K}} = \phi_{z_I} - P \left\{ \frac{\phi^{n+1}_{I,JMP,K} - \phi^{n+1}_{I-1,JMP,K}}{x_I - x_{I-1}} \right\}$$

In the same way the farfield solution can be included if a solution for ϕ_z is prescribed, i.e. by a vortex lattice method.

Scheme for free jet and highly porous walls

The wall plane z = z (JMP) is not included in the relaxation procedure, the calculations end at z = JMP-1. The second derivative ϕ_{zz} at station JMP-1 is built using the potential at the points JMP-2, JMP-1 and JMP.

$$\phi^{n+1}_{zz_{I,JMP-1,K}} = \frac{2}{z(JMP)-z(JMP-2)} \left\{ \frac{\phi^{n+1}_{I,JMP,K} - \phi^{n+1}_{I,JMP-1,K}}{z(JMP) - z(JMP-1)} - \frac{\phi^{n+1}_{I,JMP-1,K} - \phi^{n+1}_{I,JMP-2,K}}{z(JMP-1) - z(JMP-2)} \right\}$$

$\phi^{n+1}_{I,JMP,K}$ being estimated from the wall conditions

free jet: $\phi^{n+1}_{I,JMP,K} = 0.0$

highly porous P > P*: $\phi^{n+1}_{I,JMP,K} = -\frac{1}{P} \int_{-\infty}^{x} \phi_z \, dx$

In the same manner the classical far field solution of Klunker [7] in ϕ is included, allowing for an updating of ϕ not necessarily at each iteration but due to stability reasons after NGAM iterations.

The two different treatments for porous walls were recommended by Murman [10] and guarantee as well stability as the correct limiting cases solid wall (P=0) and free jet (P=∞).

4. THREEDIMENSIONAL TURBULENT BOUNDARY LAYER CALCULATIONS

Basing on the integral methods of Myring [15] and Smith [16] an integral method for compressible turbulent boundary layers has been developed and extensively tested [17]. The basic assumptions and empirical correlations included are

- o x and y momentum equations and entrainment equation are used in non-orthogonal curvilinear coordinates
- o power law profiles approximate the streamwise velocity, Mayer or Johnston correlations the crosswise velocity component in the boundary layer
- o originally Head's empirical entrainment coefficient, meanwhile replaced by the Lag Entrainment Method of Green [18]
- o Ludwig-Tillman's skin friction law
- o Eckert's reference temperature concept to account for compressibility effects.

The resulting system of hyperbolic equations is integrated by means of a fast and simple explicit finite difference scheme.

To prove the accuracy of this method a comparison is shown on figures 4 a-c as well with experimental data as with other finite difference and integral methods. It should be mentioned that in all calculations the same input was used for the external flow field, namely infinite sheared wing conditions and measured wall pressures. As shown in [17] much better agreement with the experimental data can be reached near separation if the measured velocities at the outer edge of the boundary layer are used. In general it can be stated that for wingtyp boundary layers integral methods seem to give as good answers as finite difference methods.

In the iterative cycle of calculating the viscous transonic flow this boundary layer method is used to predict the threedimensional displacement thickness surface which has to be added to the wing profiles. Its integration in the whole process can be seen from figure 3.

5. RESULTS

All test calculations were done on a wing-body combination as shown in figure 5 which belongs to the PT-series of FFA in Sweden. The wing has an aspect ratio of 4.0, a quarter chord line sweep of 35 degrees and a taper ratio of 0.4. The airfoil shape is an intermediate one using the analysis and design options of our TSP program.

5.1 Influence of Wind Tunnel Wall Conditions

To show the influence of wind tunnel walls a tunnel is assumed of 2.8 times the root chord as height and 4 times root chord as width. The same grid is used for all calculations, for free flight mesh points being added outside the walls up to z = ± 4.3 c_r and y = 2.6 c_r where far field boundary conditions are applied.

Figures 6 a,b show the influence of free jet and straight solid wall boundary conditions compared with the free flight conditions in two spanwise sections. Both sections show the same well known effects that the free jet pressures are smaller at the upper surface and higher at the lower, the shock position moved forewards. For solid walls the tunnel height with respect to the supersonic region plays an important role. Either pressures above or below the free flight data can be the result. Figure 7 shows the pressures along

the upper wall for the solid wall compared with the free flight values at this location. Unfortunately no results have been available at the time of the conference for porous or slotted walls due to some minor computer problems. Anyway, those results would lay somewhere between the solid wall and free jet data.

Figure 8 shows the necessary changes at the wall in one section to get an adjusted curved solid wall which produces wall-interference-free results. Although the angle of attack of the configuration is equal to zero due to the high local section lift the walls have to be curved to guarantee the right downwash behind the wing. The figures 9 a,b show the variation of porosity parameter along the walls for two sections to have wall-interference free results. This results might give an indication of the complexity of threedimensional adjusting of wind tunnel walls.

5.2 Influence of Viscous Effects

The influence of viscous effects on threedimensional transonic wing flow is shown by applying iteratively the displacement thickness concept. The starting solution always is the fully converged TSP solution without shock point operator. Using the resulting velocities the displacement thickness distribution is calculated and added to the wing profiles. All following TSP calculations are done using the fully conservative form with shockpoint operator. Different calculations showed that as long as there is no separation two iteration cycles proved to give converged results without any underrelaxation of the displacement-thickness. The figures 10 a,b represent the results for $M_\infty = 0.85$ and $Re = 5.4 \cdot 10^7$ 1/m at two span stations. Compared with the nonconservative inviscid results the shock moves slightly backwards and the trailing edge pressure is increased. Maximum pressures seem to be sometimes lower or even higher, depending on the threedimensional behaviour of the flow. It should be mentioned also that the displacement thickness at the lower surface can be thicker than on the upper due to threedimensional effects though the pressures on the lower surface are lower (figure 10 b). For comparison the fully conservative inviscid solution is shown also which has a shock position further aft.

Figures 11 a,b show the same effects for $M_\infty = 0.90$ and $Re = 1.1 \cdot 10^7$ 1/m. The higher recompression as well as the thicker layer due to the smaller Reynolds number produce stronger effects on both, the pressures and on the displacement thickness.

6. CONCLUSION

The present paper showed the capability of computational methods to give at least the tendencies of the influences of wind tunnel walls and boundary layers on threedimensional transonic flows. Further studies have to be made to prove results against experimental data from the wind tunnel and free flight. Relatively unexpensive studies can be done to improve adjusting wall concepts by showing the influence of different iterative adjusting procedures, effects of imcomplete adjusting etc.

Also, it seems to be very attractive to study different improved wall condition models to simulate more accurate the presence of wind tunnel walls.

7. REFERENCES

1. S. Rohlfs, R. Vanino: A Relaxation Method for Two- and Threedimensional Transonic Flows, Euromech 40, Saltjöbaden, 1973
2. W. Schmidt: Progress in Transonic Flow Computations. Analysis and Design Methods for Threedimensional Flows, VKI Lecture Series 87 Computational Fluid Dynamics, March 1976
3. W. Schmidt, S. Hedman: Recent Explorations in Relaxation Methods for Threedimensional Transonic Potential Flow, to be presented at 10th ICAS Congress, Ottawa, Oct. 1976
4. F.R. Bailey, W.F. Ballhaus: Comparisons of Computed and Experimental Pressures for Transonic Flows about Isolated Wings and Wing-Fuselage Configurations, NASA SP-347, pp. 1213-1232, 1975
5. C.M. Albone, M.C. Hall, Gaynor Joyce: Numerical Solutions for Transonic Flows past Wing-Body Combinations, Symposium Transsonicum II, Göttingen 1975
6. J. v.d. Vooren, H.W. Slooff, G.H. Huizing, A. van Essen: Remarks on the Suitability of Various Transonic Small Perturbation Equations to Describe Threedimensional Transonic Flow, Symposium Transsonicum II, Göttingen 1975
7. E.B. Klunker: Contribution to Methods for Calculating the Flow about Thin Lifting Wings at Transonic Speed, NASA-TN-D-6530, 1971
8. W. Schmidt: Fernfeld-Randbedingungen in Erhaltungsform, to be published as Dornier Report, 1976
9. B. Baldwin, J. Turner, E. Knechtel: Wall Interference in Wind Tunnels with Slotted and Porous Boundaries at Subsonic Speeds, NACA TN 3176, 1954
10. E.M. Murman: Computation of Wall Effects in Ventilated Transonic Wind Tunnels, AIAA Paper No 72-1007, Sept. 1972
11. J.J. Kacprzynski: Transonic Flow Field Past 2-D Airfoils between Porous Wind Tunnel Walls with Nonlinear Characteristics, AIAA Paper 75-81, Jan. 1975
12. F.R. Bailey: Numerical Calculation of Transonic Flow about Slender Bodies of Revolution, NASA TN D-6582, 1971
13. R.W. Barnwell: Transonic Flow about Lifting Wing-Body Combinations, AIAA Paper 74-185, 1974

14. P.A. Newman, E.B. Klunker: Numerical Modeling of Tunnel-Wall and Body-Shape Effects on Transonic Flow over Finite Lifting Wings, NASA SP-347, Pt. II, pp. 1189-1202, 1975

15. D.F. Myring: An Integral Prediction Method for Threedimensional Turbulent Boundary Layers in Incompressible Flow, RAE TR 70147, 1970

16. P.D. Smith: Integral Prediction Method for Threedimensional Compressible Turbulent Boundary Layers, ARC, R & M No. 3739, 1974

17. H.W. Stock: Results of a Calculation Method for Threedimensional Compressible Turbulent Boundary Layers, DEA Meeting, Dayton, Ohio, April 1976

18. J.E. Green, D.J. Weeks, J.W.F. Brooman: Prediction of Turbulent Boundary Layers and Wakes in Compressible Flow by a Lag-Entrainment Method, R.A.E. TR 72231, 1973

8. FIGURES

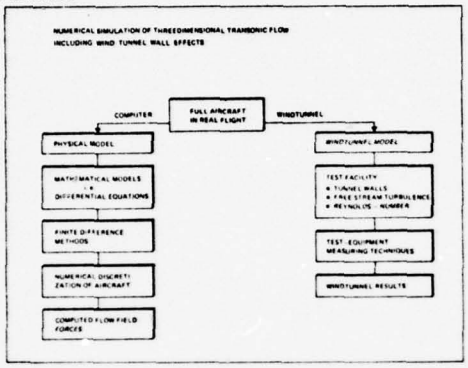

Figure 1: Computer and Windtunnel, Design Tools and their Constraints

RELAXATION METHOD TO SOLVE THE TRANSONIC POTENTIAL EQUATION

$$[(1-M_\infty^2)-(\kappa+1)\,\delta^{2/3}\,M_\infty\,\phi_x]\,\phi_{xx}+\phi_{yy}+\phi_{zz}=0$$

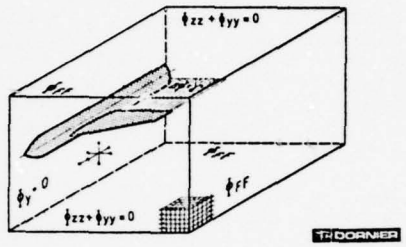

Figure 2.

Basic Arrangement for Threedimensional TSP Method

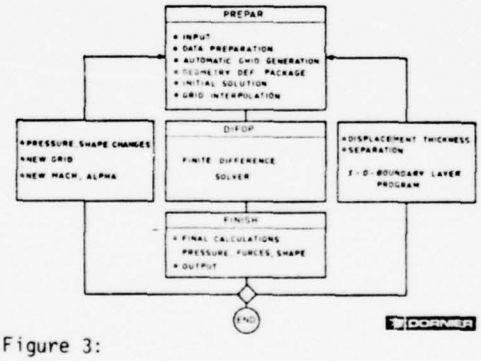

Figure 3:

Flow Chart of Numerical Simulation System

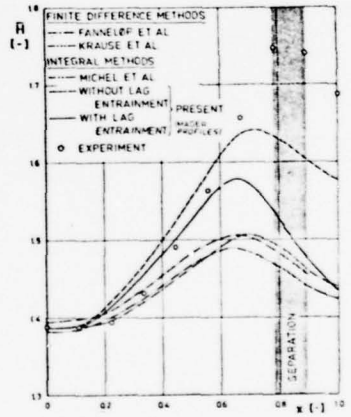

SHAPE PARAMETER DISTRIBUTION
(BERG AND ELSENAAR TEST CASE)

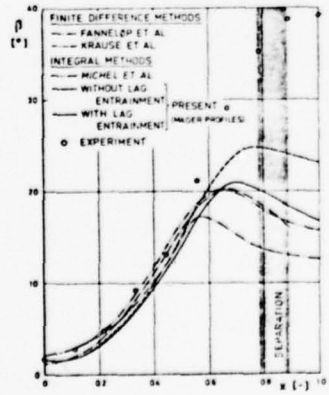

ANGLE BETWEEN THE DIRECTION OF THE WALL SHEAR STRESS AND THAT OF U_e
(BERG AND ELSENAAR TEST CASE)

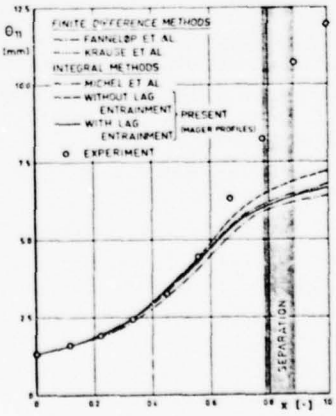

MOMENTUM THICKNESS DISTRIBUTION
(BERG AND ELSENAAR TEST CASE)

Figure 4 a-c: Comparison of Present Boundary Layer Method with Experimental Results and other Methods

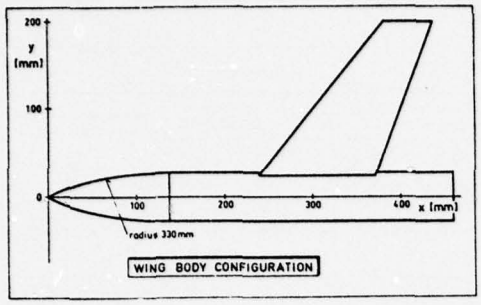

Figure 5: Planform of PT Wing Body Combination

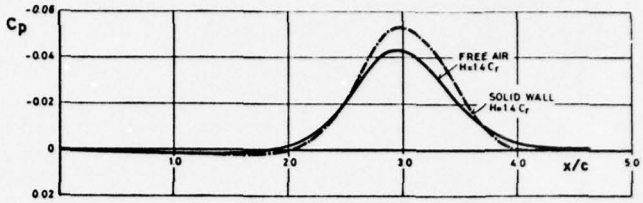

Figure 7: Pressure Distribution along the Tunnel Upper Wall at Spanstation y/s = 0,275

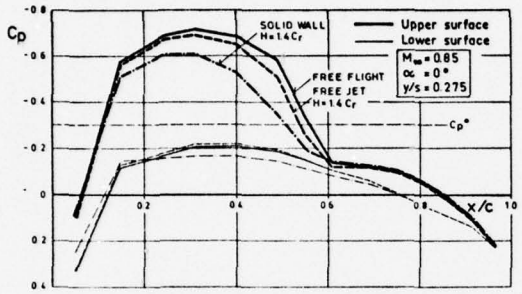

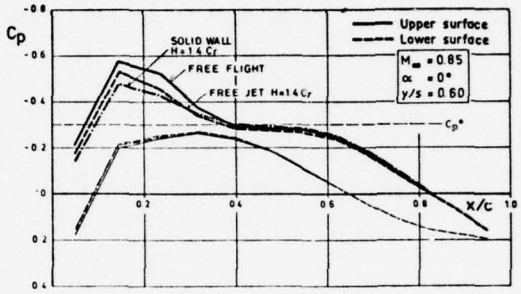

Figure 6 a-b: Influence of Windtunnel Wall Conditions at Two Spanstations

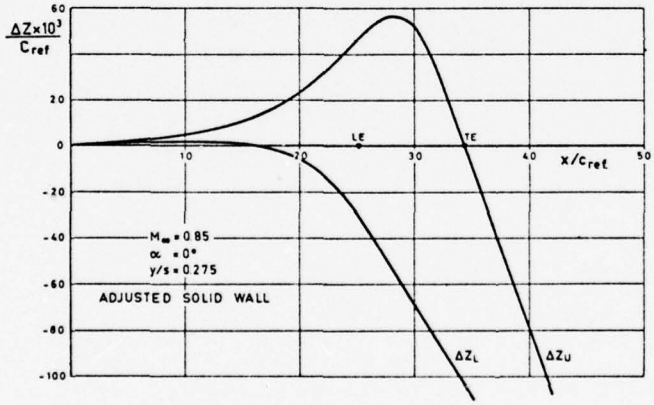

Figure 8: Contouring of Solid Upper and Lower Wall to Get Interference Free Windtunnel Walls H = ± 1.4 c_r

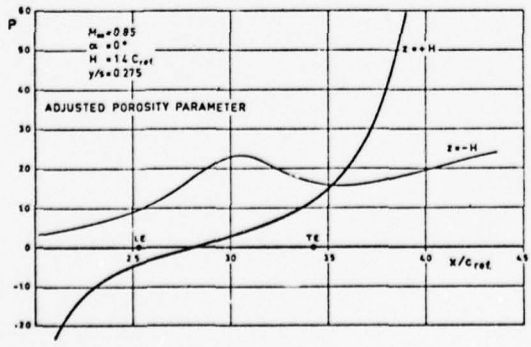

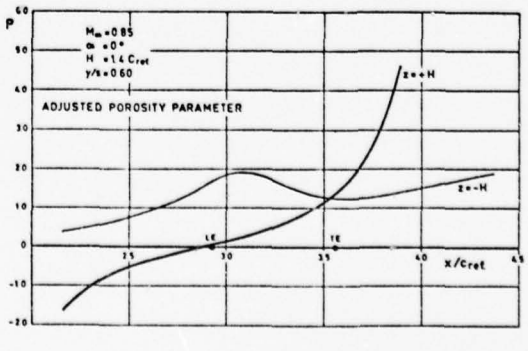

Figure 9: Adjusting of Porous Upper and Lower Wall to Get Interference Free Wind Tunnel Walls H = + 1.4 c_r

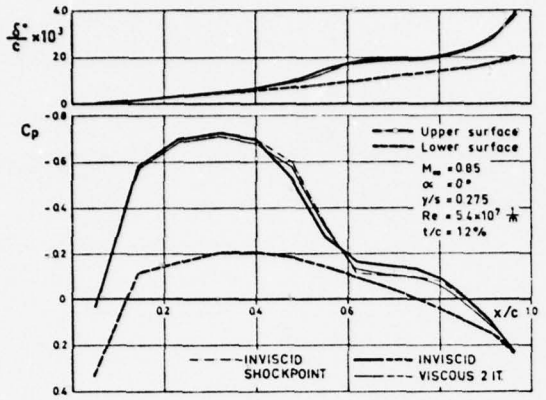

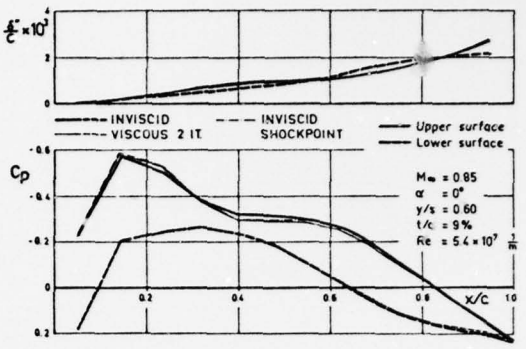

Figure 10 a-b: Influence of Viscous Effects and Shock Point Operator on Pressure Distribution and Shockposition

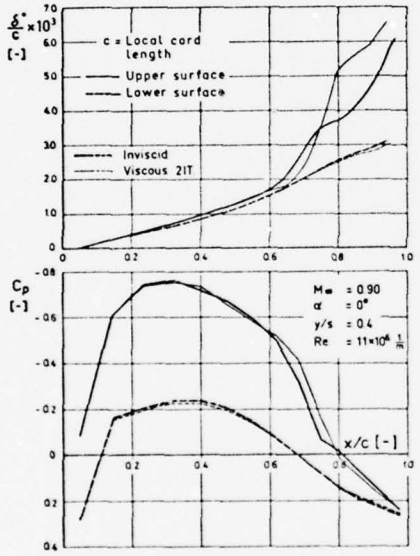

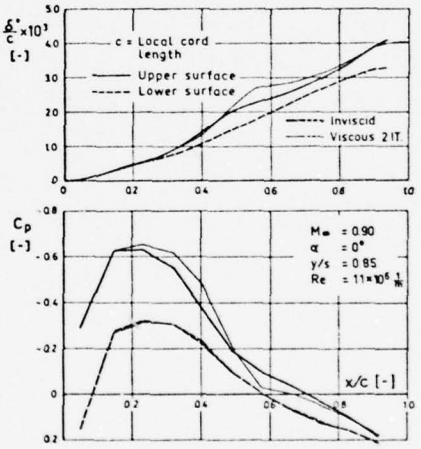

Figure 11 a-b: Influence of Viscous Effects on Pressure Distribution and Shockposition

ANALYSE DE FOURIER ET CORRELATION DE VITESSE EN AERODYNAMIQUE INSTATIONNAIRE

par

Pierre Gougat, Françoise Martin
Laboratoire d'Aérothermique du C.N.R.S.
4ter, route des Gardes
92190 - MEUDON (France)

RESUME

Le passage de l'état laminaire à l'état turbulent commence par l'apparition au sein de la couche limite d'instabilités naturelles constituées d'ondes sinusoïdales d'intermittence aléatoire.

Nous étudions la réponse de la couche limite à une vibration locale de paroi dans le but de supprimer le caractère aléatoire de cette intermittence.

Le signal sinusoïdal de déformation de la paroi est obtenu à l'aide d'un capteur capacitif de déplacement : le signal des fluctuations de vitesse dans la couche limite est donné par un anémomètre à fil chaud.

Ces deux informations peuvent être traitées séparément par analyse en temps réel, ce qui permet de mesurer le taux d'harmonique du signal de déformation et de déterminer la densité spectrale de puissance des fluctuations de vitesse.

Le traitement simultané des deux signaux se fait à l'aide d'un corrélateur en temps réel. A ce corrélateur est associé un transformateur de Fourier qui fournit le spectre mutuel des deux signaux.

Un enregistreur magnétique est utilisé pour stocker les signaux et les relire à faible vitesse ce qui facilite l'observation et l'étude des phénomènes instantanés.

1 INTRODUCTION. ETUDE

Le passage de l'état laminaire à l'état turbulent commence par l'apparition, au sein de la couche limite, d'instabilités naturelles.

Nous avons étudié le développement de ces instabilités principalement sur plaque plane. Elles sont constituées de trains d'ondes sinusoïdales intermittentes et modulées en amplitude, apparaissant de façon aléatoire dans la couche limite.

Puis, nous avons regardé l'influence d'une déformation locale de la paroi sur l'évolution de ces instabilités /1/. Une déformation, qu'elle soit en creux ou en saillie, provoque globalement une avance de la transition. A l'échelle des fluctuations de vitesse, nous remarquons que ce ne sont plus des ondes sinusoïdales qui se propagent dans la couche limite, mais nous avons des bouffées éclatées de fréquence quelconque. On voit apparaître des portions de signal de type "turbulent".

Nous étudions maintenant plus précisément la réponse de la couche limite soumise à une vibration locale de paroi dans le but de supprimer le caractère aléatoire de l'apparition des bouffées instables tout en conservant le caractère intermittent.

Nous voulons piloter l'apparition des bouffées instables par la vibration de la paroi de telle sorte que les instabilités apparaissent de façon périodique à la même fréquence que la vibration de la plaque.

Toute cette étude se fait par analyse spectrale des signaux de fluctuations de vitesse, par corrélation avec transformation de Fourier en temps réel. Les signaux de fluctuations de vitesse, d'une part, et de vibration de la paroi, d'autre part, sont traités individuellement par analyse spectrale. On en mesure aussi les valeurs moyennes et les valeurs efficaces (fig. 1).

2 DISPOSITIFS EXPERIMENTAUX

Les mesures sont faites dans une soufflerie subsonique de type Eiffel. La veine de section carrée (0,5 m x 0,5 m) a une longueur de 1 m. La vitesse de l'écoulement peut varier d'une façon continue de 4m/s à 30 m/s.

Le taux de préturbulence extérieure reste sensiblement constant et égal à 0,4 % pour des vitesses comprises entre 10 m/s et 25 m/s. Une analyse spectrale des fluctuations de vitesse de l'écoulement extérieur montre un spectre plat qui ne présente aucune singularité qui risquerait de perturber l'état laminaire de la couche limite.

L'étude des fluctuations de vitesse dans la couche limite est faite au voisinage d'une plaque plane à paroi déformable. La plaque (0,5 m x 1 m) est maintenue par quatre supports indépendants de la soufflerie. Elle présente un bord d'attaque elliptique d'allongement 12.

La paroi déformable sert de couvercle à un châssis métallique dans lequel trois cavités indépendantes et étanches ont été usinées. Chaque cavité a une longueur λ de 100 mm, et le début de la première cavité se situe à une abscisse x_o = 178 mm du bord d'attaque.

Ces cavités peuvent être alimentées en surpression ou en dépression, de telle sorte qu'il est possible d'obtenir une déformation de paroi en saillie ou en creux. La déformation ainsi obtenue a une

amplitude 2 a variant de + 1,5 mm à - 1,5 mm, sur 95 % de l'envergure de la plaque. La paroi ainsi déformée est proche d'une sinusoide de longueur λ = 100 mm et d'amplitude 2 a.

Ce système permet une grande souplesse de manipulation et de réglage de la déformation pour l'étude statique.

Nous avons maintenant aménagé un dispositif permettant de faire vibrer la partie déformable de la plaque.

Nous gardons les sources de surpression et de dépression qui alimentent la cavité en passant par un boisseau tournant entraîné par un moteur. Un capteur potentiométrique couplé avec le moteur donne un signal de rotation de celui-ci.

L'amplitude de la déformation statique de paroi et le signal de vibration, dans le cas d'une déformation non permanente, sont donnés par un capteur capacitif de déplacement.

Les mesures de fluctuations de vitesse dans la couche limite sont faites à l'aide d'une sonde miniature à film chaud.

Un dispositif de déplacement permet un réglage en ordonnée au 1/10 de mm, et en abscisse, au mm. L'ensemble du dispositif repose sur un support indépendant de la veine de la soufflerie afin d'éviter les vibrations de la sonde.

3 CHAINE D'ANALYSE. CORRELATION. TRANSFORMATION DE FOURIER

L'analyseur de spectre accomplit l'analyse de Fourier de la fonction d'entrée. Cette analyse s'effectue en temps réel, ce qui signifie que chaque échantillon de signal est pris en charge dès sa présentation et subit intégralement le traitement d'analyse indépendamment des processus déjà en cours sur d'autres échantillons.

Le signal passe dans un filtre passe bas et est converti en données numériques par échantillonnage à une fréquence de numérisation triple de la fréquence maximale de la gamme d'analyse choisie. Les données numériques sont introduites chronologiquement dans un registre mémoire qui, par décalages successifs des instants d'échantillonnage, fait circuler toutes les données à un rythme K fois plus rapide que la vitesse d'acquisition. On définit ainsi, pour une gamme d'analyse donnée, le coefficient K de compression de temps. Le signal issu de la mémoire présente un spectre de fréquences K fois plus élevées que le spectre initial et, après reconversion numérique analogique, passe dans un filtre hétérodyne à bande étroite. La compression de temps autorise une plus grande vitesse d'analyse tout en conservant une bonne précision statistique. La durée d'analyse est K fois plus faible que dans un processus d'analyse directe. La synchronisation de toutes les fonctions discontinues, échantillonnage, décalages dans la mémoire, reconversion analogique, avance pas à pas de l'hétérodynage, est assurée par une horloge interne.

La résolution de l'appareil est de 200 lignes. Chaque analyse complète est effectuée en 40 millisecondes. A titre d'exemple, pour une gamme d'analyse de 1 kHz, la résolution est de 5 Hz, et le temps d'acquisition est de 200 millisecondes. La présentation du défilement des échantillons dans la mémoire se fait sur une base de temps de 200 microsecondes. L'emploi d'un oscilloscope à deux bases de temps permet la visualisation simultanée du contenu de la mémoire et du résultat de l'analyse. Sur l'une des bases de temps la trace représente l'évolution temporelle du contenu de la mémoire dans des axes amplitude-temps. Sur l'autre base de temps, la seconde trace de l'oscilloscope correspond à l'évolution du spectre instantané dans des axes énergie-fréquence. Cet artifice de présentation est intéressant dans le cas de phénomènes intermittents : on est amené à observer soit les évolutions simultanées du contenu de la mémoire et du résultat de l'analyse sur un film, soit le blocage en mémoire d'un transitoire et de son analyse instantanée pour une photographie.

Il faut noter enfin que la sortie de l'analyseur est équipée d'un intégrateur numérique effectuant la moyenne temporelle d'un certain nombre de spectres instantanés successifs.

La fonction de corrélation détermine le degré de similitude entre deux fonctions décalées l'une par rapport à l'autre dans le temps. Elle est définie mathématiquement par :

$$f_{xy}(\tau) = \lim_{T \to \infty} \frac{1}{2T} \int_{-T}^{+T} x(t) \cdot y(t+\tau)\, dt \ ;$$

l'appareil multiplie point par point la fonction d'onde x(t) par une autre fonction d'onde décalée dans le temps $y(t+\tau)$, puis effectue la sommation ordonnée des produits pendant le temps T.

Les signaux x(t) et y(t) sont échantillonnés et convertis en données numériques à des intervalles de temps égaux au retard élémentaire τ choisi. A chaque étape d'échantillonnage, un même échantillon de x est multiplié par 100 échantillons de y arrivés dans la mémoire aux instants τ, 2 τ ..... 100 τ précédents ; les 100 multiplications sont faites avant l'arrivée d'un nouvel échantillon.

Les calculs des 100 points de mesure ainsi définis peuvent être considérés comme simultanés ; le retard τ peut varier de 1 µs à 1 s.

Un décalage de 0 à 200 τ, mis en place par section de 50 τ, permet d'étudier la fonction de corrélation symétriquement autour du zéro ou bien à des temps éloignés de zéro.

Le transformateur de Fourier, associé au corrélateur en temps réel, donne à l'ensemble de la chaîne de traitement des signaux des possibilités d'exploitation immédiate des fonctions d'intercorrélation. Le calcul de base de la transformée de Fourier est donné mathématiquement par les relations suivantes :

la Partie réelle $$a_n = \sum_k f_{xy}(k\tau) \cos\left(\frac{2\pi k n}{N}\right) ;$$

la Partie imaginaire $$b_n = -\sum_k f_{xy}(k\tau) \sin\left(\frac{2\pi k n}{N}\right)$$

Les valeurs de $f_{xy}(k\tau)$ sont les 100 valeurs obtenues à la sortie du corrélateur, k variant de 0 à 99 pour une valeur de τ choisie. La gamme maximale de fréquence est de 1 MHz. Une interpolation permet une sortie sur 1 000 points.

La fonction ainsi obtenue est une quantité complexe dont les parties réelle, imaginaire, le module, la phase peuvent être séparément présentées en fonction de la fréquence ou deux à deux en représentation paramétrique.

4 OBSERVATION DES SIGNAUX DE FLUCTUATIONS DE VITESSE

L'observation du signal des fluctuations de vitesse donné par l'anémomètre à film chaud est source de nombreuses informations nécessaires à la compréhension du phénomène de transition.

Dans l'étude des instabilités naturelles de la couche limite au voisinage de la plaque plane, nous avons observé le signal des fluctuations de vitesse par visualisation directe sur oscilloscope des informations données par le fil chaud /2/. Nous observons un signal laminaire avec des bouffées instables sinusoïdes de fréquence f modulées en amplitude, apparaissant de façon intermittente et aléatoire.

En passant par la mémoire d'entrée de l'analyseur, il nous est possible de bloquer le défilement du signal pour ne conserver en mémoire qu'une portion de signal visualisée sur l'oscilloscope (fig. 2).

Mais le défilement du signal donné par le fil chaud est très rapide, ce qui rend difficile le blocage précis d'une bouffée instable.

Nous enregistrons le signal sur bande magnétique à une vitesse de 60 ips. Nous pouvons alors relire le signal enregistré à faible vitesse soit 1 7/8 ips. Le rapport 32 entre ces deux vitesses permet de sélectionner au passage les bouffées intéressantes et de les bloquer en mémoire.

Il est intéressant pour l'étude des bouffées instables de visualiser simultanément la mémoire de l'analyseur, donc le signal des fluctuations de vitesse, et la sortie de l'analyseur qui donne le spectre instantané de la portion de signal contenue en mémoire. Nous observons ainsi une bouffée instable et son spectre instantané.

Par ailleurs, nous pouvons accumuler durant un intervalle de temps déterminé des spectres instantanés pour avoir le spectre intégré d'une portion de signal.

Sur le film projeté, nous présentons le signal instantané des fluctuations de vitesse donné par le fil chaud obtenu dans la couche limite sur plaque plane et les spectres instantanés de chaque portion de signal contenue dans la mémoire de l'analyseur.

Nous avons donc un signal de fluctuations de vitesse représentant la quantité u' en fonction du temps et le spectre correspondant, soit l'énergie des fluctuations en fonction de leur fréquence.

Nous procédons de la même façon pour faire l'observation du signal des fluctuations de vitesse en présence d'une déformation statique de la paroi. Le signal n'est plus le même, et nous observons un signal d'aspect turbulent. Il n'y a plus de bouffée instable sinusoïdale, de même qu'on ne peut plus déceler de fréquence caractéristique.

Si nous soumettons la couche limite à une vibration de paroi de faible fréquence, soit 1 Hz environ, de telle sorte que l'amplitude de la déformation varie en signal carré de 0 à + 1 mm, le signal des fluctuations de vitesse passe d'un état qu'on peut qualifier de laminaire, correspondant au zéro d'amplitude, à un état dit turbulent pour le maximum de déformation.

L'enregistrement en parallèle mais non simultané sur deux pistes différentes des signaux obtenus sur plaque plane et sur plaque déformée permet, en les visualisant simultanément, de différencier, à la lecture, les états laminaires et turbulents de la couche limite.

L'enregistrement simultané du signal de vibration de paroi et du signal de fluctuations de vitesse permet, en les relisant, d'étudier la corrélation qui les lie.

5 CORRELATION DU SIGNAL DES FLUCTUATIONS DE VITESSE ET DU SIGNAL DE VIBRATION DE PAROI

La corrélation qui existe entre les fluctuations de vitesse dans la couche limite et la vibration de paroi apparaît clairement dans l'étude simultanée des signaux donnés par le fil chaud et le capteur de déplacement. Mais une étude précise de cette corrélation est entreprise à partir de la fonction de corrélation des deux grandeurs physiques correspondantes, u'(t) fonction des fluctuations de vitesse au cours du temps et a(t) amplitude instantanée de la déformation de paroi. La fonction de corrélation s'écrit :

$$f(\tau) = \lim_{T\to\infty} \frac{1}{T} \int_0^T a(t)\, u'(t+\tau)\, dt.$$

L'étude de la fonction de corrélation se fait naturellement de pair avec une transformation de Fourier qui donne le spectre mutuel des deux quantités physiques.

Il existe un déphasage entre la réponse de la couche limite dans la zone de transition, donc à l'aval de la déformation de paroi, et la vibration de la paroi elle-même.

Nous avons remarqué qu'une déformation statique de la paroi, qu'elle soit en saillie ou en creux, provoque une avance globale de la transition, cette avance n'étant pas tout à fait la même pour les deux cas (fig. 3).

Pour une période de vibration, nous avons deux avances de la transition. La réponse de la couche limite à la vibration de paroi se fait donc à une fréquence double de la fréquence sollicitatrice F. Nous obtenons une corrélation des deux signaux à la fréquence 2 F si nous prenons la précaution de redresser le signal de vibration de la plaque pour en doubler la fréquence (fig. 1).

Mais nous conservons une corrélation à la fréquence F due à la dissymétrie des avances de la transition provoquée par une déformation positive et négative.

6 CONCLUSION

Les premiers travaux relatifs à cette étude nous avaient amenés à traiter sur ordinateur les signaux de fluctuations de vitesse dans l'optique d'une analyse spectrale. Cette démarche s'est avérée infructueuse, non pour des raisons théoriques, mais, d'une part, à cause de la complexité des signaux et, d'autre part, à cause des temps de numérisation. L'absence de couplage direct sur ordinateur n'était qu'un ennui secondaire.

Par contre, cette chaîne d'analyse et de corrélation semble parfaitement adaptée à nos besoins, et l'adjonction prochaine d'une perforatrice de ruban augmentera encore les possibilités de traitement des signaux physiques.

REFERENCES

/1/ S. BURNEL : "Influence d'un gradient de vitesse sur l'amplification des fréquences naturelles dans une couche limite". Thèse de 3ème Cycle. Paris (21 mars 1972)

/2/ P. GOUGAT, F. MARTIN : "Observation et analyse spectrale des signaux instantanés des fluctuations de vitesse dans la couche limite laminaire". C.R. Acad. Sc., Paris, t. 275, A, 1011 (13 novembre 1972)

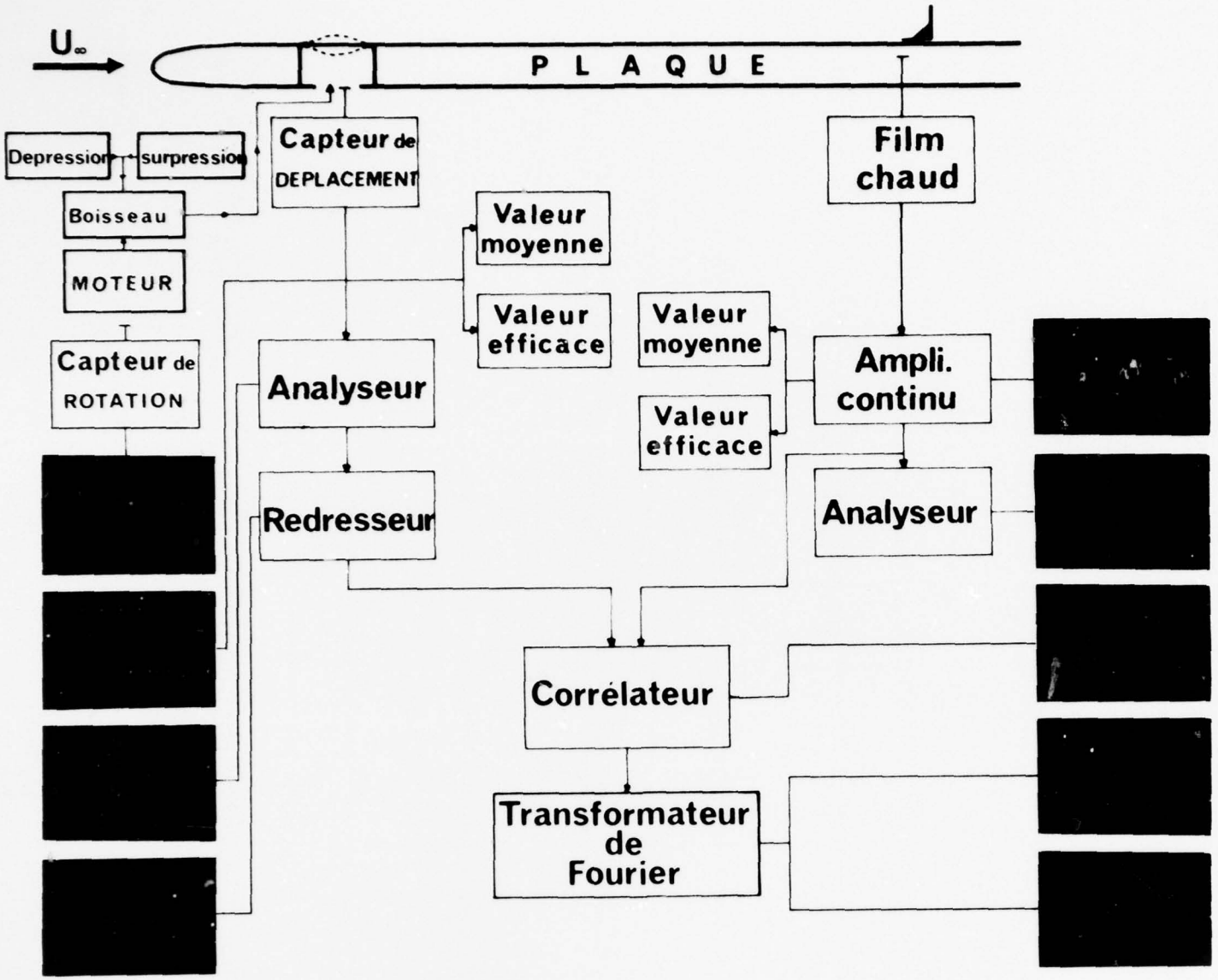
U∞
PLAQUE
Depression
surpression
Boisseau
MOTEUR
Capteur de ROTATION
Capteur de DEPLACEMENT
Film chaud
Valeur moyenne
Valeur efficace
Analyseur
Redresseur
Valeur moyenne
Valeur efficace
Ampli. continu
Analyseur
Corrélateur
Transformateur de Fourier

Fig . 1

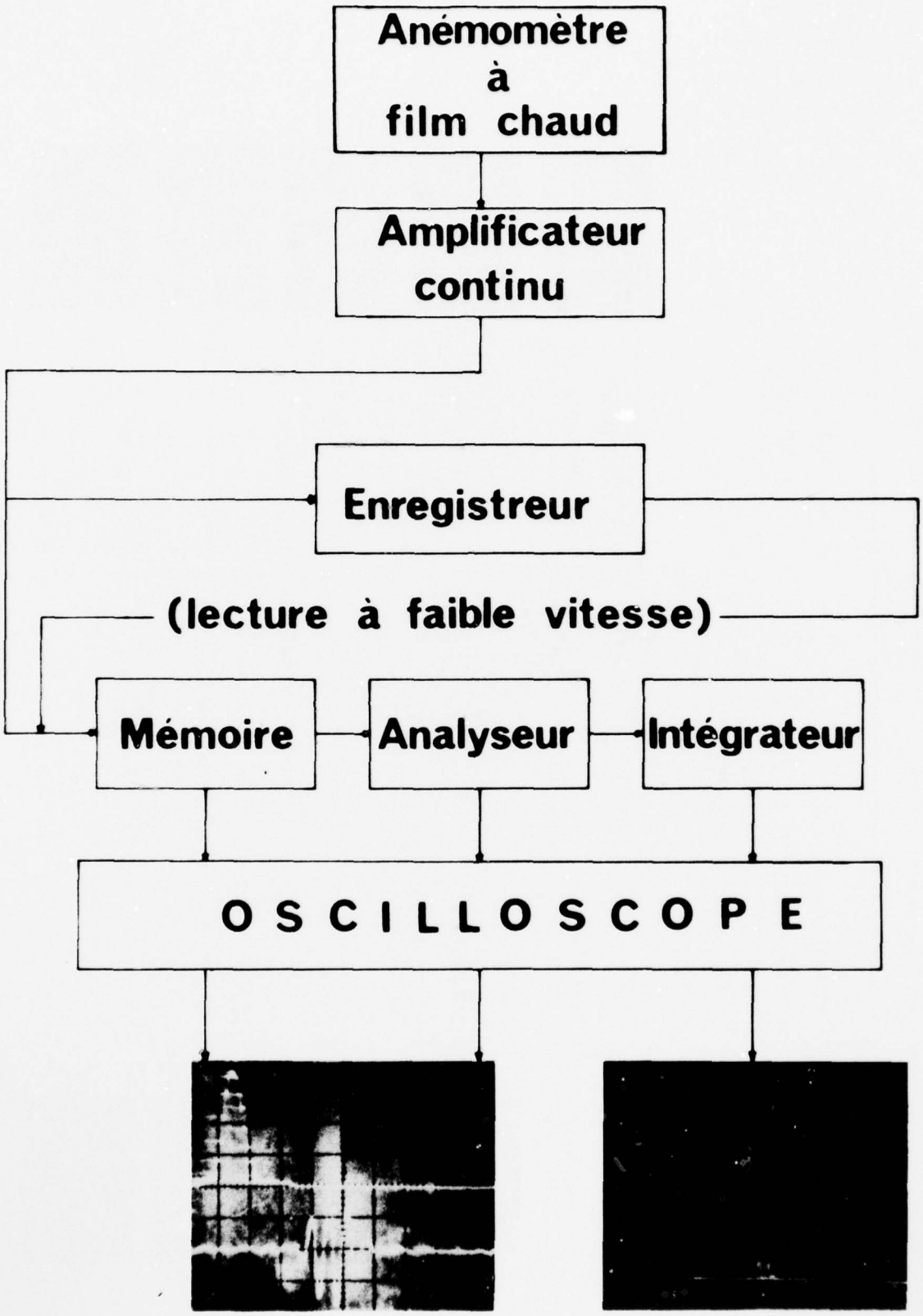
Anémomètre à film chaud
Amplificateur continu
Enregistreur
(lecture à faible vitesse)
Mémoire
Analyseur
Intégrateur
O S C I L L O S C O P E

Fig. 2

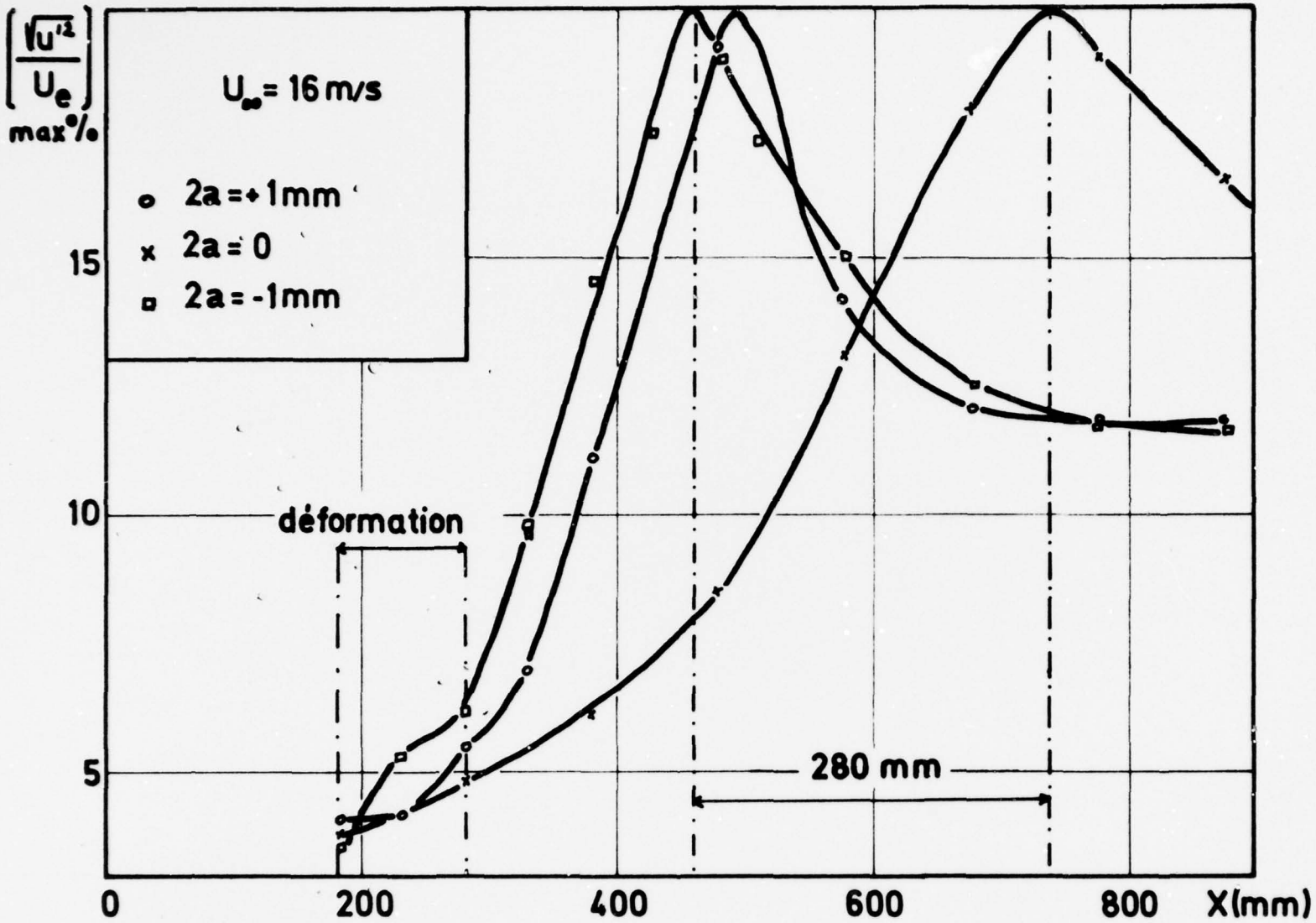
$\left[\frac{\sqrt{u'^2}}{U_e}\right]_{max}$%
U_∞ = 16 m/s
o 2a = +1mm
x 2a = 0
□ 2a = -1mm
15
10
5
déformation
280 mm
0
200
400
600
800
X(mm)

Fig. 3

PICKING UP AND GRAPHING OF THREE DIMENSIONAL FLOW FIELDS

by

H. -J. Graefe

Deutsche Forschungs- und Versuchsanstalt
für Luft- und Raumfahrt E. V.

Bunsenstraβe 10
D - 3400 Göttingen, (German Federal Republic)

Summary

This paper describes an efficient test technique for three-dimensional flow field measurements which was set up in combination of a conventional measurement technique with modern electronical equipment.

The test rig is installed in the low speed wind tunnel of DFVLR in Göttingen.
Some suggestions for graphic representations of three-dimensional flow fields are given by hand of examples.

Notation

x	mm	
y	mm	Position coordinates of the field
z	mm	
d_j	mm	Nozzle exit diameter
D	mm	Fuselage diameter
α	degrees	Angle between the local flow vector lying in the x, z-plane and the direction of undisturbed flow
β	degrees	Angle between the local flow vector lying in the x, y-plane and the direction of undisturbed flow
$\xi = x/d_j$		Dimensionless coordinates of the field
$\eta = y/d_j$		
$\zeta = z/d_j$		
q_∞	kp/m^2	Dynamic pressure of the flying speed
v_∞	m/sec	Flow velocity
q_j	kp/m^2	Dynamic pressure of the jet
$\varphi = q_j/q_\infty$		Dynamic pressure ratio
$\vartheta = T_j/T_\infty$		Temperature ratio

Indices

∞	Undisturbed flow
j	Flow in the jet

Picking up and Graphing of Three-Dimensional Flow Fields

1. Introduction

For investigations of new aerodynamic problems in a subsonic flow which will exclusively be considered here and in wind tunnel tests on complicated models as to be found in industrial aerodynamics, detailed informations are required about the steady flow behaviour in the vicinity of the model. The well known methods of flow visualization as by small tufts or smoke are indeed offering a way to get a quick general view over the flow field. For more accurate flow field analysis those methods are not sufficient however in most cases. Quantitativ results can only be obtained from real flow field measurements which enable to determine the three-dimensional distribution of the various parameters separately. Since several years there were systematical flow field measurements performed in the low speed wind tunnel of DFVLR in Göttingen. By an appropriate lay-out of electronical equipment in combination with a conventional measurement technique and automatical data reduction an efficient test rig was set up which enables to realize the normally very time-wasting investigations of three-dimensional flow field in a proper

time.

2. What is important for effectiveness of three-dimensional flow field investigations ?

At first I want to sketch the substantial postulations for an economical performance of flow field measurements (Fig. 1).

2.1 Measuring method

This is not the place to discuss about the advantages or disadvantages of single measurement methods. Nevertheless the whole instrumentation, the procedure, the data reduction and last not least the usefulness of the results are dependent on the applied test technique. The wide field of a large low speed wind tunnel demands a universal testing method by which all the parameters of the flow like pressures, velocities, temperatures and so on can be picked up completely and simultaneously.

The system has to be quickly ready to act which means the effort for calibration and adjustment and so on should be as low as possible.

If you go back to measurement methods with physically clear relation between the in-put and the out-put of the system you will get an easier data reduction. The results will become better reproducible and by that the general information will be more safe, too.

2.2 Data recording and processing

There is a great number of data which is produced by three-dimensional flow field measurements. Therefore it is important to have a sufficient electronical equipment for quick digital recording and processing by on-line. Besides of this, the flow field measurements are nearly always planned and performed as pilot measurements. It is essential that the data reduction and the out-put of the results are ensuing simultaneously with the recording of data to produce a continuous flow of information which is necessary for the control of the run-down of the measurements.

2.3 Positioning of the probe

As you know, a three-dimensional field can be felt out either point by point or continuously in a single cross section. For this you will need a sufficient translator. It must work with high velocity and must put out clear signals and data processable signals about the probe position.

2.4 Data reduction

Last not least a suitable representation of the results is important for the success of the investigation. How is it possible to give an instructive representation, referring also to the problem of a three-dimensional vector field ?
For this, there are various suggestions :

1. Representation of single parameters by isolines (isothermes, isotaches, isobars)
2. Representation of the local flow vector by arrows
3. Representation by stream-lines
4. Perspective representation of single parameters with their amount

In combination with the above mentioned two-dimensional representations there is the other problem: How is it possible to make three-dimensional effects evident ? Later on, I will point out further details.

3. Description of a suitable test rig

By the continuous accomodation on the increasing demands in the test technique there was installed a testing stand in Göttingen which satisfies the mentioned conditions rather well. The next figures (2 and 3) give the schematic description of the system after the actual situation.

3.1 Mechanical part of the system

The total pressure p_t, the static pressure p_{st}, the two differential pressures p_α and p_β for measuring the flow direction are picked up by a nine hole direction probe (Fig. 2). The flow temperature T is taken by a thermo couple which is mounted inside of the p_t-pressure pipe. The extension and design of the tiny probe head (Fig. 3) enables nearly punctual measurements. The interferences on the flow caused by the probe are neglectible. The probe is mounted on a support for automatical and very accurate positioning in x, y, z-direction of the whole space of 3 x 3 x 6 m wide wind tunnel test section. The probe can also rotate around its shaft axis. The translator is driven by stepping motors. One of the two angles of the flow vector can be determined by rotating the probe into flow direction. All the other values will be determined out of calibration curves. The maximum rotating angle of the probe is $\pm 180^\circ$ so that the reverse flows and even quasi stationary vortexes in the flow behind a body can still be picked up.

3.2 Electrical part of the system

Probe positioning is managed by programme control. In this way a two-dimensional field with numerous positions can be reached automatically point by point in a short time.
The differential pressure between both pressure holes which are lying in the plane of rotation of the probe is p_α. It is the in-put for a probe rotation control system which keeps the probe automatically staying parallel to the projection of the local flow vector in this plane. The angle of rotation indicates the angle of inclination α. The accuracy of probe adjusting can be varied by amplifying the in-put within a certain range. If the gradient of the flow vector is low, it is also possible to move the probe continuously with a suitable velocity while data will be picked up in a corresponding way. For each probe position all data of flow and probe positioning are picked up simultaneously and read on-line by a central computer. All other data which are necessary for the calculation of the local pressure p_{st} and p_t and the local temperature T as well are stored in the computer. An extensive computer programme is available to adapt data reduction, out-put of results and the process of control to many various questions and conditions of experiments. The whole process is working in real time. The out-put of the results can simultaneously be received from a printer in form of lists and from a plotter or a graphic display in form of diagrams or another manner of graphic representation. Especially the out-put on a graphic display is very advantageous. This device makes it possible to put out various graphic representations of the flow simultaneously with the measurements. This enables the testing engineer to get an idea of the flow already during the measuring phase.

4. Some suggestions for graphic representation of three-dimensional flow fields

4.1 Representation by isoclines

Isocline representation is a very good way to demonstrate flow directional distributions. The following plots (4 and 5) are showing the directional distribution of the vector of velocity in a flow field which is generated by a cross blown jet.
In this case there are plotted lines of equal inclination (that means α = const.) of the flow vector against the undisturbed flow. The advantage of this manner of representation is that the plane of drawing can be selected independently of amount and direction of the vector that should be represented. This makes possible to demonstrate the directional distribution of a vector - here a velocity component - in each plane of the three-dimensional field. Representations in only one plane of section through the flow field can give a three-dimensional idea to the observer because the assigned angle indicates the resultant direction of component and not only its projection into the plane. This figure (4) shows the plane of symmetry of the above mentioned flow field. There is a free jet generated by cold compressed air emerging vertically out of a cylindrical fuselage. The dynamic pressure ratio q_j/q_∞ is 36 and the jet Mach number M_j is 1, the jet diameter d_j = 45 mm. You can clearly separate three regions of interest.

1. An aera of upward directed flow in front of the jet with positive angles
2. The aera of the jet itself which is recognizable by 90^o limit
3. The aera of reverse flow in the dead water of the jet with angles greater than 90^o

Figure 5 gives a horizontal section at $z/d_j = 2$ through the same flow field. In the figure before, the jet axis was situated in the plane of representation while now there is shown a plane of cross section which is situated vertically to the nozzle axis. This pattern gives an idea of the directional distribution over the wideness of the aera. The three significant parts of the flow field are recognizable again. The up wash aera which as we see later is induced by a pair of vortexes in rear part of the jet extends to both sides and only slowly dies away.
Plots of planes more distant from the origin which cannot be shown here are giving an idea of the far reaching up wash flow.

4.2 Representation of stream lines

Stream lines are as know obtained by integration of directional fields. The three-dimensional coordinates of points on one stream line are following from the formulars in figure 6, if we accept that in a sufficient small interval the velocity ratios $v_y/v_x = f_i(\xi_i) = \text{const.} = \tan\beta$ and $v_z/v_x = g_i(\xi_i) = \text{const.} = \tan\alpha$ is valid.
By help of data processing it is easily possible to satisfy this condition. ξ_o and ζ_o are independent selectable starting coordinates of the stram line. α and β are the angles of direction of the flow vector. The examples of representation shown in the next two figures are giving again the flow field of a cross blown jet. Figure 7 shows the stream lines in the plane of symmetry corresponding to the above mentioned isocline field and in figure 8 a horizontal plane is plotted. For sake of clearness of the demonstration a two-dimensional representation was taken. That means the vertical component of the flow vector is neglected. This simplification is allowed in the greater part of the plane where the vertical component is small. The region of the vertical flow of the jet is saved. The stream lines disappear when the amount of the vertical component increases. It is however also possible to have a perspective representation of single stream lines for example stream lines inside of a vortex. Stream lines are especially useful because they are rather evident. Besides, it is a way to compare experimental results with potential theoretical works about flow problems.

4.3 Representation of the flow vector by arrows

Another very evident graphic representation can be seen in figure 9. Herein the projection of the velocity vector on the drawing plane is plotted with its direction and its amount. The plot is again treating the flow around a cross blown jet. We see a plane of cross section which is rather far from the origin in a region where the jet is completely developed. The represented component of the velocity gives an idea of the vortexes on the rear side of the jet.
By this picture we can understand how the up wash flow which already could be watched in the above isocline fields is generated. On its boundary the vortex is mixed with the industurbed flow. By this the flow gets a rotation impuls which leads to the resultant up wash.
This vector representation is suited for real time plotting as well. It is therefore a very good help to control measurements.

4.4 Representation by isotaches

Figure 10 contains the velocity distribution in a cross section through a cross blown hot jet. The assigned data indicate the velocity ratio v/v_∞ of the resultant local flow and the undistrubed flow. Both aeras of low intensity flow are in front and the rear part clearly recognizable. The kidney shaped deformation of the original circular jet is represented pretty well.

4.5 Representation by isothermes

Out of the simultaneously picked up temperature data figure 11 was plotted. The assigned temperature ratio T/T_{max} follows from the local measured temperature T in relation to the jet temperature T_{max} taken at the origin.

4.6 Perspective representation of parameters after their amount

At the end there still should be mentioned a possibility of perspective plotting. Sometimes a perspective graph of three-dimesnional distribution of parameter amounts can be useful. The example (Fig. 12) shows the longitudinal component of the velocity around the cross blown jet in a cross section corresponding to the isotaches field. This kind of representation will only be useful in a few special cases and therefore I don't want to give a more detailed description.

5. Conclusion

The described measurement method is very versatile. Each of the above mentioned manners of representation of flow fields is giving special information for various questions which can appear in combination with three-dimensional steady flows. If all representations are applied on one problem they can give a far reaching answer.

6. References

1. Graefe, H.-J. Analysis of the flow field of cross blown lifting jets by flow field measurements ESA TT - 165 1975
2. Graefe, H.-J. Vermessung des Außenfeldes quer angeblasener Strahlen DLR-Mitt. 74 - 18 pp. 2 - 1 to 2 - 30
3. Harms, L. Untersuchungen über das Strömungsfeld eines heissen querangeströmten Strahles DLR Mitt. 74 - 18 pp. 8 to 40 1974

DATA RECORDING

1. Application of a suitable measuring method for picking up all characteristic data (P_t, P_{st}, T, V)

2. Equipment for extensive three-dimensional probe positioning

3. Sufficient electronical equipment for
   - quick digital measurements of up to 20.000 values per measuring plane
   - control of instrumentation
   - real time data reduction

DATA REPRESENTATION

1. Referred to problem and instructive representation

2. Possibilities of representation
   - isolines
   - vectors
   - stream lines (two- and three-dimensional)
   - perspective representation of parameter amounts

3. How is it possible to make three-dimensional effects evident ?
   - representation of selected cross sections
   - three-dimensional perspective representation

Fig. 1

What is important for effectiveness of three-dimensional flow field investigations ?

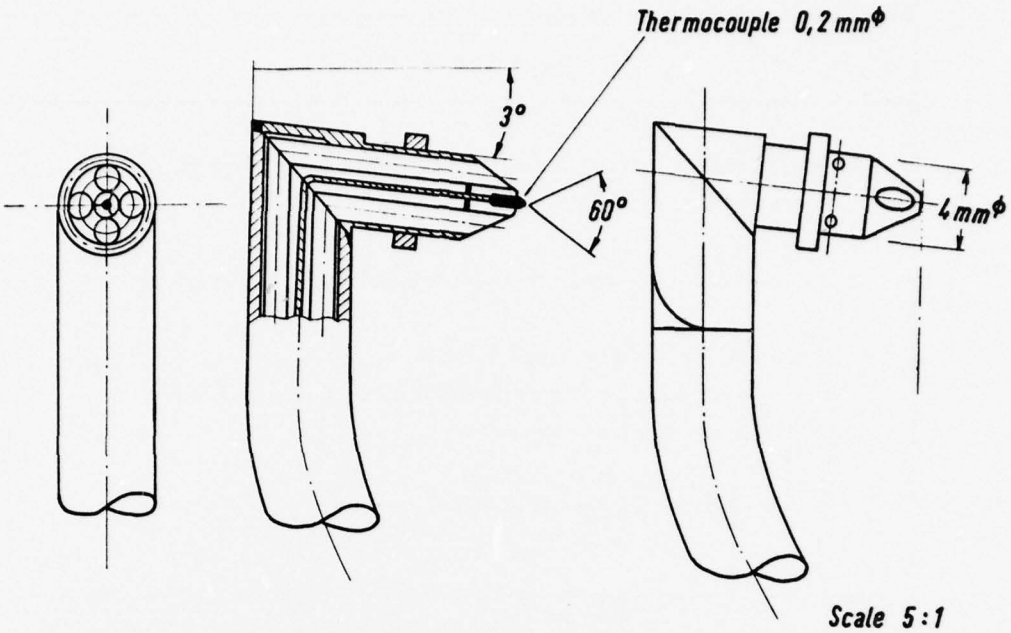

Fig. 2: Head of a 9-hole directional probe with thermocouple

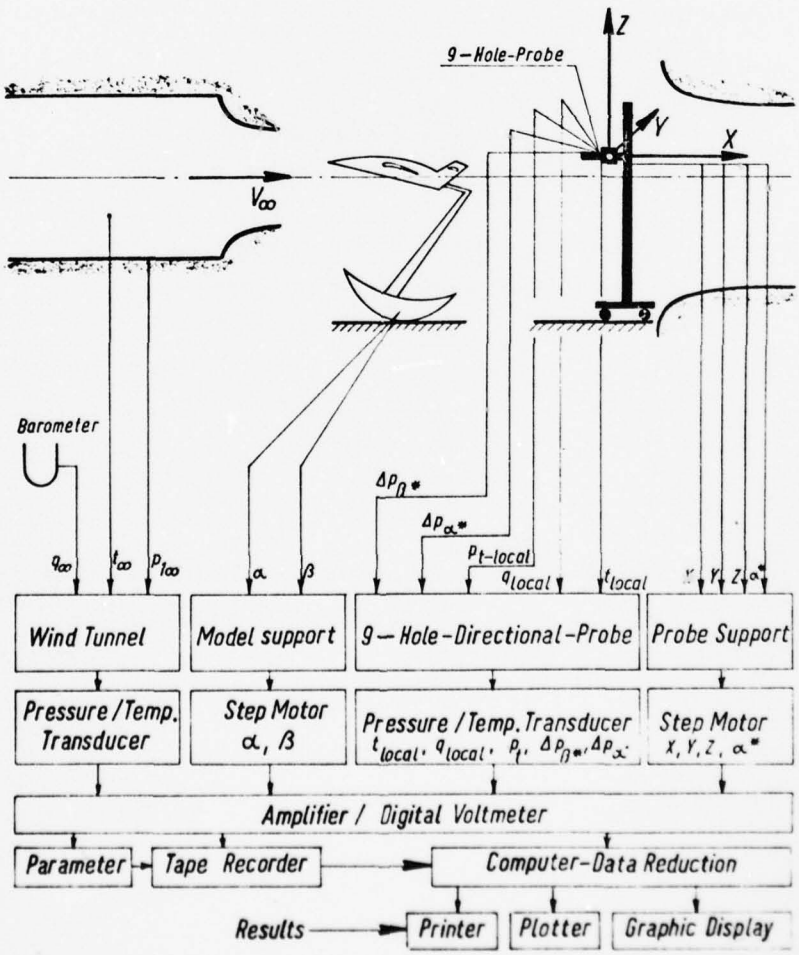

Fig. 3 : Schematic representation of a test rig for flow measurements

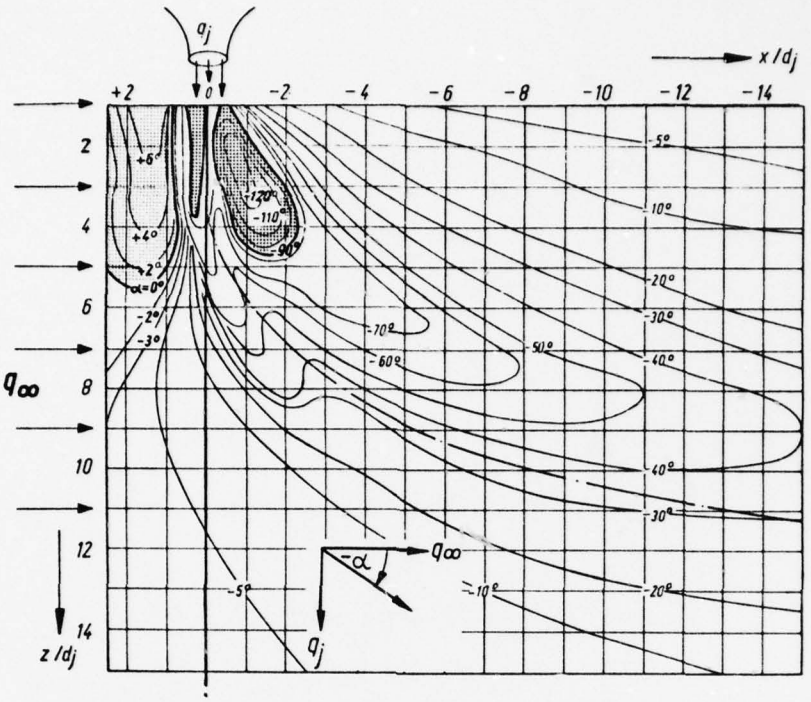

Fig.4 : Cross blown jet. Flow field in the plane of symmetry represented by isoclines (α = const.) $q_j/q_\infty = 36$, $M_j = 1$

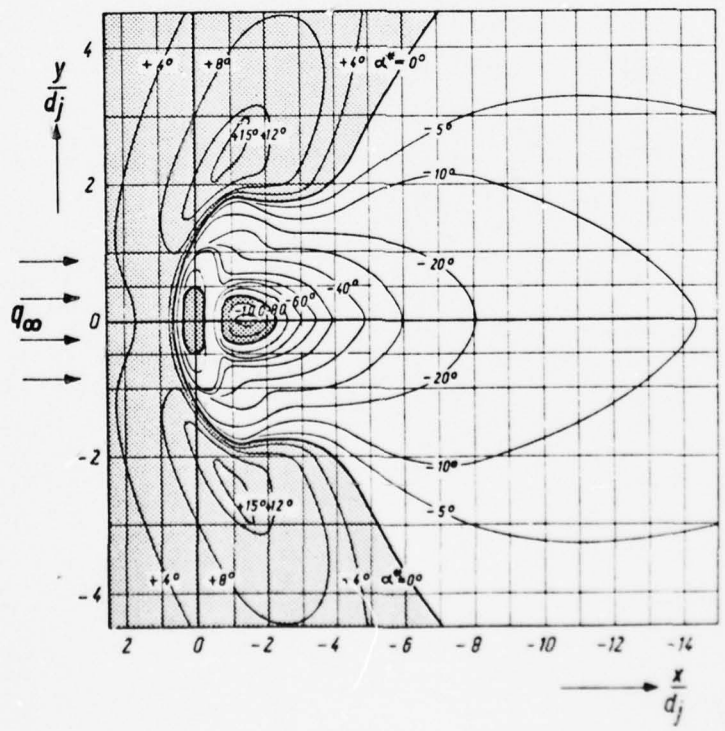

Fig.5 : Cross blown jet. Inclination of the flow vector in a horizontal plane at $z/d_j = 4$. $M_j = 1$, $q_j/q_\infty = 36$

AD-A034 324 ADVISORY GROUP FOR AEROSPACE RESEARCH AND DEVELOPMENT--ETC F/G 14/2
NUMERICAL METHODS AND WINDTUNNEL TESTING.(U)
OCT 76

UNCLASSIFIED AGARD-CP-210 NL

3 OF 3
AD-A
034 324

END
DATE
FILMED
2-15-77
NTIS

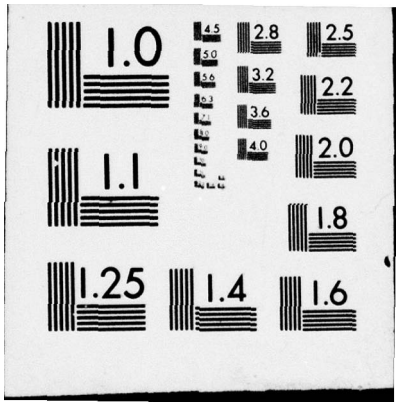
1.0
1.1
1.25
1.4
1.6
1.8
2.0
2.2
2.5
2.8
3.2
3.6
4.0
4.5
5.0
5.6

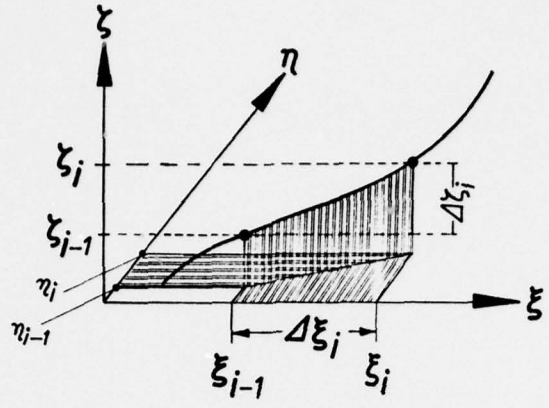

$$\xi_i = \int_0^{\Delta\xi} d\xi = \xi_{0i} + \Delta\xi_i$$

$$\eta_i = \int_0^{\Delta\xi} f_i(\xi_i)\, d\xi = \eta_{0i} + \tan\beta_i \cdot \Delta\xi_i$$

$$\zeta_i = \int_0^{\Delta\xi} g_i(\xi_i)\, d\xi = \zeta_{0i} + \tan\alpha_i \cdot \Delta\xi_i$$

Fig. 6

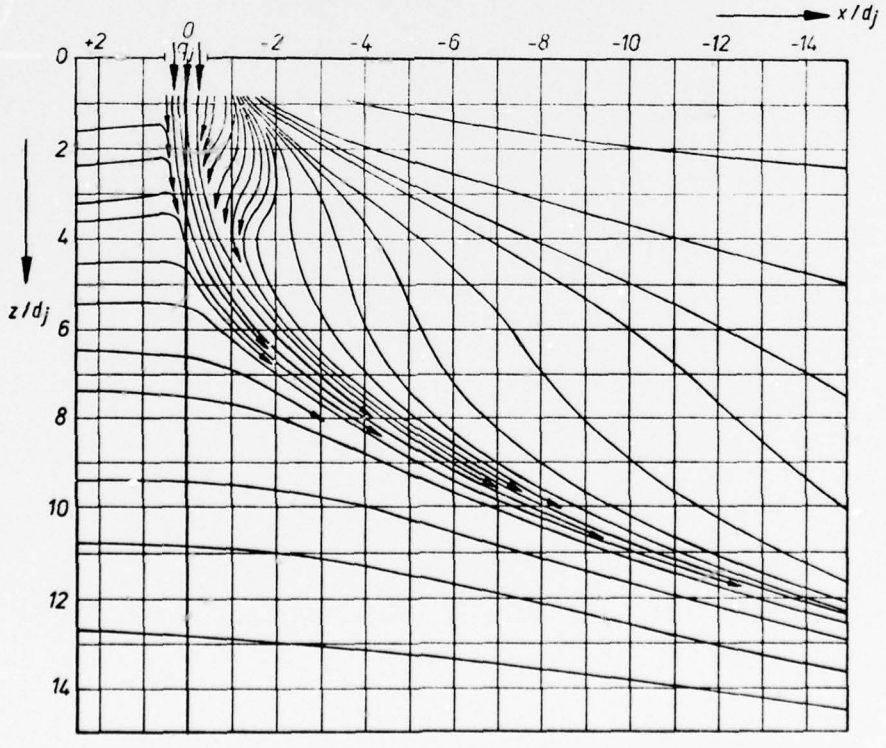

Fig. 7 : Cross blown jet. Streamlines in the plane of symmetry
$q_j / q_\infty = 36$, $M_j = 1$, $d_j = 45$ mm

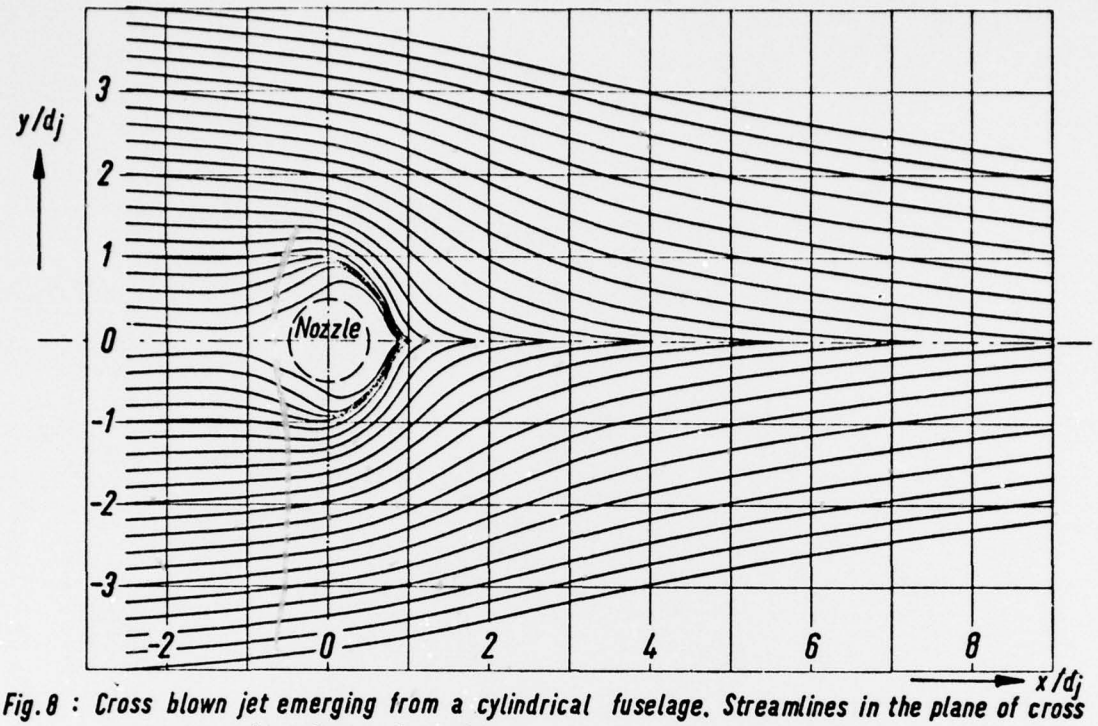

Fig. 8 : Cross blown jet emerging from a cylindrical fuselage. Streamlines in the plane of cross section at $z/d_j = 1$. $q_j/q_\infty = 36$

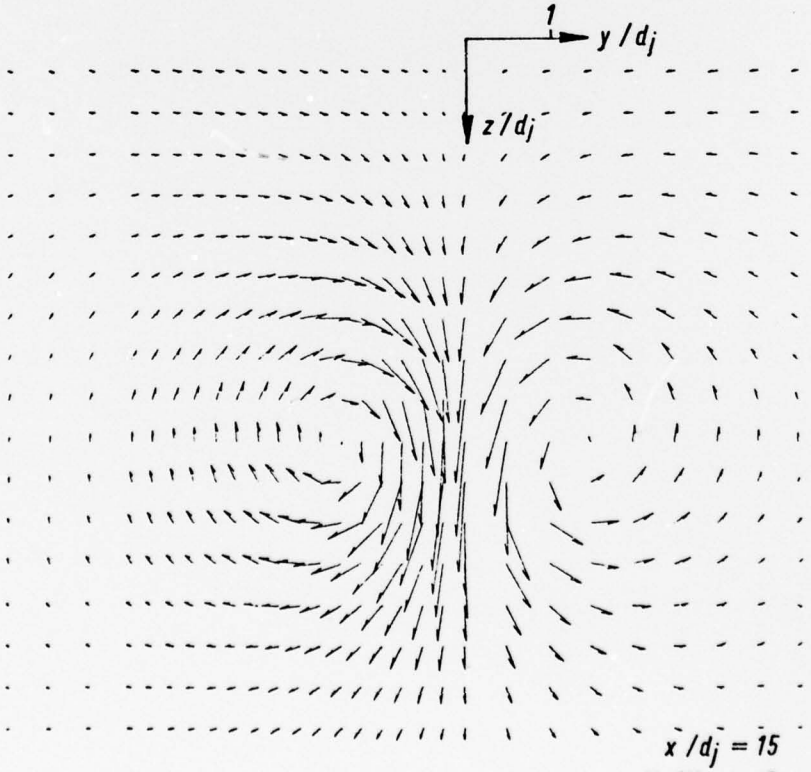

Fig. 9 : Cross blown jet.
Vector field of the flow in a y–z–plane

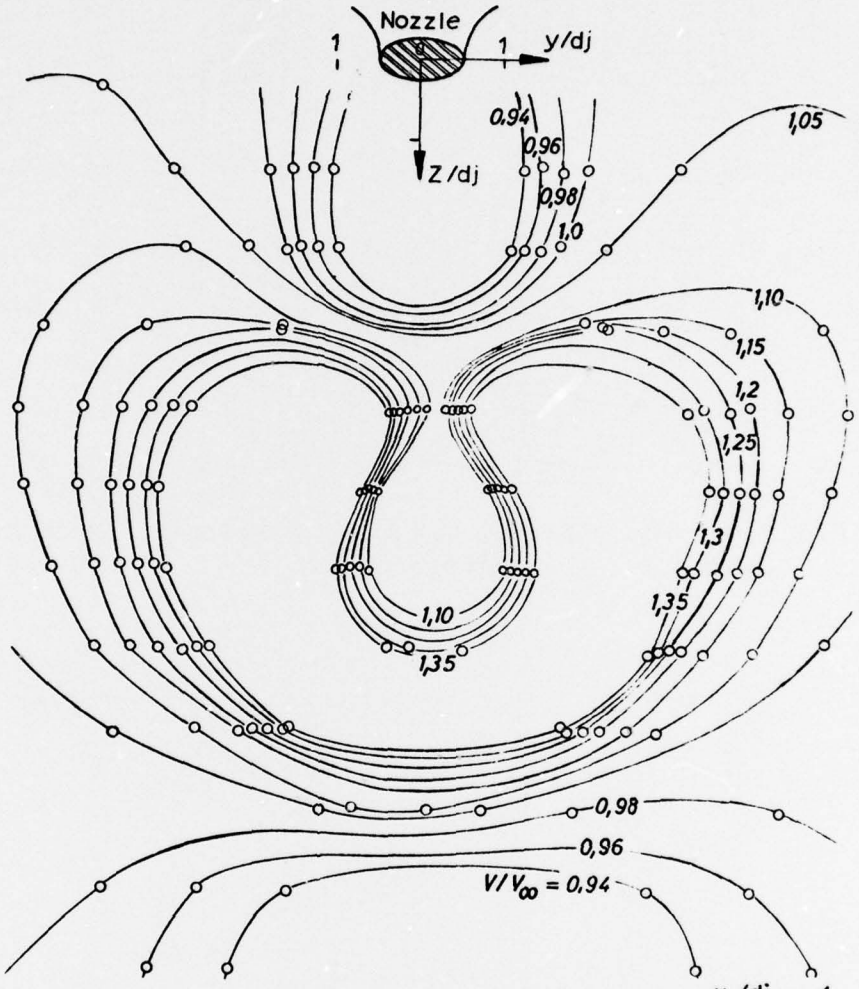

Fig. 10: Cross-blown jet.
Velocity distribution in a y-z-plane

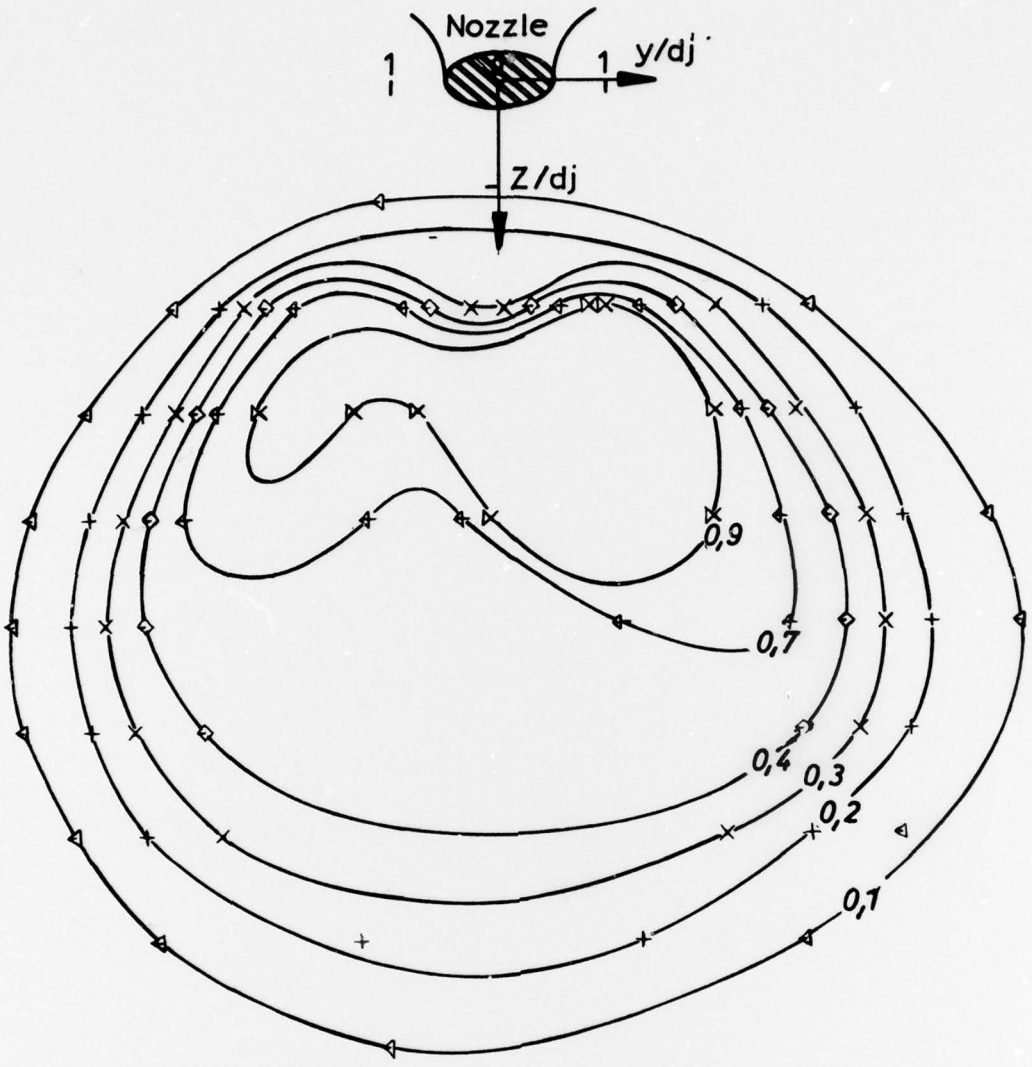

$x/dj = 4$
$V_j/V_\infty = 11,3$
$q_j/q_\infty = 64$
$T_j/T_\infty = 2$

Fig. 11: Cross-blown jet.
Temperature distribution in a z-y-plane

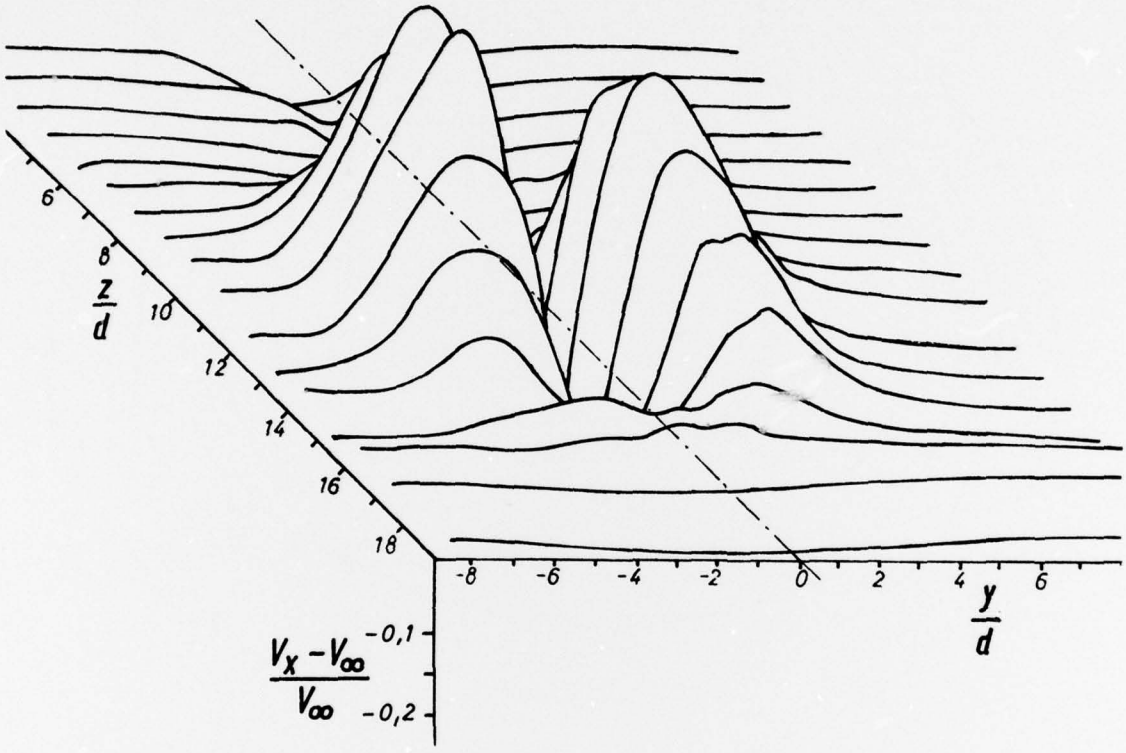

$x / d_j = 15$

$V_j / V_\infty = 8$

$q_j / q_\infty = 64$

$T_j / T_\infty = 1$

Fig.12: Cross blown jet. Three dimensional representation of the α-component of velocity in a z-y-plane

ROUND TABLE DISCUSSION

Prof. Sears :

Ladies and Gentlemen, this is a wind-up summary, and we will review what we have accomplished in the last two days, what conclusions we can come to and what points have been left dangling in the air. I am accompanied here at this table by the several chairmen of the sessions. I am M. Carrière ! You wouldn't know it by hearing my French, and I might say that you wouldn't know it by hearing my English either. But I am taking his place as far as Session 2 is concerned.

If we are to summarize and come to some conclusions, let us see what kind of conclusions we might come to that would do anybody any good. I would suggest that we look at the subjects from the following viewpoint. The last few days we have discussed, talked about and listened to a number of different aspects of the cooperation between wind tunnels and computing machines. I should think that a good way to summarize might be to look at this subject now and say what is not being done, what is missing. Or, if we can establish certain goals in the field of wind tunnel computer cooperation, how do we achieve these goals in our NATO countries and what steps toward these goals are missing from the programs ? Put bluntly, what should we be asking our various bosses and treasurers ? What should we be asking them to support that we ought to be doing ? If you agree with me to take that point of view and try to address that question, then I remind you that we have heard talks in essentially three different areas with considerable overlap.

I would say that we have heard papers (1) in the category of increasing the utility of wind tunnels, making wind tunnels more useful, more efficient and less expensive; (2) we heard papers in the category of improving the simulation provided by wind tunnels, and (3) we have heard papers in the category of complementary uses of computing hardware and software; that is, computations that would either replace the wind tunnel or complement the wind tunnel, such as the ones we heard today on improving numerical simulation as such.

Without any previous warning, I am going to call on these chairmen to try to lead off and say, in those categories, what their goals are and what ought to be done to achieve those goals. Mr. Dietz, you and your session were concerned mostly with the first category; the use of computers to increase the utility of wind tunnels. Could I ask you to think about that and talk at the same time ?

Mr. Dietz :

Thank you Mr. Chairman. You have narrowed down my avenue of approach a bit by saying that I must talk about what I would ask my bosses to support.

Prof. Sears :

No, you can go much farther than that.

Mr. Dietz :

I can say anything I wish then. I agree with you about the meeting, and I would put it in a little different context. We have talked about the use of computers in connection with wind tunnel operation, and we have also talked about the use of wind tunnels in connection with computer operation. So, we have covered the gamut from the computer supporting the wind tunnel to the reverse of that. The papers, in the Section that I chaired, dealt primarily with how the computer can improve the wind tunnel. It was obvious in those papers that a number of countries have gone a long way in using the computer to monitor the conditions in the wind tunnel and to feed back to the wind tunnel signals that will cause it to maintain set test conditions. That utilization has already increased the output per hour of the wind tunnel and increased the precision of the data that are produced by the wind tunnel. I think nothing more needs to be said about that except for AGARD to put it in the record and to have these papers widely circulated, so that others who may not have done this, could take advantage of the technology that is available. The next thing, there were several papers in the Session that talked about on-line data processing where you have the computed coefficients available to you at the very minute that they are being measured in the wind tunnel. You saw that that has been done in several nations and done with a high degree of sophistication. You are aware of the fact that the data are not only used in the control room and on the base where the wind tunnel is, but is sent to the user on-line, so that he can have it at the minute that it is being taken. There are a number of ways to use these data if you have them on-line, aside from making manual human decisions in the control room about what to do next. There were items in the papers about that; about how these were used. Remember, in the tests of rotary wing aircraft, models are very sensitive; they are not long lived, so you can use those data to trim the vehicle in the tunnel and only take those data which are essential

to your program. At least you take those 10% of the total data first, so that you know that you have them while the model is still alive. Then you take the less important data later, but you use the on-line feedback to restrict your program. That can be used either because you have a model that isn't going to last very long, or you have a limited budget, and you would like to take 1/10 of the data that we now take in order to document the performance of a bird in the wind tunnel. Remember that there are other uses for that feedback data that we didn't talk about very much in the meeting. I hope that that appears in this record, so that we can have AGARD papers on it subsequently, and that that technology would be more widely spread. I mentioned that at the outset of this meeting. That is, you can take the on-line data that you have measured from the wind tunnel and you combine that with computer output that is either purely theoretical or is also based on empirical data, but stored in the computer, and you make the wind tunnel, through that technique, produce data that ordinarily you would not otherwise have. You recall that I mentioned the situation of testing a fighter at stall, where it is going through departure. It has no engine simulators on it, but you may feed in the characteristics of the engine on the lee side and the windward side of the airplane and force a thrust differential onto that model and thereby calculate accurately its departure characteristics, even though you have no engine simulators on the model. That is a marriage of the computer and the wind tunnel that makes the wind tunnel far more useful than the wind tunnel alone. I really didn't hear enough of that in this meeting. It is being done, and the technology should be spread around through AGARD.

My recommendation about the interrelationship between the wind tunnel and the computer in response to the Chairman saying that we should recommend areas on which to spend our effort goes like this : don't let things just happen by natural events, make them happen. To make things happen, you would like to look into the future and see what might be possible. I would suggest that a future activity of AGARD or one of our individual departments might be to look at where you think the computer will be in five years, where you think the wind tunnel will be in five years, what would be their optimum interface and the optimum interaction between them five years from now to produce the best aerospace for the North Atlantic Treaty Organization. Having some estimate of where you think you ought to be, then trying to force that to happen. Make the necessary investments in computer work or the necessary investments in improved wind tunnel technology to get where you think you want to be and not just drift with the advancing technology that might happen to you.

Prof. Sears :

Let us stay on this subject for a while and see if we can get comments on this from the audience. Did Bob's remarks inspire any of the rest of you to follow up the subject ? Mr. North ...

Mr. North :

My comments will be fairly prosaic. I would think that wind tunnels in five years will be much where they are today, because of the time scales of their construction. As far as computers are concerned, to know where we shall be in five years time really seems to me to be a leap of imagination, and I imagine that many people in the computer industry would like to know that. Though I support Bob Dietz' sentiments, I certainly think that it is going to be quite difficult to come anywhere near the real situation and I think probably our guesses would be conservative.

Mr. Kelly :

I would agree with Mr. North, that it is very hard to predict where the computers will be five years from now, the changes in the last five years have been so dramatic. I think that one of the alleviating factors here is that the computer people seem to be coming up with lots of small, special purpose, relatively inexpensive pieces of equipment which can be ganged together to give you a lot of flexibility. So you don't have to make one big investment in one big piece of hardware, and then find out that you did the wrong thing five years from now. I think that we can look forward to having some adaptability in our equipment. The other point that bears on this, and I don't believe that anyone really discussed it at the meeting, is that it is possible to set up your wind tunnel experiment so that you have, in principle, an on-line parameter identification technique. You have a theoretical linearized model with which you have done the best you can before you went into the tunnel, and you play into that model your experimental results, update the linearizing parameters, and then predict the next point. We are presently trying to implement this in the rotor dynamics work, and the theory has been done; it is just that we have not quite yet done it in the tunnel. I suspect that this type of closing-the-loop between the theory and the experiment will be a very valuable thing to do. I expect to see that done in the next five years. Finally, I am quite optimistic about the adaptive wind tunnel ideas. I am hopeful that we not only will come up with computerized venting of tunnels, but in those situations where we find that it is uneconomical to vent the tunnel, we at the very minimum will come up with much better corrections with all the information being measured on the control surface. I think that there is going to be some progress there. We ought to make that happen.

Prof. Sears :

Thank you Mark. Apropos to what you said that nobody discussed, it was to some extent implied in the discussion of Mr. Slooff, wasn't it ?

Mr. Slooff :

If we think about the fact that we still have a lot of wind tunnels that are certainly not going to be self-correcting for the next five or ten or twenty years to come, there is still a lot to do with respect to classical wall interference. The thing to do really is to measure the boundary conditions at some distance from the wall and do the computations of the wall corrections using the measured boundary conditions inside of the tunnel walls. In this way we do not have to rely on the homogeneous boundary condition that everybody is using nowadays, but that nobody trusts.

Dr. Vayssaire :

Il est certain que les conditions aux limites des parois ventilées ne sont qu'une approximation mathématique. Mais lorsque les corrections de parois, associées à ces conditions linéarisées, sont appliquées, les résultats obtenus sont satisfaisants. Ces corrections sont utilisées en subsonique élevé. L'ONERA les utilise aussi et cet office nous a fourni de bons résultats.

Alors qu'est-ce que l'on cherche de mieux ? Le vrai problème transsonique est loin d'être résolu. C'est là en vérité le problème à résoudre et c'est dans ce but que l'on doit améliorer et approfondir la connaissance des conditions aux limites.

Prof. Sears :

Thank you. Are there any other comments on this subject ? The subject of corrections has been brought up and that is in my second category. As I told you, I take the place of M. Carrière, who was Chairman, and the papers of Wolf, Gunn, Chevallier, Vaucheret, Vayssaire and me all had to do with this subject.

If I take the liberty of making the opening remarks on this subject, I would say that the general problem, of course, is that we have to improve the simulation in the next decade or two. I don't think that the users of wind tunnels are going to be content. They are not content now, and they are not going to be even as content as they are today with the accuracy that we provide them. I hope I am not hurting the feelings of "wind-tunnel jockeys" in the room. I think that they are doing a fine job. But there are too many cases now where the drag is measured nicely to about three significant figures, four decimal places, which is not enough for long-range transport airplanes. If I am not mistaken, that last decimal place just mentioned, in some cases could make or break the corporation and has perhaps come close to it in some cases. There are some questions that we have not addressed today, because they are probably not related to computers. They are questions of flow quality, reduction of stream turbulence and noise, and all of that sort of thing.

In the category that we are supposed to be discussing, there are serious questions of boundary interference, together with the profound questions of what is the Mach number and what is the angle of attack that are being simulated. I said this yesterday, and I shouldn't take this advantage of you by repeating it, but I think that there are serious problems that we have to attack as we go into the future of wind tunnels. For one thing, the designers are going to have to make more elaborate calculations, as we all know and have repeated to one another in the last few days, and they are going to have more precision in their expectations. As a result of that, they and the chief engineer and the project engineer are going to demand accuracy in the range of Mach numbers, not to mention Reynolds numbers, that we are today really not able to provide. My own personal conviction, and this is certainly a prejudiced conviction, is that the use of the measurement of perturbation quantities in the stream and the deduction therefrom of conclusions about the test, the simulation that is being attempted, is a very promising direction to go. Although ONERA and some of the rest of us are doing some work in that direction, I don't think that it is enough. I think that the questions of what is to be measured, how it is to be measured, and how the wall geometry is going to be altered to provide this simulation have so many possible answers that a lot of them ought to be followed up, and they are not, to date. The Southampton group, the ONERA group, and the Calspan group are each doing something a bit different from one another, which is good. However, I think that there are more possibilities and opportunities for invention and original work than are being followed up. I will tell you what we need, if I am correct that this is an important line of work : we need more monetary support.

M. Chevallier, would you say something here.

M. Chevallier :

I have few comments; I wish that many people work on the subject of adaptive walls for there are many ideas yet to be applied. In another way, I think that the new concepts derived from the virtual external flow may be useful even for a conventional wind tunnel : for example to determine the Mach number from the set of wall pressure distributions. It is not a trivial question, as mentioned.

One of the questions for me is now to use adaptive walls in both the subsonic and supersonic ranges, as the flow patterns are then quite different. Nevertheless, I hope that adaptive walls will be a solution for transonic testing in the future.

Prof. Sears :

Are there any more comments on this subject ?

Dr. Schmidt :

I have one question concerning the adaptive wall technique. As far as I know, all the results we saw were done on two-dimensional cases and also cases including no lift or just a very small portion of lift. What do you think about three dimensions, let us say modelling wind tunnel walls for very complex wing-body combinations ? That actually means that the walls will be quite complex, shaped also in a very complex form. Do you think it would be possible to do a modelling like that in three dimensions ? Also, do you think it will be possible to do a modelling for highly loaded high lift systems having the right wake curvature and thus Kutta condition.

Prof. Sears :

We have to clarify our concepts here. Several of us are working with the concept where you don't ever have to model the flow in the vicinity of the airplane model. You measure the perturbation quantities around the outside, some way away from the model. You are not even allowed to know what that model is .. that is your competitor's model! .. and you only know the perturbation quantities. You eliminate thereby the question of whether you are able to calculate the flow-field of an airplane. You only calculate the flowfield outside of a surface on which you have measured perturbation quantities.

Dr. Schmidt :

Even the flowfield on that, let us say a tube, is quite complicated and complex and is changing quite a lot along the tube surface. So it is still the same problem. It is caused by complex aircraft, so finally the flowfield will depend on the shape of that aircraft.

Prof. Sears :

Granted, but I was put off by your mentioning the Kutta condition. That doesn't seem to have any relation to what we are talking about here.

Dr. Schmidt :

It will have some relation in the fact that the disturbances on the tube depend on the lift that is produced.

Prof. Sears :

If the Kutta condition is not satisfied, then the perturbations will be different, and I don't have to know that.

Dr. Schmidt :

Actually you satisfy the Kutta condition, but the wake curvature is different from the one you will have in real flight. That will cause differences on the lift.

Prof. Sears :

Negative. I don't agree.

Dr. Schmidt :

On high lift systems, due to the wind tunnel walls you will have different wake curvature.

Prof. Sears :

In the three-dimensional configuration with lift, certainly the downstream conditions that are modelled are affected by the fact that there are trailing vortices. But they are there; I don't have to worry about them, they are there. There can be a sheet of them, or two of them, or rows of them, etc. I don't have to know that. The problem is only to be able to calculate,and we saw this morning that there is some progress in this direction. We have to be able to calculate a three-dimensional transonic flow with given boundary conditions. The boundary itself will be very simple and the boundary values given on the boundary will not be that simple. They will be functions of the two variables, hopefully with some symmetry. That does not seem to me to be the difficult part of the problem. The difficult part of the problem is to decide, in the cases of the three-dimensional tunnel, at how many spots on the top, bottom and sides you have to control the wall configuration. I don't know the answer to that, but I think it will be "infinity", where "infinity is .. ? M. Chevallier, what will be the infinite number of spots ? Thirty or so ? In some ways the three-dimensional problem will be simpler than the two-dimensional problem, as you know, because there will be three-dimensional attenuation of the errors that you make by your crudity, that you make by having only a finite number of screwjacks.

Also, I wanted to object a little bit to your saying that there was no lift. We went up over the stall in those data that you saw. They went up and stalled and had lift coefficients above one or something like that, with an NACA 0012. One must not say that there is no lift. However, it was two-dimensional. It seems to me that some of the questions that were asked of me at the end of my talk yesterday about how much it is going to cost and how soon these things are going to be in operation and things like that were a little silly, because it is clear that we are in the stage where we don't have enough information on this type of wind tunnel to know about its cost effectiveness compared to whatever the alternative is, i.e., building a great big wind tunnel or doing

everything in flight, etc. So, I think that questions that would depend on real hard numbers for hardware and things like that are a few years too early now. My point, and M. Chevallier agrees with me, is that this is a possibility that has or seems to have a great deal of power in certain non-linear regimes where nothing else is quite clear, so it ought to be investigated to the point where decisions can be made. But the decisions are not here. Is that fair ?

M. Chevallier :

Perhaps, I can add some comments on the questions we heard about the new concepts. The adaptive walls idea is very young and, like a baby, cannot give a satisfactory answer to all questions. But are some of them, for example the effects of the limited length of the test section, well-known even for the conventional walls ? Indeed, we can be more demanding with our new baby, as we hope he may be better after all than his forefathers; but give him time to solve all your problems.

Prof. Sears :

By the way, speaking of instrumentation as I did, I meant to make a wisecrack that I already tried out on Prof. Young. That is, that this is a remarkable meeting for the last few days, since nobody said "LDV" for two whole days. When I have talked about adaptive walls schemes to other audiences, almost invariably some optimistic fellow says, "Your instrumentation problems are all going to be solved. You are going to have an LDV scheme that has all the readings of two or more perturbation quantities all around a thereby defined surface S". I don't think anybody is looking into that; maybe it is too early. The LDVs ... is there anybody here who loves the LDVs and thinks that they are going to be the solution instead of probes and wall pressures and things that we are using today ? (LDV = Laser Doppler Velocimeter).

Mr. Kelly :

I hate to be put in the position of being the optimist because I am usually the pessimist, but we have had very good experiences with the two-dimensional laser velocimeter that we have used in our 7 by 10 foot tunnel. We have used this, incidentally, coupled directly into a small computer. This is one of our experiences that convinces me that, in the future, we are going to see a lot of small special purpose instruments like this that actually are quite sophisticated and read the information out directly in the terms of what the man wants to see, namely, in this case, non-dimensionalized velocities. You can synchronize the data sampling with rotor speed so that you can freeze the flow. You can do lots of nice things like that. I was so enthusiastic, as a matter of fact, that I decided that we were going to build one for the 40' by 80' wind tunnel. I ran into a problem in that, with a two-dimensional instrument the mounting provisions to get it up where we wanted it in order to scan a large part of the flow ended up being a very expensive proposition. Mechanical mounting cost as much as the instrument itself. We dropped back and decided that we would build a three-dimensional instrument first for the 7' by 10' wind tunnel, because then the mounting is very much simplified; you can mount the instrument anywhere you want, probably on the floor where you can service it and focus it on any place in the test section within limits and have a very powerful tool, which I think should be very practical. We are building the three-dimensional instrument, and I have great confidence that Dr. Kenneth Orloff, who has been so successful with the two-dimensional instrument, will make the three-dimensional instrument work eventually, if not the first time. The two-dimensional instrument, once it is hooked up and operating, is very easy to use. In some aspects it has been like a well-developed computer. If it works it works right, and the need for calibrations are practically non-existent. If it doesn't work, you have to call the expert and get into the box. It seems to me that this really is a powerful tool for making these measurements on the control surfaces, in that it could be set up in one location, and it could scan a number of places. You could have an adaptive scan so that you could take a lot of data points in regions of high rates of change and a very few data points in regions of low rates of change, and probably program that. It can all be resolved on the computer, in terms of getting the components that you want. Therefore, I am quite encouraged about the potential of the LDV, and I think it does fit in very nicely with the need for extensive measurements on the control surface. I do envision a lot of problems with putting, say, 100 static pressure taps in the floor, or 100 directional pitots on the floor, and having people kick dirt into them or stumble over them and break them, etc. In fact, I think that the laser velocimeter might well end up having less upkeep than a bunch of probes or static pressure taps.

Prof. Sears :

Are there more comments on this general topic of using computers to improve the simulation ?

Mr. Slooff :

I will make a few remarks on a slightly different subject, but still very closely related, which was not discussed I think, in the past two days of this meeting. This is the problem of support interference, sting support interference in particular, which can be quite important. If I remember one of those pictures, I think in one of the Dornier papers, where they had a very small store on really a tremendous sort of sting, I could imagine that when a fellow would try to drop his load on a particular object, it would fall on the next one or something, because of the interference. I think here is another point where computational methods might help in establishing the magnitude of interference. One can compute the flow about a configuration without the sting support and with the sting support represented and determine the interference from the difference. This kind of procedure should become more or less a standardized treatment in future wind tunnel testing.

Prof. Sears :

May I suggest that we go on to my third category then, i.e., using computers to replace or complement wind tunnels, to carry out numerical simulations in parallel with, or in lieu of, wind tunnel simulations. We have three chairmen to open this subject !

Prof. Smolderen :

I must first of all say that I enjoyed very much Mr. Slooff's contribution, not only because he is one of our brilliant former students, but also I think he gave many interesting remarks. In particular, things that are somewhat overlooked when comparing wind tunnels vs numerical computations. In fact, for instance, it is very easy to change a configuration in a numerical computation and very difficult to do so in a wind tunnel test, but on the other hand it is very easy to obtain many different measurement points in the wind tunnel, and the cost of numerical computation for difficult cases is proportional to the number of, for instance, incidence points that you want to look at. These are things which I think one does not always take into account when making general discussions about these things. I also was very much interested, perhaps personally more than anything else, in his remark on inverse problems, which certainly have not received, as he said, enough attention both from theoretical and applied people. Both inverse problems and optimization problems which I think can be classed into the same category. There were some implications in the results that indicate that maybe some of these inverse problems are not well posed. I don't think one can generalize here and say that any inverse problem is not well posed. However, there are some which are not well posed. I think that the example he gave was more an example of extreme sensitivity of the results to a given inverse problem, and probably not really to the not-well-posed nature of the problem mathematically. I think that these should be studied in more detail by theoretical people for the simple examples. I think that there are perhaps other people who would like to say something about that. The paper by Mr. Jones, I found also very interesting, since it is perhaps a rather specific application, but a very nice application of calculations which finally lead to instrumental methods. Both the idea of using computations of a parameter which is very sensitive to Mach numbers for Mach numbers very close to one is a very good idea, and also let us say, that it is quite a feat to be successful in computing exactly such a parameter as the stand-off distance at Mach numbers so close to one. I was still a little disturbed about a remark he made on the unsuccessful application of time-dependent methods. I suppose that the time-dependent method used was not one of the best ones. The last paper by the Dornier people was somewhat out of the general idea of the Session. I think the comments that Bob Dietz made earlier are pertinent to this paper, namely, that one should use computation to prepare a test in order to have efficient testing conditions. I do not think that I can really draw general conclusions from these three papers, because they are either not completely related to the subject or are rather specific, but I must say that I found them all very interesting.

Dr. Wirz :

There are three very different papers to talk about briefly. The first, presented by Mr. Marvin from NASA Ames, was one of the most appealing to me since the objective of the work is of fundamental importance. The combination of numerical simulation of compressible turbulent flows with carefully designed and controlled experiments to enhance turbulence modelling, seems to be indispensable (and therefore fundamental) to verify closure concepts for the numerical treatment of the time-averaged Navier-Stokes equations. The actually used eddy viscosity model (two layers) is, of course, a rather classical one, while the algebraic relaxation model seems to improve significantly the validity of the theoretical results, although a question mark may be put whether this model is sufficiently invariant. One could, for instance, suggest to model a relaxation process in turbulent flows by considering an additional differential equation.

The second paper, presented by Mr. Couston from VKI, essentially deals with problems associated with transonic blade-to-blade flow computations at the trailing edge and where a time-dependent (finite area) approach to solve the full Euler equations has been used. A rather simple theoretical model to treat approximately the trailing edge region (base pressure problem) has been employed showing good agreement with experiments. It appears that the base pressure has only a weak influence on the trailing edge shock strength and the exit flow direction.

The last paper of this Session, presented by Dr. Schmidt and Dr. Stock from Dornier, is a very ambitious attempt to compute the three-dimensional transonic flow field around a complete aircraft configuration including even the boundary layer effects. The calculations are based on the small disturbance equations which are, of course, a very limited model to treat flows around aircraft configurations. Furthermore, it appears to be difficult to formulate proper boundary conditions, if a wind tunnel must be simulated. Obviously, there exists a need to replace the relaxation methods, since it seems to become more and more difficult to obtain with those techniques three-dimensional transonic flow fields.

As far as the viscous part is concerned, I pointed out already earlier that the key problem to solve numerically three-dimensional boundary layer flows seems not to be the numerical method being used (integral or finite difference method), but the turbulence model. Due to the limited flexibility of integral methods, finite difference methods seem to be superior (at the expense of more computer time, however).

A few remarks may close this summary. Of course, it was not possible to cover all topics of Computational Fluid Dynamics where remarkable progress has been accomplished recently. The paper of Mr. Marvin again may serve as a good example to demonstrate the potential of close collaboration between theoretically-numerically oriented scientists and experimentalists. There is, of course, also a need for more fundamental research as far as the development of theoretical models (i.e. turbulence modelling) and numerical methods is concerned. A certain danger in simply using existing methods cannot be denied, as examples often show.

Dr. Schmidt :

I would like to stress that there is quite a large lack of experiments on three-dimensional boundary layers. There are not many data available to compare with. Also we are missing good experiments on the pressures and the boundary conditions on wind tunnel walls. As long as we don't know very much about the boundary conditions, there is no chance really to simulate, as Prof. Wirz said, those conditions in the numerical procedures. What I would like to point out is that we are able to simulate whatever we know. If we know the conditions, if we have the right physical model, and if we can formulate the differential equations, then it is no problem to incorporate those conditions in the numerical calculation. Our problem is that we don't know the differential equation. We even don't know the physical model. There should be some more research and some more work on very good experiments on the wind tunnel walls to know all the conditions on slots and porous walls, etc.

The second comment pertains to the session which was chaired by Prof. Smolderen, referring to the paper given by Dr. von der Decken. We should keep in mind that there were actually two points. One was that with the combination of computational methods and wind tunnel techniques, there is a chance to take care of all the influences that you are not able to really represent in the wind tunnel, like jets. Therefore, we have an option in our computational cycle to take care of the additional flow field which is generated by the jet of an engine. We can take the flow around the engine pod and also the mass flow through the engine. This gives an increment of flow field velocities around the configuration. That could be added in the forces and integration of the path of the external store. On the other side, we can take care of the sting. In fact, not of a sting like that shown on the schematic drawing, but on the real sting which is much smaller. We calculate the forces acting on the sting and then substract sting forces and take account of the base drag in the computation. So we are adjusting the sting to simulate the real trajectory.

Mr. James :

I have been asked to put this question on behalf of Mr. Shaw, who had to leave early. It really concerns papers in the first three sessions, so now seems an appropriate time to voice it. I should also mention that it is particular to industrial applications, rather than the experimental and theoretical approaches. His question is in two parts. "With the limited funds available and assuming these funds are not sufficient to fund both tunnel and computer based methods, would the panel comment on the following two suggestions :
1. That we use existing tunnels to create test case data to be used in validating and improving the next generation of computer based fluid dynamic methods. Any funds thus saved could be used in developing relevant soft-ware, such as systems to allow existing or the next generation of general computers parallel processes.
2. The main function of these new fluid dynamic methods would be used to aid interpretation and extrapolation of wind tunnel data acquired in the normal development of a new aircraft project".

What he is suggesting in the second question, is that we use the normal wind tunnel that we have now, and the new fluid dynamic methods be used as an extrapolation of the existing wind tunnel work, rather than spending money to improve the wind tunnels.

Prof. Sears :

The first question was whether we would recommend using existing wind tunnels for wind research, or research on wind tunnel techniques, or wind tunnel soft-ware.

Mr. James :

Yes, really, to validate and improve the next generation of computer fluid dynamics.

Mr. Dietz :

Regarding the first question about whether we could select some typical kind of test conditions or models in a wind tunnel and use those as standard test cases for computer methods, and therefore improve computer methods or get more confidence in them, there is a study that AGARD has underway on that subject. Dr. Barche is the study chairman. The discussion we had recently was that it is going to be very difficult to select those example cases. That is a career in itself. As people have been mentioning, Mr. Kelly may have said it and Bill Sears said it, that in a typical wind tunnel test, as of current day at least, we don't really know the angle of attack precisely, we don't know the Mach number precisely, and we don't know the wall interference effects precisely. We don't know the model shape precisely. When you take all that ignorance into account, it is kind of hard to choose this typical test case. When I mentioned five years as my target about saying where wind tunnels would be and where computers would be, it is based

on the idea that within five years we will have many of those things in modern tunnels overcome, not that you will build a new tunnel, but you may install a magnetic suspension system or you will know a lot more about sting effects. You will be able to measure model angle of attack and model shape precisely in the test section. You will make the measurements suggested by someone in the audience that say that wall interference is negligible. It may not tell you how to correct wall interference, but you will know when it can be ignored. Those things you can see happening in the wind tunnels, the technology is almost here today and the hardware isn't like building a new wind tunnel. You could say where wind tunnels will be five years from now. They will be much better tools than they are today. At that point we could make some test cases that the computer people could use as trial balloons, so to speak. Dr. Barche's study will throw some more information on that, and the man that raised that question should follow that study.

Dr. Vayssaire :

Je suis d'accord avec M. Dietz. Un exemple très simple prouve qu'il a raison. La soufflerie Sigma 4 de l'Institut de St Cyr, avec ses parois déformables, a été créée en 1956. Elle a fonctionné dès 1960. Les ordinateurs ont trouvé leur épanouissement à partir de 1967/1970 pour devenir opérationnels en soufflerie. Et ce n'est qu'à partir de 1969/1972 que l'on s'est sérieusement intéressé aux effets de parois ventilées. Ce qui prouve que, bien que possédant une soufflerie de bonne réalisation technologique, il faut envisager son amélioration très rapidement. Les recherches pratiques et théoriques, propres à cette amélioration, qui marchent en parallèle, se font une concurrence acharnée.

Aussi, il est difficile de faire un choix aujourd'hui pour proposer des principes, des montages ou des essais de base.

Quoiqu'il en soit, en attendant les souffleries futures, on doit toujours améliorer les souffleries existantes - ce qui est possible comme on vient de le dire - pour en tirer le meilleur parti : une bonne soufflerie aujourd'hui sera excellente demain, si l'on sait l'utiliser.

Prof. Sears :

Now, in closing this discussion, let us make sure that everybody has had a chance to talk.

Mr. Marvin :

I would like to make two comments. First, there are cases where wind tunnels will probably never give correct simulation : for example, very high altitude, high velocity situations where scale and chemical reactions of high temperature air cause nonequilibrium effects to occur. These are situations where computational fluid dynamics will provide the best simulations. We face this problem with the space shuttle vehicles. We have, in the past year, actually used computational methods to simulate the flow field and heating over the vehicle in order to evaluate the design methods used by the developer of the vehicle. Essentially the computed flow field was used to assess the engineering extrapolation of wind tunnel data to flight. The results indicated that our extrapolation techniques worked pretty well. For heat protective systems of the type used on the shuttle there is some "forgiveness" in the design because if the heat transfer rates are off somewhat, you can absorb this uncertainty in the heat shield material. We are continuing to assess the design, but our confidence in it is increasing because we were able to properly simulate the flow field through computation. In the future, I would expect numerical simulation to be relied on extensively to guide our extrapolation of wind tunnel data to full scale and flight.

The second comment I have is on the employment of the simple eddy viscosity models in our attempts to simulate turbulent separated flows. We were driven to this, as I mentioned, by excessive computational times. With the recent "speed-up" in our codes, we will move on to more sophisticated models that really can build some physics into the problems. We are actually getting into programming multi-equation models now. I am optimistic that there will be marked improvements in our ability to model separated flows.

Mr. Jones :

My subject is a little bit off the main topic of the meeting, but I just would like to answer Prof. Smolderen, because he brought up the fact of the time-dependent methods and, in fact, three time-dependent methods have been used to try and do this blunt body transonic computation. The first one is based on Moretti's type of scheme. That one gave us the kinky behaviour in the shock wave and the convergence was also very slow, even at Mach number about 1.2. The second method was the one mentioned in my presentation, due to Aungier, which was programmed by Hsieh (AEDC) and that took 22 hours at Mach number 1.05. The third and probably the best method these days, is Rizzi's finite volume method. The latest results he sent me still hadn't converged after 75 seconds on the CDC 7600 computer. The 7600 is 60 times faster than the computer that I have available. That was at Mach number 1.05. If you go lower in Mach number it takes much longer.

Dr. Schmidt :

I have one short comment on that subject. In fact, I think he is completely true to say that with Mach numbers very close to one, you have those problems he is mentioning. But as far as I know, there exists one method which is slightly better in that region than those he is mentioning. That is the one done by Rösner in Freiburg (now in Karlsruhe). He succeeded in getting quite good results down to Mach numbers of 1.05 using a time-dependent

technique which is based on the Russian method of Rusanov. This is a completely implicit method which seems to overcome some of those problems. If you write a letter to him, you might get his results to compare with.[x]

Prof. van Ingen :

I would like to start with the morning session and make some remarks about that first. I would like to stress again the fact that the wind tunnel is becoming a part of a large computing system. It is just a hybrid computer where we have an analog part doing the difficult calculations around complicated shapes. With the concept of adaptive walls, in existing tunnels, we may be able to increase the size of the models which we dare to test in them. This increase in size may go on as long as we can improve our calculation methods.

It is quite clear that flow field computations will be very difficult. It is also clear that the computations will become less difficult the farther away we are from complicated shapes. That means, they will be easier away from the model, so that the calculations you have to do to get the configuration of adaptive walls or whatever you use in that region, are bound to be simpler than the full computations. This was reflected in one of the earlier remarks about Kutta conditions. That is going to be a difficult part of the computation. You single out this difficult part and let the wind tunnel computer do it.

Of course, the wind tunnel computer uses the right equations as Mr. Slooff put it this morning. You have, however, the wrong boundary conditions. Part of this is due to the sting support system which you can't solve by adaptive walls. The other part comes from the nearness of the walls and this can be solved by the adaptive walls, etc. If you ask me what the situation will be five years from now, I think that a good advice to people planning new facilities, is that they should make sure that they have enough space around the test sections to install these new gadgets. Because, in that way, the tunnel will be able to do work of increasing usefulness in coming years.

Another point I planned to make, but which in the meantime was already mentioned by Bob Dietz, is the need for carefully designed experiments. It is important to realize that an experiment should not just be done, it should be designed. One of the very good examples, is the NLR work on three-dimensional turbulent boundary layer flow. That was a very carefully designed experiment, having in mind the needs of people developing computational schemes. The plans AGARD has to define more of these experiments should be strongly supported by industry as well.

Now, I come to the afternoon sessions. Two papers we had this afternoon give good examples of the situation which arises now, that the intimate linkage between measuring apparatus and computational devices is already well underway. This is only going to pose a problem to our budget authorities, because they always are more reluctant, at least in my surroundings, to allow you a computer than they are to allow you some measuring apparatus. Therefore, you should be aware that as soon as you can call something an instrumentation system rather than a computer, you better do so.

There is another point I would like to stress, it has been said that, from an industrial viewpoint, it is very important to see what you are doing when making wind tunnel tests. You may select your measuring points much more carefully when you have on-line data reduction and hence can see where you are going. The academic people should not neflect this in their teaching and in the projects they give to their advanced students. We should not allow our students to keep on working with old-fashioned things, and not trying to bring these types of techniques into teaching. One thing which struck me earlier this week, was that one of the speakers first showed an old-fashioned manometer board and afterwards decided that his output from his nice computer should be brought in the same form as the original board. You get a very nice quick-look device if you just keep your old manometer board, but add to this, very carefully designed electronic equipment. It can be done, we have one of these things in our department. It is just an old-fashioned manometer board, but with additional photocells and electronic equipment, it works quite nicely.

Prof. Sears :

Thank you very much. I think that we ought to close this session, although many of you have profound things to say. Before we close we have one member of the audience who can speak to us with real authority, because he didn't attend any of it and hasn't heard the papers. I would like to call on Prof. Young, who is the Chairman of the Board of the VKI to tell us what he thought of the meeting.

Prof. Young :

Thank you Prof. Sears. As Prof. Sears has said, I am in a very unique unbiased position to comment on this meeting. However, one or two points did strike me from the little I have heard. Some 10 years ago, I remember a computer enthusiast saying that in 10 years time we will be able to solve the Navier-Stokes equations complete with turbulent flow and separation for any boundary conditions. By simply pressing the appropriate button you will be able to solve any problem you want. Therefore, we will not need any

---

[x] Rösner and Wieland estimated 5 hours computer time at M = 1.05 (private communication to Mr. Jones).

wind tunnels, and all wind tunnel people had better start thinking of other jobs. It appears that that prophesy of 10 years ago, judging by this meeting, is still a long way off from fulfillment, and I personally think that we shall never see it fulfilled. There is a less extreme position for the computer enthusiast to take and to some extent this was reflected in something that Prof. Wirz said, that if only we had a lot more reliable wind tunnel data then we can get rid of wind tunnels. Even that strikes me as a little bit illogical.

The right answer, which was evident at this meeting, is that, of course, wind tunnels and computers are complementary. They are not in any sense rivals, one will help the other. We can look forward to their development in harness in various ways. It has been said that the wind tunnel, after all, is a very good analog computer, and the computer is a very good thing for numerical experiments. If you combine these two in various ways, you should be able to achieve much more effective results than in the past. I am quite sure that we shall go on wanting better wind tunnels, and perhaps more specialized, smaller and more effective computers than in the past.

And now putting on my other hat, as the Chairman of the Board of Directors of VKI, it is opportune for me to say thank you very much to all of you who have participated in this gathering, in particular, to our Chairman here and his colleagues, for making this meeting the success that it has obviously been. As you will know, this meeting has not only the object of bringing together specialists in this particular field, but also, because of the timeliness and the appropriate nature of the subject, it marks the occasion of the 20th Anniversary of the VKI. The actual ceremony will take place tomorrow. I am glad that the meeting has been a success, and I hope that all of you will choose to stay and join in the proceedings of tomorrow. This will help round off our celebrations. Once more, I thank all who have contributed to this meeting and helped in its organisation, especially the hard working translators sitting in their hot eyrie at the top there, and particular thanks to those who chaired the various sessions.

AGARD
NATO OTAN
7 RUE ANCELLE · 92200 NEUILLY-SUR-SEINE
FRANCE
Telephone 745.08.10 · Telex 610176

DISTRIBUTION OF UNCLASSIFIED AGARD PUBLICATIONS

AGARD does NOT hold stocks of AGARD publications at the above address for general distribution. Initial distribution of AGARD publications is made to AGARD Member Nations through the following National Distribution Centres. Further copies are sometimes available from these Centres, but if not may be purchased in Microfiche or Photocopy form from the Purchase Agencies listed below.

NATIONAL DISTRIBUTION CENTRES

BELGIUM
Coordonnateur AGARD – VSL
Etat-Major de la Force Aérienne
Caserne Prince Baudouin
Place Dailly, 1030 Bruxelles

CANADA
Defence Scientific Information Service
Department of National Defence
Ottawa, Ontario K1A OZ2

DENMARK
Danish Defence Research Board
Østerbrogades Kaserne
Copenhagen Ø

FRANCE
O.N.E.R.A. (Direction)
29 Avenue de la Division Leclerc
92 Châtillon sous Bagneux

GERMANY
Zentralstelle für Luft- und Raumfahrt-
dokumentation und -information
D-8 München 86
Postfach 860880

GREECE
Hellenic Armed Forces Command
D Branch, Athens

ICELAND
Director of Aviation
c/o Flugrad
Reykjavik

ITALY
Aeronautica Militare
Ufficio del Delegato Nazionale all'AGARD
3, Piazzale Adenauer
Roma/EUR

LUXEMBOURG
See Belgium

NETHERLANDS
Netherlands Delegation to AGARD
National Aerospace Laboratory, NLR
P.O. Box 126
Delft

NORWAY
Norwegian Defence Research Establishment
Main Library
P.O. Box 25
N-2007 Kjeller

PORTUGAL
Direccao do Servico de Material
da Forca Aerea
Rua de Escola Politecnica 42
Lisboa
Attn: AGARD National Delegate

TURKEY
Department of Research and Development (ARGE)
Ministry of National Defence, Ankara

UNITED KINGDOM
Defence Research Information Centre
Station Square House
St. Mary Cray
Orpington, Kent BR5 3RE

UNITED STATES
National Aeronautics and Space Administration (NASA),
Langley Field, Virginia 23365
Attn: Report Distribution and Storage Unit

THE UNITED STATES NATIONAL DISTRIBUTION CENTRE (NASA) DOES NOT HOLD STOCKS OF AGARD PUBLICATIONS, AND APPLICATIONS FOR COPIES SHOULD BE MADE DIRECT TO THE NATIONAL TECHNICAL INFORMATION SERVICE (NTIS) AT THE ADDRESS BELOW.

PURCHASE AGENCIES

Microfiche or Photocopy
National Technical
Information Service (NTIS)
5285 Port Royal Road
Springfield
Virginia 22151, USA

Microfiche
Space Documentation Service
European Space Agency
114, Avenue Charles de Gaulle
92200 Neuilly sur Seine, France

Microfiche
Technology Reports
Centre (DTI)
Station Square House
St. Mary Cray
Orpington, Kent BR5 3RF
England

Requests for microfiche or photocopies of AGARD documents should include the AGARD serial number, title, author or editor, and publication date. Requests to NTIS should include the NASA accession report number. Full bibliographical references and abstracts of AGARD publications are given in the following journals:

Scientific and Technical Aerospace Reports (STAR),
published by NASA Scientific and Technical
Information Facility
Post Office Box 8757
Baltimore/Washington International Airport
Maryland 21240, USA

Government Reports Announcements (GRA),
published by the National Technical
Information Services, Springfield
Virginia 22151, USA

Printed by Technical Editing and Reproduction Ltd
Harford House, 7–9 Charlotte St, London W1P 1HD

ISBN 92-835-0178-0